



HAL
open science

Multi-scale study of straw buildings hygrothermal, environmental and mechanical behavior

Ghadie Tlaji

► **To cite this version:**

Ghadie Tlaji. Multi-scale study of straw buildings hygrothermal, environmental and mechanical behavior. Materials. Université Clermont Auvergne, 2022. English. NNT : 2022UCFAC084 . tel-04416366

HAL Id: tel-04416366

<https://theses.hal.science/tel-04416366v1>

Submitted on 25 Jan 2024

HAL is a multi-disciplinary open access archive for the deposit and dissemination of scientific research documents, whether they are published or not. The documents may come from teaching and research institutions in France or abroad, or from public or private research centers.

L'archive ouverte pluridisciplinaire **HAL**, est destinée au dépôt et à la diffusion de documents scientifiques de niveau recherche, publiés ou non, émanant des établissements d'enseignement et de recherche français ou étrangers, des laboratoires publics ou privés.

Université Clermont Auvergne

École Doctorale

SCIENCES POUR L'INGÉNIEUR DE CLERMONT-FERRAND

THESIS

Presented by

Ghadie TLAIJI

Presented for obtaining

The degree of University Doctor

Specialty: Materials

Thesis title

Multi-scale study of straw buildings hygrothermal, environmental and mechanical behavior

Publicly defended on December 12, 2022 in front of the jury composed of:

Mr. Steve GOODHEW, Professor, University of Plymouth	Reviewer
Mr. Rafik BELARBI, Professor, Université de La Rochelle	Reviewer
Mr. Jean-Philippe COSTES, Professor, Ecole Nationale Supérieure d'Architecture de Clermont-Ferrand	Examiner
Mrs. Hasna LOUAHLIA-GUALOUS, Professor, Université de Caen Normandie	Examiner
Mrs. Florence COLLET, Associate Professor, Université de Rennes 1	Examiner
Mr. Pascal BIWOLE, Professor, Université Clermont Auvergne	Supervisor
Mr. Salah OULDBOUKHITINE, Associate Professor, Université Clermont Auvergne	Co-Supervisor
Mrs. Fabienne PENNEC, Associate Professor, Université Clermont Auvergne	Co-Supervisor
Mr. Erick RIGAUDIE, Société Activ'Home	Guest

Université Clermont Auvergne

École Doctorale

SCIENCES POUR L'INGÉNIEUR DE CLERMONT-FERRAND

THÈSE

Présentée par

Ghadie TLAIJI

Pour obtenir le grade de

DOCTEUR D'UNIVERSITÉ

Spécialité : Matériaux

Titre de la thèse

**Étude multi-échelle du comportement hygrothermique, environnemental et mécanique
des bâtiments paille**

Soutenue publiquement le 12 décembre 2022 devant le jury composé de :

M. Steve GOODHEW, Professeur des Universités, University of Plymouth	Rapporteur
M. Rafik BELARBI, Professeur des Universités, Université de La Rochelle	Rapporteur
M. Jean-Philippe COSTES, Professeur des Universités, Ecole Nationale Supérieure d'Architecture de Clermont-Ferrand	Examineur
Mme Hasna LOUAHLIA-GUALOUS, Professeur des Universités, Université de Caen Normandie,	Examinatrice
Mme Florence COLLET, Maître de conférences, Université de Rennes 1	Examinatrice
M. Pascal BIWOLE, Professeur des Universités, Université Clermont Auvergne	Directeur
M. Salah OULDBOUKHITINE, Maître de conférences, Université Clermont Auvergne	Encadrant
Mme Fabienne PENNEC, Maître de conférences, Université Clermont Auvergne	Encadrant
M. Erick RIGAUDIE, Société Activ'Home	Invité

Abstract

Bio-based materials such as straw have generally a low embodied energy. Therefore, they are becoming a promising alternative to improve buildings energy performance and reduce their carbon footprint. When compared to common building construction materials, bio-based materials allegedly provide better control of the indoor temperature and relative humidity variations, thus ameliorating thermal comfort. Although widely studied, there is still a lack of data concerning the thermal, hygric, and energetic performance of such structures. The purpose of this thesis is to provide some of the answers through experimental and numerical work.

A literature review analyses the work that has been carried out by the research community and compared the results. It shows that on the fiber scale, straw is composed of two main elements, cellulose, and lignin. The first provides thermal insulation and the second provides mechanical resistance. At the bale scale, experiments show that the thermal conductivity varies between 0.033 W/m.K and 0.19 W/m.K based on the bale density, temperature, relative humidity, and fiber orientation. Mechanically, straw bales have a non-linear stress-strain curve at low loading levels and elastic behavior since the bale exhibit a complete recovery of deformation after removing the loads. At the wall scale, the time lag and the decrement factor of a multilayered straw envelope are found to be about 7 hours and 0.1, respectively. The sound reduction index of this type of wall is between 45-58 dB. Fire tests done on plastered straw walls reveal a resistance of 2 hours. At the building scale, many full-scale studies show that this type of construction has less embodied energy and consumes less final energy during operation than conventional buildings. Despite all of these findings, studies on energy behavior, cost analysis, and how interior air moisture is self-regulated in straw buildings are still needed at the building size. It was also found that more research is needed to improve the sound resistance of the straw wall by adding new layers capable of absorbing acoustic waves.

Experimental and numerical characterization of straw fibers and bales is carried out on straw material collected from local farms. The experimental characterization includes thermal conductivity, specific heat, sorption-desorption, and moisture buffer capacity measurement. It is discovered that straw fibers and bales have good thermal and hygric performance with an average thermal conductivity of 0.078 W/m.K, a thermal capacity of 1500 J/kg.K, and an average water vapor resistance diffusion factor of 1.58. The numerical work proposes a mathematical model for the prediction of the bale's thermal conductivity as a function of chemical composition, temperature, density, relative humidity, and fiber orientation. The effective thermal conductivity increases by 25 % when the cellulose content decreases by 10 %. The most affecting factor is the fibers' orientation.

At the wall scale, a fire resistance test is conducted on a new type of straw wall integrating a mineral foam layer at the interior side. The results show that this wall can be classified as EI 180 meaning that the sample exposed to fire on one side can prevent the temperature from rising for 180 minutes. Then, a numerical assessment of the hygrothermal performance of multi-layered straw walls with different boundary conditions is conducted using WUFI software. Results show that straw walls with cement and/or wood covering can be used in tropical and temperate climates, coated straw walls with additional air layers in dry climates, while insulated straw walls are best fitted in continental climates. In the latter, the dryness rate varies between 7 and 40 % with a low condensation risk of value in the range of 0-12 %.

At the building scale, an experimental study on a full-size straw building shows that indoor hygrothermal comfort is assured 54 % of the time, and indoor thermal comfort shows a TCI of 2 °C during summer and 6 °C during winter. The experimental work is completed by a numerical model built on EnergyPlus software to study the hygrothermal and energetic performance of the straw-based building under different climates and wall layouts. This section is followed by a sensitivity analysis to study four important factors, density, initial water content, sorption isotherm curve, and thermal conductivity vs RH. The assessment is done by calculating the sensitivity index that shows the parameter impact on the

results. The higher index is obtained for the thermal conductivity function of RH. The EP model predicted the cooling and heating demands of six different cases under four extreme weather. It is showed that straw walls are good insulators and can decrease the heating demand by more than 30 % based on the wall configuration. The straw wall composition affects slightly the heating and cooling load while the exterior condition impacted highly the energy consumption. In addition, it is noticed that wood-straw buildings are not recommended in tropical climates since it increases the cooling demand. From an environmental point of view, straw and wood reduce the net carbon emissions of the building due to the carbon sequestration effect. Buildings composed of straw-wood envelopes have net carbon emissions of -124.6 kg of CO₂ per habitable surface area. Buildings composed of straw-cement envelopes have net carbon emissions of 151.8 kg of CO₂ per habitable surface area. Buildings composed of straw-wood-cement have a net carbon emission varying between 34.6 and 61.5 kg of CO₂ per habitable surface area. From an economic point of view, straw buildings are not cost-effective in Brazil (Aw) due to the cooling cost that makes savings impossible compared to standard buildings. The walls' environmental and economic performances are considered to associate them with the appropriate climates. Thus, case 1 should be used in tropical climate (Aw), case 2 in a cold desert climate (Bwk), case 3 in mediterranean climate (Csa), and cases 4 and 5 in subarctic continental (Dfc). Regarding mechanical stability, a numerical study is carried out by using Robot structural analysis. This study shows the stability of straw structures under horizontal seismic acceleration of 1.6 m/s² and severe climate conditions.

Keywords: straw material, thermal properties, hygrothermal performance, indoor comfort, numerical model, experimental validation,

Résumé

Les matériaux biosourcés, tels que la paille, ont généralement une faible énergie intrinsèque. Ils deviennent donc une alternative prometteuse pour améliorer la performance énergétique des bâtiments et réduire leur empreinte carbone. Comparés aux matériaux de construction courants, les matériaux biosourcés permettraient un meilleur contrôle de la température intérieure et des variations d'humidité relative, améliorant ainsi le confort thermique. Bien que largement étudié, il y a encore un manque de données concernant la performance thermique, hygrique et énergétique de telles structures. L'objectif de cette thèse est d'apporter une partie des réponses à travers des travaux expérimentaux et numériques.

Une revue de la littérature analyse les travaux réalisés par la communauté des chercheurs et compare les résultats. Elle montre qu'à l'échelle de la fibre, la paille est composée de deux éléments principaux, la cellulose et la lignine. Les premiers assurent l'isolation thermique et les seconds la résistance mécanique. À l'échelle de la botte, les expériences montrent que la conductivité thermique varie entre 0.033 W/m.K et 0.19 W/m.K en fonction de la densité de la botte, de la température, de l'humidité relative et de l'orientation des fibres. Du point de vue mécanique, les bottes de paille présentent une courbe contrainte-déformation non linéaire à des niveaux de charge faibles et un comportement élastique puisque la botte présente une récupération complète de la déformation après le retrait des charges. À l'échelle du mur, le déphasage thermique et le coefficient d'amortissement d'une enveloppe de paille multicouche sont d'environ 7 heures et 0.1, respectivement. L'indice d'affaiblissement acoustique de ce type de murs se situe entre 45 et 58 dB. Les essais au feu effectués sur des murs en paille plâtrée révèlent une résistance de 2 heures. A l'échelle du bâtiment, de nombreuses études montrent que ce type de construction a une énergie grise moindre et consomme moins d'énergie finale en fonctionnement que les bâtiments conventionnels. Malgré tous ces résultats, des études sur le comportement énergétique, l'analyse des coûts et la manière dont l'humidité de l'air intérieur est autorégulée dans les bâtiments en paille sont encore nécessaires à l'échelle du bâtiment. Il a également été constaté que des recherches supplémentaires sont nécessaires pour améliorer la résistance au bruit du mur de paille en ajoutant de nouvelles couches capables d'absorber les ondes acoustiques.

Une caractérisation expérimentale et numérique des fibres et des bottes de paille est réalisée sur un matériau collecté dans des fermes locales. La caractérisation expérimentale comprend la conductivité thermique, la chaleur spécifique, la sorption-désorption et la mesure de la capacité tampon de l'humidité. On découvre que les fibres et les bottes de paille ont de bonnes performances thermiques et hygriques avec une conductivité thermique moyenne de 0.078 W/m.K, une capacité thermique de 1500 J/kg.K et un facteur de diffusion moyen de la résistance à la vapeur d'eau de 1.58. Le travail numérique propose un modèle mathématique pour la prédiction de la conductivité thermique de la botte en fonction de la composition chimique, de la température, de la densité, de l'humidité relative et de l'orientation des fibres. La conductivité thermique effective augmente de 25 % lorsque la teneur en cellulose diminue de 10 %. Le facteur qui a le plus d'influence est l'orientation des fibres.

À l'échelle du mur, un essai de résistance au feu est réalisé sur un nouveau type de mur en paille intégrant une couche de mousse minérale sur la face intérieure. Les résultats montrent que ce mur peut être classé EI 180, ce qui signifie que l'échantillon exposé au feu sur un côté peut empêcher la température d'augmenter pendant 180 minutes. Ensuite, une évaluation numérique de la performance hygrothermique de murs en paille multicouches avec différentes conditions limites est réalisée à l'aide du logiciel WUFI. Les résultats montrent que les murs de paille avec un revêtement en ciment et/ou en bois peuvent être utilisés dans les climats tropicaux et tempérés, les murs de paille enduits avec des couches d'air supplémentaires dans les climats secs, tandis que les murs de paille isolés sont mieux adaptés aux climats continentaux. Dans ces derniers, le taux de dessiccation varie entre 7 et 40 % avec un faible risque de condensation d'une valeur comprise entre 0 et 12 %.

A l'échelle du bâtiment, une étude expérimentale sur un bâtiment en paille montre que le confort hygrothermique intérieur est assuré dans 54 % des cas et que le confort thermique intérieur présente un indice de confort thermique de 2 °C en été et de 6 °C en hiver. Le travail expérimental est complété par un modèle numérique construit sur le logiciel EnergyPlus pour étudier les performances hygrothermiques et énergétiques d'un bâtiment à base de paille sous différents climats et dispositions des murs. Cette section est suivie d'une analyse de sensibilité pour étudier quatre facteurs importants, la densité, la teneur en eau initiale, les isothermes de sorption et la conductivité thermique en fonction de l'humidité relative. L'évaluation est effectuée en calculant l'indice de sensibilité qui montre l'impact du paramètre sur les résultats. L'indice le plus élevé est obtenu pour la conductivité thermique en fonction de l'HR. Le modèle EP a prédit les demandes de refroidissement et de chauffage de six cas différents sous quatre conditions météorologiques extrêmes. Il est démontré que les murs en paille sont de bons isolants et peuvent réduire la demande de chauffage de plus de 30 % en fonction de la configuration du mur. La composition des murs en paille affecte légèrement la charge de chauffage et de refroidissement, tandis que les conditions extérieures ont un impact important sur la consommation d'énergie. En outre, il est à noter que les bâtiments en bois-paille ne sont pas recommandés dans les climats tropicaux Aw car ils augmentent la demande de refroidissement. D'un point de vue environnemental, la paille et le bois réduisent les émissions nettes de carbone du bâtiment grâce à l'effet de séquestration du carbone. Les bâtiments composés d'une enveloppe en paille et bois ont une émission nette de carbone de -124.6 kg de CO₂ par surface habitable. Les bâtiments composés d'une enveloppe en paille et ciment ont des émissions nettes de carbone de 151.8 kg de CO₂ par surface habitable. Les bâtiments composés de paille-bois-ciment ont des émissions nettes de carbone variant entre 34.6 et 61.5 kg de CO₂ par surface habitable. D'un point de vue économique, les bâtiments en paille ne sont pas rentables au Brésil (Aw) en raison du coût du refroidissement qui rend impossible toute économie par rapport aux bâtiments standard. Les performances environnementales et économiques des murs sont analysées pour les associer aux climats appropriés. Ainsi, le cas 1 devrait être utilisé en climat tropical (Aw), le cas 2 en climat de désert froid (Bwk), le cas 3 en climat méditerranéen (Csa) et les cas 4 et 5 en continental subarctique (Dfc). En ce qui concerne la stabilité mécanique, une étude numérique est réalisée en utilisant l'analyse structurelle Robot. Cette étude montre la stabilité des structures en paille sous une accélération sismique horizontale de 1.6 m/s² et dans des conditions climatiques sévères.

Mots clés : matériau paille, propriétés thermiques, performances hygrothermiques, confort intérieur, modèle numérique, validation expérimentale,

Acknowledgments

My first thanks go to my project directors, Prof. Pascal Biwole, Dr. Fabienne Pennec and Dr. Salah Ouldboukhitine. First and foremost, thank you for providing me with the opportunity to complete this thesis on such an interesting topic and in such a pleasant work environment. I want to thank you for believing in me throughout this process and for teaching me so much on both intellectual and professional levels. I'd like to emphasize your human qualities and your unbreakable supervision, which have contributed to the success of this project.

I would like to thank the members of the jury for taking the time to read my work. Especially the reviewers, Prof. Steve Goodhew and Prof. Rafik Belarbi, who had the difficult task of carefully reading the lengthy manuscript and providing constructive feedback. I also want to thank the other members of the jury, Prof. Jean-Philippe Costes, Prof. Hasna Louhalia-Gualous, and Dr. Florence Collet, for their insightful comments, advice, and direct or indirect contributions to my thesis work.

My deepest thanks go to Clermont Auvergne University, Ecole doctorale Science Pour Ingénieur, and Institute Pascal. Their financial support is greatly appreciated.

Thank you to everyone at the Institute Pascal and IUT Clermont Auvergne at Montluçon who helped me with my research. I'd like to thank Myriam, Stephane, and Gael for our scientific discussions and your assistance with the test's instrumentation and data collection throughout this thesis.

I'd like to thank my doctoral colleagues for inspiring me to get up every morning (but not before 9 a.m.) and come to work.

One final thought goes to my family, who has always supported me and has always been there for me, in good and bad times. They gave me everything possible to enable me to reach higher education levels. I only hope that they know how their love, support, and patience encouraged me to fulfill my and their dream...

Nomenclature

a	Extinction coefficient	(-)
A	Surface area	(m ²)
ASH	ASHRAE standard	(-)
AR	Aspect Ratio	(-)
ASTM	American Society for Testing and Materials	(-)
C_n	Fibers' orientation distribution	(%)
C	Volumetric heat capacity	(J/m ³ .K)
C_g	Natural gas cost	(\$/kWh)
C_e	Electricity cost	(\$/kWh)
CE	Carbon emissions	(kg of CO ₂)
CNC	Carbon neutral coefficient	(-)
C_p	Thermal capacity	(J/kg.K)
CR	Condensation risk	(-)
COP	Coefficient of performance	(-)
D_ϕ	Liquid conduction coefficient	(kg/(m.s))
Diff	Thermal diffusivity	(m ² /s)
D	Mean pore diameter	(m)
d_g	Diameter of the gas molecules	(m)
DR	Dryness rate	(%)
DVS	Dynamic Vapor Sorption	
DSC	Differential scanning calorimetry	
DL	Dead load	(N)
EAD	Equivalent Area Diameter	(m)
EN	European Norm/standard	
EU	European Union	
e	Thickness	(mm)
E	Modulus of elasticity	(kPa)
EC	Energy cost	(\$)
Eff	Thermal effusivity	(J/K.m ² .s ^{1/2})
EP	Energyplus	
ESC	Energy annual saving cost	(\$)
F	Load	(kN)
f	Decrement factor	(-)
$f_{cellulose}$	Content of cellulose	(%)
FEM	Finite element method	
g	Gravitational acceleration	(m/s ²)
GWP	Global Warming Potential	(kg CO ₂ equivalent)
G	Global vertical radiation	(W/m ²)
g_v	Water vapor flux density	(kg/m ² .s)
H	Total volume enthalpy	(J/m ³)
h	Heat transfer coefficient	(-)
h_v	Evaporation enthalpy of water	(J/kg)
h_{net}	Net heat flux	(W/m ²)
\dot{h}_c	Convection heat flux	(W/m ²)
\dot{h}_r	Radiative heat flux	(W/m ²)
ICP-MS	Inductively Coupled Plasma Mass Spectroscopy	
IC	Initial cost	(\$)
IEEP	Institute of European Environmental Policy	
IL	Imposed load	(N)
l	Fibers' length	(m)
l_f	Means free path of the air molecules	(m)

L	Sample height	(mm)
LCA	Life cycle assessment	
LCC	Life cycle cost	
m_i	Weight	(g)
M_{in}	Internal moisture gain	(g/m ³)
M_{HVAC}	Moisture gain or loss due to HVAC	(g/m ³)
MS	Dry matter	(%)
MC	Moisture content	(%)
MG	Mold growth	(-)
MBV	Moisture Buffering Value	(g/(m ² .%RH))
n	Refraction index	(-)
N	Number of fiber possible orientations	(-)
N_l	Lifetime	
Nu	Nusselt number	(-)
P	Pressure	(Pa)
Pr	Prandtl number	(-)
P_s	Static pressure	(Pa)
P_0	Atmospheric pressure	(Pa)
$P1, P2$	Gas pressure before and after the equilibrium state	(Pa)
PEI	Primary Energy Intensity	(J)
P_{sat}	Saturation pressure	(Pa)
P_{sv}	Saturated water vapor pressure	(Pa)
PWF	Present worth factor	(-)
Q	Specific heat output	(J/kg.K)
q	Sensible heat flux density	(W/m ²)
Q_h	Annual heating load	(kWh/year)
Q_c	Annual cooling load	(kWh/year)
r	Distance between the thermocouple and the heat source	(m)
r_d	Discount rate	
R	Specific gas constant of water vapor	46.15 J/kg.K
Ra	Rayleigh number	(-)
RH	Relative humidity	(%)
$RMSE$	Root mean square error	(W/m.K)
RFCP	French association "Réseau français de la Construction Paille"	
R_f	Roughness surface factor	(-)
R_{rain}	Mass flow rate of rain water	(kg/s)
R_w	The Weighted Sound Reduction Index	(dB)
SEM	Scanning Electron Microscope	
SI	Scatter index	(%)
S	Weight of moisture-free cellulose sample	(g)
s	Material layer thickness	(m)
S_{acc}	Accidental snow load	(N)
sd	Vapor diffusion thickness	(m)
SL	Snow load	(N)
t	Time	(second)
T	Temperature	(K) (°C)
TCI	Thermal comfort index	(-)
TCP	Total carbon emissions due to materials production	(kg of CO ₂)
T_g	Air temperature inside the furnace	(°C)
T_m	Surface temperature of the material	(°C)
T_r	Radiation temperature inside the furnace	(°C)
THW	Transient hot wire method	
TWC	Total water content	(kg/m ³)

TAPPI	Technical Association of the Pulp and Paper Industry	
U	Heat transfer coefficient	(W/m ² .K)
V _g	Gas volume	(m ³)
V _s	Sample volume	(m ³)
V _z	Wind speed	(m/s)
VOC	Volatile Organics Compounds	(%)
v	Vapor content	
w	Moisture content	(%) or (kg/m ³)
Wash	Weight of ash	(g)
W _{cellulose}	Weight of cellulose	(g)
W _i	Sound power	(W)
W _{lignin}	Weight of lignin	(g)
W _{SE}	Weight of solvent extractive	(g)
W _{α-cellulose}	Weight of α-cellulose	(g)
WL	Wind load	(N)
x	Insulation thickness variable	(cm)
2-D	Two dimensional	

Greek letters

α	Thermal diffusivity	(m ² /s)
α _c	Coefficient of convection	(-)
α _s	Coefficient of solar absorptance	(-)
α _l	Coefficient of liquid absorptance	(-)
β	Thermal expansion coefficient	(1/K)
θ _n	Angle of orientation	(°)
k	Thermal conductivity	(W/(m.K))
k _B	Boltzmann constant	k _B = 1.38×10 ⁻²³ (kg.m ²)/(s ³ .K ⁴)
k _{cellulose}	Thermal conductivity of cellulose	(W/m.K)
k _{lignin}	Thermal conductivity of lignin	(W/m.K)
ν	Kinematic viscosity	(m ² /s)
ξ	Accommodation coefficient	(-)
Π	Volume fraction	(-)
ρ	Density	(kg/m ³)
σ	Stephan-Boltzmann constant	σ = 5.670374 e-08 W/(m ² K ⁴)
φ	Heat flux density	(W/m ²)
φ and φ	Relative humidity	(%)
φ	Time lag	(hour)
φ _r	View factor	(-)
λ	Thermal conductivity	(W/(m.K))
δ _p	Water vapor permeability	(kg/(m.s.Pa))
μ	Water vapor diffusion resistance factor	(-)
δ	Water vapor diffusion coefficient in air	(kg/ms.Pa)
ε	Strain	(%)
ε _m	Thermal emissivity of the material	(-)
ε _f	Thermal emissivity of the fire	(-)
ΔL	Elongation	(mm)
Δm	Weight variation	(kg)
ΔRH	Relative humidity variation	(%)
Δt	Time between two successive weightings	(s)
ΔP	Pressure variation	(Pa)

γ	Surface tilt angle	(°)
η	Heating system efficiency	(-)
σ	Stress	(kPa)

Subscripts

B	Brasilia-Brazil
<i>c</i>	Conductive
C	Xinjiang-China
comf	Comfort
<i>eff</i>	Effective
ext and e	Exterior
<i>f</i>	Fiber
F	Nice-France
<i>g</i>	Gas
int and i	Interior
max	Maximum
min	Minimum
op	Operative
out	Outdoor
<i>p</i>	Pores
<i>par</i>	Parallel
<i>r</i>	Radiative
R	Arkhangelsk-Russia
<i>s</i>	Solid
<i>se</i>	Exterior surface
<i>Ser</i>	Series
<i>si</i>	Interior surface

Table of contents

Abstract	i
Résumé	iii
Acknowledgments	v
Nomenclature	vi
Greek letters	viii
Subscripts	ix
Table of contents	x
Tables of figures	xiii
Table of tables	xviii
General introduction	1
First part: Literature Review	5
1. Straw fiber scale	5
1.1. Anatomy and microscopic characteristics	6
1.2. Chemical composition and physicochemical properties	7
1.3. Sorption-desorption isotherms.....	9
1.4. Discussion and perspectives	11
2. Straw bale scale	12
2.1. Density and porosity.....	13
2.2. Thermal properties.....	14
2.3. Water vapor diffusion factor and thickness	20
2.4. Mechanical properties	20
2.5. Discussion and perspectives	23
3. Straw wall scale.....	24
3.1. Hygrothermal properties.....	25
3.2. Acoustic performance.....	27
3.3. Fire resistance.....	29
3.4. Economic and environmental performance	31
3.5. Straw embedded in composite construction materials	33
3.6. Discussion and perspectives	34
4. Straw building scale	35
4.1. Construction systems.....	36
4.2. Regulations on straw construction.....	38
4.3. Energy and life cycle assessment of straw buildings	39
4.4. Discussion and perspectives	41

5.	Thesis positioning.....	42
5.1.	Bibliographic study synthesis.....	43
5.2.	Thesis objectives	45
5.3.	Thesis methodology.....	46
Second part: Straw fibers and bales characterization		39
6.	Experimental study.....	47
6.1.	Straw preparation.....	48
6.2.	Experimental methods	50
6.3.	Experimental results	63
7.	Thermal conductivity numerical model.....	77
7.1.	Model description.....	78
7.2.	Validation of the model	84
7.3.	Parametric study	86
Third part: Straw wall Characterization		91
8.	Fire resistance test	92
8.1.	Experimental work	93
8.2.	Experimental results	97
8.3.	Numerical model	99
8.4.	Numerical results validation.....	102
8.5.	Proposed solution	103
9.	Hygrothermal numerical study	104
9.1.	Numerical modeling approach	105
9.2.	Model validation.....	106
9.3.	Case study.....	112
9.4.	Hygrothermal criteria	116
9.5.	Results and discussion.....	117
9.6.	Proposed Solutions	123
Fourth part: Building characterization.....		127
10.	Experimental straw building's thermal performance	128
10.1.	Experimental setup	129
10.2.	Methodology and assessment criteria.....	132
10.3.	Experimental results	133
11.	Numerical study of thermal and energetic performance of straw buildings.....	139
11.1.	General description of EnergyPlus	140
11.2.	Model description and validation	141
11.3.	Sensitivity analysis	145
11.4.	Case study description.....	148

11.5.	Numerical results.....	149
12.	Environmental and economic study	154
12.1.	Previous studies.....	155
12.2.	Environmental assessment.....	155
12.3.	Economic assessment	158
13.	Straw building’s mechanical performance	163
13.1.	Case study description.....	164
13.2.	Numerical model of the structure	164
13.3.	Results	171
	General conclusion and perspectives.....	173
	Reference.....	179
	French version : Résumé détaillé	196
	Appendices	214
	Appendix A1: Isolation method	215
	Appendix A2: Mechanical properties of Glued Laminated Timber GL24h and Steel S 235.....	216
	Appendix A3: Staple dimensioning based on Eurocode 5	217
	Appendix A4: French regions location category	218
	Appendix A5: Wind load calculation in France	219
	Appendix A6: List of publications	222

Tables of figures

Figure 0.1: Experimental and numerical articles on straw bale construction between the years 1990 and 2020.....	3
Figure 0.2: Number of articles done worldwide between the years 1990-2020.....	3
Figure 1.1: SEM analysis images of the surface of wheat straw (a), (d), and (e), barley straw (b) and (f), and rice straw (c) at low and high magnification factors (based on [24–27])	6
Figure 1.2: Diagram showing the different steps of the isolation method [32].....	8
Figure 1.3: Sorption and desorption isotherm of wheat and rice straw [36]	10
Figure 1.4: Comparison of wheat and barley sorption and desorption curves [25].....	10
Figure 2.1:Variation of the thermal conductivity with respect to the density of vertical and horizontal oriented fibers (based on data from [47])	14
Figure 2.2: Thermal conductivity data for wheat and barley straw as a function of temperature and density (based on [28,43,49])	15
Figure 2.3: Thermal conductivity for different orientations with respect to (a) temperature, (b) RH, and (c) density [48]	16
Figure 2.4: Vertical and horizontal strain variation (VS and HS) according to the applied load for bales oriented horizontally and vertically (HO and VO) (A the first loading path and B the second loading path) (based on [14,71])	21
Figure 2.5: Variation of the deformation modulus of bales oriented horizontally and vertically [14]..	22
Figure 2.6: Stress-strain behavior for bales oriented horizontally and vertically [14]	23
Figure 3.1: Variation of straw temperature (dotted line) and outside temperature (black line) as a function of time [14].....	25
Figure 3.2: Relative humidity in different locations in the straw bale wall [14].....	25
Figure 3.3: Variation of the relative humidity while varying the temperature at a different location in the wall between 2009 and 2012 with respect to the Fraunhofer Institute isopleth limits (FIB-Mold expected growth) [76].....	26
Figure 3.4: Sound absorption coefficient and sound reduction index of straw and stone (based on [60,82]).....	28
Figure 3.5: Sound reduction index of a 50 cm thick straw wall according to the ISO 717-1 [60].....	29
Figure 3.6: Temperature-time curve of the ASTM E-119, the furnace, and the unexposed surface of the straw bale wall (based on [85])	30
Figure 4.1: Load-bearing wall and roof plate construction [104].....	36
Figure 4.2: Infill wall and structure section [104].....	37
Figure 4.3: Steps of the GREB technique [3].....	37
Figure 4.4: Main parts of a prefabricated straw wall [84]	38
Figure 5.1: Diagram showing the different applications of straw	44
Figure 6.1: High-density rectangular balers model « BigBaler » from « New-Holland » and the concept of the compression chamber [119,120]	48
Figure 6.2: High-density round baler from John Deere 900 [119].....	48
Figure 6.3: Schematic presentation of the straw mold of 40 cm width, 40 cm length, and a variable height from 20 to 60 cm that gives a variable density from 80 kg/m ³ to 120 kg/m ³	49
Figure 6.4: Different types of samples used in the experiments. Samples I and II are fibers, and III, IV, and V are bales with different dimensions and densities.....	50
Figure 6.5: Digital microscope Keyence VHX 6000	51
Figure 6.6: Principle of an optical microscope where the tested object is placed at AB, the actual image through the objective lens is seen at A'B', the image observed through the ocular lens is seen at A''B'' [122]	51
Figure 6.7: Process followed to obtain a digital microscopic image	52
Figure 6.8: Schematic representation of the Van Soest method.....	53

Figure 6.9: Sorption isotherm classification given by IUPAC	54
Figure 6.10: Climatic chamber, RH digital sensor, and Digital scale used for sorption isotherm test..	55
Figure 6.11: Schematic representation of the volumetric method for determining equilibrium gas-solid adsorption/desorption isotherms.....	56
Figure 6.12: RH variations versus time at a constant ambient temperature	57
Figure 6.13: Neotim FP2C conductivity meter with the needle probe.....	59
Figure 6.14: Schematic representations of the Calvet-type calorimeter based on [139]	61
Figure 6.15: Calvet cryo calorimeter.....	61
Figure 6.16: Sensor distribution in the tested type IV straw bale.....	62
Figure 6.17: Temperature and relative humidity variations in the climatic chamber (1, 2, 3, and 4 refer to the first, second, third, and fourth scenarios, respectively)	63
Figure 6.18: A wheat stalk with its different parts	64
Figure 6.19: Transversal cross-section of an internode wheat straw by using Keyence® digital microscope	65
Figure 6.20: Longitudinal cross-section of an internode wheat straw by using Keyence® digital microscope	66
Figure 6.21: Sorption desorption curves of three samples of straw fibers tested by the volumetric method	67
Figure 6.22: Comparison of the straw bale and fiber average sorption curves to the numerical model of Merakeb applied to straw, average sorption curve of wood [148], and average sorption curve of glass wool [149]	68
Figure 6.23: Relative humidity and weight of straw bale Type III (sample 1) variations during three cycles proposed by Nordtest.....	69
Figure 6.24: Average moisture buffer value variation according to the number of cycles and the different tested samples.....	69
Figure 6.25: Water vapor permeability and diffusion resistance factor values of five straw samples of type III.....	70
Figure 6.26: Thermal conductivity variation versus temperature and relative humidity for wheat straw bales having perpendicular fibers and density (a) 80 kg/m ³ , (b) 100 kg/m ³ , and (c) 120 kg/m ³	71
Figure 6.27: Thermal conductivity variations versus temperature and relative humidity for wheat straw bales having parallel fibers and density (a) 80 kg/m ³ , (b) 100 kg/m ³ , and (c) 120 kg/m ³	72
Figure 6.28: Specific heat variation of straw fibers using the DSC Calvet type	73
Figure 6.29: RH variations inside the climatic chamber, at the exposed surface, and inside the bale ..	73
Figure 6.30: RH variations inside the climatic chamber, at the exposed surface, and inside the bale ..	74
Figure 6.31: RH variations in the climatic chamber, inside the bale, and at the surface of the bale versus time	75
Figure 6.32: Temperature variations in the climatic chamber, inside the bale, and at the surface of the bale versus time	76
Figure 7.1: Schematic representation of the heat path in uncompressed and compressed straw fibers	81
Figure 7.2: Schematic structure of straw bales having randomly oriented fibers.	82
Figure 7.3: Gaussian normal laws of straw fibers' orientation distribution in a bale [43]	82
Figure 7.4: Representative volume element of a straw bale and its thermal electrical analogy model .	83
Figure 7.5: Comparison of the numerical and experimental thermal conductivity for bales having densities from 80 kg/m ³ to 120 kg/m ³ and temperature from 15 °C to 55 °C, at 25 % RH	85
Figure 7.6: Numerical and experimental thermal conductivity variation versus RH for bales having density (a) 80 kg/m ³ , (b) 100 kg/m ³ and (c) 120 kg/m ³ , at 15 and 45 °C	86
Figure 7.7: Solid, gas, radiation, and effective thermal conductivities versus density for two types of straw composed of 38 % and 48 % of cellulose	87
Figure 7.8: Solid, gas, radiation, and effective thermal conductivities versus temperature for a straw bale of RH 10 % and density 120 kg/m ³	88

Figure 7.9: Solid, gas, radiation, and effective thermal conductivities versus RH for a straw bale of temperature 20 °C and density 120 kg/m ³	89
Figure 7.10: Solid, gas, and effective thermal conductivities versus RH for a straw bale at a temperature of 25 °C and density of 100 kg/m ³ with fibers mostly perpendicular ($\mu=90^\circ$, $\sigma=45^\circ$) and mostly parallel ($\mu=180^\circ$, $\sigma=45^\circ$) to the heat flux.	90
Figure 8.1: Side view of the sample showing its composition	94
Figure 8.2: Sample preparation steps and the thermocouple placement inside and on the surfaces of the wall	94
Figure 8.3: (a) furnace 1 m wide, 1 m deep, and 2 m high used for the experiment with two burners, (b) section sketch of furnace setup showing the flame and thermometer locations, and the smoke and heat path	95
Figure 8.4: Temperature variation inside the furnace compared with ISO-834 curve	96
Figure 8.5: Installation of a straw wall. Insulation material is added at the edges between the wall and the furnace before starting the experiment	96
Figure 8.6: Smoking indications on edges of the exposed face of the wall.....	97
Figure 8.7: Transient temperature variation during the experiment at different locations in the wall ..	98
Figure 8.8: Post-fire sample aspect showing a hole in the fermacell that caused the straw to burn.....	99
Figure 8.9: Thermal conductivity, specific heat capacity, and density variations with respect to the temperature of straw, fermacell, mineral foam, and wood.....	101
Figure 8.10: Boundary conditions at the interior and exterior sides of the test wall	102
Figure 8.11: Comparison of the experimental (noted by test) and numerical (noted by SI) results at locations 2, 5, 6, 7, and 8.....	102
Figure 8.12: Comparison of the numerical results for the wall with (noted by GAP) and without (noted by FULL) fire seal paste.....	103
Figure 9.1: Location of thermocouples and humidity probes in the straw wall [15].....	106
Figure 9.2: Monthly average outdoor temperature and relative humidity in the Picardy region	107
Figure 9.3: The variation of the inner and outer surfaces' temperature and RH [15]	108
Figure 9.4: Straw material's hygrothermal functions showing the variation of thermal conductivity vs temperature (a), thermal conductivity vs relative humidity (b), and moisture content vs relative humidity (c) (based on [15,36,43,48])	109
Figure 9.5: Comparison of the experimental and simulated weekly average temperature variations over one year for wall surfaces under Picardie weather conditions	110
Figure 9.6: Comparison of the experimental and simulated weekly average RH variations over one year for wall surfaces under Picardie weather conditions	110
Figure 9.7: Variation of the interior and exterior surface temperature for the numerical model (WUFI) and the experiment [15] for 24 hours on 25 April 2010.....	111
Figure 9.8: Monthly average outdoor temperature and relative humidity in Brasilia-Brazil, Xinjiang-China, Nice-France, and Arkhangelsk-Russia over one year.....	115
Figure 9.9: Annual variation of the indoor dry air temperature (a) and the indoor air relative humidity (b)	116
Figure 9.10: Day-averaged total water content variation for cases three, four, and five over four years under R-the Arkhangelsk-Russia weather and B- the Brasilia-Brazil weather	118
Figure 9.11: Dryness rate of all cases in all climate conditions for four years.....	119
Figure 9.12: Time percentage where the condensation might occur for all cases over four years.....	120
Figure 9.13: Isopleth for case 4 (left) and case 5 (right) tested with Arkhangelsk-Russia climate condition	121
Figure 9.14: Relative humidity distribution inside the wall (3-R) through all the layers during 100 days in winter.....	122
Figure 9.15: Daily total water content of case 3 (3-R/360) with a straw thickness of about 36 cm and case 5 (5-R) under high indoor relative humidity in Arkhangelsk-Russia for four years	123

Figure 9.16: Isoleth for case 4 with vapor retarder layer (left) and with high straw thickness layer (right) tested with Arkhangelsk-Russia climate condition	124
Figure 9.17: The isopleth for case 1-R with ventilated rain screen and lime layer	125
Figure 10.1: Experimental straw building located in Reugny, France	129
Figure 10.2: Composition of the straw wall used in the experimental building.....	129
Figure 10.3: Weather station installation at six meters away from the experimental building	130
Figure 10.4: Motion sensor, T and RH sensors installed in the walls	131
Figure 10.5: Drawing plan of the building with the location of the sensors (red and blue)	131
Figure 10.6: Fauconnier’s model showing the hygrothermal comfort zone based on the temperature and RH combination	133
Figure 10.7: Comparison of the daily outdoor air (weather station) and indoor (on the second floor) temperature and relative humidity.....	134
Figure 10.8: RH and temperature daily variation of the internal and external surfaces of the north and south facing walls on the second floor of the test building	135
Figure 10.9: Comparison between the operative temperature of the first floor (F1), the second floor (F2), the CIBSE and ASHRAE maximum and minimum acceptable temperature over one year from August 1 to July 31	136
Figure 10.10: Indoor RH variations at the first (F1) and second floors (F2) with reference to the maximum and minimum RH recommended by ASHRAE 55 over one year from August 2020 to July 2021	137
Figure 10.11: <i>Top</i> and RH values of the indoor air of the first and second floors with respect to the hygrothermal comfort zone defined by Fauconnier’s model.....	138
Figure 11.1: Daily outdoor air temperature (T _{out}) and relative humidity (RH out) at Reugny obtained for one year from August 1 to July 31	142
Figure 11.2: Test building geometry using Sketchup and EnergyPlus plugins.....	142
Figure 11.3: Comparison of numerical and experimental findings for the south internal surface temperature and the relative humidity on the second floor from August 1 to July 31	144
Figure 11.4: Comparison of the numerical and experimental findings for the indoor air temperature and the relative humidity on the second floor from August 1 to July 31	144
Figure 11.5: First order sensitivity index of the four variable inputs on the indoor air temperature and relative humidity.....	146
Figure 11.6: Monthly average indoor air temperature and relative humidity variations by varying the density (1, 2, and 3 are the case number)	147
Figure 11.7: Monthly average indoor air temperature and relative humidity variations by varying the moisture content (4, 5, and 6 are the case number)	147
Figure 11.8: Monthly average indoor air temperature and relative humidity variations by varying the sorption isotherms curve (7, 8, and 9 are the case number)	147
Figure 11.9: Monthly average indoor air temperature and relative humidity variations by varying the thermal conductivity dependent RH curve (10, 11, and 12 are the case number).....	148
Figure 11.10: Equipment, occupants, and light schedule during 24 hours.....	148
Figure 11.11: Comparison of the indoor operative temperature of cases 1 (Top-1), 2 (Top-2), 3 (Top-3), 4 (Top-4), 5 (Top-5), and ASHRAE maximum and minimum limits under the Brazilian climate over one year from January 1 to December 31.....	149
Figure 11.12: Comparison of the indoor operative temperature of cases 1 (Top-1), 2 (Top-2), 3 (Top-3), 4 (Top-4), 5 (Top-5), and ASHRAE maximum and minimum limits under the Chinese climate over one year from January 1 to December 31	149
Figure 11.13: Comparison of the indoor operative temperature of cases 1 (Top-1), 2 (Top-2), 3 (Top-3), 4 (Top-4), 5 (Top-5), and ASHRAE maximum and minimum limits under the French climate over one year from January 1 to December 31	150

Figure 11.14: Comparison of the indoor operative temperature of cases 1 (Top-1), 2 (Top-2), 3 (Top-3), 4 (Top-4), 5 (Top-5), and ASHRAE maximum and minimum limits under the Russian climate over one year from January 1 to December 31	150
Figure 11.15: Hygrothermal indoor comfort of the six cases under Brasilia, Xinjiang, Nice, and Arkhangelsk weather	151
Figure 11.16: Simulation results of the annual heating and cooling energy consumption for all cases based on the weather and the wall composition	152
Figure 12.1: Heating and cooling annual CO ₂ emissions of the studied cases	157
Figure 12.2: Total energy cost of the different cases	160
Figure 12.3: Initial cost of the studied cases	161
Figure 12.4: Life cycle cost of the studied cases	161
Figure 13.1: Straw-wood building modeled in RSA (Robot Structural Analysis) software	165
Figure 13.2: I- section steel beams (left) and angle steel (right) profiles	165
Figure 13.3: Honeycomb with stiffener panel dimension annotation	166
Figure 13.4: Staples dimension annotation [265]	166
Figure 13.5: Surface and linear dead loads applied to the whole structure	167
Figure 13.6: Imposed loads applied to the living spaces	168
Figure 13.7: Snow load applied to the roof	168
Figure 13.8: Wind loads applied to the building	169
Figure 13.9: French seismic zonation map [268]	170
Figure 13.10: Mesh of the panels	171
Figure 13.11: Panels stresses map based on Von Mises criterion for Comb 1 (left) and Comb 3 (Right)	172
Figure 13.12: Recommended type 1 elastic spectrum response applicable for ground from type A ..	172
Figure A4. 1: France map showing the location categories based on the snow charge [270]	218
Figure A5. 1: France map showing the location categories based on the wind speed [271]	219
Figure A5. 2: Pressure coefficient based on the zone of the building [271]	221

Table of tables

Table 1.1: Dimensions of barley fibers [24].....	6
Table 1.2: Chemical composition of the cereal straw [31].....	7
Table 1.3: Organic substance components of wheat, barley, and triticale straw using standard isolation [32]	8
Table 1.4: Macro and microelements composition of Wheat, Barley, and Triticale straw [32])	8
Table 1.5: Phosphate, potash, magnesium, and Sulphur in a different kind of straw [34]	9
Table 2.1: Typical bale size versus density and weight [34].....	13
Table 2.2: Average hygrothermal parameters of the straw compared to other construction materials (based on [45,46]).....	14
Table 2.3: Different propositions of thermal conductivity correlations (with ρ the density, t the thickness, T the temperature, and RH the relative humidity).....	17
Table 2.4: Bale thermal conductivity according to density and fiber orientation (cases that do not have a distinct direction might be thought of as a combination of horizontal and vertical fiber orientation.)	18
Table 2.5: Straw bale load-deformation characteristics (based on [71]).....	21
Table 3.1: Different wall material comparisons [93]	31
Table 3.2: Calculation of straw bale and brick wall costs per m ² [95]	32
Table 3.3: Price and environmental impact of different types of the wall [97].....	32
Table 4.1: Different countries' regulations concerning straw bale construction (based on [108])	39
Table 4.2: Materials used in the Straw Bale Cabin and its embodied energy classification [65].....	40
Table 4.3: Advantages and disadvantages of the load bearing, infill, and prefabricated methods (based on [80]).....	41
Table 5.1: Properties of different construction materials	45
Table 6.1: Content of wheat straw's components obtained by the Van Soest method.....	66
Table 9.1: Straw buildings materials' basic properties extracted from WUFI materials database and literature at 20 °C and 20 % RH.....	107
Table 9.2: Straw buildings materials' basic properties extracted from WUFI materials database and literature at 20 °C and 20 % RH.....	112
Table 9.3: Different layers composition of five considered cases.....	113
Table 9.4: Köppen–Geiger Climate classification for the four chosen cities	114
Table 9.5: c and h values used in equation (9.8) and equation (9.9) for each country	116
Table 9.6: Computed results from the straw walls cases regarding the ASHRAE standard (ASH) ...	122
Table 9.7: Computed results from the straw walls cases regarding time lag and decrement factor....	123
Table 11.1: Materials hygric and thermo-physical properties at 20°C.....	143
Table 11.2: Studied inputs values (No. 2, 6, 8, and 11 present the experimental case)	145
Table 12.1: CO ₂ emission factor of the used construction materials, electricity, and natural gas	156
Table 12.2: Results showing the total CO ₂ emission due to the materials production process, the carbon neutral coefficient, and the net carbon emissions of the building	156
Table 12.3: Gas price, electricity price, discount rate, and present worth factor in four countries	158
Table 12.4: Materials average price	158
Table 12.5: Materials total price of the studied cases.....	159
Table 12.6: Payback period of straw buildings	162
Table 13.1: Eurocode 1 load categories for different areas [266]	167
Table 13.2: Eurocode 8 requirements for different building types to resist the horizontal acceleration	170
Table A2.1: Mechanical properties of GL24h and S235.....	216
Table A3.1: Dimension of two staples used in the assembling step.....	217

Table A3.2: Dimensions of the two staples in the assembling step.....	217
Table A4.1: Snow charge in the different location categories [270].....	218
Table A5.1: Roughness length and minimum height of a building based on its land category.....	219
Table A5.2: Calculation of the wind intensity [271].....	220
Table A5.3: Calculation of the pressure coefficient [271].....	221

General introduction

Thesis context:

The modern world's rapid development requires an ever-increasing demand for energy, raising serious concerns about the extraction and distribution of fossil energy resources, with serious environmental consequences. Environmental awareness has paved the way for a low-carbon economy and a new green growth model. Accelerating Europe's transition to a low-carbon economy is both a huge opportunity and an urgent necessity. Through its energy policies and international actions, the European Union is well positioned to successfully lead this transition. The European Commission has adopted new measures "Clean Energy for All Europeans" in response to COP21 directives, intending to reduce CO₂ emissions by 40% by 2030 starting from 1990. The goal for European countries is to position themselves as global leaders in energy transition, not just to implement directives. To successfully meet this challenge, the emphasis is on energy efficiency and the development of renewable energy sources.

The construction industry is a major driver of the energy transition because it has the greatest untapped potential for energy savings. This sector is also a key area in the fight against global warming. It is responsible for 40 % of final energy consumption, 36 % of greenhouse gas emissions, and 120 million tons of CO₂ each year in Europe [1]. The European real estate market is an investment opportunity, not only because the construction industry is the most energy-intensive, but also because 75 % of European buildings are inefficient in terms of energy use.

In France, to make the building sector more energy-efficient and reduce its carbon footprint, strict energy consumption standards are applied for new buildings. These criteria propose the use of low embodied energy and bio-based products with the implementation of the RE2020 environmental regulation on January 1, 2022, to replace RT2012 [2]. Wheat, rice, oat, and barley straw are examples of bio-based materials that are able to offset CO₂ emissions. The agriculture waste product is a renewable material from local agricultural activities that are considered carbon-neutral [3].

Despite its numerous uses, cereal straw is produced and available in large amounts that are sufficient to produce compressed straw bales. The world produces about 2000 million tons of different straw types per year. In the EU, several studies have evaluated the ability of straws to save energy [4]. A study done by the Institute of European Environmental Policy shows that 110 million tons per year of dry straw were produced in 27 member states [5]. For example, France is an agricultural country with about 32 million hectares of useful agricultural area out of the 55 million hectares of the country [6]. Regarding cereal production, about 9 million hectares are devoted to it, which allows France to produce 50 to 70 million tons of grain per year where the majority of these grains being wheat. It is estimated that 10% of the straw produced each year would be enough to insulate all the housing built during a year [7–9]. Today, the agriculture field in France is processing approximately 20 million tons of wheat straw, which can supply around 5000 straw bale buildings. There are about 500 new straw buildings each year which is constantly increasing [10]. Therefore, if 1% of new buildings were made of straw, it would require 1% of straw production, which is well below the differences in production that may be due to climate or other conditions [11].

Primitive straw houses were built on the African plains since the Paleolithic Era, 3.3 million years ago and the revival of these constructions began more than 100 years ago. The first construction was located in Nebraska (USA) in 1886, because of the lack of wood and other building materials at that time [10]. In France, this mode of construction first appeared in 1920. The interest in this type of construction decreased by the end of the 20th century because of industrialization of the building construction and the growing interest in new materials. Note that straw, as a structural or insulating material, concerns the construction of buildings of all sizes: from single-family homes to multi-store buildings, industrial sheds to public buildings. For example, Walker *et al.* [12], Mesa and Arengi [13], Ashour *et al.* [14], and Douzane *et al.* [15] studied the mechanical and hygrothermal properties of different types of straw constructions. In addition, straw can be added to conventional materials to enhance their mechanical and

thermal properties. Amin *et al.* [16], Agwa *et al.* [17], Saad *et al.* [18], and Heniegal *et al.* [19] studied the effects of the nano cotton stalk, palm leaf ashes, straw, banana, and palm leaf on the concrete.

Since the development of these structures, numerous studies have been conducted which reflect the importance of straw construction. Based on Google Scholar statistics, the number of articles containing straw as a construction material in their titles and abstracts is increasing. **Figure 0.1** shows the trend of publications about straw bale construction from 1990 until 2020. It can be noted that the majority of papers are experimental concerning thermal, mechanical, and hygrothermal properties. Of all the noted articles, about 70% have been carried out by university laboratories, and the rest have been done in collaboration between companies and universities. **Figure 0.2** presents the distribution of articles over the world. This statistic shows that about 50% of the total published articles worldwide on straw bale construction come from France, the UK, Italy, and the USA. Since the authors of some articles come from different countries, the total number of studies in **Figure 0.1** and **Figure 0.2** is greater than the total number of articles collected and cited.

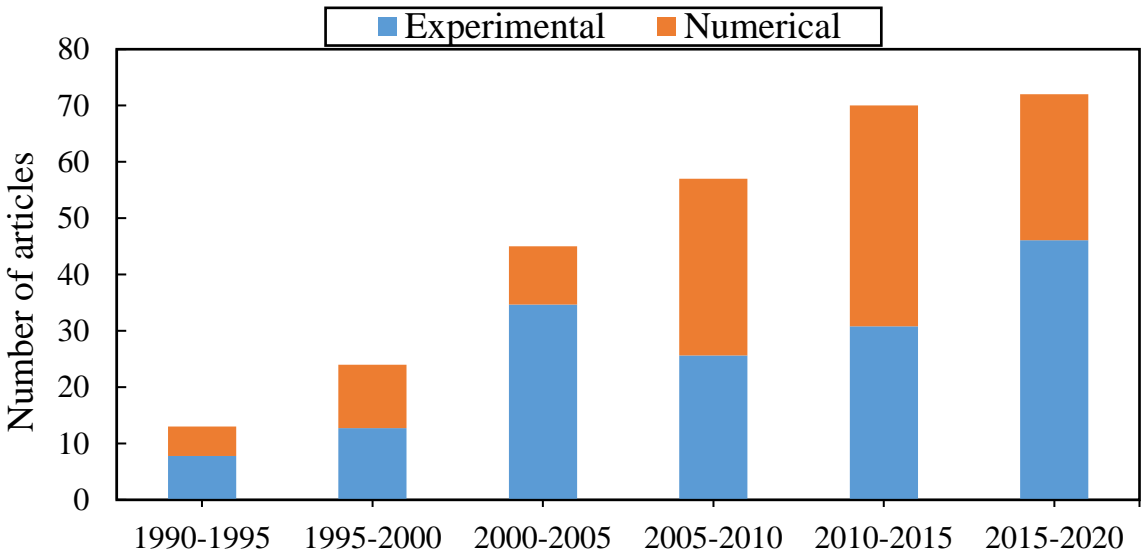


Figure 0.1: Experimental and numerical articles on straw bale construction between the years 1990 and 2020

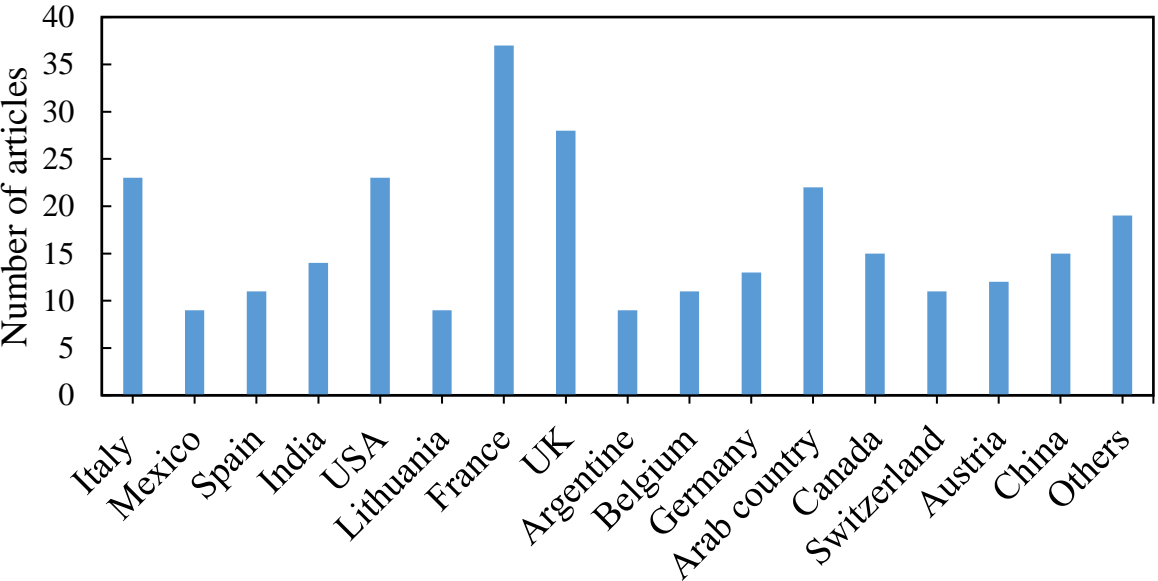


Figure 0.2: Number of articles done worldwide between the years 1990-2020

Thesis question and methodology:

The lack of some information and explanations in the literature prompted the establishment of this research. Specifically, it is still unclear whether the alleged increased hygrothermal comfort and diminution of energy consumption of straw buildings can be scientifically documented. Similarly, experimental and numerical studies are needed for estimating the fire and the mechanical resistance of such structures by adding new covering materials that may improve the results. These questions still prevent the dissemination of straw buildings. Thus, this thesis aims to provide scientific answers to these questions. The composite material belongs to bio-based materials, which are made up of straw as vegetal fibers that act as a thermal and mechanical reinforcement in a wood box. The methodology is both experimental and numerical on several scales (fiber, bale, wall, and building) starting from the study of thermal and hygric characteristics of straw fibers and bales to the study of the indoor air comfort and energy consumption of straw buildings, passing through the wall hygrothermal and fire resistance characterizations.

Manuscript Layout:

The dissertation is divided into four parts:

- The first part provides an overview of the existing academic literature and industry practice on straw-based construction. The review is divided into five chapters. First, it reports investigations on the microscopic structure and chemical composition of the straw material. Then, research on straw bales is detailed with a focus on the bale's density, porosity, thermal conductivity, specific heat capacity, effusivity, diffusivity, water vapor diffusion, load-deformation mechanical properties, and PH measurements. At the wall scale, works regarding the hygrothermal behavior, fire resistance, acoustic performance and environmental impact of straw-based envelopes are presented. The existing literature on a full-scale straw building is discussed next, from the viewpoints of construction systems, regulations, and energy behavior. In the synthesis section, the main findings of the existing literature are critically assessed and, more importantly, the needed future research directions are outlined to fill in the gaps in the existing knowledge.
- The second part is divided into two chapters. The first chapter shows the experimental work done to characterize straw at fiber and bale scales. The material preparation process is described with the experimental methods used. The characterization results are shown at the end of the chapter. Based on the experimental results, the second chapter proposes an analytical model of thermal conductivity in straw bales. The model takes into consideration the density, temperature, humidity, and fibers' orientation of the bales.
- The third part focuses on the experimental and numerical investigation of multilayered straw walls. A WUFI model is used to predict hygrothermal problems that may occur in certain conditions for five straw walls with different configurations. The new straw wall proposed by the thesis industrial partner Activ'home is then tested for fire resistance. Using Abaqus software, a numerical model is proposed after the experiment.
- The fourth part studies the indoor comfort of the straw building. This part is completed by an energetic study to predict the consumption of such structures by using Energyplus models for different scenarios. A sensitivity study is done to determine the parameter that affects mostly the indoor air temperature and relative humidity. In addition, the mechanical resistance is tested by using the ROBOT structural analysis model. In the end, an economic and environmental analysis is done to show the cost of straw buildings and their net carbon emissions.

This thesis work was carried out at the Clermont Auvergne University, within the Institut Pascal, in the framework of the ECOMAT project funded by the 2015-2021 French state-region development plan contract (CPER).

First part: Literature Review

1. Straw fiber scale

This chapter presents the different characteristics of the straw fibers used in the construction field. The characterization includes the microstructure of different types of straw with their chemical composition and their sorption-desorption curves. The porous structure may lead to a low thermal conductivity and water diffusion factor. The chemical composition of wheat, barley and rice straw seems to forecast good hygrothermal properties and mechanical strength at the fiber scale with availability in most countries. As result, it is noticed that further investigations are required to compare straw fibers to other natural and synthetic fibers whether microstructurally and chemically. These properties are important in defining a heat transfer model for straw bales.

Table of contents

1.1. Anatomy and microscopic characteristics.....	6
1.2. Chemical composition and physicochemical properties.....	7
1.3. Sorption-desorption isotherms.....	9
1.4. Discussion and perspectives.....	11

Chapter 1. Straw Fiber Scale

1.1. Anatomy and microscopic characteristics

Natural fibers are used in bio-based composites to improve the material's mechanical and thermal properties. Natural fibers-based materials may be divided into several groups. They comprise plant-based materials like straw and wood, as well as animal-based materials like wool and silk, and mineral-based materials like asbestos and basalt. Plant fibers, particularly straw, have recently attracted more attention than other varieties due to their excellent thermal performance and lightweight properties [20–23]. This popularity is explained by their availability all over the world.

Straw is an agricultural coproduct formed following grain harvesting in various varieties of wheat, barley, oats, and others. Laborel-Preneron *et al.* [24] utilized ImageJ and analyzed processed images to identify the size distribution and morphology of fibers. The experiment consisted of studying fibers fixed on a metal substrate under vacuum with a 15-kV accelerating voltage. This approach is only suitable for a small number of non-spherical fibers [25–27]. The findings, which came in the form of a contrasting scanned image of the particles on a black backdrop, allowed for the length and width of the straw fibers to be calculated. The aspect ratio (AR) and the Equivalent Area Diameter (EAD) may be calculated using these two dimensions. By dividing the length by the width, the AR is computed. Its value indicates whether a fiber is short (near 1) or long (greater than 1). Equation (1.1) computes the EAD of a circular cross-section (A) fiber. The average values of the barley fiber diameters, EAD, and AR, as well as their variations, are shown in **Table 1.1**. AR is about 4.1 mm, greater than 1, which means that the fibers are noticeably lengthy.

$$\text{EAD} = \sqrt{\frac{4 \cdot A}{\pi}} \quad (1.1)$$

Table 1.1: Dimensions of barley fibers [24]

Dimension	Barley straw
Major (mm)	7.6 ± 4.4
Minor (mm)	2.3 ± 1.5
EAD (mm)	4.0 ± 2.1
AR	4.1 ± 3.7

The length and distribution of straw inside a bale are critical in determining its mechanical properties. Barley straw, according to Ashour and Wu [28], have higher mechanical properties than wheat straw fibers because the fibers are shorter. For both barley and wheat, the proportion of fibers smaller than 2 mm long is roughly 95% for barley and 76 % for wheat, with the remainder ranging from 2 mm to 50 mm.

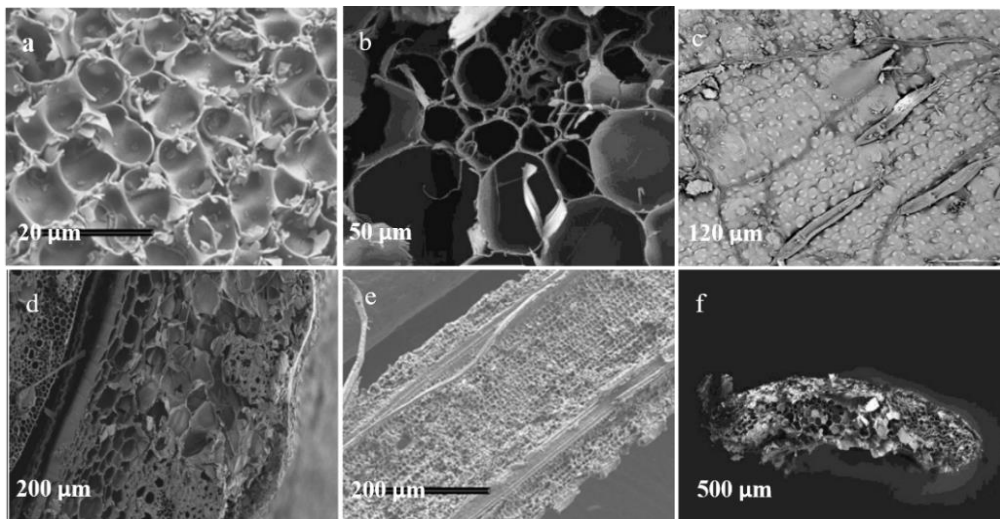


Figure 1.1: SEM analysis images of the surface of wheat straw (a), (d), and (e), barley straw (b) and (f), and rice straw (c) at low and high magnification factors (based on [24–27])

Chapter 1. Straw Fiber Scale

Laborel-Preneron *et al.* [24] and Bouasker *et al.* [25] used a high-resolution Scanning Electron Microscope (SEM) to visually examine the porosity structure and morphology of straw fibers. The microstructures of rice, barley, and wheat straw are shown in **Figure 1.1 (b), (c), (d), and (f)**. Rice has an ordered and compact surface, while barley and wheat have porous multi-scaled morphologies that range from 2 μm to 100 μm and 7 μm to 20 μm , respectively. Halvarsson *et al.* [27] used SEM to do a morphological examination of wheat straw in the context of research on medium-density fiberboards. The surface of a 0.6 mm long wheat straw fiber is shown in **Figure 1.1 (a) and (e)**. The pores have the same dimensions as the rice. According to Halvarsson *et al.* [27], these complex forms can include hydrophobic and inorganic elements like silicon, which slow the absorption of water.

A porous structure leads to a decrease the thermal conductivity and lowers the water diffusion factor, which influences the heat transmission mechanism in the bale. This is due to a material's porosity, which determines how much water it can store based on the pore's dimensions and sorption properties of the material.

1.2. Chemical composition and physicochemical properties

Plants satisfy their nutritional demands for development from soil nutrients, water, air, and sun. This explains the variations in the chemical composition of straw based on the location, climate, and type. The chemical composition of construction materials provides information about their durability, stability, thermal, and mechanical properties. The durability is determined by the moisture content and hemicellulose [29]. The lignin component improves stability and mechanical strength. The cellulose component improves the material's thermal insulation and mechanical property [30].

In France, the national comity [31] determined the chemical composition of cereal straw as cited in **Table 1.2**. These findings showed two main values the dry matter and cellulose by about 88% and 42 % respectively, making the straw a mechanically resistant material, with high thermal resistance. The mechanical resistance and the lifetime of vegetal fibers depend highly on their moisture content which should be less than 15 %.

Table 1.2: Chemical composition of the cereal straw [31]

	Average value	Extreme value
Dry matter (%)	88	85-90
Mineral matter (% MS)	7	5-10
Total nitrogen (% MS)	3.5	2-5
Soluble nitrogen (% N total)	25	20-30
Crude cellulose (% MS)	42	40-50
Calcium (g/kg de MS)	3	2-5
Phosphorus (g/kg de MS)	0.8	0.3-1.5
Magnesium (g/kg de MS)	1	0.5-1.5

In the continental Croatian field, Plazonić *et al.* [32] determined the organic compounds of wheat, barley, and triticale straw samples by applying the isolation method described in **Figure 1.2** and appendix **A1**. The ash content (W_{ash}), the solvent extractives content (W_{SE}), the klason lignin content (W_{Lignin}), the cellulose content ($W_{cellulose}$) and the α -cellulose content ($W_{\alpha-cellulose}$), presented in **Table 1.3**, are calculated by applying the procedures cited in **Figure 1.2**. Results showed that wheat straw had a better composition because it has a combination of high contents of cellulose and lignin by about 48% and 25%, respectively, and low moisture content of about 7%. The composition of this type of fiber is similar to wood since the main three components; cellulose, lignin, and hemicellulose exist in both.

Chapter 1. Straw Fiber Scale

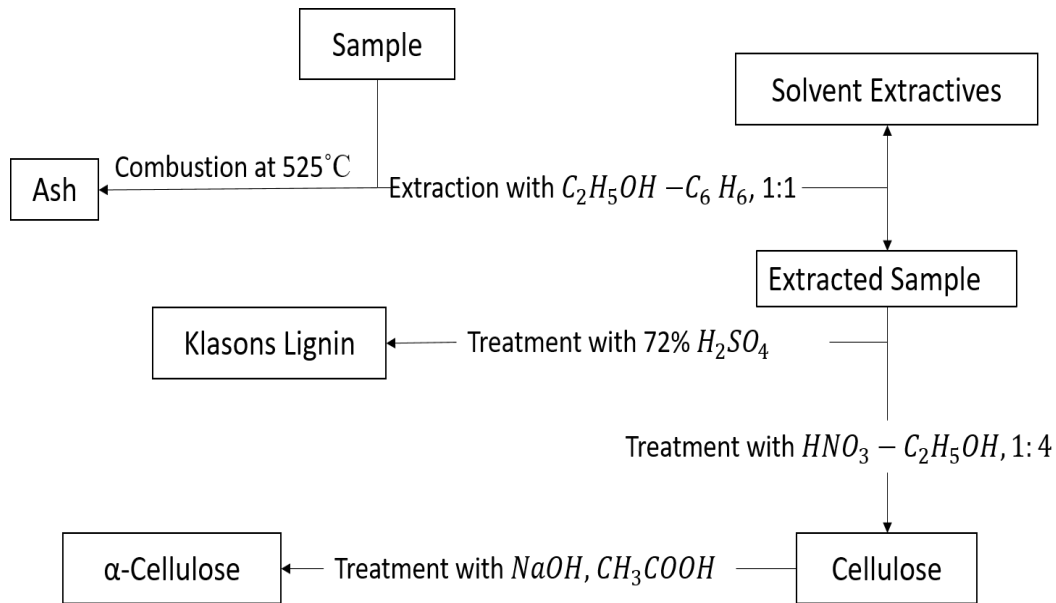


Figure 1.2: Diagram showing the different steps of the isolation method [32]

Table 1.3: Organic substance components of wheat, barley, and triticale straw using standard isolation [32]

W, %	Wheat	Barley	Triticale
Moisture	6.94	6.62	7.73
Ash 525 °C	9.27	7.14	5.27
Klason lignin	24.66	21.71	12.59
K-H cellulose	48.28	45.9	52.88
α-cellulose	31.47	37.97	44.22

On the other hand, Plazonic *et al.* [32] used the ICP-MS (Inductively Coupled Plasma Mass Spectroscopy) approach to detect the inorganic elements mentioned in **Table 1.4**. ICP-MS is an ionization source that fully decomposes a sample into its constituent elements and transforms those elements into ions. The ions are separated based on their mass to charge ratio and are then subjected to signals that detect the element concentration based on reference material. In Plazonic *et al.* [32] experiment, the process consisted of dissolving the ash obtained in the above experiments since it doesn't contain organic compounds. Findings showed that the highest macro element composing the tested fibers is potassium, which helps in maintaining a balance in water content [33].

Table 1.4: Macro and microelements composition of Wheat, Barley, and Triticale straw [32]

Nutrient	Wheat (g/kg)	Barley (g/kg)	Triticale (g/kg)
K	10.34	5.01	13.97
Ca	3.3	3.63	2.77
Mg	1.05	0.66	0.897
P	0.59	1.30	0.48
Zn	0.054	0.18	0.023

Chapter 1. Straw Fiber Scale

Fe	0.047	0.102	0.036
Mn	0.031	0.0015	0.073
Al	0.19	0.16	0.032
Bi	0.117	0.15	0.202
Si	0.071	0.147	0.007
Ba	0.042	0.0028	0.053

In a technical study published by the HGCA (Cereals and oilseeds division of the Agriculture and Horticulture Development Board) in the United Kingdom, Nicholson *et al.* [34] provided the usual levels of nutrients found in straw fibers, as indicated in **Table 1.5**. The purpose of this study was to see how straw fibers affected the physical qualities of soil. For example, in five tons of winter wheat straw, 6 kg P₂O₅, 47.5 Kg K₂O, 6.5 kg MgO, and 6.5 Kg SO₃ may be predicted. These components are all important and decrease the need for inorganic fertilizers once added to the soil.

Table 1.5: Phosphate, potash, magnesium, and Sulphur in a different kind of straw [34]

Straw type	Phosphate (Kg P ₂ O ₅ /t)	Potash (Kg K ₂ O/t)	Magnesium oxide (Kg MgO/t)	Sulfur (Kg SO ₃ /t)
Wheat (winter)	1.20	9.50	1.30	1.30
Barley (spring)	1.50	12.50	1.20	No data
Oat	1.60	16.70	2.20	No data
Rye	2.10	10.00	1.00	No data

The physicochemical property as well as the surrounding environment determine the straw durability in buildings. Among the factors that influence the durability and stability of the material is the presence of microorganisms. The microorganisms grow and thrive when the conditions within the bale are ideal for their development. These conditions are determined by the pH of the straw. In a neutral environment, bacteria develop at their slowest pace. Ashour *et al.* [14] measured the pH by drying the straw at a high temperature (105 °C) and mixing it with distilled water in a 1:9 ratio. An average value of 7.29 was discovered and represented a neutral-alkaline environment. Bouasker *et al.* [25] determined the pH of barley straw using a pH meter. Straw fibers were mixed in NaCl solution and NaOH for 24 hours to remove moisture from the bale. The pH value was 8.3 in the experiment, indicating the presence of mold. Halvarsson *et al.* [27] used the technique of Johns and Niazi [35] to determine the pH and pH-buffering capacity of wheat straw by extracting the aqueous solutions from the straw and measuring its pH with a digital pH meter. The pH value and pH-buffering capacity were both found to be 7.5.

To sum up, throughout the plant growth process, the chemical components of straw are influenced by the kind of soil and climate conditions. With availability in most regions, the chemical composition of wheat, barley, and rice straw appears to predict a low thermal conductivity, high hydric absorption, and good mechanical resistance at the fiber scale. These properties cannot be helpful if the internal conditions of the bale are acidic or alkaline. Therefore, to be safe, straw fibers should be stored at a neutral pH.

1.3. Sorption-desorption isotherms

Water has an impact on the physical straw properties, such as thermomechanical properties and stability. The interaction of straw and water has been studied in the literature through sorption-desorption isotherms. This type of graph shows the equilibrium moisture content at a given climatic condition

Chapter 1. Straw Fiber Scale

(temperature and relative humidity). The equilibrium is achieved through an increase (absorption) or a decrease (desorption) in moisture content.

Yin *et al.* [36] used the DVS (Dynamic Vapor Sorption) method to analyze the sorption-desorption isotherm of rice and wheat straw. In general, straw is a hygroscopic substance that goes through five phases of water absorption. It starts with single-layer adsorption and progresses to super saturation. Despite the differences in microstructure between wheat and rice, **Figure 1.3** indicates that the sorption and desorption curves of both straw types are almost identical. Bouasker *et al.* [25] compared the sorption-desorption curves of wheat and barley straw. They noticed different behavior during desorption due to the slow desorption kinetics of the barley at high relative humidity values as shown in **Figure 1.4**.

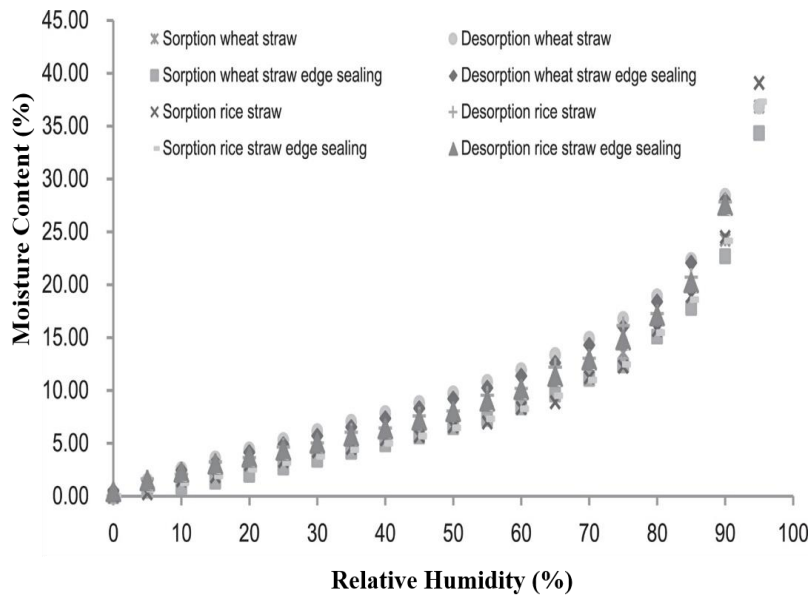


Figure 1.3: Sorption and desorption isotherm of wheat and rice straw [36]

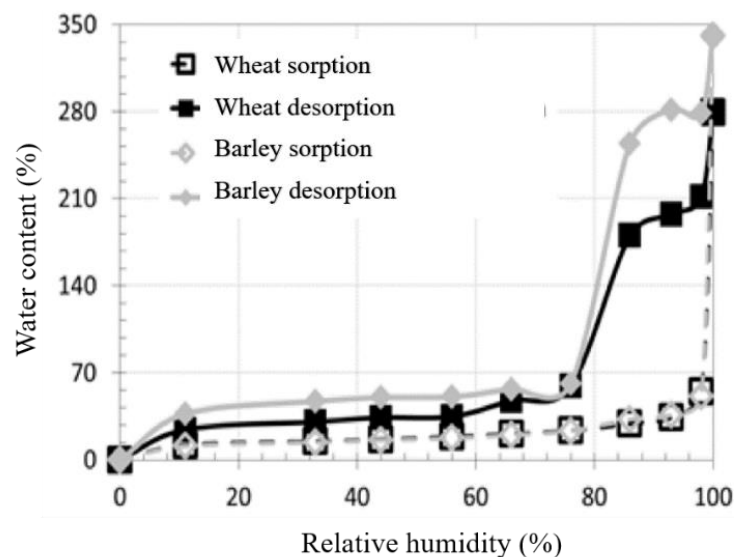


Figure 1.4: Comparison of wheat and barley sorption and desorption curves [25]

In both studies, the amount of water trapped by the pores during desorption causes a difference between the sorption and desorption curves called hysteresis. The hysteresis is higher when the solid part of the fiber is denser and porous. Liuzzi *et al.* [37] measured the water content at 23 °C under various relative

Chapter 1. Straw Fiber Scale

humidity values in the climatic chamber to study the hygrothermal behavior of barley straw fibers. They discovered that the sorption curve's form matches type II isotherms, which have a sigmoid shape and an inflection point that denotes a shift from mono- to poly-molecular fixation, and define the meso- and macroporous structures. This classification is based on the IUPAC recommendations regarding the six types of physisorption isotherms [38]. As a result of this feature, the straw can serve as an effective hydric regulator, enhancing hygrothermal comfort.

1.4. Discussion and perspectives

The size and the distribution of the pores and fibers as well as the amount of the major straw components were discovered during the investigation of the chemical composition and microstructure of the straw fibers. Such features are responsible for the heat transfer mechanism inside the material and can affect its thermal and mechanical properties. The fibers inside a bale are mostly short (1-2 mm) and very porous, according to SEM and imaging examinations, which can improve the mechanical properties of bales. Straw is composed mainly of cellulose, lignin, and hemicellulose. It is apparent that the chemical structure of many types of straw is the same as that of wood. However, additional research into the comparison of straw fibers to other natural and synthetic fibers is needed. The fibers' microstructural properties should be analytically linked with their mechanical and thermal properties. In the literature, there is no model yet of heat transport in a straw porous media and no data concerning the straw fibers' ultimate tensile strength and fracture toughness. In addition, further pH-related studies should be carried out as they have a strong effect on the inner bale conditions and durability.

2. Straw bale scale

Straw bale is a group of fibers stacked and compressed in a way that provide good thermal and mechanical properties for building application. These properties are highly dependent of the density of the material and the fibers orientation in the bale. On one hand, this chapter shows the thermal and hygric properties of bales such as thermal conductivity and vapor resistance factor. On the other hand, it presents the mechanical properties of the material, through experimental studies on elastic stress-strain behavior of straw bales. At the end, this chapter discusses the other measurements that can be performed to make a complete characterization for the material.

Table of contents

2.1. Density and porosity	13
2.2. Thermal properties.....	14
2.2.1. Thermal conductivity.....	14
2.2.2. Heat capacity.....	19
2.2.3. Thermal effusivity and diffusivity.....	19
2.3. Water vapor diffusion factor and thickness.....	20
2.4. Mechanical properties.....	20
2.5. Discussion and perspectives.....	23

Chapter 2. Straw Bale Scale

2.1. Density and porosity

The straw bale is an agricultural product resulting from the harvest of various kinds of cereal. During the manufacture of this material, a harvesting machine is required to separate the grains from the straw/stem and a baler is required to gather the straw by pressing it in the shape of a bale. This gathering phase determines the size and shape of the bale [39], as well as the fiber orientation inside it [40]. Bales can be circular or square, small or large, with two or three strings [41] depending on the dimensions of the compression channel. Between 1940 and 1980, the baler channel developed and the work rate reached 25 tons per hour [34]. The machine can then produce 45 to 50 rectangular bales per hour.

The manufacturer while respecting some limits can impose the dimensions of the compression channel. In general, a rectangular bale's height ranges from 60 to 130 cm, its width from 70 to 120 cm, and its length from 50 to 280 cm, whereas a round bale's diameter ranges from 80 to 190 cm and its height from 100 to 120 cm. **Table 2.1** shows examples of straw bales' various shapes and densities. Many nations consider a density of more than 80 kg/m³ to be sufficient for straw construction. Furthermore, large bales (such as rectangular three-string bales) are employed in buildings because they provide a more solid structure in terms of density and weight. Other limits can be found in the research literature. Wimmer *et al.* [42] used small bales having a width of 46 cm, a height of 36 cm, and a variable length between 40 cm and 110 cm. The density of a bale is determined primarily by its size, density, water content, straw type, and the compressive force exerted by the baler [28]. According to Costes *et al.* [43], ordinary straw bales can have densities ranging from 74 kg/m³ to 103 kg/m³. Watts *et al.* [40] measured lower densities for barley straw bales, ranging from 54.6 kg/m³ to 78.3 kg/m³, and comparable densities for both oat and wheat straw bales, ranging from 81 kg/m³ to 106.3 kg/m³. Before beginning the construction process, it is critical to assess the density because it has an impact on the material's porosity, the envelope's thermal properties, and the structural stability. High density, for example, results in reduced porosity, increased thermal conductivity, and improved mechanical stability. To find an acceptable density and porosity, a compromise between mechanical and thermal properties should be made.

Table 2.1: Typical bale size versus density and weight [34]

Bale		Bale size (cm)			Density (kg/m ³)	Weight (kg)
		width	Height	Length		
Round	Small	120	150	-	118	250
	Large	150	180	-	103	400
Square	Small	80	90	250	160	280
	Medium	120	90	250	160	420
	Large	120	130	275	140	550

Another important property of straw bales is porosity. Natural fibers and specifically straw bales are regarded as porous materials. The blank gaps allow water and other foreign molecules to flow through them. The porosity of the samples is inferred from their apparent and actual density. The manufactured coating (composed of sand, straw fibers, and clay), the industrial coating (composed of aggregates and a mixture of sand and clays supplied in bags), and the concrete have the lowest porosities of about 24 % and the highest densities of about 2000 kg/m³, as indicated in **Table 2.2**. The wood board (composed of wood fibers) and the straw bales (composed of straw fibers) have better porosity and density. Wihan [44] studied straw bales that have a porosity of about 90%. Different values can be always noted due to the dispersion of the properties of the bio-based material. Porosity has an impact on the material's absorption that rises as the porosity increases. This is explained by the quantity, distribution, and size of the pores in the substance. As a result of water and vapor absorption, the porosity of the straw bale impacts its long-term durability and stability.

Chapter 2. Straw Bale Scale

Table 2.2: Average hygrothermal parameters of the straw compared to other construction materials (based on [45,46])

Parameters	Straw bale	Concrete	Wood fiber board	Industrial coating	Manufactured coating
Density [kg/m ³]	100	1450	570	2051	1600
Porosity [%]	93	24	50	24.8	30
Capillary absorption [kg/(m ² .S ^{1/2})]	0.0155	0.003	0	0.068	0.047
Total absorption [%]	203.9	13	17.5	8.8	15.6
MBV [g/(m ² .%RH)]	1.853	0.9-1.1	1.929	--	--

2.2. Thermal properties

2.2.1. Thermal conductivity

Thermal conductivity is a measure of a material's ability to conduct heat. According to the literature, density, porosity, moisture content, fibers' orientation, structural imperfections, and temperature affect the thermal conductivity of straw bales. Straw bale made of barley, wheat, rice, and oats offers high thermal insulation capabilities and can reduce building energy use.

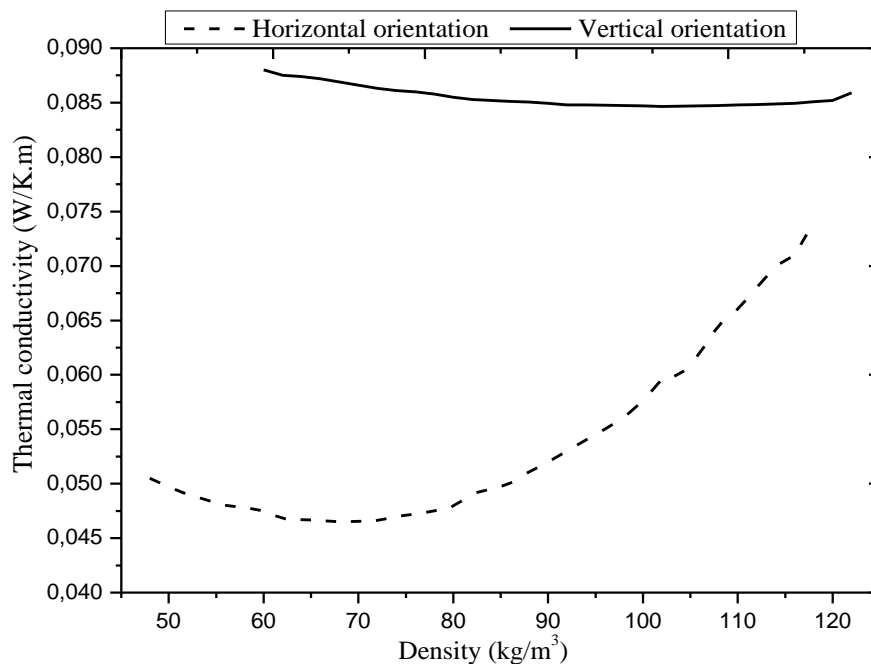


Figure 2.1: Variation of the thermal conductivity with respect to the density of vertical and horizontal oriented fibers (based on data from [47])

Firstly, McCabe [41] investigated the effect of the fibers' orientation on the thermal conductivity of wheat straw bales using the hot guarded plate device. Samples had the same density, temperature, and moisture content of 133 kg/m³, 20°C, and 8% MC, respectively. Results showed an important difference between the perpendicular oriented fibers' thermal conductivity of 0.046 W/m.K and the parallel oriented fibers' thermal conductivity of 0.061 W/m.K. Sabapathy *et al.* [48] evaluated the impact of this factor by varying each time the temperature, RH and density. The parallel fibers' thermal conductivity

Chapter 2. Straw Bale Scale

reached 0.1 W/m.K while the perpendicular fibers' thermal conductivity was about 0.06 W/m.K. Vejeliene [47] examined the influence of the orientation and length of the fibers (chopped straw) on thermal conductivity. As seen in **Figure 2.1**, the thermal conductivity rises when the fibers are positioned horizontally and decreases when they are orientated vertically relative to the heat flux direction. Variations in air volume in the heat flow path cause this behavior. Concerning fiber length, chopped straws had better thermal conductivity than long fibers.

Secondly, Ashour and Wu [28,49] studied the impact of the straw type on thermal conductivity. The experiment consisted of measuring the thermal conductivity of wheat and barley straw bales 60 cm long, 38 cm wide and 36 cm high. **Figure 2.2** presents the variation of the thermal conductivity with respect to the density for both straw types at different temperature levels. The chemical composition of wheat and barley fibers differs, which explains the differences in the observed results. It can be noticed that wheat bales had higher thermal conductivity than barley bales. In addition, this experiment highlighted the effect of the density variations. In both circumstances at 10°C, 20°C, and 30°C, as density rises, the thermal conductivity decreases until it reaches a point where it stabilizes, after which it begins to rise again. Costes *et al.* [43] also measured the thermal conductivity of 13 straw bales treated at 23°C and 50% RH using the guarded hot plate technique. It is worth noting that their results differ from those of Ashour and Wu [28,49], which might be owing to Costes *et al.* [43]'s non-mentioned orientation. Shea [50] also used a flow meter to test the thermal conductivity of straw bales with varying densities. Comparable to previously mentioned, as the density grew from 63 kg/m³ to 123 kg/m³, the observed thermal conductivities increased from 0.059 W/m.K to 0.064 W/m.K.

Thirdly, Palumbo *et al.* [51] tested the effect of the RH or MC on the thermal conductivity of a mixture of 81 % of barley straw and 19 % of cornstarch. RH had a significant impact on the thermal conductivity of this material due to the replacement of the air or gaps with water. This can be explained by the porous nature of this material. In the experiment of Sabapathy and Gedupudi [48], represented in **Figure 2.3**, similar findings were observed for rice straw bales. When the RH rose from 40% to 60%, the conductivity increased from 0.06 W/m.K to 0.07 W/m.K, as illustrated in **Figure 2.3 (b)**.

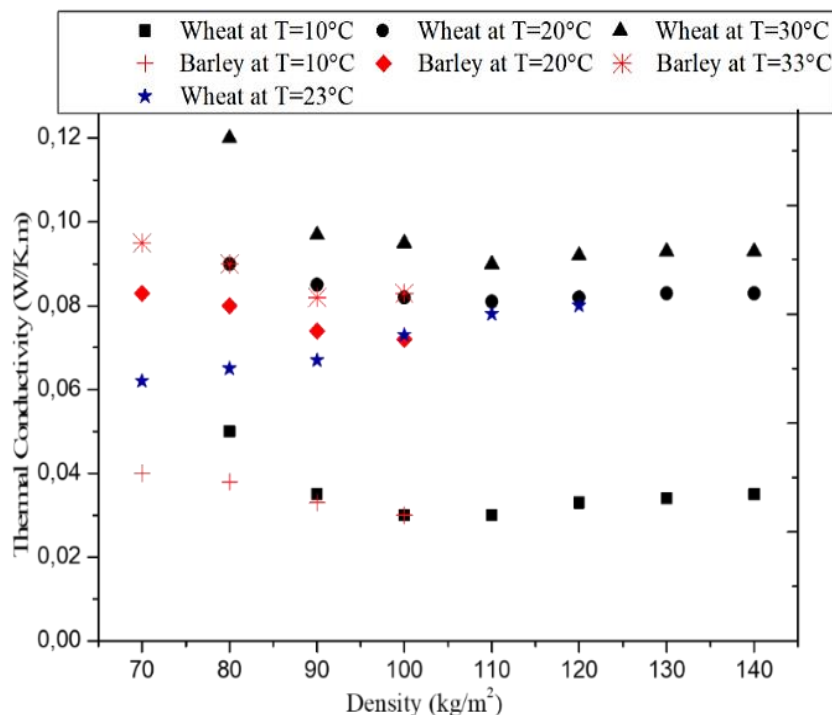


Figure 2.2: Thermal conductivity data for wheat and barley straw as a function of temperature and density (based on [28,43,49])

Chapter 2. Straw Bale Scale

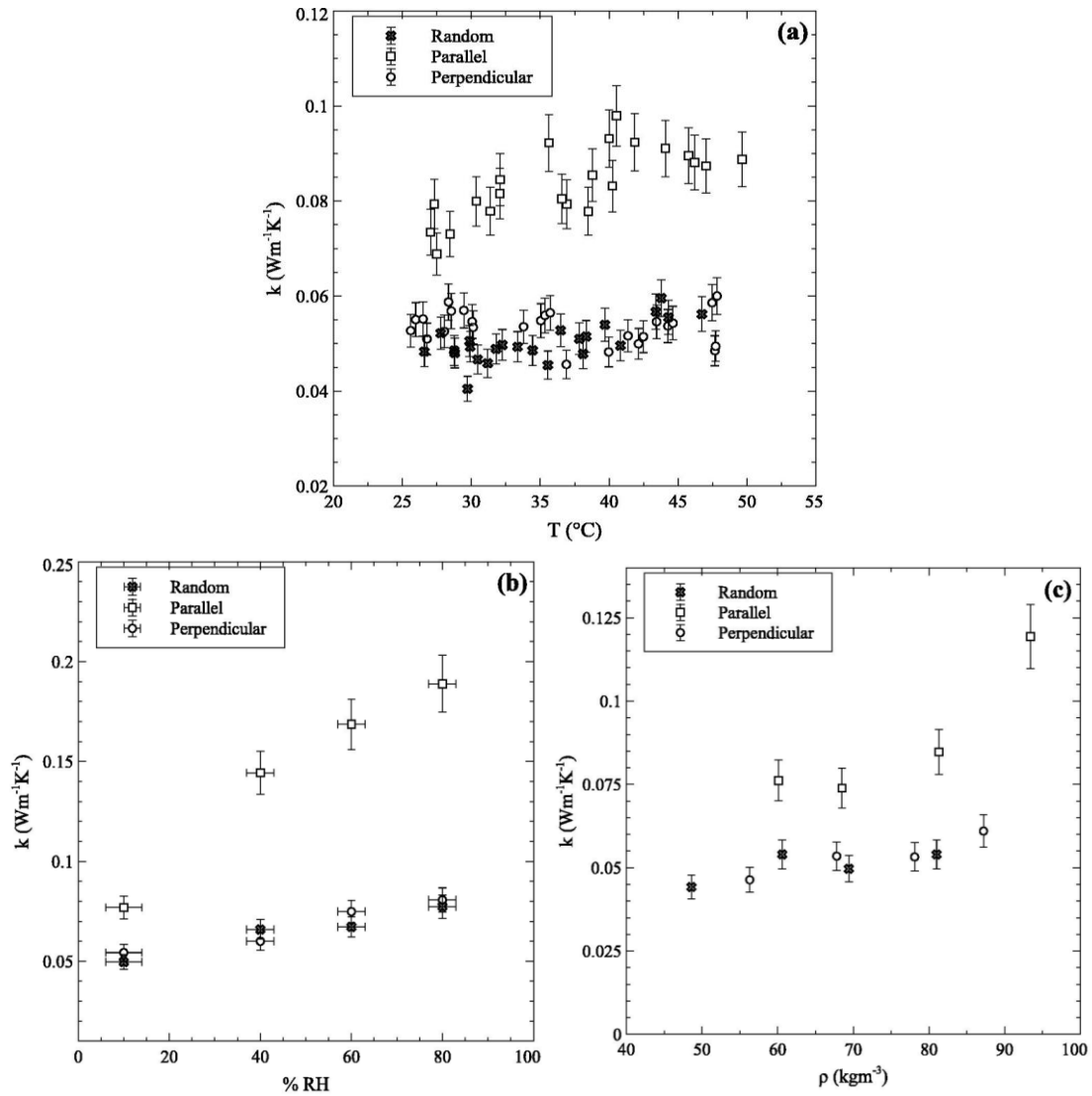


Figure 2.3: Thermal conductivity for different orientations with respect to (a) temperature, (b) RH, and (c) density [48]

Between the years 1993 and 2019, several experiments measured the thermal conductivity for a narrow range of parameters. **Table 2.3** shows the researchers' findings, which include correlations that can predict thermal conductivity as a function of temperature, RH, and density for wheat, rice, and barley. **Table 2.4** presents the experimental findings of several authors' thermal conductivity tests. These investigations revealed that as density and moisture content rise, so does thermal conductivity. To sum up, as shown in equation (2.1), a single value for the thermal conductivity of straw cannot be determined since various factors (density, humidity, fiber orientation, temperature, and others) can influence its thermal characteristics.

$$0,033 [\text{W}\cdot\text{m}^{-1}\cdot\text{K}^{-1}] \leq \lambda \leq 0,19 [\text{W}\cdot\text{m}^{-1}\cdot\text{K}^{-1}] \quad (2.1)$$

Chapter 2. Straw Bale Scale

Table 2.3: Different propositions of thermal conductivity correlations (with ρ the density, t the thickness, T the temperature, and RH the relative humidity)

Proposed correlation for λ (W/K.m)	Considered conditions	Fiber orientation	Straw type	Ref.
$0.048 + 0.00029\rho - 0.0113t$ $0.0444 + 0.000272\rho$	$\rho=68-123 \text{ kg/m}^3; T=23^\circ\text{C}; RH=50\%$	---	---	[43]
$0.046(1 + 0.009T)$ $0.067(1 + 0.0078T)$	$\rho=80 \text{ kg/m}^3; T=10-40^\circ\text{C}$	Perpendicular parallel	---	[52]
$0.037 + 0.019(RH)$	$\rho=107.5 \text{ kg/m}^3; T=10^\circ\text{C}; RH=10-90\%$	---	Barley + corn starch	[51]
$0.09637 - 0.00146\rho + 0.0000107\rho^2$ $0.10312 - 0.00036\rho + 0.0000175\rho^2$	$\rho=60-120 \text{ kg/m}^3; T=10^\circ\text{C}; RH=50\%$	Perpendicular parallel	Barley	[47]
$0.00399 - 0.00023\rho + 0.00269T$ $0.0625 - 0.0005\rho + 0.002237T$	$\rho = 82-138 \text{ kg/m}^3$ $\rho 68-98 \text{ kg/m}^3$	---	Wheat Barley	[49]
$-0.0002\rho^2 + 0.317\rho + 0.315(RH) - 0.042T + 30.794 \text{ [mW/m.K]}$ $-0.0103\rho^2 + 2.196\rho + 1.573(RH) + 0.478T - 46.072 \text{ [mW/m.K]}$	$\rho=60-120 \text{ kg/m}^3; T=10-50^\circ\text{C}; RH=10-90\%$ $\rho=45-200 \text{ kg/m}^3; T=10-50^\circ\text{C}; RH=10-90\%$	Perpendicular Parallel	Rice	[48]

Chapter 2. Straw Bale Scale

Table 2.4: Bale thermal conductivity according to density and fiber orientation (cases that do not have a distinct direction might be thought of as a combination of horizontal and vertical fiber orientation.)

Year	Authors	Straw type	Moisture content/ Relative humidity MC/RH (%)	Mean Temperature (°C)	Density (kg/m ³)	Fiber orientation	thickness (+plaster) (mm)	Thermal conductivity (W/m.k)
1993	McCabe [41]	Wheat	MC 8.4%	20	133	perpendicular	419	0.047
		parallel				584	0.06	
		Rice			123	Random	450	0.08
1997	CEC/ATI [53]	Rice	MC 11%	23	107	perpendicular	406	0,0811
						parallel	584	0,1471
2003	Ashour [49]	Wheat	----	----	82-138	----	----	0,033
		Barley		----	69-98			0,034
2004	Beck <i>et al.</i> [54]	Barley	----	40	80	perpendicular	22	0.041
	CEBTP [55]	----	RH 50%	23	77	----	----	0.066
2009	FASBA [56]	Wheat	0	----	81-111	perpendicular	----	0,044
					105	parallel		0,067
2011	Vejeliene [47]	Barley	RH 50 %	10	60-120	parallel	----	0,0845-
		50-120			perpendicular	0,0875		
		35-80			random	0.039-0.045		
		Barley chopped			35-80	random		0.037-0.044
2012	Shea <i>et al.</i> [50]	Wheat	RH 50 %	----	63-123	random	300	0,059-0,064
			----	----	115		490	0,087
2015	Wei <i>et al.</i> [57]	Rice	MC 10-18%	30	200-350	----	40	0.051-0.053
2016	Conti <i>et al.</i> [58]	Wheat	MC 12,5%	19	65,7	parallel	530	0,062
			MC 11,5%		84,1			0,07
2017	Gallegos-Ortega <i>et al.</i> [59]	----	RH 10%	25	115	-----	----	0.094
2017	D'Alessandro <i>et al.</i> [60]	----	RH 45%	22	80	----	450	0.052
2019	Cascone <i>et al.</i> [61]	Wheat	MC 8%	35	78	random	20	0.069
2019	Sabapathy and Gedupudi [48]	Rice	RH 40 %	30	68	random	---	0,06
						perpendicular		0,057
						parallel		0,15
						random	---	0,07
						perpendicular		0,08
						parallel		0,17
						random	---	0,07
						perpendicular		0,075
						parallel		0,19

Chapter 2. Straw Bale Scale

2.2.2. Heat capacity

Heat capacity, measured by a calorimeter, is the ratio of the absorbed heat to the temperature elevation. Marques *et al.* [62] calculated the thermal capacity of rice straw with densities ranging from 80 kg/m³ to 100 kg/m³ and temperatures ranging from 0 °C to 40 °C without accounting for the pores between the fibers. Thermal capacity was determined to be between 1075 J/kg.K and 2025 J/kg.K. Concerning wheat straw, the volumetric heat capacity factor rose from 164 kJ/m³.K to 276 kJ/m³.K, when the density varied from 82 kg/m³ to 138 kg/m³ and the heat capacity was reported as 2000 J/kg.K [49]. According to Goodhew and Griffiths [63], the specific and volumetric heat capacity of straw bales with a density of 60 kg/m³ were 600 J/kg.K and 36.8 kJ/m³.K, respectively, while the clay-straw having a density of 440 kg/m³, they were 900 J/kg.K, and 400 kJ/m³.K, respectively. For the same reasons as thermal conductivity, a single number for thermal capacity cannot be determined. The heat capacity of straw fluctuates within the range provided by equation (2.2), according to [64,65].

$$1338[J.kg^{-1}.K^{-1}] \leq C_p \leq 2000 [J.kg^{-1}.K^{-1}] \quad (2.2)$$

2.2.3. Thermal effusivity and diffusivity

Thermal effusivity and diffusivity are parameters related to the thermal conductivity, density, and heat capacity of material as indicated in equation (2.3) and equation (2.4), respectively. Thermal effusivity, also known as thermal permeability, explains how a material exchanges heat when exposed to another substance [66], whereas thermal diffusivity indicates a material's capacity to transport warmth across its many surfaces and extremities. These two parameters were inferred by Chaussinand *et al.* [64] from the range fluctuation of thermal conductivity and capacity. Equation (2.5) and equation (2.6) yield the effusivity and diffusivity values of the straw bales, respectively.

Ashour [49] investigated the thermal diffusivity and effusivity of wheat straw by varying the density from 82 kg/m³ to 138 kg/m³. They found that the thermal diffusivity fell from 3 x 10⁻⁷ m²/s to 1.5 x 10⁻⁷ m²/s while the thermal effusivity rose from 1.49 J/K.m².h^{0.5} to 1.79 J/K.m².h^{0.5}. The thermal diffusivity of a straw bale with a density of 60 kg/m³ was 18.2 x 10⁻⁷ m²/s, according to Goodhew and Griffiths [63]. This value dropped to 4.6 x 10⁻⁷ m²/s for a density of 440 kg/m³, after combining the straw with clay. Sabapathy and Gedupudi [48] determined the heat diffusivity of a straw bale with a density of 68 kg/m³. The values obtained varied from 2.4 x 10⁻⁷ m²/s to 15.3 x 10⁻⁷ m²/s. They proposed at the end correlations predicting the thermal diffusivity for the vertical, horizontal, and random orientations as indicated in equation (2.7), equation (2.8), and equation (2.9), respectively.

Straw walls assist in gaining heat to raise the interior temperature, because of their low thermal effusivity. Straw bales, on the other hand, have a low diffusivity, which might alter the wall's heat buildup. As a result, when the sun heat is high, in the summer weather conditions, an overheating problem might arise [64]

$$Eff = \sqrt{\lambda \cdot \rho \cdot C_p} \quad (2.3)$$

$$Diff = \frac{\lambda}{C_p \cdot \rho} \quad (2.4)$$

$$417 [J.K^{-1}.m^{-2}.s^{-1/2}] \leq Eff \leq 775 [J.K^{-1}.m^{-2}.s^{-1/2}] \quad (2.5)$$

$$0,1 \times 10^{-6} [m^2.s^{-1}] \leq Diff \leq 3,6 \times 10^{-6} [m^2.s^{-1}] \quad (2.6)$$

$$diff = (9.75 \times 10^{-4})\rho^2 - 0.152\rho + 0.0109(\%RH) + (8.76 \times 10^{-3})T + 6.2 \quad (2.7)$$

$$diff = (-3.28 \times 10^{-4})\rho^2 - 0.0429\rho + (8.2 \times 10^{-4})(\%RH) + (8.96 \times 10^{-4})T - 0.96 \quad (2.8)$$

$$diff = (1.29 \times 10^{-6})\rho^2 + (-9.44 \times 10^{-3})\rho + (-8.32 \times 10^{-4})(\%RH) + (4.3 \times 10^{-4})T + 1.01 \quad (2.9)$$

Chapter 2. Straw Bale Scale

2.3. Water vapor diffusion factor and thickness

The vapor diffusion resistance factor μ of construction materials is a decisive element in terms of condensation in building insulation applications. It indicates the ability of a material to allow water vapor passage [67]. For the same material, measurements taken at various degrees of relative humidity (dry-cup and wet-cup) may provide different results. This is due to surface diffusion, which is more evident at greater humidity levels. In porous materials such as straw, diffusion takes place in the pores. According to [68], μ can be defined by equation (2.10).

$$\mu = - \left(\frac{\delta_{air}}{g_v} \right) \cdot \frac{dp}{dx} = \frac{\delta_{air}}{\delta} \quad (2.10)$$

where g_v is the flux density, δ is the diffusion coefficient at a specific temperature, δ_{air} is the diffusion coefficient of the air and p is the pressure.

The French network for straw bale construction (RFCP) [10] measured the μ -value for dry straw bales having a density of about 100 kg/m^3 . The tested bale had a μ -value of 1.15. Labat *et al.* [69] found that a straw-clay sample with a density of 350 kg/m^3 had two distinct values for the water vapor diffusion factor of 2.92 (using the wet cup technique) and 4.77 (using the dry cup method). Marques *et al.* [62] used the dry cup method to determine the water vapor diffusion factor for rice straw bales with densities ranging from 80 kg/m^3 to 100 kg/m^3 . This parameter varied from 3 to 5 regarding the density. Liuzzi *et al.* [37] measured the water vapor diffusion factor according to EN 12086 [70]. They found a value of 2.59 ± 0.78 for a straw bale mixed with sodium silicate solution and having a density of 152 kg/m^3 .

The vapor diffusion thickness sd is computed using a number of assumptions, including constant temperature and μ -value. If the air's vapor diffusion resistance is the same as the material layer's thickness s , then both flux densities are identical, and the material's thickness sd is given by equation (2.11). The sd -value of straw, for example, is 0.41 m for a thickness of 36 cm and μ of 1.15.

$$sd = \mu \cdot s \quad (2.11)$$

2.4. Mechanical properties

The mechanical behavior of a bale depends on two main parameters; the strain ε and modulus of elasticity E , calculated by equation (2.12) and equation (2.13), respectively. These parameters depend on the height (L), its variation (ΔL), and the stress (σ).

$$E = \frac{\Delta L}{L} \quad (2.12)$$

$$E = \frac{\sigma}{\varepsilon} \quad (2.13)$$

Konecny *et al.* [71] investigated the effect of fiber orientation on the mechanical properties of wheat straw bales 70 cm long, 40 cm wide, and 30 cm high. As shown in **Table 2.5**, the samples had perpendicular and parallel fiber orientations with varying densities. A plywood board was utilized with three wood beams to spread the load during the compression tests. Ashour *et al.* [14] evaluated straw bales positioned horizontally and vertically, i.e. perpendicular to the load direction and parallel to the load direction, to demonstrate their mechanical properties using the compression test. The density of the bales was 102.6 kg/m^3 in all cases, with a moisture content of 11%. According to the case in question, the bales were 61 cm long, 36 cm high and 43 cm wide. From 2 kN to 10 kN, the vertical force applied to the bale was raised by unit increments. A dimension measurement was performed after each increment. The results of these tests are shown in **Figure 2.4** and **Table 2.5**. Straw bales were found to be very deformable. The vertical strain of vertically oriented bales was almost proportionate to the applied load. **Figure 2.4** shows an inflection at 10 kN when the straws were squeezed, accompanied by a crushing sound. In the opposite example, when the fibers are perpendicular, an initial linear deformation of up to 8 kN was followed by a substantial softening and hardness. In the examined cases of **Table 2.5**, complete recovery was not seen, but Ashour *et al.* [14] found that straw bales were restored to their original dimensions after unloading.

Chapter 2. Straw Bale Scale

Table 2.5: Straw bale load-deformation characteristics (based on [71])

No.	Experimental data				Results			
	Fiber orientation	Density (kg/m ³)	Load rate (mm/s)	Load (kN)	Deformation (mm)	Stress (kPa)	Strain (%)	Modulus of elasticity (kPa)
I-1	parallel	No data	0.05	9.4	22.5	26	7.5	347.7
II-1	parallel	83.6	0.2	9.7	46.9	28.2	15	187.7
II-2	parallel	83.4	0.2	8.8	48.6	28.1	15.3	183.5
III-2	perpendicular	92.9	0.4	8.4	38.4	21.3	12.7	167.8
III-3	perpendicular	97.5	0.4	7.6	56.4	20.2	18.5	109.2
III-4	perpendicular	80.6	0.4	13.8	54.7	32.4	17.2	188.2

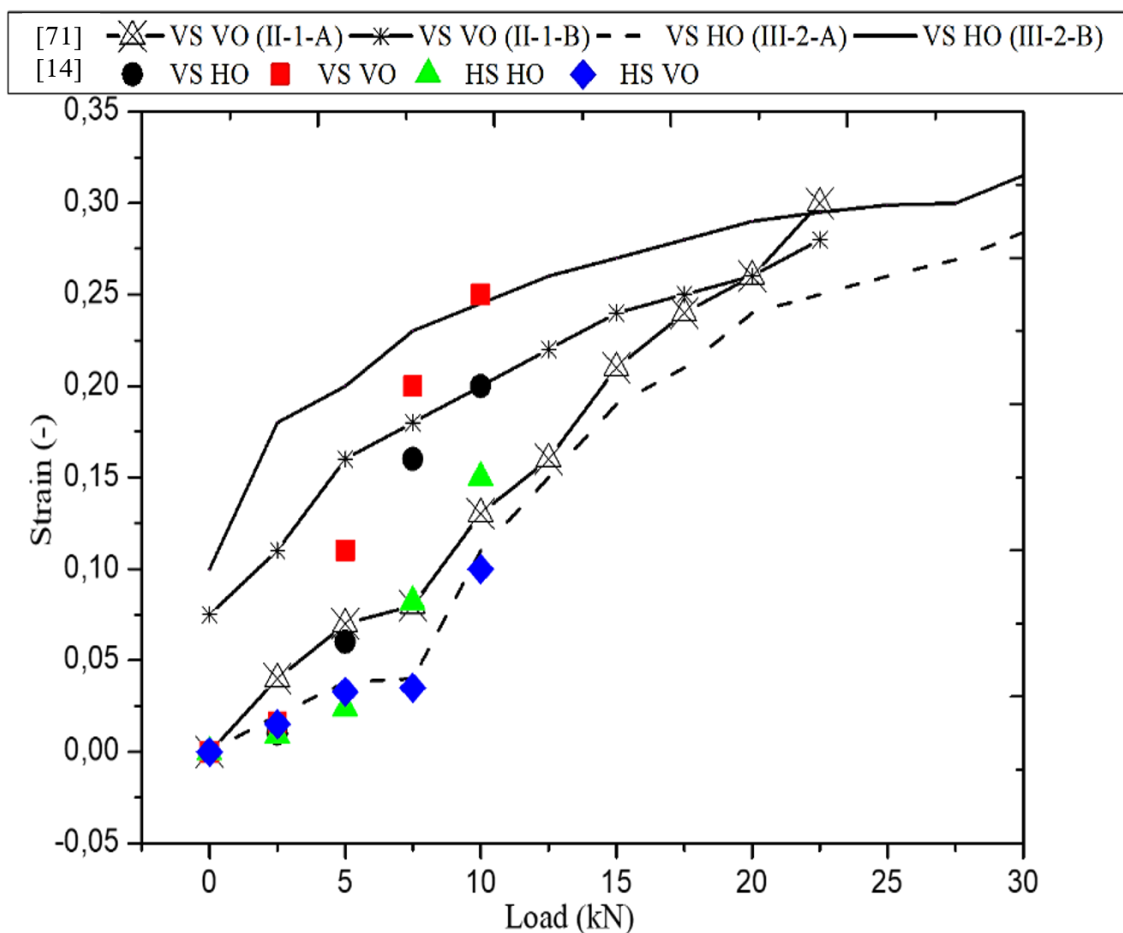


Figure 2.4: Vertical and horizontal strain variation (VS and HS) according to the applied load for bales oriented horizontally and vertically (HO and VO) (A the first loading path and B the second loading path) (based on [14,71])

Chapter 2. Straw Bale Scale

In both experiments, the horizontal bales had lower stresses and strains than the vertical bales. The horizontal bale's maximum strain was 0.2, whereas the vertical bale was 0.25. Furthermore, the graph revealed that the strain variation was nearly proportionate to the load and that the resistance of bales to deformation increased over time. These investigations indicated that horizontal and vertical bales have nearly identical anisotropic behavior. It is worth noting that horizontally oriented bales have better resistance to deformation, implying that the building structure is more stable.

During the experiments to assess the elasticity of the straw bales, the deformation modulus, also known as the elasticity modulus, was studied. The modulus of elasticity varies with the load fluctuations, as seen in **Figure 2.5**. When the applied load rose, this value dropped. To conclude the investigation, Ashour *et al.* [14] provided the stress-strain curve, shown in **Figure 2.6**, which is used to compute the modulus of elasticity. At low loads, the strain fluctuation was nonlinear. These outputs assure the bale's ductile nature by allowing it to absorb a large amount of applied energy. The vertical and horizontal straw bales reverted to their original proportions after 13 minutes of compression testing and resetting the load. Ashour *et al.* [14] and Konecny *et al.* [71] experiments showed the same modulus of elasticity as seen in **Figure 2.6** and **Table 2.5**. The modulus of elasticity ranged between 160 kPa and 189 kPa while the densities were between 80 kg/m³ and 100 kg/m³.

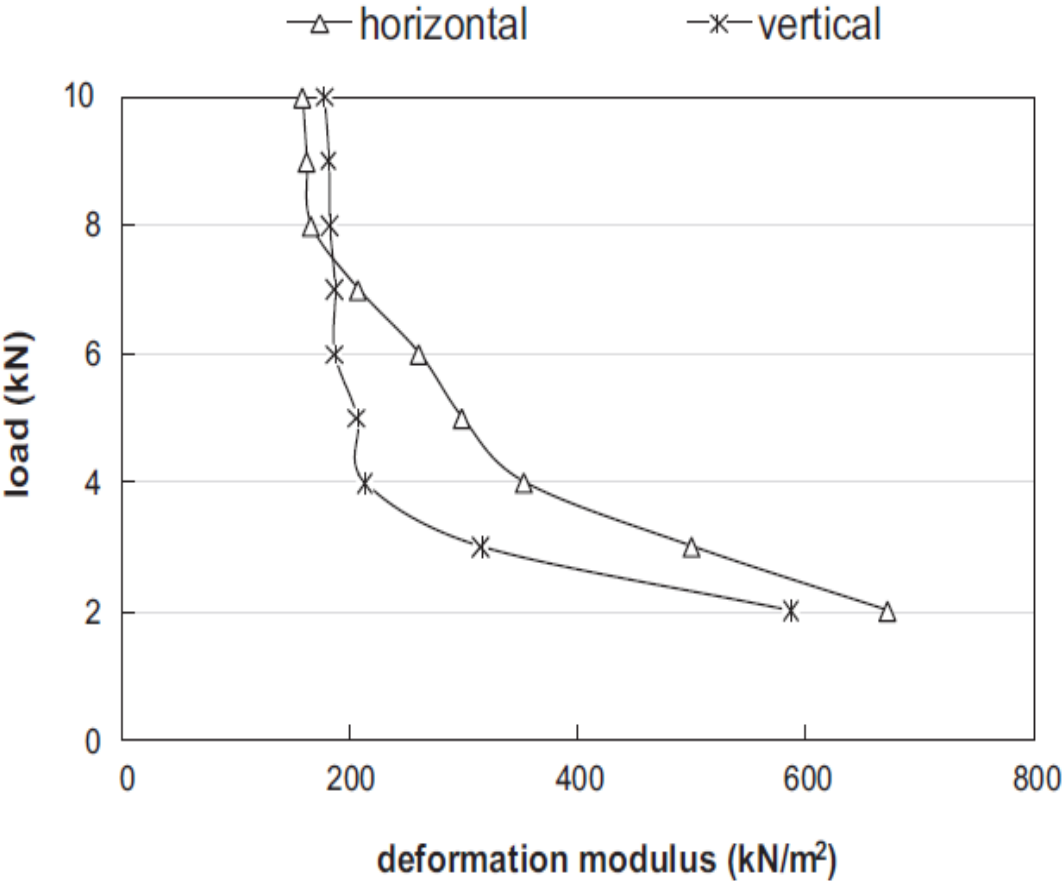


Figure 2.5: Variation of the deformation modulus of bales oriented horizontally and vertically [14]

Chapter 2. Straw Bale Scale

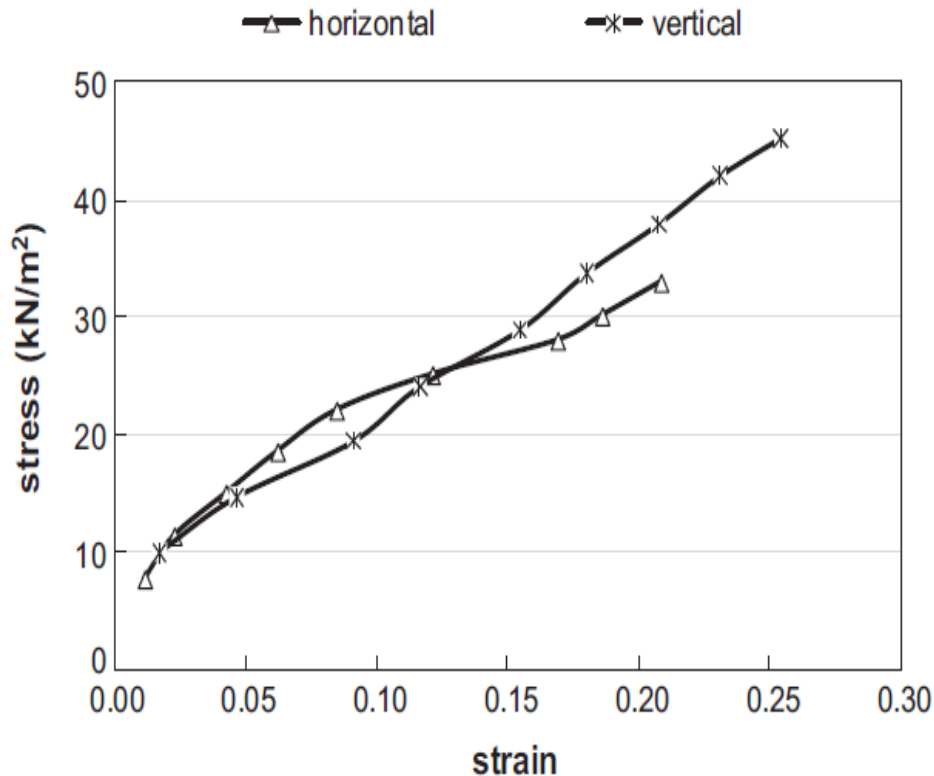


Figure 2.6: Stress-strain behavior for bales oriented horizontally and vertically [14]

According to [72], the straw has a modulus of elasticity varying from 200 kPa to 800 kPa for densities between 115 kg/m^3 and 140 kg/m^3 . Ashour *et al.* [73] explored the mechanical behavior of plastered straw bales. The modulus of elasticity of this type of construction was about 9.45 MPa. According to Goodhew *et al.* [74], the ultimate load for the unplastered wall was 19.2 kN/m, while it was 66 kN/m for the lime-plastered wall using the same procedure. In addition, in the first example, a deflection of roughly 170 mm was detected, whereas, in the second situation, a deviation of around 55 mm was noted. In the second example, the lime coating increased the wall's resilience. Vardy and MacDougall [75] investigated plastered wheat bales with dimensions of 30 cm x 40 cm x 60 cm and a density of 85 kg/m^3 . The modulus of elasticity for on-edge bales was 18 MPa, and the ultimate load was around 30 kN/m, whereas the modulus of elasticity for flat bales was 12 MPa, and the ultimate load was 60 kN/m. According to Konecny *et al.* [71], the observed modulus of elasticity is largely dependent on the density of the tested sample, including humidity, fiber orientation, straw type, growing region, and bale preparation.

2.5. Discussion and perspectives

Before being employed, the bale, which is considered a non-structural wall divider, should be thermally and mechanically examined. The behavior of the walls and the entire structure is determined by this part's characterization. The majority of investigations, according to the available literature, focused on the fluctuation of thermal conductivity of the bale with regard to density, temperature, humidity, and fiber orientation. The results for thermal conductivity varied from 0.03 W/m.K to 0.19 W/m.K, indicating that the material possesses insulating properties and that density, temperature, relative humidity, and fiber orientation are parameters to meticulously adjust to maximize the bale's thermal insulating capabilities. Straw bales are tough and strong from a mechanical standpoint because they may recover quickly once compressive stresses are removed. The thermal conductivity, as well as the bale thermal capacity, effusivity, diffusivity, and diffusion factor of water, were not numerically confirmed. Sensitivity analysis studies are needed to assess the factor that impact highly the characteristics of the straw. Similarly, numerous additional mechanical tests may be made to determine the impact of parameters such as load intensity, load direction, dynamic load rate, bale density, straw type, fiber orientation, and Young's modulus of the straw bale

3. Straw wall scale

This chapter presents the existing literature on straw construction at the wall scale. The bales’ density, thickness and moisture content, as well as the other wall layers such as finishing plaster, affect straw walls U-value, the most important property in presenting the thermal insulation capacity of a wall. This chapter shows the hygric and thermal behavior of a straw wall and its different reported U-values that affect the time lag and the decrement factor of the wall. In addition, this chapter adds other studies that investigated the acoustic properties of straw wall. At the end, it was found that further are needed in order to predict moisture issues that may occur because of the exterior and interior climates.

Table of contents

3.1. Hygrothermal properties25

3.2. Acoustic performance.....27

3.3. Fire resistance.....29

3.4. Economic and environmental performance.....31

3.5. Straw embedded in composite construction materials.....33

3.6. Discussion and perspectives.....34

Chapter 3. Straw Wall Scale

3.1. Hygrothermal properties

The wall's inner temperature and relative humidity are influenced by its surrounding environment as well as the properties of the layers composing it. The orientation and placement of the wall indicate the quantity of solar radiation and absorb rainwater, and temperature and humidity fluctuations owing to climatic change. According to Walker *et al.* [12], the aerobic and anaerobic degradation of straw is dependent on the amount of time it was exposed to humidity, water, and severe outdoor conditions. Mesa and Arengi [13] investigated the hygrothermal characteristics of 38 cm straw walls with lime plaster on the outside and clay plaster on the inside by adjusting the temperature and humidity of a climatic chamber. The experimental data were then compared to the computational results generated using a WUFI model, which was found to be similar. It was noticed that the temperature achieved equilibrium after three days, whereas the humidity reached equilibrium after 10 days. This characteristic is explained by the high thermal and moisture storage capacity of the straw. To explore the change of temperature and RH at different levels in a straw wall, Ashour *et al.* [14] conducted an experimental investigation on a ground stage wall in Germany. Mud stucco was used to cover the straw, which had a total thickness of 50 cm. At a height of 140 cm from the floor, the sensors (RH and T) were mounted on the surfaces and within the wall. Despite the severe temperature and the differences between day and night, the temperature sensors within the straw bales indicated a roughly steady temperature. The smoothed internal temperature variation showed the ability of the straw to decrease the influence of outside temperature changes on the interior temperature. The low difference between the temperature of the exterior plaster and the temperature at a distance of 20 cm within the bale was noticed because of the thermal insulation offered by the straw bales. The mentioned insulation characteristic of the straw explains also the indoor thermal comfort. **Figure 3.1** depicts the progressive drop of the straw layer average temperature from 23.6 °C to 23.2 °C after 450 hours.

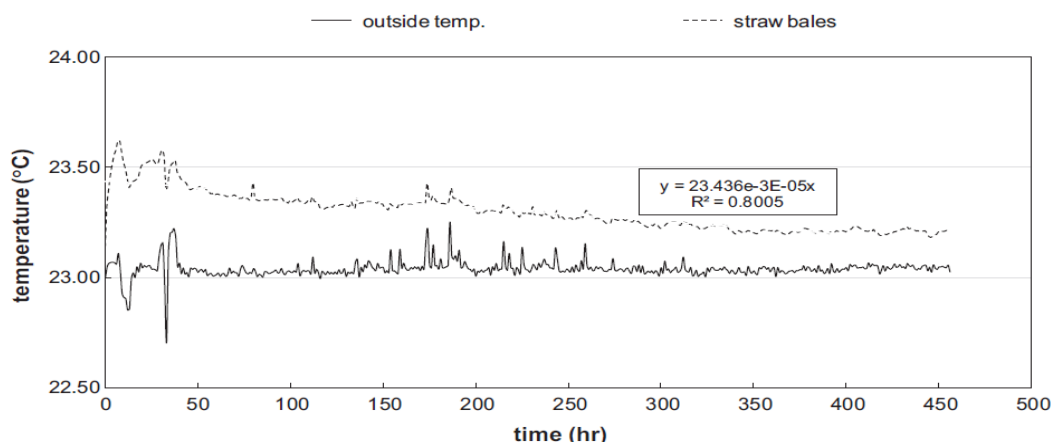


Figure 3.1: Variation of straw temperature (dotted line) and outside temperature (black line) as a function of time [14]

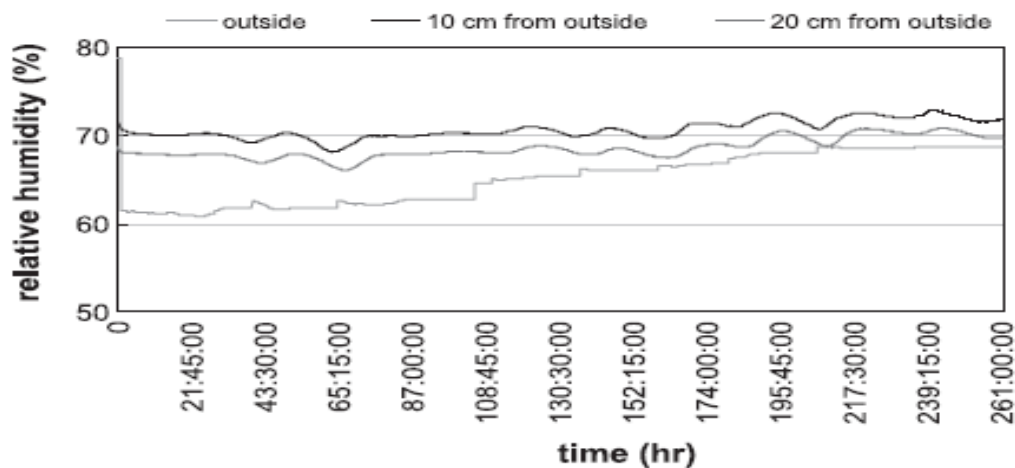


Figure 3.2: Relative humidity in different locations in the straw bale wall [14]

Chapter 3. Straw Wall Scale

Ashour *et al.* [14] also tracked the fluctuation in humidity in the straw wall, as seen in **Figure 3.2**. During the 24 hours, the difference in RH between the exterior and interior of the bale reduced from roughly 10% to 7%. After 261 hours, the disparity continues to shrink, reaching roughly 2.63 %. The RH curves revealed that humidity absorption was slow, since it may take more than 300 hours to reach the outside RH value. It was noticed in this experiment that the RH movement through the straw wall is minimal and that the straw walls give enough thermal comfort indoors.

Thomson and Walker [76] followed the temperature and humidity fluctuations of a 36 cm straw bale wall with 3.5 cm of outside lime layer subjected to a wind-driven wet climate for three years to track moisture-induced deterioration. As a result, the outside layer was shown to be the source of the initial increase in RH. During the experiment, it was discovered that mold would form at some RH levels at specified temperatures as indicated in **Figure 3.3**. To verify this result, a core of the outer layer was extracted from the lower half of the wall to conduct a gravimetric measurement of the straw moisture content. Moisture content was found to be 28.5% more than 20%, which speeds up the material breakdown. A degradation test was also carried out to track the microorganism's progress by adjusting the temperature and humidity to 21.5 °C and 87 %, respectively, and by measuring the CO₂ level. Straw at 28.5% MC was found to be safe from bacteria development because the CO₂ level used as a mold indicator, stayed steady for around 20 days.

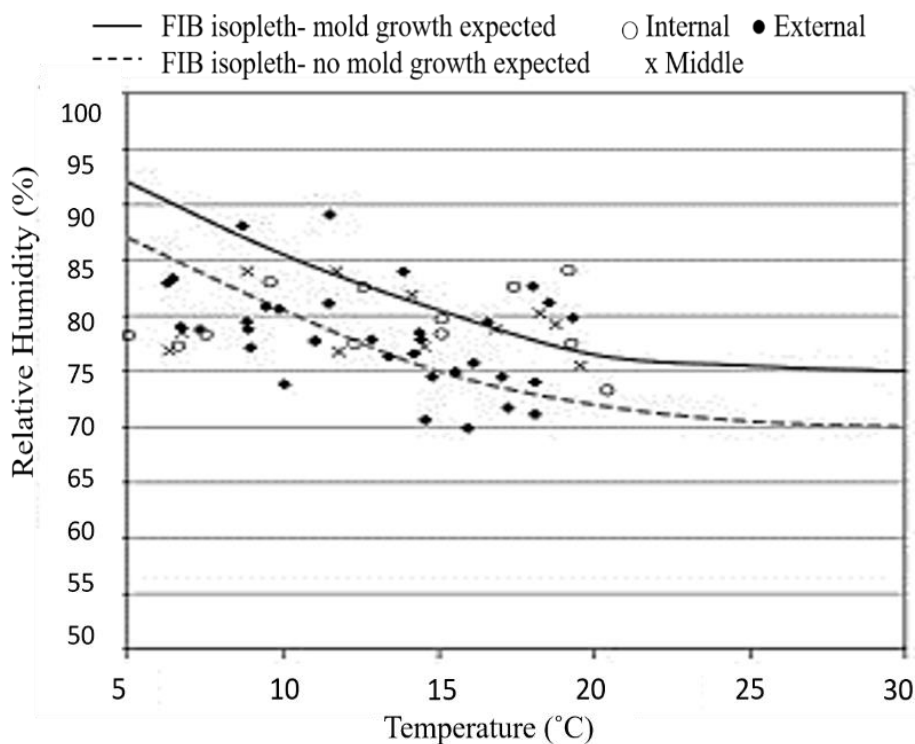


Figure 3.3: Variation of the relative humidity while varying the temperature at a different location in the wall between 2009 and 2012 with respect to the Fraunhofer Institute isopleth limits (FIB-Mold expected growth) [76]

Robinson *et al.* [77] evaluated the influence of moisture content in straw walls of a test house having a floor area of 8.5 m² that was coated twice with a 20 mm lime mortar layer with a 12-day break between each treatment. The coating procedure is done in stages to increase water absorption. The application of a moist layer on top of a dry layer had no impact on moisture absorption. Between days 0 and 12, and days 21 and 37, respectively, a 5% rise in moisture was noticed following the application of the first layer on the exterior and inner sides. Furthermore, it was discovered during the experiment that the moisture level of the straw bales ranged between 20 % and 25 %.

Rice straw walls were experimentally examined by Sabapathy and Gedupudi [78] to demonstrate their hygrothermal properties. The walls were 10 cm thick and were part of a 4 m² cell. On the outside and interior of the walls, a thermocouple network was built. Temperature and humidity sensors also monitored indoor and outdoor air quality. The indoor and outdoor relative humidity (RH) ranged from

Chapter 3. Straw Wall Scale

40 % to 80 % and 50 % to 95 %, respectively. Indoor and outdoor temperatures averaged 28 °C and 40 °C, respectively. Even though the walls were exposed to high humidity levels for a long period, the straw did not store a large amount of water. Lime renders and clay plasters generally used to cover the straw layer have an important vapor permeability, which prevents the moisture deterioration of the material. To reduce the moisture issues, Walker *et al.* [12] suggested quantitatively assessing the hygrothermal performance of the straw wall before beginning construction. Based on the local circumstances, steady-state and dynamic models can determine if the moisture risk within the building exists.

To estimate the wall thermal inertia the surface temperature variations may be utilized to calculate the time lag and decrement factor as detailed in equation (3.1) and equation (3.2), respectively. The time lag is the length of time it takes for a heat wave to go from the outside to the inner surface, and it is determined by the maximum temperature of the interior and exterior surfaces ($t_{int,max}$ and $t_{out,max}$). The decrement factor is the ratio of inner to exterior surface temperature fluctuations, and it is determined by the highest and minimum temperatures of the interior and external surfaces ($T_{int,max}$, $T_{int,min}$, $T_{out,max}$ and $T_{out,min}$). A large time lag ($\phi > 10$ hours) indicates strong dynamic thermal performance, whereas a time lag $\phi < 6$ hours indicates poor performance. A smaller decrement factor implies greater ability of the wall to reduce the amplitude of the periodic heat wave conveyed.

$$\phi = t_{int,max} - t_{out,max} \quad (3.1)$$

$$f = \frac{T_{int,max} - T_{int,min}}{T_{out,max} - T_{out,min}} \quad (3.2)$$

The results of Douzane *et al.* [52] revealed a 6-hour time lag and a 0.08 decrement factor. Gallegos-Ortega *et al.* [59] conducted research on a straw house in Mexico and discovered a 9.12-hour time lag and a 93.5 % temperature drop, despite the fact that the RH within the straw was only approximately 10 %.

The U-value is used to determine the thermal insulation of the wall and its capacity to resist heat transfer from the system to the environment or vice versa. The U-value of a straw wall in Montholier [55] composed of 36 cm of straw with 2-cm lime plaster coatings and 2-cm hemp-lime plaster was found to be 0.25 W/m². K. The low thermal conductivity of 0.095 W/m.K suggests excellent thermal stability. Rye and Scott [79] found a U-value of 0.16 W/m². K for a 43.5 cm straw wall covered by lime plaster. For a wall composed of a 1.3 cm interior plasterboard, 2.7 cm air gap, 20 cm straw, 2 cm air gap, and 2.5 cm exterior stone panel, Cascone *et al.* [61] found a U-value of roughly 0.281 W/K.m². Barbara [80] found that a 45 cm unplastered straw wall has a U-value of 0.11 W/m².K, but a wall made up of 10 cm brickwork, 7.5 cm mineral fiber, 10 cm light concrete block, and 13 cm lightweight plaster has a higher U-value of 0.33 W/m².K. Those values might be compared to those of a wall made of 10 cm concrete block, 7.5 cm mineral fiber, 10 cm concrete block, and 1.3 cm plaster has a U-value of 0.4 W/m².K, whereas another made of 10 cm concrete block, 7.5 cm mineral fiber, 10 cm concrete block, and 1.3 cm plaster which has a U-value of 0.29 W/m².K. These results highlight the important thermal insulation of straw.

3.2. Acoustic performance

Building acoustics is the science that investigates sound reflection, absorption, transmission, and insulation to control noise and create a room with special acoustic characteristics. Sound is a pressure wave that propagates in the air or through any material. To prevent these waves from passing through the wall they should be absorbed [60]. This can be achieved by giving the structure sufficient mass using low porosity and high-density materials. According to ISO 10140-2, the sound absorption coefficient and the sound reduction index are used to examine the sound resistance of a wall, as indicated in equation (3.3) and equation (3.4), respectively. These equations depend on the incident and the radiated sound power (W_1 and W_2) and the sound power radiated by the surrounding elements around the tested wall (W_3). The standard walls sound reduction index surpass 60 dB [81].

Chapter 3. Straw Wall Scale

$$R = 10 \log \frac{W_1}{W_2} \tag{3.3}$$

$$R_w = 10 \log \frac{W_1}{W_2 + W_3} \tag{3.4}$$

Straw bales are characterized by their high porosity and low densities but once applied to a wall, it shows acceptable sound resistance. D'Alessandro *et al.* [60] determined experimentally the acoustic properties of a straw wall at frequencies ranging from 50 to 1600 Hz. Before being applied to the structure, the bales had a density of 55 kg/m³. **Figure 3.4** depicts the sound absorption coefficient at 7 cm and 5 cm from the inside surface. The sound absorption coefficient at 7 cm was larger and reached 0.78 before dropping to 0.6 at 1.6 kHz. The growing and then reducing behavior at both sites verified the porous nature of the straw. The same behavior and shape curve was found by Trabelsi and Kammoun [82] which characterized a 45 cm thick straw wall. The bale's density was 120 kg/m³ and the superficial density of the unplastered and plastered straw wall was around 52 kg/m³ and 67 kg/m³, respectively. The findings show that at middle and high frequencies, the acoustic absorption coefficient is 58 dB. This value is acceptable in the construction field. Trabelsi and Kammoun [82] also compared straw walls to stone walls. Straw walls exhibited greater reduction index values, although only by 1 to 10 dB depending on the frequency. The same test was repeated on a 50 cm straw bale wall. The result can be seen in **Figure 3.5**. The apparent sound reduction index was 42 dB at 500 Hz. This experiment demonstrates through the obtained curves acoustic performance similar to the previous studies.

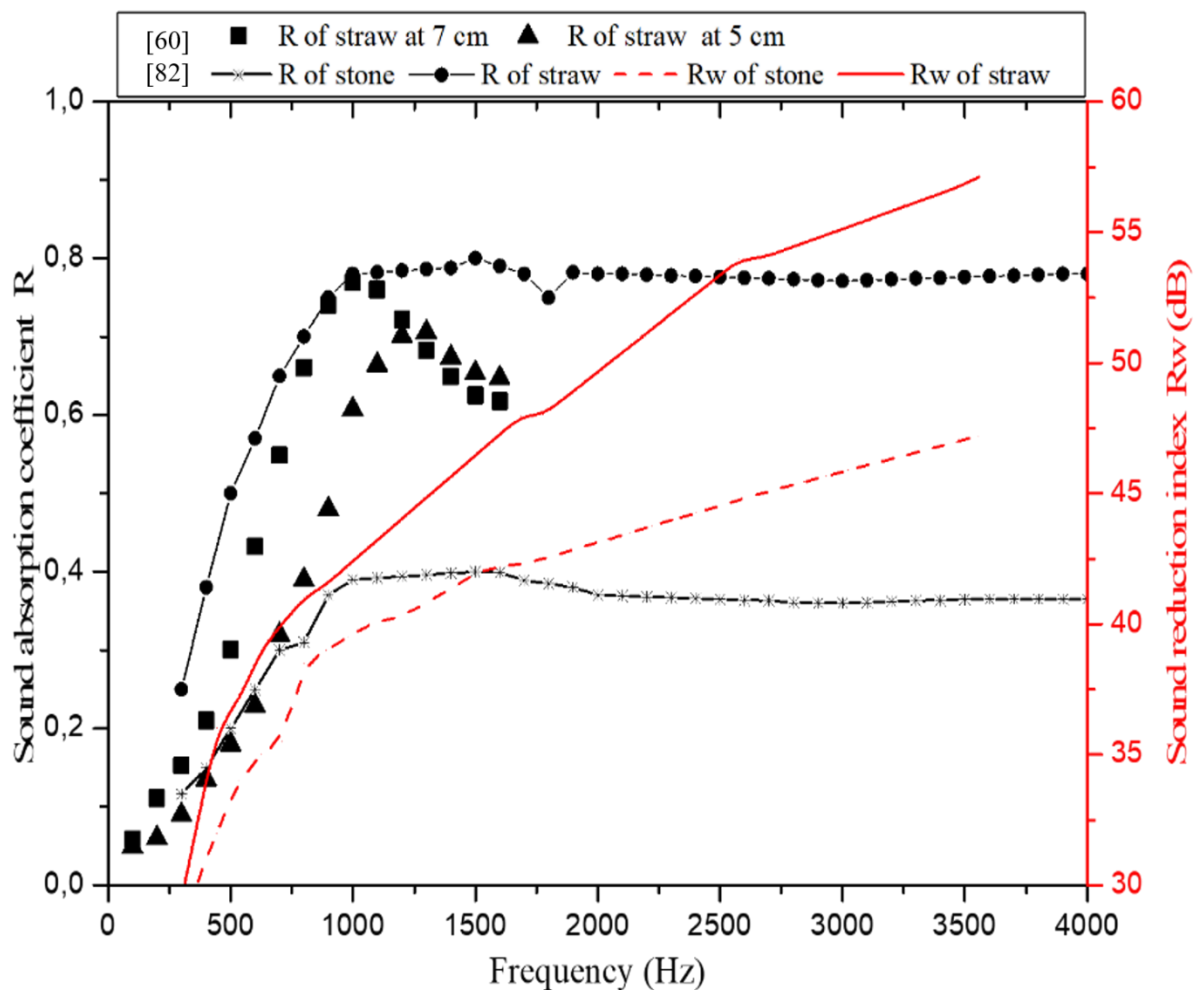


Figure 3.4: Sound absorption coefficient and sound reduction index of straw and stone (based on [60,82])

Chapter 3. Straw Wall Scale

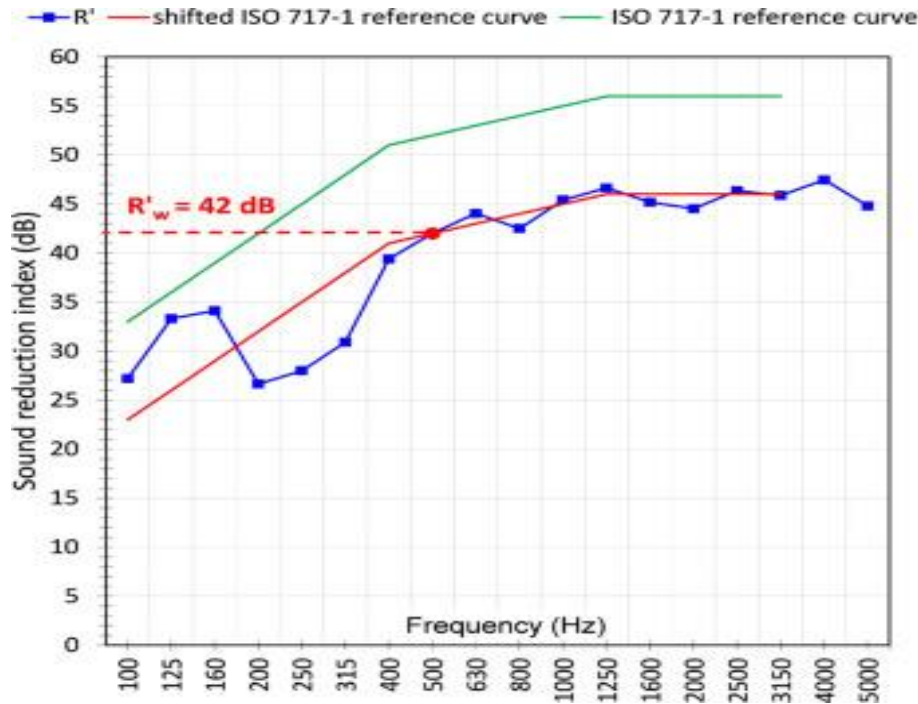


Figure 3.5: Sound reduction index of a 50 cm thick straw wall according to the ISO 717-1 [60]

Dalmeijer [83] recorded a sound reduction index of 53 dB for a 46-cm-thick straw bale wall covered with 2.5 cm and 3.5 cm thick clay layers at the inside and outside surfaces, respectively. Wall *et al.* [84] recorded a sound reduction index of 44 dB for a 35 cm straw wall covered by 3.5 cm of lime render layer. The experiment consisted of monitoring the background noise to determine the reduction of the sound index after generating 100 dB of white noise to the outer side.

The study of walls' acoustics has gained attraction in the building industry since it has the potential to improve indoor comfort. As a result, building materials should be able to both absorb and resist the propagation of sound waves. The experiments showed that the sound reduction index of straw walls varies between 42 to 53 dB depending on its thickness and outside/inside surface layers.

3.3. Fire resistance

The capacity of a structure to withstand fire is known as fire resistance, the important factor that determines its security. Standard fire testing in accordance with ASTM E119 and ISO 834-1 has been used to calculate fire resistance ratings in hours based on equation (3.5) and equation (3.6) [85]. These equations that give the air temperature of the furnace (T) depend on the test time (t) and the initial material temperature (T_0). The test can be done by using laboratory furnaces to model the fire through the wall.

$$T = 345 \log_{10} (8.t+1) + 20 \quad (3.5)$$

$$T = 750 [1 - e^{-3.79553\sqrt{t}}] + 170.41 \sqrt{t} + T_0 \quad (3.6)$$

On a small scale, straw bales were demonstrated, by [86], as a fuel product with low flashover (B), low smoke (S1), and no flame droplets (d0). The low oxygen level in bales after compression explains these features since they do not promote burning [87,88]. Janowska-Renkas *et al.* [89] observed the material behavior of straw bale samples covered by clay once subjected to a direct flame using a thermal imaging camera. The clay prevented the flames from reaching the straw. After 15 min, it burnt out and the flame reached the straw at a 3 mm depth. Despite charring, when the torch was off, no fire spread was observed inside the samples due to their good density (above 108 kg/m³).

Chapter 3. Straw Wall Scale

On a bigger scale, the international building code [90] requires, for walls, a fire resistance rating of between 2 and 4 hours depending on their composition. For this purpose, several tests were conducted to classify a straw wall. In 1980, the National Research Council of Canada [85] showed that straw walls covered by a cement layer could resist fire temperatures above 1000 °C for two hours. Similarly, Theis [91] compared the resistance of unplastered and plastered straw walls. The temperature fluctuations in the first type barely fulfilled the required standards of 2 hours resistance while in the second type the resistance increased to up to 3 hours. During the experiment, it was discovered that the junctions between the bales were vulnerable areas since the burns appeared there first. In 2001, two different studies in Austria [86,87] and Denmark [91] investigated plastered straw walls under high temperatures and direct flames. The wall withstood for 90 minutes in the first trial, but only 30 minutes in the second when the first fracture appeared, and there was no temperature variation on the unexposed side of the wall. In 2006, in the United States, the Ecological Building Network [85,92] tested a 15.5 m² non-loadbearing straw bale wall covered by a 1.3 cm cement layer. The temperature variation of the unexposed surface and the furnace temperature, which adhered to the standard, are given in **Figure 3.6**. The wall passed the two hours limit at 1900 °C and the unexposed surface temperature reached the 150 °C.

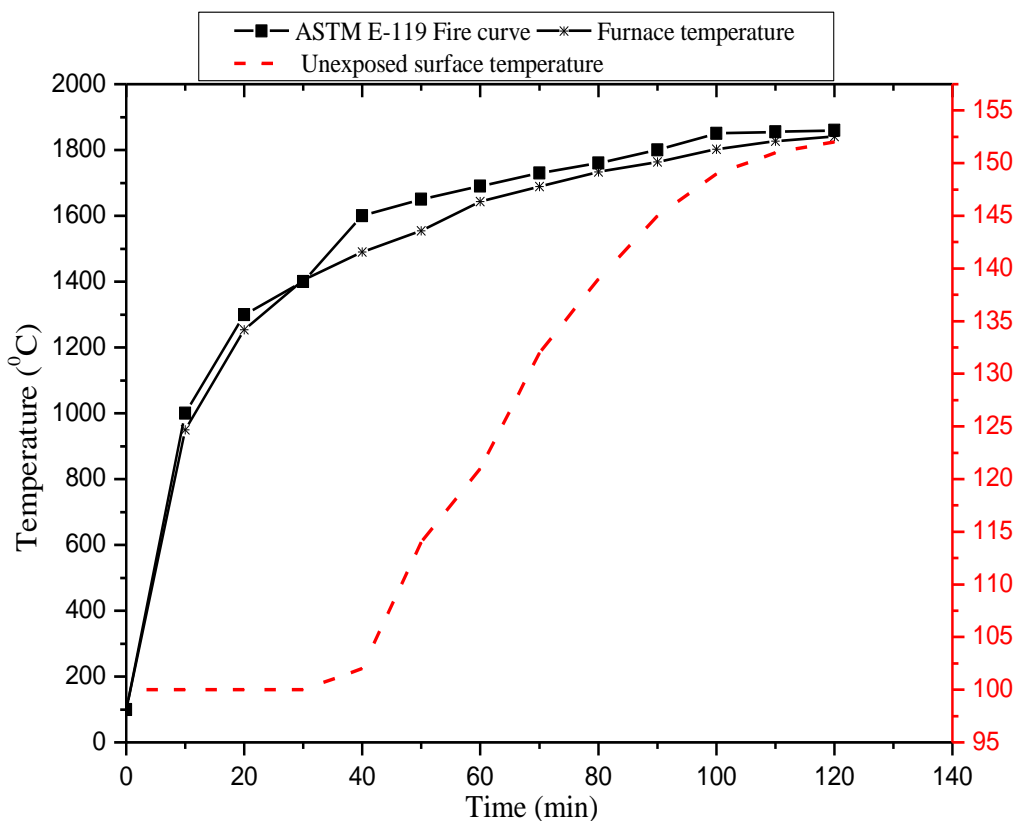


Figure 3.6: Temperature-time curve of the ASTM E-119, the furnace, and the unexposed surface of the straw bale wall (based on [85])

Furthermore, loadbearing plastered straw walls were tested in accordance with Czech norms, to demonstrate the effect of compression on fire resistance by increasing the applied load rate [85]. The wall resisted fire for 2 hours and 26 minutes when loaded at 200 N/s, but only for 1 hour and 6 minutes when loaded at 333 N/s. In 2009, Wall *et al.* [84] examined the fire resistance of a straw wall coated by a lime render layer. At a total air pressure of 101345 Pa, the furnace temperature was increased to 700°C for 30 minutes, then to 900 °C for 44 minutes until reaching 1000 °C. After 90 minutes, the lime render started to peel away from the wall and after 135 minutes, the wall crashed. The temperature on the opposite side of the wall rose from 13 °C to 50 °C during the experiment. This type of wall surpasses the requirements of UK construction norms by more than four times.

Chapter 3. Straw Wall Scale

In terms of time, a straw-filled structure takes more than two hours to collapse after a fire, several tests yielded excellent results. The type of coating layer and the density of the bales may affect the outcome. As a result, well-covered straw walls may easily be compared to other construction materials.

3.4. Economic and environmental performance

Construction materials as principal components of a building have economic and environmental aspects depending on their properties. The selection of material takes into account the climate conditions, availability, price, and carbon footprint. Lately, to reduce pollution, bio-based materials such as straw bales replaced traditional materials such as concrete hollow blocks. In this regard, to know the environmental and economic performance of straw walls, many studies determined their CO₂ emissions and energy consumption.

Table 3.1 compares walls made of fired bricks to those made of concrete blocks, straw-clay walls, and straw bales. In this experiment, Gonzales [93] studied 140 m² envelopes composed respectively of different materials to determine their thermal transmittance, CO₂ emissions, and the energy needed to construct the wall. Results showed that straw has the lowest thermal conductivity, and straw walls have the lowest CO₂ emissions and energy consumption. This lowest ecological impact is due to the small transportation distance of the straw. The embodied energy of 500 straw bales brought from 700 kilometers distant is about 27 MJ per bale. Szasz *et al.* [94] studied the differences between brick and straw bale walls. Their study showed remarkable differences from a thermal and ecological point of view. Straw walls had a U-value of 0.094 W/m².K, while brick walls had a U-value of 0.2 W/m².K. Brick has a global warming potential (GWP) of 85 kg CO₂/m² and a PEI of 1400 MJ/ m², whereas straw bale has a GWP of -70 kg CO₂/m² and a PEI of 400 MJ/ m².

Table 3.1: Different wall material comparisons [93]

Number of required per m ² of wall	Thermal conductivity (W/(m. K))	Thermal transmittance U-value (W/(m ² .K))	Energy per m ² wall (MJ/m ²)	Emission of CO ₂ (kg CO ₂ /m ²)
85 fired bricks	0.9	3.9	488	30
11 concrete blocks	0.64	3.2	169	9.6
7 straw-clay blocks	0.18	0.86	40	3.4
3 straw bales	0.07	0.16	28	2.5
3 half straw bales	0.07	0.32	14	1.3

Borjan *et al.* [95] also examined the cost and environmental impact of a straw wall and a brick wall, having both a U-value of 0.12 W/m².K. The primary energy (PEI) and global warming potential (GWP) of the examined walls showed a significant difference. The PEI of the brick wall was 985.65 MJ/m² and the GWP was 61.5 kg CO₂ equivalent, whereas the PEI of the straw was around 104.83 MJ/m² and the GWP was roughly -50 kg CO₂ equivalent. **Table 3.2** highlights the cost of each layer composing the straw wall and brick wall based on the Australian market to show the economic advantage of the straw. The prices did not include the structural frame and logistics tools cost. The overall price of the brick

Chapter 3. Straw Wall Scale

wall is found to be 14% more per one-meter square than the straw wall due to the local commodity of straw. It should be noted that in case the straw is imported, the price increases because of the transportation cost.

Table 3.2: Calculation of straw bale and brick wall costs per m² [95]

Walls	Material	Thickness (m)	Price (€/m ²)
Strawbale wall	Loam plaster	0.035	12.07
	Straw bale	0.04	22.5
	Loam plaster	0.02	6.89
	Lime plaster	0.015	6.25
	Total	0.47	47.71
Brick wall	Lime cement plaster	0.02	3.88
	Honeycomb brick	0.25	15.51
	EPS	0.28	31.92
	Lime cement plaster	0.015	2.91
	Total	0.565	54.22

The thermal resistance, environmental effect, and pricing of conventional and straw walls are shown in **Table 3.3**. The difference is observed at the environmental level through the negative greenhouse gas emission of the straw walls. The price of the thermal resistance unit per m² of straw is lower by 33% than the cellular concrete wall. In this study, the total price of the straw wall is more expensive than a conventional isolated wall by 100 euros per m² due to the transportation and the construction technique. In Italy, Mutani *et al.* [96] estimated the cost of a straw wall to be approximately 1200 €/m² and the cost of a regular wall to be around 1500 €/m². This modest differential was most likely attributable to the cheap cost of straw and the high cost of specialist building labor.

Table 3.3: Price and environmental impact of different types of the wall [97]

comparison of conventional walls with straw walls	U-value (W/m ² .K)	Price (€/m ²)	Thermal resistance price per m ² (€/m ²)	Greenhouse gas emission (kg CO ₂ /m ²)	gray energy (kWh/m ²)
Conventional wall isolated from the inside	0.33	166	55	+35	129
Conventional wall isolated from the outside	0.22	185	42	+41	212
Wall with distributed insulation (cellular concrete)	0.26	209	55	+75	208

Chapter 3. Straw Wall Scale

Coated straw wall on both surfaces	0.14	266	37	-14	76
Straw wall with cladding and plasterboard	0.13	231	30	-52	101

To summarize, the straw material's environmental benefits are not its sole advantage; it can also be utilized as a low-cost construction material with great heat resistance. Despite its sometimes-greater price per meter square, straw is a competitive material because of its increased heat resistance that can reduce the energy bills during the building's lifetime, and its reduced greenhouse gas emissions.

3.5. Straw embedded in composite construction materials

Composite building materials are generally durable and mechanically strong due to the combination of the characteristics of the material that compose the final product. They consist of reinforcing a typical material such as concrete or hollow bricks by using natural or synthetic fibers such as straw fibers.

Belhadj *et al.* [98] mixed barley straw with sand concrete to compare the mixture's thermal characteristics to the sand concrete by applying them to the exterior wall of a building in an arid region. By a combination of sand with a mass per volume of 1316 kg/m^3 and cement with a mass per volume of 350 kg/m^3 , the mixture's total density was determined to be 2042 kg/m^3 . The mass per volume values of the sand, cement, and barley were 1245 kg/m^3 , 350 kg/m^3 , and 15 kg/m^3 , respectively, and their mixture total density was about 1895 kg/m^3 . The improvement was not only for the density but also for the thermal conductivity, the time lag, and the decrement factor of the envelope. Firstly, the sand concrete's density decreased by 8% after adding the fibers. Second, the material without fibers had a thermal conductivity of 1.4 W/K.m , which was greater than the material with fibers' thermal conductivity of 1.32 W/K.m . Thirdly, the amelioration of the time lag and decrement factor was estimated by 1 h and 20% respectively.

Zhang *et al.* [99] used straw and cement blocks to cover a solar greenhouse's north wall from the outside to demonstrate straw's capability to store heat and offer adequate thermal insulation. The thermal conductivity of the wall was estimated at 0.075 W/m.K and the volumetric specific thermal capacity was about $0.187 \times 10^6 \text{ J/m}^3.\text{K}$. Results showed that the indoor temperature was higher than the outside by 3.4°C during winter and 11.5°C during summer. These figures demonstrate the ability of the material to store heat and provide good thermal insulation.

Hou *et al.* [100] filled hollow concrete blocks with straw fibers to study the heat and moisture transfer properties of this type of envelope. The thermal conductivity of the straw and the concrete were 0.04 W/m.K and 1.515 W/m.K , respectively, and their densities were 257 kg/m^3 and 2050 kg/m^3 , respectively. The presence of straw inhibited heat and moisture transmission in the building due to its low thermal conductivity and water vapor permeability coefficient.

Sabapathy and Gedupudi [101] added a 10 cm straw layer to a concrete wall to study the effects on the cooling and heating loads of the building. The cooling and heating loads were reduced to 45 W/m^2 and 40 W/m^2 , respectively and the energy savings ranged from 67 % to 96 %.

Ahmadi *et al.* [102] isolated fired clay hollow bricks by using 55 kg/m^3 dense wheat straw bales to study the thermal effect. Results showed that the thermal transmittance of a straw-filled brick wall varied between $0.87 \text{ W/m}^2.\text{K}$ and $1.0 \text{ W/m}^2.\text{K}$, whereas that of an empty brick wall varied between $1.78 \text{ W/m}^2.\text{K}$ and $2.07 \text{ W/m}^2.\text{K}$. The efficacy ratio of energy savings is 42.97 %.

Chapter 3. Straw Wall Scale

Therefore, compressed straw fibers can be used to insulate already existing conventional walls or can be added to conventional construction materials to enhance their mechanical/thermal properties, save energy and reduce the environmental impact.

3.6. Discussion and perspectives

In general, to keep the fibers from deteriorating, the straw walls should be sealed. Plasters have a variety of qualities that might have beneficial or adverse effects on straw walls. It can increase the insulating characteristics and mechanical strength of the straw wall, but it may not create a sufficient vapor barrier. The composition of a straw wall (plaster type, air gap, layer thickness) is crucial and has a significant impact on hygrothermal, environmental and economic performance, but it is also highly reliant on climatic circumstances. As a result, the hygrothermal characteristics of various types of walls must be evaluated and/or computed experimentally and/or theoretically under varied exterior and interior situations. There is a need for further information on the fire tolerance test of various types of walls. In terms of acoustic efficiency, there are few researches on how to improve the sound resistance of the straw wall by adding new layers with the ability to absorb acoustic waves. New studies are also needed to detect the mechanical characteristics of straw walls under high stress, such as testing to determine the wall's capacity to withstand storm and wind power. These tests should compare the straw walls of different layer architectures and suggest ways to strengthen them. These future researches should allow offering simple wall building regulations under different climatic and extreme conditions.

4. Straw building scale

The first part of this chapter presents the main straw bale construction systems and discusses their respective advantages and drawbacks. In the second part, the straw bale construction regulations from different countries are reported. The next part deals with previous works on the life cycle assessment of straw buildings, to show their economic and environmental performance that may fulfill the purpose of the use of bio-based material. At the end, it is noticed that there are still very few numerical studies on the energy behavior of straw-based buildings depending on the wall structures, the building location, and its scenarios of occupation and operation. Based on the energy results, the economic feasibility of such buildings should be more intensively searched, especially in terms of payback period and life cycle cost.

Table of contents

4.1. Construction systems.....	36
4.1.1. Structural bale house or load-bearing method.....	36
4.1.2. Nonstructural bale or infill method.....	37
4.1.3. Prefabricated panels method.....	38
4.2. Regulations on straw construction.....	38
4.3. Energy and life cycle assessment	39
4.4. Discussion and perspectives.....	41

Chapter 4. Straw Building Scale

4.1. Construction systems

Walker *et al.* [12] described three basic types of in situ straw construction known as load bearing, infill, and prefabricated panel methods. To prevent mold and hygric issues, straw bales or walls should be produced and stored in a dry atmosphere for all three techniques mentioned. The minimum acceptable density of a bale is 80 kg/m^3 and it should have a rectangular form, as stated in the preceding sections. The direction of the bale and the fibers inside it determine the wall's mechanical stability. Horizontal fibers and bundles arranged on their largest flat face had the highest performance.

4.1.1. Structural bale house or load-bearing method

This method entails choosing the foundation materials and preparing them before stacking the bales one on top of the other to build a wall [28,103]. Slabs on grade and raised floor foundations are the two most common types of foundations. In some circumstances, it can be adjusted to reduce, for example, the quantity of concrete or other common materials used. The straw blocks are next pinned together and secured to the foundation. This process is continued until the desired height is achieved. The roof plate closes the constructed zone at that height. Because there is no structural structure in this design, the bales bear the weight of the roof. It is important at the end to properly fix the envelopes to stabilize the whole building and to distribute the weight. The technique of building the bales according to the load-bearing system is depicted in **Figure 4.1**.

Small holes between the compressed bales may form, due to irregular flaws in the geometric shape of the bales. Those imperfections cause hygric problems by allowing the water and humidity to cross the wall. To prevent this phenomenon, bundles of straw fibers should fill the holes. The windows, the doors, and every aperture area must be done by specifying their boundaries with wood boxes fixed to the bales while piling up the bales to build the wall. The finishing step in all construction projects is the envelopes coating. In straw buildings, specific plaster types are used to keep moisture out of the wall and improve its acoustic, and fire resistance. Walker *et al.* [12] stated that lime- and earth-based coatings are more popular in Europe, whereas cement (frequently coupled with nonhydraulic lime) coatings are more common in North America.

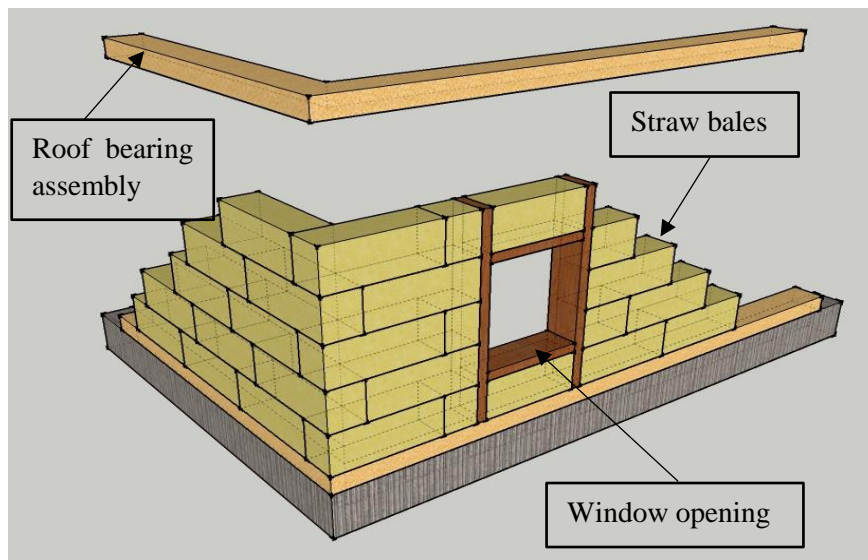


Figure 4.1: Load-bearing wall and roof plate construction [104]

For reasons of safety and stability, the existing approach contains criteria that should be followed [28]. The wall thickness, for example, should be greater than 36 cm since it is an important structural component of the structure. Using huge bales and covering layers, this thickness may usually be readily achieved. The maximum height of a 58.4 cm thick wall is 3.3 m, however skilled engineers can go higher. Furthermore, the applied load or compression load is discovered to be the most essential characteristic that impacts the thermal qualities, fire resistance, and sound resistance. On the top of the straw walls, the live and dead loads are restricted to 1757 kg/m^2 and must be applied at the wall center.

Chapter 4. Straw Building Scale

4.1.2. Nonstructural bale or infill method

This method is characterized by the presence of concrete, steel, or wooden beams and posts in the load-bearing structure. After completing the foundation, the first stage in this procedure is to install the new cited parts. Following that, the bales are used to fill-in the gaps and construct the walls to provide thermal insulation properties. Before the filling step, the bales are compressed and tested to control their initial moisture content. **Figure 4.2** depicts the construction process using the infill approach. The beams and posts rather than the bales support the roof's weight. As previously stated, the envelope should be plastered after the procedure is completed.

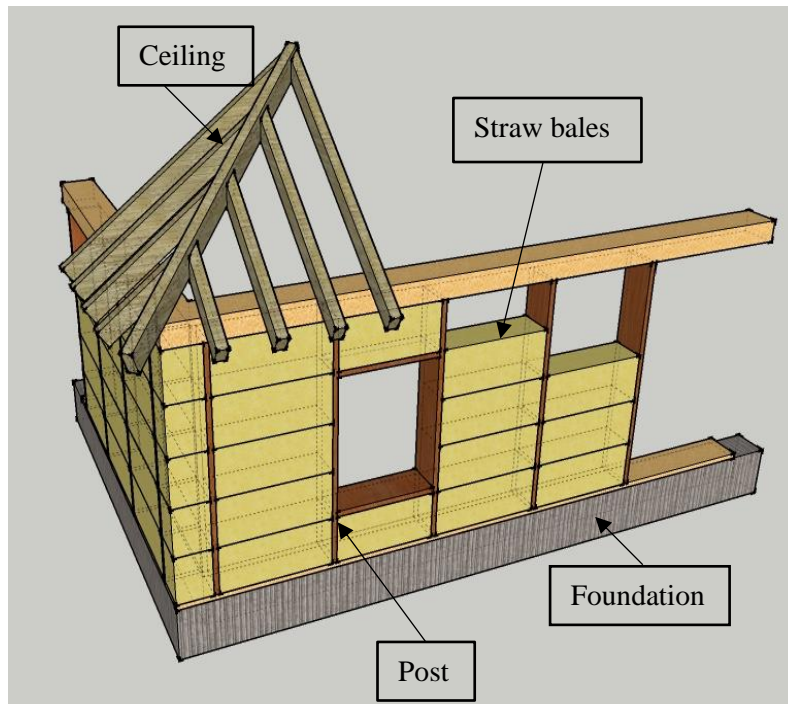


Figure 4.2: Infill wall and structure section [104]

The GREB (Groupe de Recherches Écologiques de la Baie) technique, which has the same steps as the infill approach, is shown in **Figure 4.3**. It consists of putting the straw bales in a double frame mold (timber) and fixing all elements with strips and metal connectors (screws and nails). Thus, both the straw and the timber support the weight of the roof [3,105]. The load should be distributed as evenly as possible throughout the structure.

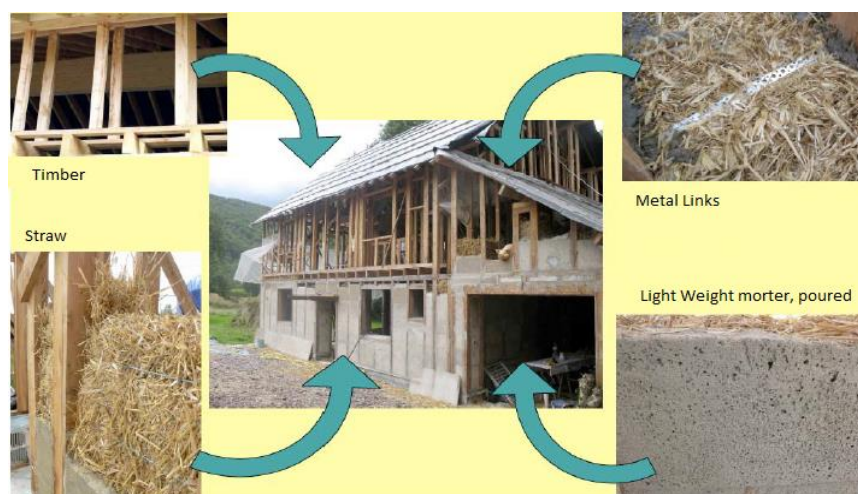


Figure 4.3: Steps of the GREB technique [3]

Chapter 4. Straw Building Scale

In this approach, some rules should be respected to ensure the durability and stability of the building. The foundation and the first row of straw bales should be spaced with at least 15 cm of wood or any other material [28,80]. The length of an unsupported wall with a thickness of 58.4 cm can exceed 3.3 m and reach about 7.6 m. The apertures are considered structural features in this manner, and substantial frames are used to sustain the wall and roof loads. Installations for electrical and plumbing parts can be made on the internal surfaces of walls and roofs, as well as in designated vacant places. The wire or tubes should have a minimum depth of 3.2 cm from the wall's interior finish.

4.1.3. Prefabricated panels method

The basic idea behind this method is to prefabricate boxes and load them with straw bales at the workshop or on-site as shown in **Figure 4.4**. Rainscreen panels and coating can subsequently be applied to the prefabricated wall. The installation varies depending on the building site's limits (size of the elements, machines available, etc.). The boxes can be created out of a variety of materials (solid wood, lattice beams, I-beams, etc.) with varying thermal performance. To prevent hygric issues, the prepared wall should be protected from rain and humidity before applying it in situ.

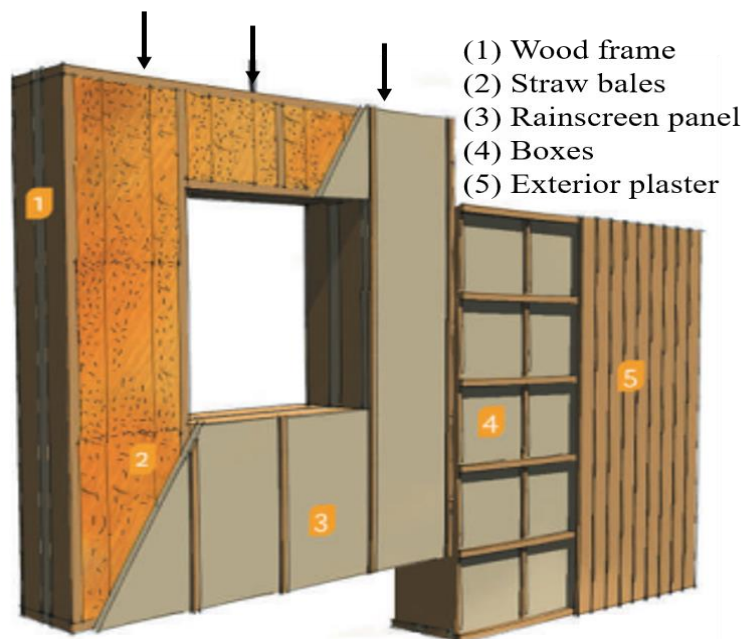


Figure 4.4: Main parts of a prefabricated straw wall [84]

4.2. Regulations on straw construction

Every country has developed its laws in the construction industry to promote human safety and comfort. The layers of building walls, the indoor thermal comfort, the wall sound resistance, and many other important factors are all specified in regulations, as shown in **Table 4.1**. In 2011, straw construction codes were introduced in Canada to include specific information for the type of structure. They were particularly concerned with their thermal and mechanical properties as well as their acoustic and fire resistance. The straw building's endurance was particularly examined, as it is strongly dependent on the moisture content inside the construction. In 2015, the International Residential Code (IRC) included an appendix for bale construction, which began to be used for one and two-story structures [106]. The IRC appendix offers a glossary of words as well as technical information regarding straw bales and straw walls.

Any type of straw, such as wheat, rice, barley, or oat, can be used to make a bale. Rectangular bales with a minimum height and thickness of 30 cm are utilized in the building construction. Synthetic or natural fibers, as well as metal, having a thickness of less than 0.8 cm can be used to bind the bales together to maintain the bale density at around 104 kg/m³. The MC of the bale should not exceed 20% of the total weight. To create a sturdy wall, bales are pinned both internally and externally by steel, wood, or bamboo

Chapter 4. Straw Building Scale

pins with diameters of 13 mm to 19 mm, spaced by 61 cm. If properly maintained and covered, a straw construction can live for 100 years as is the case of the French building that exists since 1920 [107]. Plasters prevent the walls from degradation caused by moisture and microorganisms and strengthen them mechanically. The minimum thickness of the cement, clay, or other materials plasters is 1 cm.

Table 4.1: Different countries' regulations concerning straw bale construction (based on [108])

Country	About the regulation	year
Denmark	The Danish Building and Urban Research Institute published a guide for all testing and design issues concerning straw construction.	1994
USA	The straw bale building code acted as a pioneering document for the industry and the other straw bale building codes.	1996
Belarus	The code includes requirements for the quality, moisture content, and density of the straw bales, which can only be used for insulation infill and not to support the weight.	1999
Germany	Straw can be used only to thermally insulate the building.	2006
Canada	The building code of Canada defined the process of construction, the maintenance procedure, and the fire system of straw buildings.	2011
France and the Czech Republic	The code was carried out by the government. Therefore, straw buildings should have a technical detailed report to obtain a building permit.	_____
Australia	The building Code of Australia classified straw construction as an alternative solution in the building construction sector.	_____

4.3. Energy and life cycle assessment of straw buildings

A typical life cycle assessment of a building concerns the examination of the whole life cycle of the structure starting from the materials manufacturing to the building construction, its usage, and destruction, and finally the materials recycling. Thus, the environmental impact of the building depends on the material that composes it. From here, it can be noticed that a straw building saves energy because of the straw insulating properties and low embodied energy.

In the United Kingdom, Atkinson [65] considered a 40-m² straw based little cottage built using the load-bearing technique. The utilized materials are listed in **Table 4.2**. As can be observed, the used materials embodied energy rates varied between extremely high and very low. The straw wall's total embodied

Chapter 4. Straw Building Scale

energy was estimated at around 2360 kWh, with an average of 73 kWh/m³ for the wall and around 6000 kWh/m³ for the roof. The very high difference between the roof and the wall is explained by the use, for the latter, of bio-based materials having a very low embodied energy. In Switzerland, Chaussinand *et al.* [64] evaluated a 300 m² office structure made of wheat straw and wood frames against two sets of temperatures (winter and summer) using the ASHRAE 14-2002 technique [109]. The total amount of energy consumed was estimated to be roughly 3800 kWh. Knowing that the primary to final energy ratio of the wood is 0.7, the building's primary annual energy (PEI) was estimated to be around 8.9 kWh/m². The results also revealed that 19 m² of solar panels were sufficient to generate yearly the building's mechanical ventilation, residential hot water, and lighting. The annual electricity use was around 2080 kWh, 10% lower than the energy consumption of a typical office building.

Table 4.2: Materials used in the Straw Bale Cabin and its embodied energy classification [65]

		Volume (m ³)	Embodied energy (energy rating)
Foundation	Steel chassis	0.07	Extremely high 0 %
	Supporting timber	0.45	Low 6%
Walls	Wheat straw	28.2	Very low 85%
	Lime plaster	1.35	Medium 7%
	Clay plaster	0.93	Very low 85%
	Plastic straps	---	Extremely high 0 %
Windows and doors	Softwood windows	0.17	Medium 7%
	Double glazed units	0.04	Very high 0 %
	Redwood doors	0.19	Medium 7%
Roof	Cedar shingles	1.3	Very low 85%
	Stainless steel nails	---	Extremely high 0 %
	Roof timber	0.8	Low 6%
	Wood fiberboard	0.45	Medium 7%
	Clay plaster	0.32	Very low
Floor	Plywood	0.12	High 2%
	Timber joists	0.57	Low 6%
	Thermafleece	5.43	Very low 85%
	Floorboard	0.24	Medium 7%

Alcorn and Donn [110] conducted a Life-Cycle Analysis of 18 dwellings (with a total area of 200 m²) to determine the embodied energy and embodied CO₂-eq of the materials. As a result, they discovered that straw bale constructions with a timber frame emit approximately 1900 kg of CO₂ equivalent per year and consume approximately 37.9 GJ of energy per year, whereas a standard house with

Chapter 4. Straw Building Scale

conventional insulation, wood timber, and concrete floor consumes approximately 41.7 GJ of energy per year and emits approximately 2197 kg of CO₂ equivalent per year. These findings demonstrate the value of straw as a bio-based material for lowering heating loads and CO₂-eq emissions.

4.4. Discussion and perspectives

Various building methods have emerged since the introduction of straw as a construction material, such as the load-bearing, frame infill, and prefabricated panels methods. **Table 4.3** shows the main characteristics of each strategy. The literature, on the other hand, indicates that such approaches have not been fully described in terms of their inherent benefits and limitations from thermal, mechanical, and engineering perspectives. It's still unknown, for example, which building method delivers the highest thermal comfort, energy savings, and seismic resistance. To this objective, experimental and numerical research should be conducted to detect the best technique. Simultaneously, a set of measurements and simulations on straw structures are needed to evaluate their life cycle from harvesting to disposal.

Table 4.3: Advantages and disadvantages of the load bearing, infill, and prefabricated methods (based on [80])

	Advantages	Disadvantages
Load-Bearing method	Simplest and fastest method with flexible designs and shapes.	Straw bales should be stored in a dry environment even during the building process.
	Requires basic principles.	Less than 50 % of the wall area can be windows and doors.
	Possibility to have multi-store buildings.	The maximum unbraced wall length is 6 m.
Infill method	The roof can be placed before the straw bales.	More complicated than the Nebraskan style.
	The frame can be steel, concrete, or wood and made off-site.	Specific skills are needed to construct the frames.
	The openings frame is more stable than the Nebraskan style	It uses a large amount of timber or wood.
Prefabricated panels method	Walls can be fabricated in the workshop	Necessitates a lot of lifting equipment for implementation
	Walls can be fabricated on site	Functioning and protected location is required for its incarnation
	Fastest way to construct a straw building	

5. Thesis positioning

This last chapter of the bibliographic study includes a detailed synthesis of the literature to highlight the results achieved so far by studies on straw as a construction material. The synthesis shows the main characteristics of the straw construction at different scales. Despite all the existing research, some information to characterize and standardize the material is still missing in the literature. Therefore, the following part identifies aspects that need to be further investigated based on the previous sections. The perspectives concern the mechanical, thermal and hygric studies. At the end, the objectives of this thesis work are stated.

Table of contents

5.1. Bibliographic study synthesis.....43

5.2. Thesis objectives.....45

5.3. Thesis methodology.....45

Chapter 5. Thesis positioning

5.1. Bibliographic study synthesis

Straw bale construction dates back to the invention of the baling machine and appeared in the USA around 1886. It was imported to Europe in the early eighties during the energy crisis. Now it is gaining attention to decrease the CO₂ emissions and the energy consumption caused by conventional construction materials. This review shows the performance of straw as an agricultural byproduct construction material, starting from the microscopic scale to the building scale, passing through the bale and wall scale.

Straw fibers size distribution and morphology analysis showed that, regardless of the straw type, the majority (76-90%) of fibers are 2 mm long, which gives bales more important mechanical properties than long and continuous straw fibers. In addition, it showed that fibers have a porous structure, which leads to lower thermal conductivity and water vapor diffusion resistance factor. Straw's mechanical and thermal properties are also affected by the chemical composition of this material. The composition of cereal plants, including wheat, barley, and triticale is similar to wood. They contain about 45% of KH-cellulose, 30% of α -cellulose, and 7% of moisture, which provide a stable and durable material. They also contain about 25% of Klason lignin which is responsible for increasing their mechanical strength properties. Bales, in their different dimensions and shapes, can have a variety of densities for construction utility that range between 80 kg/m³ and 130 kg/m³. This variation affects the thermal conductivity of straw bales. Several researchers showed that thermal conductivity depends not only on the density of the bale but also on the straw type, the fibers' orientation, and the relative humidity or moisture content. For a heat flow perpendicular to the fibers' main orientation, the thermal conductivity increases with the increasing density, while when the heat flow is parallel, the thermal conductivity increases with increasing bale density. This can be explained by the resistance of the air and the straw walls against the heat flow when it is perpendicular, and by only the air resistance when it is parallel. In general, straw bales can feature thermal conductivity as low as 0.033 W/K.m and up to 0.19 W/K.m. Their heat capacity varies between 1338 J/kg.K and 2000 J/kg.K. Straw bales' water vapor diffusion resistance factor is about 1.5 and their moisture buffer capacity is 1.853 g/m².%RH which represents a material having the ability to exchange RH and water vapor.

Experimental characterization of mechanical resistance shows that straw bales feature non-linear stress-strain behavior at lower loading level and higher anisotropic behavior with the vertical strain when the fibers are vertically orientated than when they are horizontal. After removing the loads, bales generally exhibit a complete recovery of deformation, which illustrates their elastic behavior. The modulus of elasticity ranges between 200-300 kPa for low densities (80-90 kg/m³) bales. The stress-strain curves show the flexibility of the material since the modulus of elasticity varies little under elastic loads and stays within the linear regime. The bales' density, thickness, and moisture content, as well as the other wall layers such as plaster finishing, affect the straw wall's U-value, the most important property in presenting the thermal insulation capacity of a wall. Experiments on different thicknesses and densities showed that a straw wall transmittance can be optimum with a value of about 0.25 W/K.m². In all cases, for such types of walls, the time lag for the propagation of heat from the outer surface to the inner surface is about 6 to 10 h for a decrement factor lower than 0.1, which are good thermal inertia properties.

Regarding sound insulation, straw bale walls cannot be considered good sound insulating structures, since their lightweight limit their efficiency at low frequencies. Studies showed that the sound reduction index R_w ranges between 45-58 dB which is lower than 60 dB for conventional wall materials. Due to the lack of oxygen inside the compressed bales, the material offers a high tolerance to flame and temperature rise. Various fire tests revealed that straw walls meet national building code requirements. Plastered straw walls, for example, according to ASTM E119-05a have a fire endurance of 2 hours. From 1994, regulations appeared all over the world to specify the shape, density, and size of bales, pins type, ties, and moisture content. In order to ensure the protection of the material, walls should be finished and protected from the weather (RH) and fire. Many full-scale studies describe the construction

Chapter 5. Thesis positioning

techniques of straw houses, in Nebraska, Infill and prefabricated, giving each one's pros and cons. In all literature cases, straw buildings have less embodied energy and consumed less final energy during operation than conventional buildings, thus fulfilling the purpose of the use of bio-based material. A topology diagram, seen in **Figure 5.1**, sums-up the different applications of straw material in buildings. **Table 5.1** presents the properties of several construction materials when compared to straw.

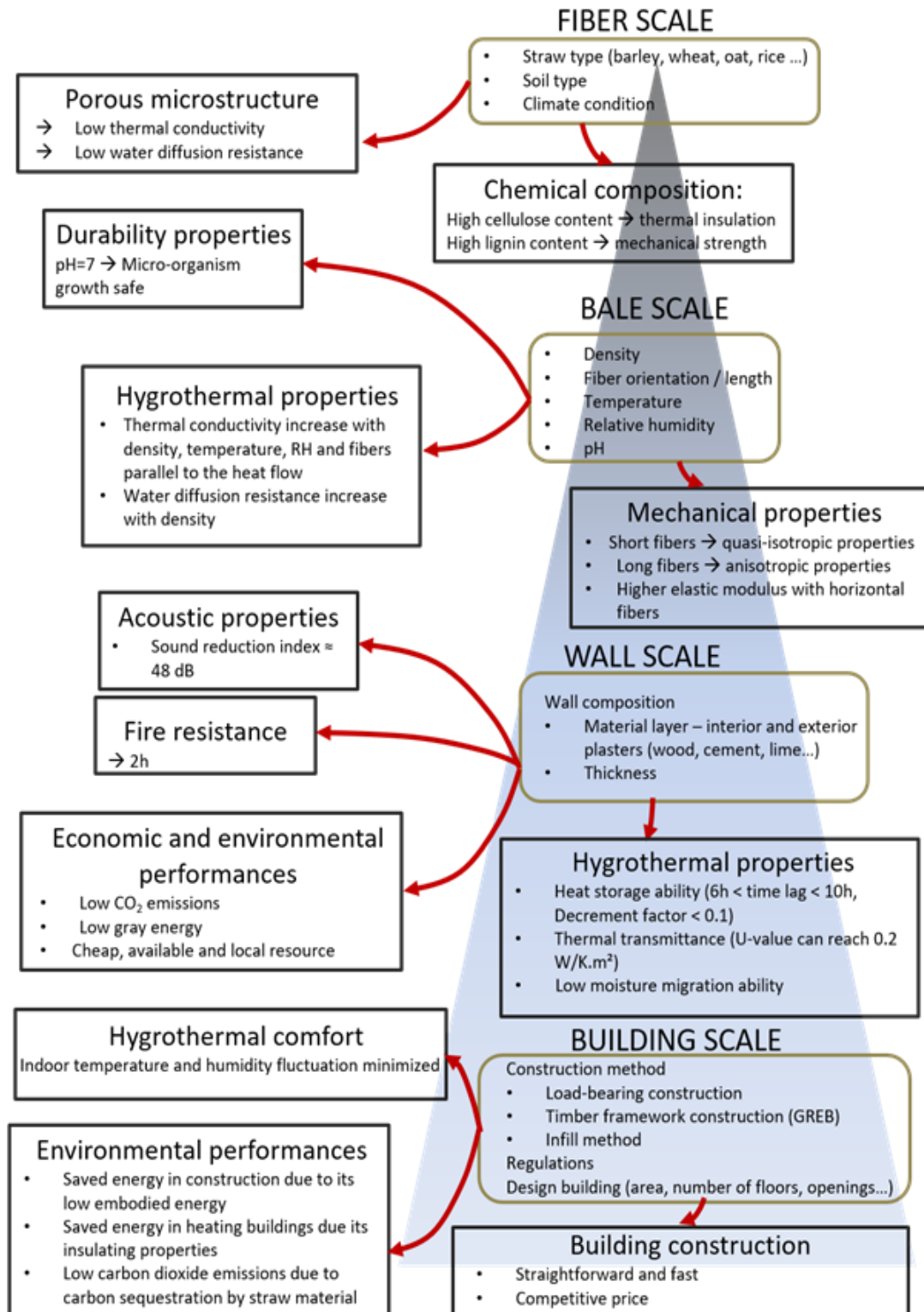


Figure 5.1: Diagram showing the different applications of straw

Chapter 5. Thesis positioning

Table 5.1: Properties of different construction materials

Material	Thermal conductivity (W/m.K)	Density (kg/m ³)	Specific heat (J/kg.K)	Water vapor diffusion resistance factor μ
Concrete	1.13 [111]	1440-2400 [111]	1000 [111]	50-150 [112]
Straw	0.05-0.12 [64]	70-200 [34]	1500 [64]	1.5 [112]
Brick	0.3-1.1 [113],[114]	1600-1800 [111],[114]	1000 [111]	15 [112]
Steel	45 [113]	7800 [113]	480 [113]	106 [112]
Wood/timber	0.14-0.22 [115]	600-1500 [113],[115]	1200 [115]	40 [112]
Fiberglass	0.045 [116]	1500 [117]	700 [118]	1 [112]
Gypsum	0.5 [111]	1300 [111]	1000 [111]	7-10 [112]

The aim of this review was to highlight the results achieved so far by studies on straw as a construction material, as well as to identify aspects that need to be further investigated. The general idea of having bio-based buildings is to minimize the environmental impact i.e. energy consumption and CO₂ emissions while preserving a thermally comfortable indoor environment. Over the years, straw bale construction has evolved and spread all over the world. Straw bale has good fire and sound resistance, can create an insulating layer, and resist the flow of heat. This product can last many years but it has to be protected from moisture, vapor, and water by using different kinds of coatings as mentioned in several international regulations. Some of the analyzed studies represent an important step forward in the dissemination of straw bale buildings as a recognized construction technique. Especially, in-lab and in-situ testing provide a quantitative assessment of the physical and mechanical properties. However, a lack of consistent data among these studies was noticed due to the wide variety of characteristics that this material presents. For example, many studies were focused on construction methods and thermal and mechanical characterization, but so far, a consistent compromise between the density, the relative humidity of the bales, and all the other factors that affect the material properties has yet to be proposed. This is a needed step toward the accurate prediction of the thermal and energy behavior, CO₂ emission reduction as well as cost analysis of buildings made from this promising material. Regarding the mechanical characterization, while the strain under compressive stress and the modulus of elasticity have been searched, the literature lacks studies on straw bale response to torsional and shear stresses. More important, information on the effect of the bending stress on the bale thermal conductivity is missing while bale bending may happen when employed as floor or roof material.

5.2. Thesis objectives

Despite all researches, some information to characterize and standardize the material is still missing in the literature. Regarding thermal characterization, more experiments concerning the variation of the thermal conductivity versus the moisture content for different types of straw are needed. Researchers studied extensively the conductivity and its variations while the variation of the specific heat, the diffusion factor, and pH have been insufficiently searched. These factors should be studied in detail while varying the density, the relative humidity, the fiber's orientation, and the type of straw. On the wall scale, studies on mold formation on straw wall surfaces are lacking. In this respect, no condensation isopleths as a function of the wall structure for varying hygrothermal boundary conditions can currently

Chapter 5. Thesis positioning

be found in the literature. At the building scale, there are still very few numerical studies on the energy behavior of straw-based buildings depending on the wall structures, the building location, and its scenarios of occupation and operation. The role of straw as a regulator of indoor air moisture is also insufficiently documented. Such future studies should take into account the variability of the results, due to the changing nature of the thermo-physical properties of this bio-based material over time. Based on the energy results, the economic feasibility of such buildings should be more intensively searched, especially in terms of payback period and life cycle cost. Straw building mechanical resistance should be studied under climatic loads and seismic accelerations. This thesis aims at providing new data regarding these issues.

5.3. Thesis methodology

The methodology is both experimental and numerical for the thermal and mechanical aspects. It consists of multi-scale characterization starting from the microscopic scale to the building scale, passing through the bale and wall scale. The planned tasks are as follows:

- I- Fiber scale: carry out micro and macroporous experimental characterization in order to deduce the microstructure of the straw that can have an impact on the heat and moisture transfer mechanisms in the bale.
- II- Bale scale: test experimentally straw bales to deduce the thermal conductivity, sorption isotherm, specific heat, resistance to water vapor diffusion coefficient, etc. Numerically, a heat transfer model should be designed based on the microstructure of the material and its measured hygrothermal characteristics.
- III- Wall scale: study the hygrothermal property of typical multi-layered straw walls under different boundary conditions by using numerical models through WUFI software. In addition, experimentally, a fire resistance test should be conducted for a straw wall covered by wood and mineral foam supplied by the industrial partner Activ'home. The objective is to attain a 180 minutes resistance.
- IV- Building scale: investigate experimentally the thesis' straw test building located in Reugny-France by analyzing the temperature and humidity variations of the surfaces and the indoor and outdoor environment. The results should help validate a numerical model and an uncertainty analysis built on EnergyPlus software. Afterward, the EnergyPlus model should be used in order to test the building behavior under different climates and scenarios. For the mechanical prospects, a numerical model should be developed by using ROBOT software. For the environmental prospects, a life cycle analysis should be accomplished for straw constructions.

Second part: Straw fibers and bales characterization

6. Experimental study

This chapter first describes the preparation of the straw samples. The type of the sample is chosen regarding the experimental requirements. The next section details the experimental methods including the equipment used and the steps that need to be followed. The experimental study includes the microstructure characterization, the chemical composition, the measurement of the moisture buffer value, the water vapor permeability, the adsorption/desorption curves, the thermal conductivity and heat capacity.

Table of contents

- 6.1. Straw preparation.....48
 - 6.1.1. Straw bales fabrication process.....48
 - 6.1.2. Samples to be tested.....49

- 6.2. Experimental methods..... 50
 - 6.2.1. Microstructure characterization.....50
 - 6.2.2. Hygric characterization.....53
 - 6.2.3. Thermal characterization.....58
 - 6.2.4. Hygric and thermal stability of a straw bale.....62

- 6.3. Experimental results.....63
 - 6.3.1. Microstructure characterization.....64
 - 6.3.2. Hygric characterization.....66
 - 6.3.3. Thermal characterization.....70
 - 6.3.4. Hygric and thermal stability.....73

Chapter 6. Experimental methods

6.1. Straw preparation

6.1.1. Straw bales fabrication process

The straw bale is, above all, an agricultural product derived from cereal cultivation. Its creation necessitates the observance of several stages, each of which is equally important. Because production and harvesting techniques vary, it can be difficult for those outside the agricultural world to understand how they work or even their utility. The goal is to briefly present the most common cultivation methods and the tools used throughout the harvesting and production of the straw bale.

Cereal production is widespread in France and is manifested by the cultivation of several types. Wheat and barley are the most common, but other cereals such as spelt, oats, etc. are very often found. Generally, in the summertime, agricultural machines such as combine harvesters and balers invade the fields for the harvest process that consists of separating the grain and the straw. Following this separation, the grain is stored and the straw is temporarily laid out to dry in the wind (strip continuous loose straw). The obtained fibers are then collected and compressed with a baler. This step determines the shape, density, dimension of the bales, and orientation of the fibers. High-density rectangular balers, shown in **Figure 6.1**, are among the most common tools for producing high-density bales weighing between 150 and 220 kg/m³ and ranging in length from 50 to 250 cm. Rectangular bales with smaller dimensions (30 - 150 cm length) and lower density (70 - 150 kg/m³) can also be produced using medium-density rectangular balers. The second type that cannot be used in the construction field is the round bales produced with high-density round balers shown in **Figure 6.2**. Round bales' density is between 100 kg/m³ and 170 kg/m³, and the height is between 100 cm and 180 cm.

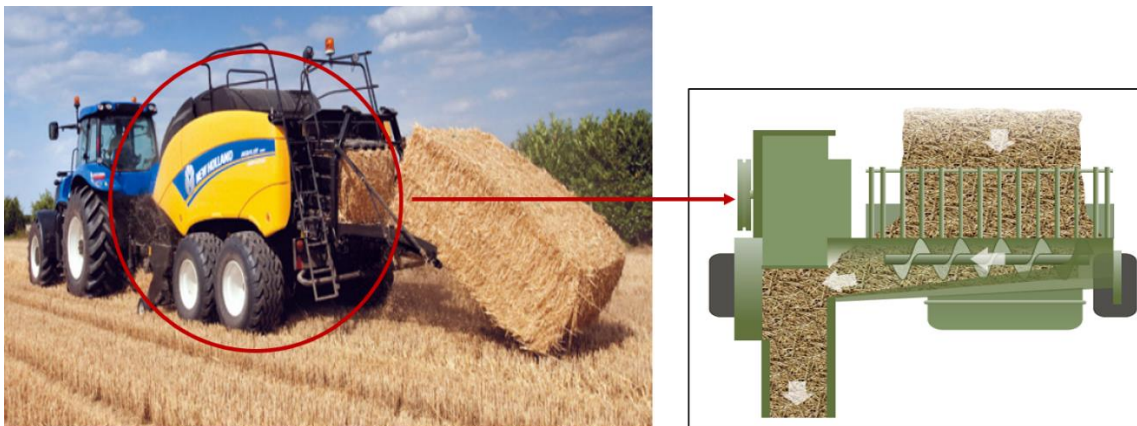


Figure 6.1: High-density rectangular balers model « BigBaler » from « New-Holland » and the concept of the compression chamber [119,120]



Figure 6.2: High-density round baler from John Deere 900 [119]

Before being applied in a building, the bales are stored under shelters of various types; hayloft, open hangar, closed hangar, etc. These shelters allow the bales to retain their properties without being damaged by adverse weather conditions. Thus, they should provide good protection against direct and

Chapter 6. Experimental methods

driving rain. In addition, the quality of the shelter walls must ensure that no moisture intrusion other than rain (infiltration, for example) alters the quality of the bales in contact with the various walls. To do this, it is possible to place pallets or gratings, on the floor, before the storage of the bundles, this precaution also serves to maintain good ventilation. It is possible also to cover the bales with a waterproof canvas to protect them.

6.1.2. Samples to be tested

Activ'home [121], a local French company, is an exclusive distributor of multilayered straw envelopes using wheat straw bales from French Auvergne farms (a region located at the center of the country). The original bales used are 50 cm wide, 83 cm long, and 35 cm high, with a density of 90 kg/m^3 . The large size of the bales prevents their direct application in experimental procedures that require smaller sizes and different shapes. Thus, several samples were prepared from the selected bales. The form of the samples depends on the targeted physical property and the considered experimental method. Part of the testing necessitates samples in the form of fiber bundles, while other necessitates small straw bales. In the rest of the manuscript, the term 'fiber' refers to the internode of a wheat straw stalk (**Figure 6.18**).

The first type of sample (I) is prepared from 3 g of chopped fibers to fill a 4 cm^3 cylindrical volume. The second type (II) is also made from 5 g of chopped fibers to fill a 7.7 cm^3 cylindrical volume. In both types, the fibers were about 5 mm to 20 mm in length and weighted about 3.6 g each. The third type (III) has the form of a 10 cm high, 20 cm wide, and 15 cm thick bale, of mass 0.25 kg. The fourth type (IV) is a cylindrical bale of mass 0.67 kg, a diameter of 7 cm, and a height of 36 cm. It is obtained by coring a straw wall. The extracted part is then inserted into a polycarbonate cylinder to conserve the total density obtained after stacking the bales. The cylinder is open at its upper and bottom surfaces to allow temperature and RH exchange. The last type (V) is a rectangular bale having a mass of 5 kg, a height of 20 cm, and a length and width of 40 cm. For this last type, the challenge was to prepare at the laboratory scale, a sample of the bale that can have different densities by compressing it without losing fibers. Thus, a transparent polycarbonate box was made with one sliding plate at the top and holes at each side to introduce the sensors and facilitate heat and mass transfers with the straw. After filling the box with straw fibers and compressing it, the sliding plate is fixed with screws from each side to determine the height, as shown in **Figure 6.3**. Polycarbonate is used in this study since it does not affect the hygrothermal behavior of the straw and can withstand the force needed for compression. All samples are represented in **Figure 6.4**. In the three last types, the density was set between 80 and 120 kg/m^3 to reflect the density of the material when used in construction as recommended by the RFCP for straw buildings.

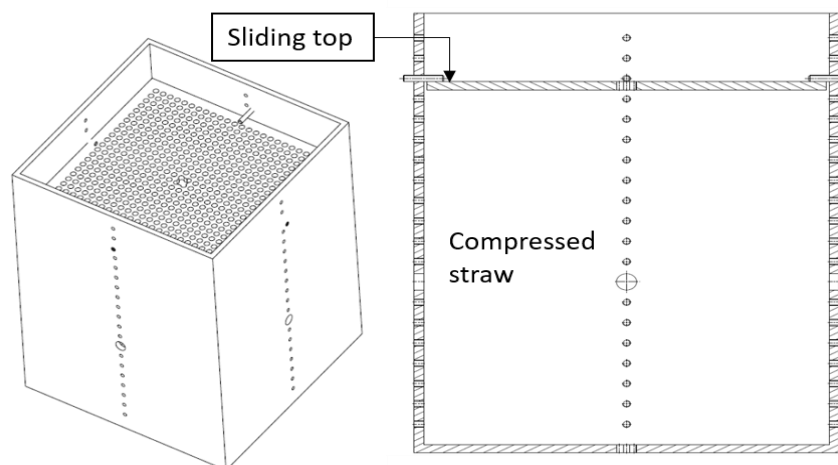


Figure 6.3: Schematic presentation of the straw mold of 40 cm width, 40 cm length, and a variable height from 20 to 60 cm that gives a variable density from 80 kg/m^3 to 120 kg/m^3

Chapter 6. Experimental methods



Figure 6.4: Different types of samples used in the experiments. Samples I and II are fibers, and III, IV, and V are bales with different dimensions and densities

6.2. Experimental methods

6.2.1. Microstructure characterization

6.2.1.1. Microscopic images

i. Principle

The characteristics of a porous material, such as the geometry of its solid parts and pores, are revealed through microstructure characterization. Pores in this sort of material are responsible for enhancing the material's specific surface area, as well as affecting heat transmission. According to IUPAC classification [38] pores of diameter, less than 2 nm are called micropores, those between 2 and 50 nm mesopores, and those greater than 50 nm are called macropores. Pores can be open, closed (fluid-inaccessible), blind (open on one side only), or linked. The microstructure characterization can be achieved by using microscopic images that show pores and matter distribution. The characterization allows the optimization of the studied material according to its applications.

ii. Equipment

The apparatus Keyence VHX 6000 used to test sample II is shown in **Figure 6.5**. It is located in the Laboratory of Engineering Sciences and Environment (LaSIE, UMR CNRS 7356) at La Rochelle University. The setup contains a control unit equipped with communication software connected to a console and a camera unit.

Chapter 6. Experimental methods



Figure 6.5: Digital microscope Keyence VHX 6000

iii. Measurement protocol

The optical microscope has traditionally been used to expand the image of small objects by using sequential lenses. Generally, a basic microscope's optical system consists of an objective lens and eyepieces. The objective lens is used to magnify an item to clarify the vision. During the observation, the specimen is positioned near the focal plane of the objective lens in object space, and an intermediate plane is used to generate a magnified actual picture of the specimen. Because the intermediate plane is on the eyepiece's focus plane, the eyepiece acts as a magnifier, enlarging the picture projected on the intermediate image plane. Finally, the viewer is given an enlarged, virtual, inverted image. **Figure 6.6** presents the concept of this imaging tool.

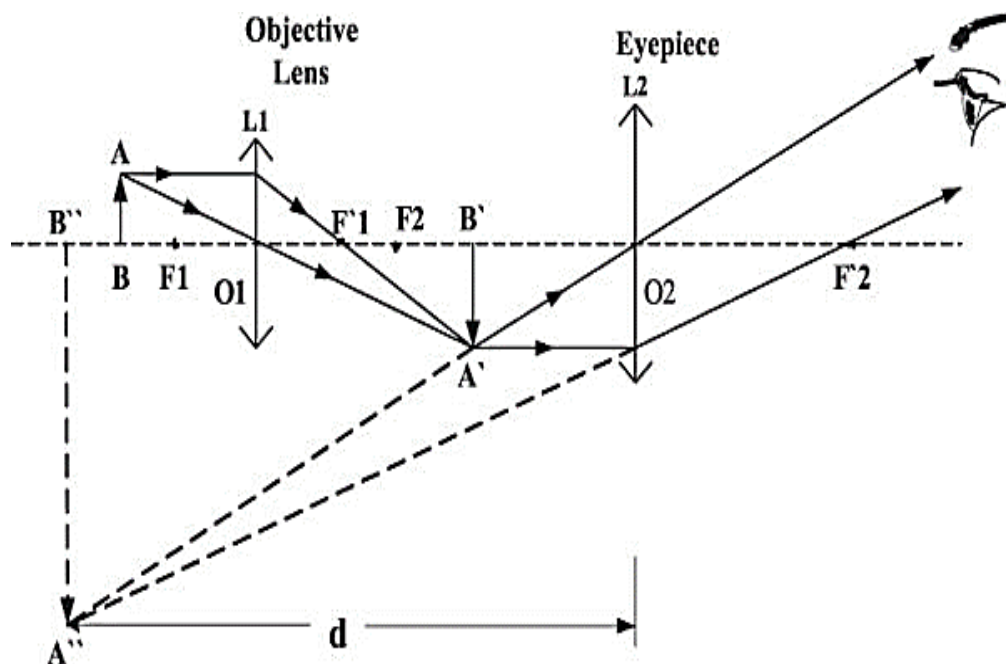


Figure 6.6: Principle of an optical microscope where the tested object is placed at AB, the actual image through the objective lens is seen at A'B', the image observed through the ocular lens is seen at A''B'' [122]

With the advancement of technology and the unique needs of research projects, many novel microscopic imaging technologies have been created based on the optical microscope such as the digital microscope that allows for obtaining pictures with higher resolution. The digital microscope is an image capture tool that includes a camera and magnifying optics rather than an eyepiece and displays the image of the sample on a screen in real-time. The system is intended for use in a wide range of domains such as in laboratories, R&D departments, and quality assurance departments to monitor, measure, and record data for different types of materials. According to [123], image capturing is done by converting image

Chapter 6. Experimental methods

information carried by electrons into a light signal, which is then sent to the charge-coupled device (CCD) to be digitalized and saved on the computer as illustrated in **Figure 6.7**.

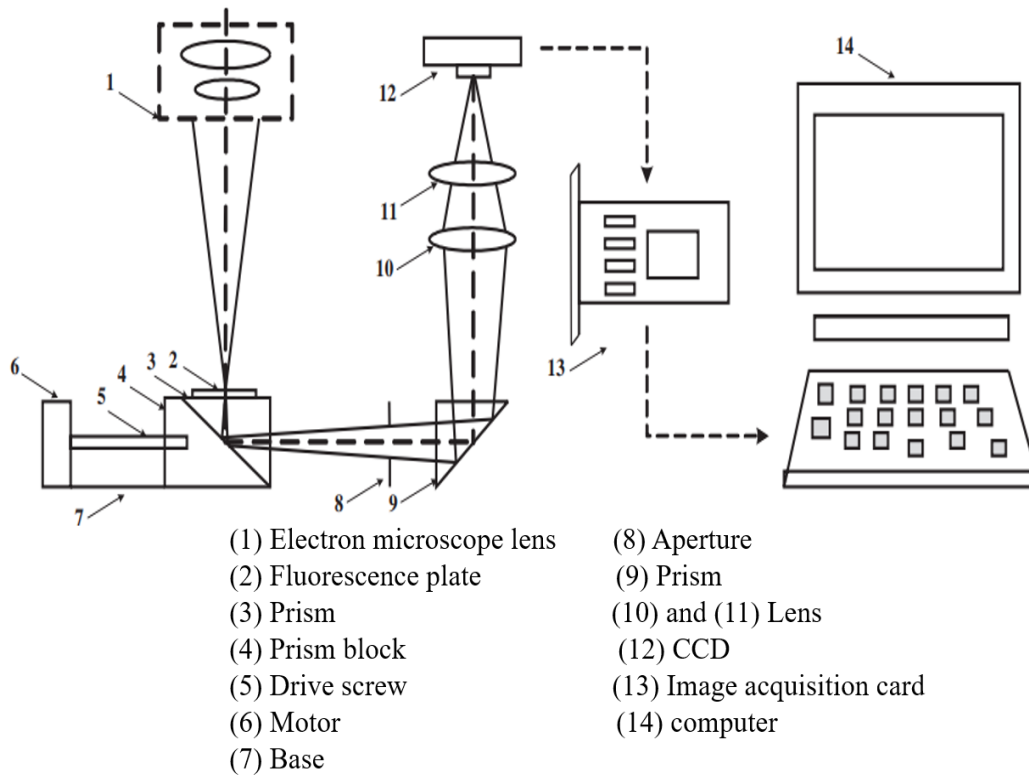


Figure 6.7: Process followed to obtain a digital microscopic image

6.2.1.2. Chemical composition

i. Principle

The principle of this experiment is to determine the chemical composition of wheat straw by using the Van Soest method [124]. This gravimetric method allows the sequential determination of constituents by treatment with neutral and acidic detergents. It is applied on dried and grinded fibers to make the sample homogeneous. This method allows obtaining an estimation of the lignin, cellulose, and hemicellulose content.

ii. Equipment

The Van Soest method is usually done in a Van Soest analyzer. The analysis was performed at the Bio-Valo Laboratory located in Clermont-Ferrand.

iii. Measurement protocol

The sample is successively subjected to the action of neutral detergents, then acid, and finally to the action of concentrated sulfuric acid under the XP U44-162 [124], EN 15414 [125], and EN 15403 [126] standards. The hemicellulose, lignin, and cellulose content are determined by a weight difference based on the mineral matter weight. The method is described in **Figure 6.8**.

Chapter 6. Experimental methods

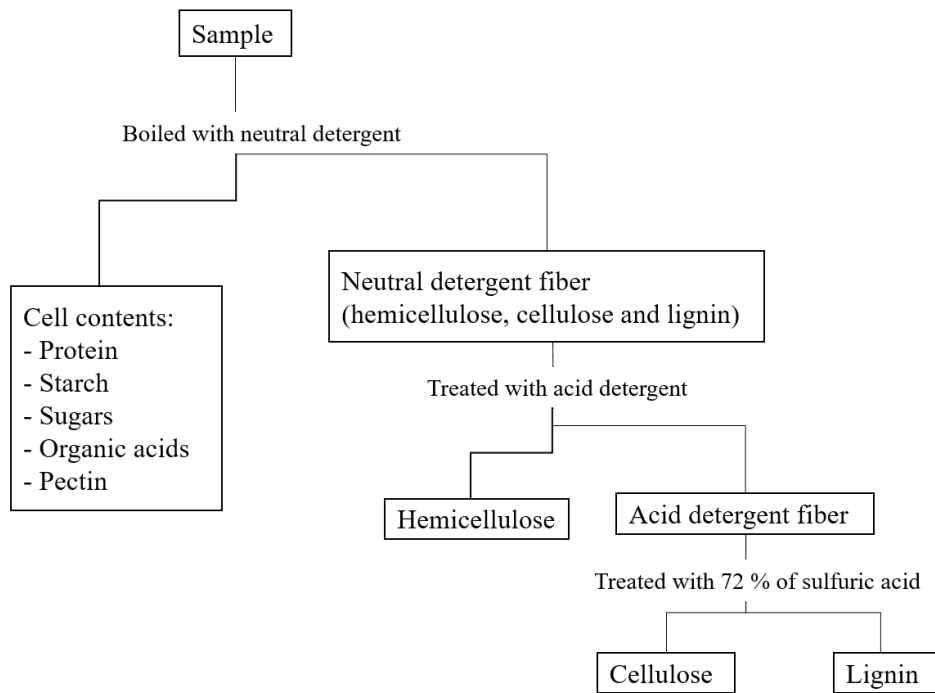


Figure 6.8: Schematic representation of the Van Soest method

6.2.2. Hygric characterization

Humidity is the principal driver of material deterioration. Porous samples physically absorb water molecules on their whole surface. The intermolecular forces of Van Der Waals acting on the vapor molecules are the cause of this occurrence. The adsorption is monomolecular when a single layer of water molecules is present on the surface of the pores at a relative humidity lower than 20 %. For RH between 20% and 50%, the adsorption is multimolecular with many layers of water molecules on the surface. Capillary condensation occurs when the RH is beyond 50 %. The degradation might result in a reduction in sound or thermal insulation, mechanical resistance, and mold presence that affect indoor air quality and causes health problems. The hygric properties also determine the mass transfer to and from the indoor environment. It is therefore essential to determine a material's hygric characteristics. For this purpose, this study employed the volumetric adsorption approach, the Nordtest protocol, and the water vapor permeability test to determine the material's hygric properties.

6.2.2.1. Adsorption and desorption curves

i. Principle

Construction materials are subjected to the daily and seasonal fluctuations of the surrounding air temperature and relative humidity. Water vapor moves from the air to the material and inversely when their partial pressures of water vapor are not equal. The moisture storage capacity of a material is defined by its sorption curve, also known as the sorption isotherm, at a given temperature. This property explains the equilibrium of bound and free water in a hygroscopic material. It is also used to extract texture information that affects the hygric properties of the material. Strong growth of moisture content at low relative humidity suggests the presence of small pores, while limited growth at a relative humidity of less than 30 % implies the presence of big pores. The existence of a prominent hysteresis ring shows that the sample is mesoporous, and the size of these mesopores is determined by their location [127]. The quantity of gas adsorbed at 100 % RH may be used to determine the total volume of mesopores and micropores.

According to the IUPAC classification [38], there are 6 types of sorption isotherms and 4 subtypes as shown in **Figure 6.9**. The condensation of gas in a microporous sample corresponds to the isotherm I. For non-porous or macroporous materials, isotherms II and III correspond to multilayer adsorption of a

Chapter 6. Experimental methods

wetting (II) or non-wetting (III) surface. In a mesoporous sample, isotherms IV (wetting) and V (non-wetting) indicate capillary condensation. The isotherm VI describes the adsorption of a highly ordered substance like graphite. Isotherms II and IV, each, feature two subcategories (H3, H4, and H1, H2) that allow information on the mesoporous texture to be obtained based on the hysteresis cycle shape. H1 denotes a limited distribution of homogenous mesopores, H2 denotes a network of linked pores of various sizes, H3 denotes capillary condensation occurring in a non-rigid structure but not a distinct mesoporosity, and H4 denotes microporous absorbents with sheets bound together.

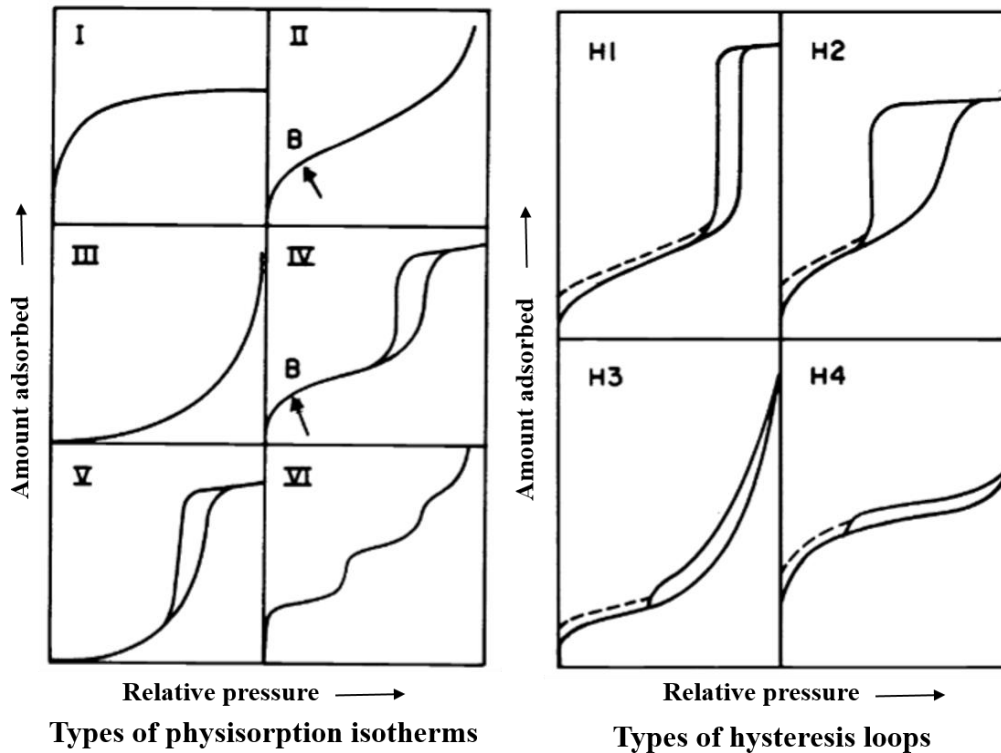


Figure 6.9: Sorption isotherm classification given by IUPAC

ii. Equipment

To obtain the adsorption/desorption curves of gas by a solid, two different techniques can be used based on the same method, the volumetric adsorption method [128]. The first experiment is done by using the "BELSORP Aqua³" device located at the laboratories of La Rochelle University. The device includes a gas dosing function, pressure transducers, a vacuum pump, and valves. It can test simultaneously three samples of type I. The other experiment uses a climatic chamber, a precision scale, and an HYT 939 Digital humidity sensor, as shown in **Figure 6.10**, to test a cylindrical bale (type IV) located at the Institut Pascal lab in Montluçon. The chamber provides constant temperature and RH conditions in the range [-10 °C - 70 °C] and [10 % - 90 %], with a precision of ± 0.1 °C and ± 0.5 %, respectively, and the RH sensor provides measurements with a precision $\pm 1.5\%$.

Chapter 6. Experimental methods

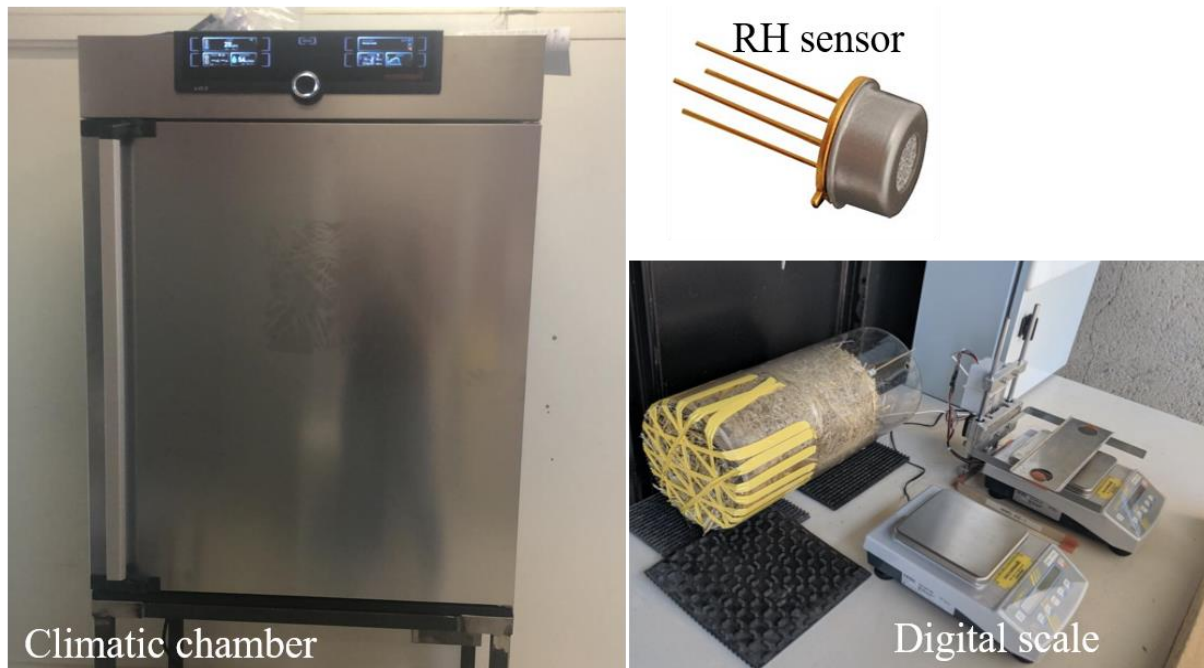


Figure 6.10: Climatic chamber, RH digital sensor, and Digital scale used for sorption isotherm test

iii. Measurement protocol

In the present study, the experiment is done based on the ISO 24353:2008 norm [129] that concerns the determination of adsorption/desorption properties in response to RH. Two different techniques are used based on the volumetric adsorption method [128]. The first experiment is done on type I samples to determine the sorption isotherm of straw fibers. It uses a "BELSORP Aqua³" device which includes a gas dosing function, pressure transducers, a vacuum pump, and valves. It can test simultaneously three samples of type I. The experiment consists of dosing a certain gas volume V_g of pressure P_1 through a volume V that contains the sample of volume V_s . A pressure transducer measures the pressure P_2 in V and V_s after reaching the equilibrium state. A schematic representation of the apparatus is shown in **Figure 6.11**. As adsorption occurs at the gas-solid interface, the weight of the solid increases and the pressure of gas decreases. Thus, the adsorbed volume can be calculated by the difference between P_1 and P_2 and the free space in V . The described process is repeated at different gas pressures. The whole system is maintained at a constant temperature during the experiment. In general, this method is rapid and precise but requires the use of a vacuum pump, a manometer, and a closed glass tube system. Proper temperature control is critical to this method, and volatile constituents may contribute to the pressure exerted by the material.

Chapter 6. Experimental methods

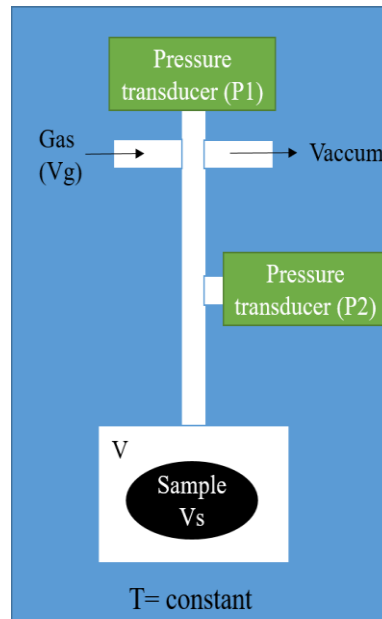


Figure 6.11: Schematic representation of the volumetric method for determining equilibrium gas-solid adsorption/desorption isotherms

The second experiment is done on type IV samples to determine the sorption isotherm of straw bales. It uses a climatic chamber, a precision scale, and an HYT 939 Digital humidity sensor, as shown in **Figure 6.10**. After drying the material at 70°C to obtain a weight of 675 g, it is placed in the climatic chamber at a fixed temperature of 23 °C. The RH of the climatic chamber is then varied from 5 % to 75% % with a step of 5 %. At each RH level, the sample is weighted and the absorbed moisture is calculated according to Merakeb *et al.* [130] procedure. The procedure uses random variations of the ambient humidity and temperature to reflect the phase equilibrium of the water bound to the material with the environmental vapor pressure, known by the sorption isotherms. The moisture content function is interpreted as a thermodynamic property of the material which confines the water to a level of energy according to the hydric state of the material. This energy level stabilizes with the external environment's relative humidity to give information on the energetic state of the pores surface layer.

6.2.2.2. Moisture buffer value (MBV)

i. Principle

The water exchange between the material and its environment reflects its hygroscopic capacity measured by the moisture buffer value. The MBV indicates the ability of a material to maintain stable indoor RH conditions against strong variations of outdoor RH. Cascione *et al.* [131] reviewed the existing theoretical and experimental approaches concerning the measurement and calculation of the moisture buffer value. They showed that the Nordtest is a reliable utilized approach that is applied in this study. The Nordtest project establishes a test for determining the moisture buffer value experimentally. The idea is based on exposing a specimen to 24-hour environmental fluctuations in the form of a square wave.

ii. Equipment

The experiment includes a Memmert HPP260 constant climate chamber and a precision scale located at the Institut Pascal's premises in Montluçon. The chamber provides constant temperature and RH conditions in the range [-10 °C - 70 °C] and [10 % - 90 %], with precision ± 0.1 °C and ± 0.5 %, respectively.

iii. Measurement protocol

The experiment consists of subjecting five types III samples to periodic square fluctuations of RH while maintaining a constant temperature as shown in **Figure 6.12**. The first type of fluctuation maintains in

Chapter 6. Experimental methods

the climate chamber a high RH of 75 % for 8 hours and a low RH of 33 % for 16 hours while the other one changes every 12 hours between the same high and low RH. The temperature is always maintained at 23 °C. The first cycle scenario is chosen to reflect the daily RH schedule in a building. As indicated in the Nordtest procedure, only one side of the sample is exposed to mass exchanges with its surrounding with a surface of 0.03 m², while the other material surface is waterproof. Before starting, the initial weight of each sample is noted after conservation at 23 °C and 10% RH for 48 hours. During the test, each sample is weighed six times during a single adsorption/desorption period. In this study, each sample was subjected to only three consecutives 8h + 16h adsorption/desorption periods since the differences in the measured weight were below 5%. Each sample's MBV in each cycle is then calculated according to equation (6.1) while the final MBV is calculated using the mean value of all samples for all cycles. A material with an MBV of 0.2 to 0.5 g/ (m². % RH) is considered to have limited moisture buffering capacity, of 0.5 to 1 a moderate buffering capacity, of 1 to 2 a good buffering capacity, and above 2 an excellent buffering capacity.

$$MBV = \frac{\Delta m}{A \cdot \Delta RH} = \frac{m_{75\%} - m_{33\%}}{A \cdot (75 - 33)} \quad (6.1)$$

where Δm is the weight variation between 75 % RH and 30 % RH, A is the exposed surface area and ΔRH is the relative humidity variation.

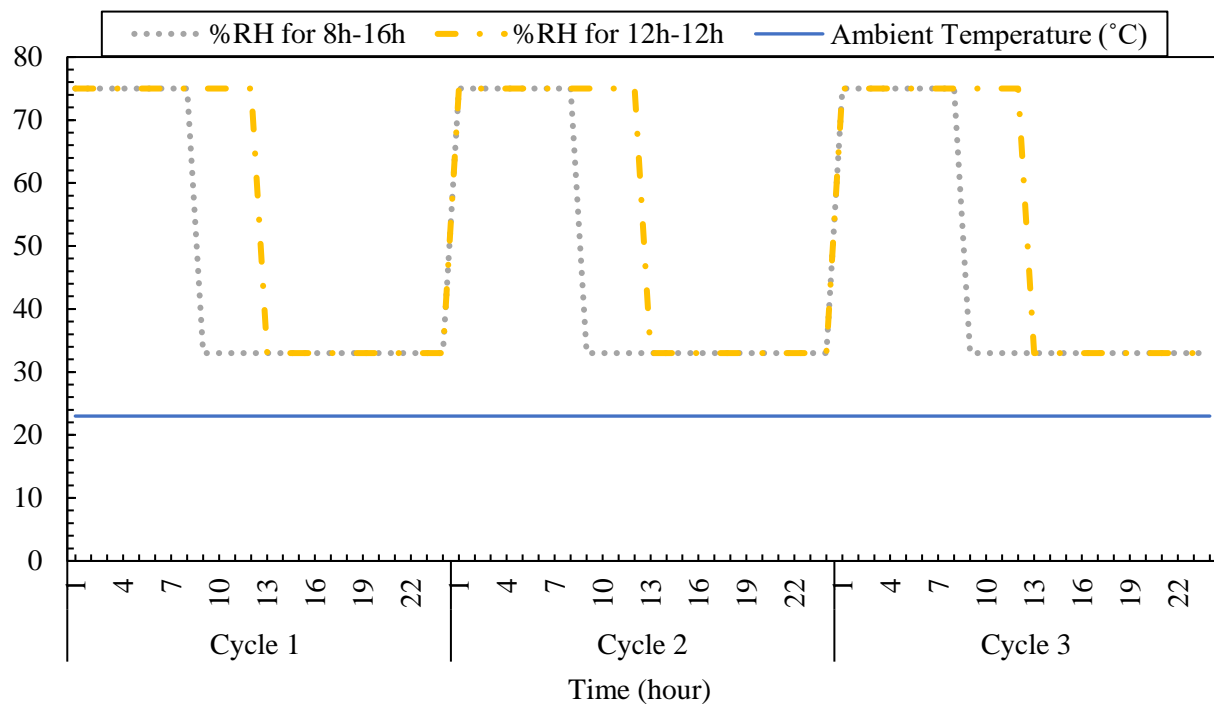


Figure 6.12: RH variations versus time at a constant ambient temperature

6.2.2.3. Water vapour permeability

i. Principle

Water vapor permeability is the most widely used property in the field of building when assessing condensation risks and hygrothermal performance. Internal condensation occurs in a wall if the vapor pressure is locally equal to the saturation pressure. This can result in permanently wet areas, resulting in a loss of thermal insulation, insulation deconstruction, and the appearance of mold.

The vapor permeability of a material determines the rate of the vapor that passes it under a given set of ambient RH and temperature. Generally, vapor transfers from the heated side of the material to its cold

Chapter 6. Experimental methods

side. All materials enable gas to cross through them by entering their atomic structure. Some materials are considerably better at enabling vapor to pass through them than others, while some are superior barriers. Vapor permeability includes transfer by diffusion (collision of gas molecules), transfer by effusion (collision with pores' walls), and liquid transfer (capillary condensation).

The ISO 12571 [132] and EN 12086 [133] standards impose to study the permeability of samples at 23 °C and 75 % RH for 24 hours. Several weight measurements of the material are carried out when the steady state is established to determine the water vapor transmission coefficient g described by equation (6.2). The final value of g is considered obtained when it does not vary by more than 5 % over the last five measurements. From the knowledge of this coefficient, several other parameters characterizing the water vapor transfer can be calculated, such as the water vapor permeability π calculated by equation (6.3) and the vapor diffusion resistance factor, calculated by equation (6.5). The water vapor permeability depends on the variation of the pressure ΔP due to RH variations calculated by equation (6.4).

$$g = \frac{\Delta m}{A \cdot \Delta t} \quad (6.2)$$

$$\pi = \frac{g \cdot e}{\Delta P} \quad (6.3)$$

$$P = RH \cdot 100 e^{\left(18.986 - \frac{4052}{235.89 + T}\right)} \quad (6.4)$$

$$\mu = \frac{\pi_{air}}{\pi} \quad (6.5)$$

$$\pi_{air} = \frac{0.083}{R \cdot T} \cdot \frac{P_0}{P} \cdot \left(\frac{T}{273}\right)^{1.81} \quad (6.6)$$

where Δm is the weight variation of the tested material, e the thickness of the sample, A the exposed surface, Δt the time between two successive weightings and π_{air} the water vapor permeability of the air is calculated by equation (6.6). T is the surrounding temperature, P_0 the atmospheric pressure equal to 10125 Pa, P the atmospheric pressure during the test, and R the specific gas constant of water vapor equal to 46.5 J/kg.K.

ii. Equipment

The experiment uses a Memmert HPP260 constant climate chamber and a digital balance at the Institut Pascal's premises in Montluçon, to test sample III. The chamber provides constant temperature and RH conditions in the range [-10 °C - 70 °C] and [10 % - 90 %], with precision ± 0.1 °C and ± 0.5 %, respectively.

iii. Measurement protocol

The experiment consists of exposing the type III sample to 75 % RH and 23 °C for 24 hours. This step is repeated three times for five samples. After each cycle, the final weight of the sample is measured and π is calculated. This experiment is based on EN 12086 [70] and ASTM [134] norms. The final results consider an average value for each sample.

6.2.3. Thermal characterization

The thermal characteristics of straw bales are the major focus of the characterization. Particularly the thermal conductivity, which directly affects the assumed thermal performance of the material and the specific heat capacity, which indicates the ability of the material to store heat. Both parameters are studied experimentally for wheat straw using the hot wire method and a calorimeter Calvet type, respectively.

Chapter 6. Experimental methods

6.2.3.1. Thermal conductivity

i. Principle

The thermal conductivity of insulating materials can be measured by stationary methods such as flux meters and hot guarded plates or by transient methods such as hot wire and flash methods. In this study, the hot wire approach (THW) is used according to ISO 8894-2:2007 [135] to measure the thermal conductivity of straw bales. This method is applied since the straw is opaque and dry. The measuring principle is to locally heat the material a few degrees above ambient temperature by a hot wire or probe and to measure the temperature rise over time [136]. Then, by mathematical processing of the signal, the conductivity k of the material can be determined. The mathematical process is based on the linear heat source equation with which the temperature T at a distance r from the heat source at time t can be determined by equation (6.7). The temperature variation ΔT during the measuring time is an important data to obtain the thermal conductivity. The temperature increases ΔT between t_1 and t_2 with a specific heat output Q , is given by equation (6.8), which is used to calculate the unknown thermal conductivity. At the end of the test, results are displayed in a logarithmic time-temperature diagram. The thermal conductivity can then be determined from the slope of the straight line. The derived results are only valid in the linear part of the graph. The measurement accuracy of the device is 5 % and its reproducibility is 3%. The advantages of such methods are the very short measurement time (less than 10 minutes). Current devices generally guarantee thermal conductivity measurement results from 0.02 to 5 Wm.K. The magnitude of the thermal conductivity of our straw material falls within this range, as shown by Ghadie *et al.* [137].

$$T(r, t) = \frac{Q}{4.\pi.k} \left[\ln \left(\frac{4.\alpha.t}{r^2} \right) - \gamma \right] \quad (6.7)$$

$$\Delta T = T_2 - T_1 = \frac{Q}{4.\pi.k} \ln \left(\frac{t_2}{t_1} \right) \quad (6.8)$$

ii. Equipment

The experiment is done by using a Memmert HPP260 constant climate chamber, K thermocouples, HYT 939 Digital humidity sensor, and Neotim FP2C conductivity meter with a needle probe shown in **Figure 6.13**, designed for flexible and granulate materials that allow for easy insertion without the need for pre-drilling. The temperature and relative humidity are measured with precisions of $\pm 2.2^\circ\text{C}$ and $\pm 1.5\%$, respectively. The equipment is located at Institut Pascal lab in Montluçon.

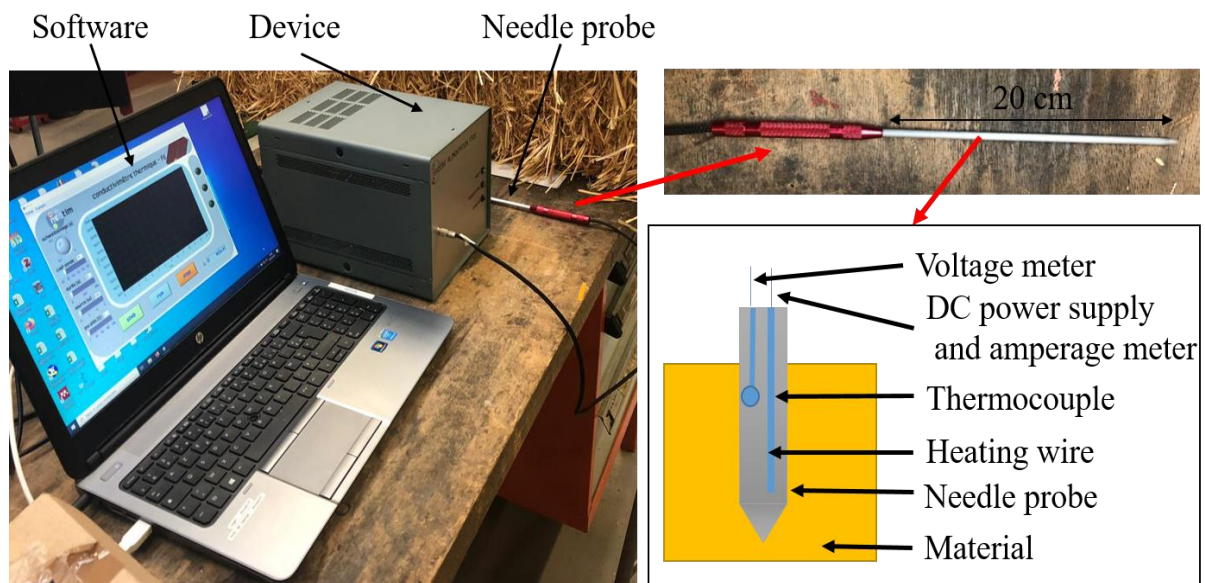


Figure 6.13: Neotim FP2C conductivity meter with the needle probe

Chapter 6. Experimental methods

iii. Measurement protocol

In order to control the temperature and humidity of the material, a type-V sample is introduced into the climatic chamber. The needle probe, temperature, and RH sensors are inserted into the bale's core. The needle probe is inserted either parallel or perpendicular to the fiber's main orientation, to examine the impact of the fiber orientation on the thermal conductivity. Each measurement of the thermal conductivity is done after the chamber has reached the equilibrium state, which takes roughly 24 hours. The equilibrium state is monitored by comparing the temperature and the RH of the chamber to those of the probes inside the bale. Three measurements of the thermal conductivity are done for each sample and each needle orientation and the final value is calculated as the average of the three measured values. These steps are repeated for different RH in the range of 10 % to 90 % with an increment of 5 %, different ambient temperatures from 15 °C to 55 °C with an increment of 5 °C, for both perpendicular and parallel fibers.

6.2.3.2. Specific heat

i. Principe

Heat capacity is a thermophysical property that determines the amount of heat required for a unit change in a material's temperature. The specific heat capacity (C_p) refers to a material's heat capacity divided by its mass, which is the amount of energy needed to raise the temperature of one kilogram by one degree Celsius (or one Kelvin). The precise analysis of a sample's temperature and its heat exchanges with the environment can be done using differential scanning calorimetry (DSC). The basic idea behind this is to change programmatically the temperature of a cell containing the tested material. A thermally inert reference body such as sapphire, zinc, lead, and benzoic acid that does not undergo any physical, chemical, or biological transformations [138] is housed in a second cell. The whole system is placed under an insulating chamber and a permanent vacuum to improve insulation and avoid moisture condensation. The DSC can measure the quantity of heat absorbed or emitted by the sample across the investigated temperature range by calculating the difference in heat flux between the sample and the reference. In fact, for a sample of mass m , C_p is calculated as given by equation (6.9) and the flux ϕ between the sample and the exterior by equation (6.10).

$$C_p = \frac{1}{m} \cdot \frac{\partial h}{\partial T} \quad (6.9)$$

$$\phi = m \cdot C_p \cdot \frac{dT}{dt} \quad (6.10)$$

Where $\frac{\partial h}{\partial T}$ is the ratio of the enthalpy-temperature variations of the material and $\frac{dT}{dt}$ is the ration of the temperature-time variations during an isobaric transformation.

The original DSC presents difficulties because of the water evaporation at ambient pressure and temperature range. This drawback can be mitigated by employing a Calvet DSC with a three-dimensional heat flux detector using ring thermocouples that surround the sample [128], as represented in **Figure 6.14**. The radial arrangement of the sensors ensures the integration of 94 % of the heat for any temperature. The advantage of the setup is the sensitivity of the calorimeter, which is independent of the flow rate, and the size of the sample.

Chapter 6. Experimental methods

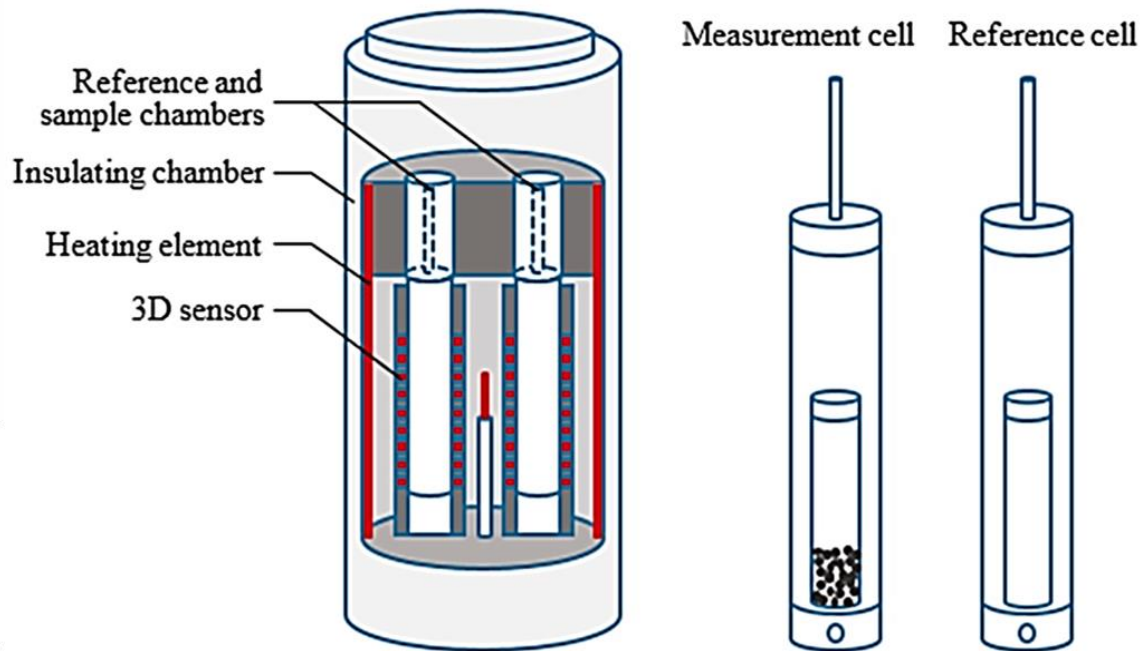


Figure 6.14: Schematic representations of the Calvet-type calorimeter based on [139]

ii. Equipment

The experiment is done by using a CALVET CRYO calorimeter represented in **Figure 6.15**, which is located at the laboratories of La Rochelle University. The temperature and enthalpy accuracies are ± 0.5 °C and ± 0.2 %, respectively. The studied sample is from type II.



Figure 6.15: Calvet cryo calorimeter

iii. Measurement protocol

The DSC analyzes were carried out within the framework of the EN 11357 standard [18]. The considered temperature range is -10°C - $+45^{\circ}\text{C}$. The temperature cycle is defined as an isotherm at -10°C , an increase from -10°C to 45°C with a temperature speed of 0.36 °C/s, and then an isotherm at 45°C . After determining the fibers' mass, they are introduced into the measurement cell, and the DSC curves from the reference cell and sample cell are plotted. Then, the calibration of the device is carried out by using

Chapter 6. Experimental methods

a sapphire with a well-known specific heat capacity. The heat capacity is calculated directly from the heat flow signal after measuring the difference in the heat flow rates in the chambers.

6.2.4. Hygric and thermal stability of a straw bale

i. Principle

High RH can cause mechanical stress on construction materials and damage them due to mold growth, while temperature variations cause natural aging and increase the deterioration reaction rates. Both parameters equally affect the thermophysical properties of materials. For this reason, the following experiment monitors the temperature and RH inside a straw bale after it is subjected to several RH and temperature scenarios.

ii. Equipment

The experiment is done at the premises of Institut Pascal lab in Polytech Clermont-Ferrand, by using a climatic chamber, three K thermocouples, and HYT 939 Digital humidity sensors having precisions of $\pm 2.2^\circ\text{C}$ and $\pm 1.5\%$, respectively.

iii. Measurement protocol

The tests are carried out according to the DIN 52620 norm [140], using a type IV sample. The T/RH sensors in the bale are evenly distributed at the center, surface, and outside the bale as shown in **Figure 6.16**. To study the effect of the humidity, the RH is increased from 4% and set to 55 % for 100 hours while conserving the 21°C as a first scenario. In the second scenario, the RH is cyclically increased five times from 30 % to 80 % with a constant temperature of 30°C . To study the temperature effect, the temperature in the chamber climatic is varied between 21°C and 23°C with 42 % RH during 24 hours. The cycle is repeated four times. Then, the temperature is increased from 20°C to 35°C for 24 hours. At last, the ambient temperature is decreased to -10°C , followed by an increase to 35°C with a constant RH of 60 %. These scenarios are presented in **Figure 6.17**. These scenarios are taken randomly to see the effect of the exterior temperature and RH on the bale.

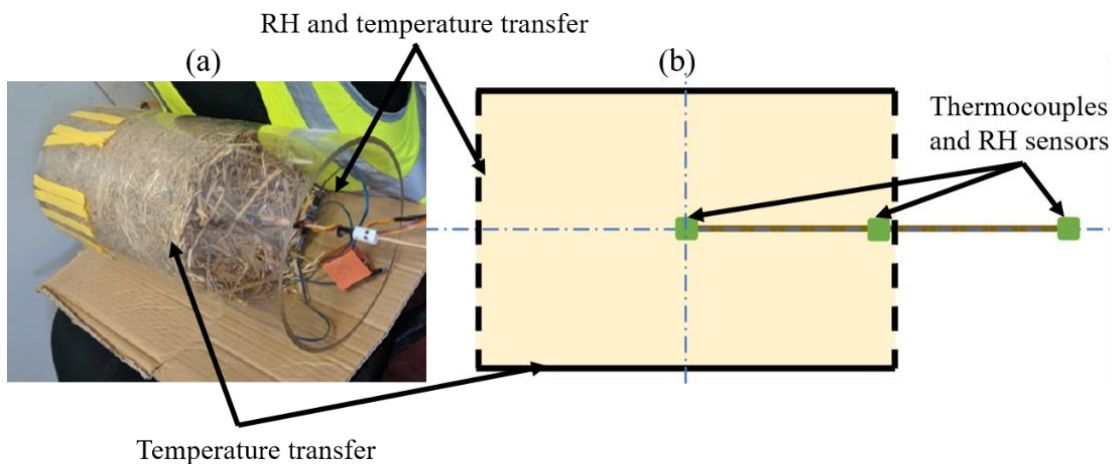


Figure 6.16: Sensor distribution in the tested type IV straw bale

Chapter 6. Experimental methods

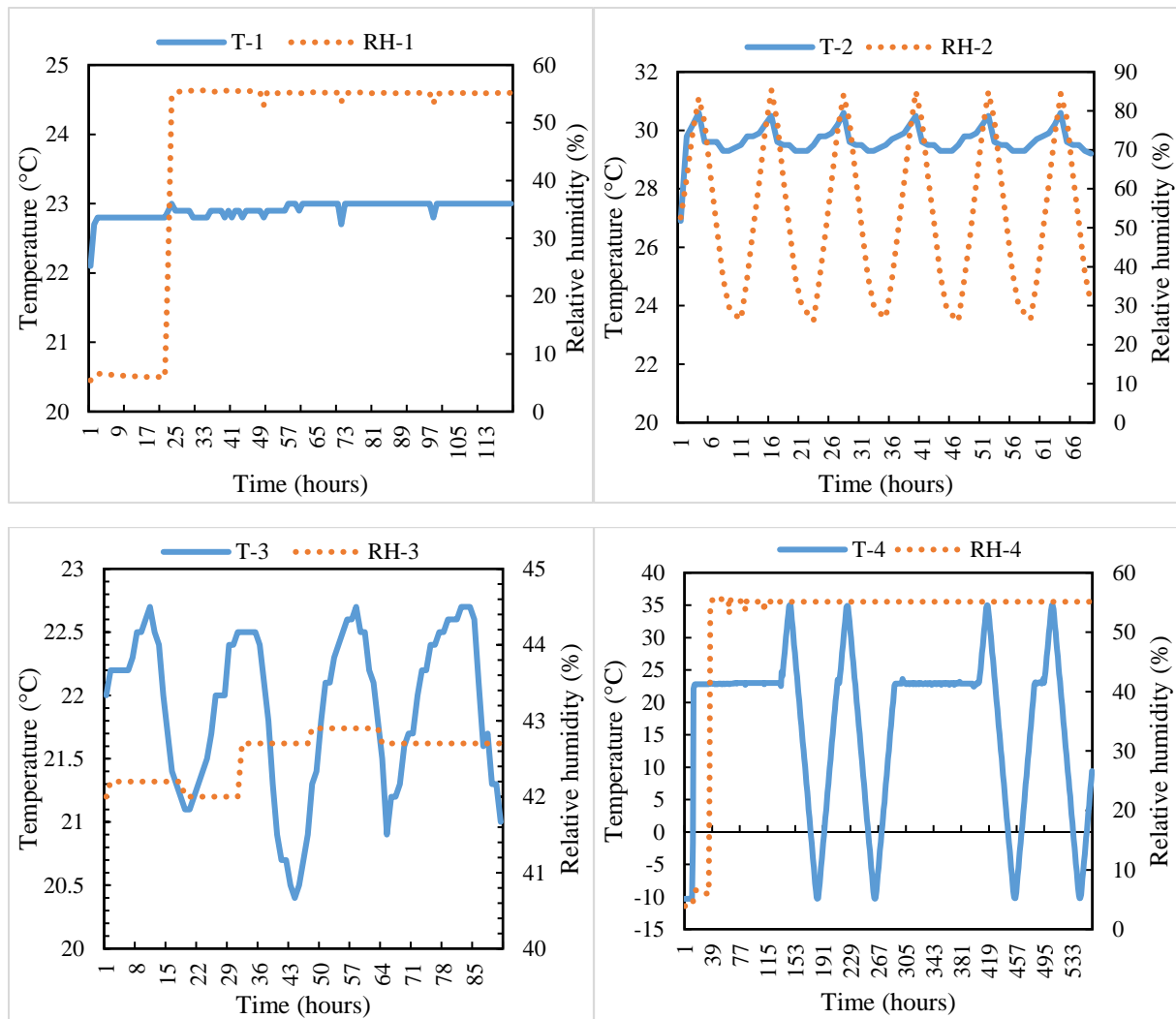


Figure 6.17: Temperature and relative humidity variations in the climatic chamber (1, 2, 3, and 4 refer to the first, second, third, and fourth scenarios, respectively)

6.3. Experimental results

The characterization of the straw thermophysical properties is an essential step in the product development process toward building applications. Straw-based composite materials are not new in the construction field but their properties remain little known in the scientific literature. In order to satisfy the criteria of building thermal insulation standards like EN 1362 [141], EN 13500 [142], and ACERMI [143], the current research intends to enhance the literature on this type of material and to enable building designers and manufacturers to make decisions based on the provided data.

Besides the regulatory aspect, the results of this chapter are intended to be used in the heat transfer models of the following chapter, involving physical parameters of the material and in numerical simulations on the study of the thermal behavior of buildings including such insulators.

The physical characterizations of materials fall into the structure, thermal, and hygric groups. This makes it possible to complete the studies already done for straw and to classify them in relation to other existing materials. The characterization of the material carried out during this thesis is part of the Activ'home project. It should be noted that some relevant characterizations of the material have been carried out by other laboratories due to difficulties in accessing certain equipment or lack of time.

Chapter 6. Experimental methods

6.3.1. Microstructure characterization

6.3.1.1. Microscopic images

The straw bale is made of a composite material that consists of two phases (fibers and air). Holes typically have sizes on the nanometer scale. These phases' morphology is seen using a digital microscope with various magnifications. The sample preparation is challenging because they need to be cut carefully to avoid changing the material's morphology.

A wheat stalk is composed of three main parts, grain head, nodes, and internodes as shown in **Figure 6.18**. According to Motte *et al.* [144], 57% of the total mass is localized in the internode, 18% in the leaves, 10% in the nodes, and the rest in the chaff and the rachis. The stem, made of nodes and internodes, has a cylindrical shape with a hollow space inside. The outer layer of the internodes is rich in lignin, cellulose, and hemicellulose and has on its surface a silica layer. The microstructure morphology of a wheat fiber internode was visualized using a Keyence® digital microscope at different levels of magnification. This device gives high-resolution colored images that rival scanning electron microscopy and allows observing the straw in accordance with ISO/TS 24597 [145].

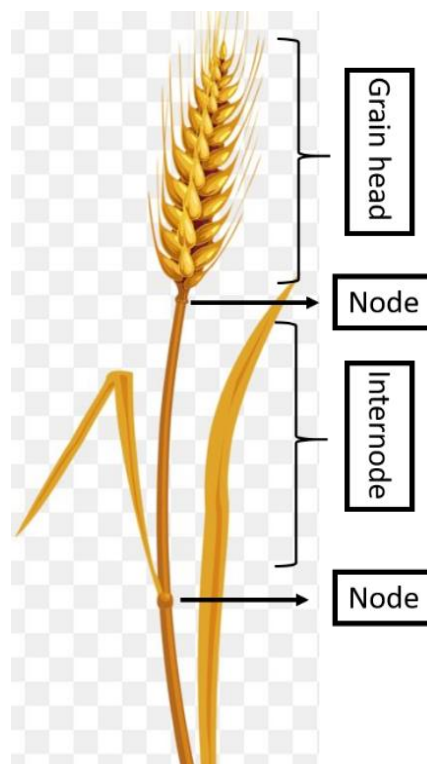


Figure 6.18: A wheat stalk with its different parts

Figure 6.19 represents the transversal cross-section of a wheat straw internode. The stems of straw are tubular cylinders with spaces and pores on their surface. The tested straw has a diameter of 3176 μm with a 312 μm -thick stem. It is worth noting that the internode part includes the epidermis, parenchyma, and vascular bundles as described by Ghaffar and Fan [146]. The epidermis is composed of around 100 μm -thick wall cells that regulate gas exchange and water balance. It also protects the interior vascular system and improves the mechanical performance of the fiber. The vascular bundles are spread as short and long polygonal cells having a bubble shape. The diameter of the pores in the stem varies between 5 μm and 45 μm and is distributed randomly all over the section. To complete the morphology description of this type of fiber, the vascular bundles were observed throughout the longitudinal section, as shown in **Figure 6.20**. In some parts, the vascular bundles have some heavily lignified thickenings (consisting of cellulose) in the secondary wall that create spiral structures to generate horizontal vessels. According to Lui *et al.* [147], these vessels are created during the autumn season, before they break down during the growth and create an internodal cavity.

Chapter 6. Experimental methods

The interconnections and the void distribution are key in determining the heat transfer model of the material. On one hand, the interconnections, including their chemical composition, are responsible for the variations in thermal conductivity due to the mass, temperature, and humidity variations. Cellulose and hemicellulose are sources of thermal insulation. An increase in cellulose amount leads to a decrease in thermal conductivity. On the other hand, the void amount affects significantly the thermal conductivity since it contributes to the thermal insulation. Thus, in wheat fiber, the three principal elements responsible for the thermal conductivity variations are lignin, cellulose, and air.

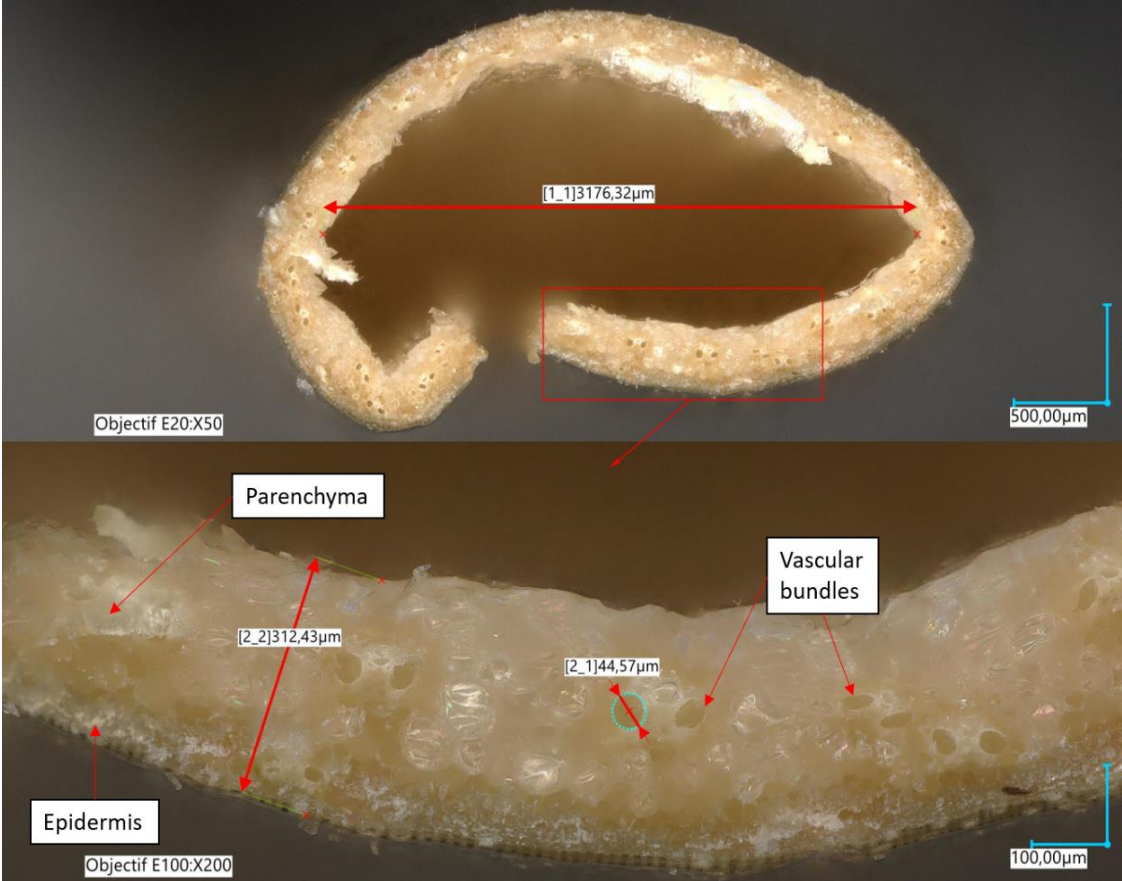


Figure 6.19: Transversal cross-section of an internode wheat straw by using Keyence® digital microscope

Chapter 6. Experimental methods

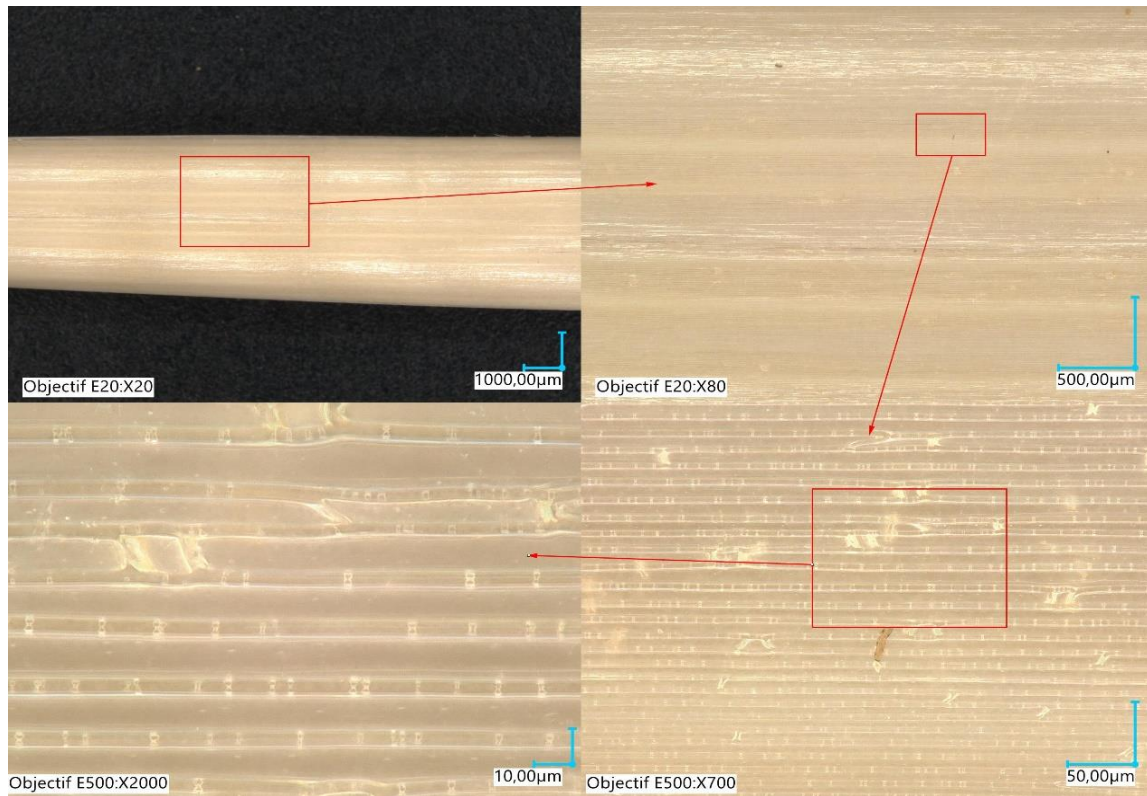


Figure 6.20: Longitudinal cross-section of an internode wheat straw by using Keyence® digital microscope

6.3.1.2. Chemical composition

The content of the different components is described in **Table 6.1**. The tested sample has lower cellulose and lignin content than the wheat straw tested by Plazonic *et al.* [32]. The moisture content is higher by 4.6 % while the ash, cellulose, hemicellulose, and lignin are lower by 4.57 %, 5 %, 25.9 %, and 17.3 %. These differences are explained by the agricultural conditions of each sample. The tested wheat straw may have lower thermal insulation properties and mechanical resistance based on its chemical composition.

Table 6.1: Content of wheat straw's components obtained by the Van Soest method

Component	Average value
Dry matter (g/100g MS)	92.3
Mineral matter (g/100g MS)	6.1
Organic matter (g/100g MS)	86.2
Moisture content 105 °C (% MS)	11.5 (77 g/100g MS)
Soluble fraction (% MS)	20.1
Hemicellulose content (% MS)	22.3
Cellulose content (% MS)	36.4
Lignin content (% MS)	7.3
Ash content 550°C (% MS)	4.72

6.3.2. Hygric characterization

Insulating materials are often compared based on their thermal conductivity. Due to their increased density, bio-sourced materials frequently have a little higher value than traditional insulators like mineral wool and expanded foam (around 0.04 W/m.K). Therefore, it is crucial to emphasize the hygric qualities of bio-sourced materials, i.e. their capacity to retain or let moisture travel through them in the form of

Chapter 6. Experimental methods

vapor or liquid, in order to promote them. An insulating system can react in different ways to water vapor. The system can be perspiring or closed to vapor transfer. Similarly, for the transfer of liquid water, an insulator can be hydrophobic or more or less capillary active. In terms of moisture storage, bio-sourced materials have, like other hygroscopic materials, the essential property of being able to exchange moisture with the surrounding air.

6.3.2.1. Adsorption and desorption curves

At equilibrium, the relationship between water content and relative humidity of a material can be graphically represented by a curve, called the sorption isotherm. The material is then considered as a set of three phases: the solid phase, the liquid phase, which corresponds to the liquid absorbed from the surface of the material, and the gas phase within the pores, where water vapor and air are in equilibrium. For each moisture value, a sorption isotherm indicates the corresponding water content value at a given constant temperature. If the composition or quality of the material changes, then its sorption behavior also changes. Due to the complexity of sorption processes, isotherms cannot be determined explicitly by calculation but must be recorded experimentally for each product.

The sorption-desorption isotherms are plotted for two types of samples (I and IV) to see the effect of the density. **Figure 6.21** presents the isotherms plotted for three samples of type I. The sorption phase starts from 3% RH with 1 % WC to 30 % RH with 5 % WC, 50 % RH with 7.2% WC and 90 % RH with about 21 % WC. The desorption phase decreases from 90 % RH with 21 % WC to 50 % RH with 11 % WC, 30 % RH with 8 % WC and 3 % RH with 1.8 % WC. According to IUPAC classification, the presence of such hysteresis corresponds to the II H3 pattern, characteristic of a macroporous sample consisting of pores of different sizes.

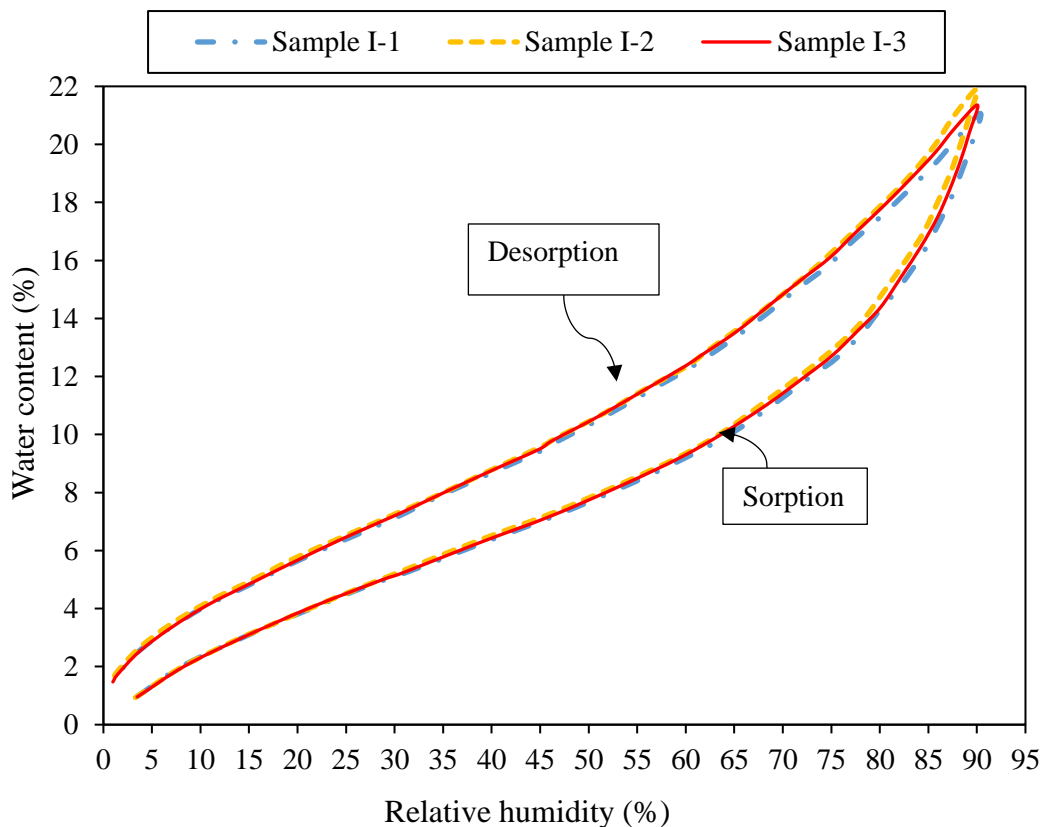


Figure 6.21: Sorption desorption curves of three samples of straw fibers tested by the volumetric method

Chapter 6. Experimental methods

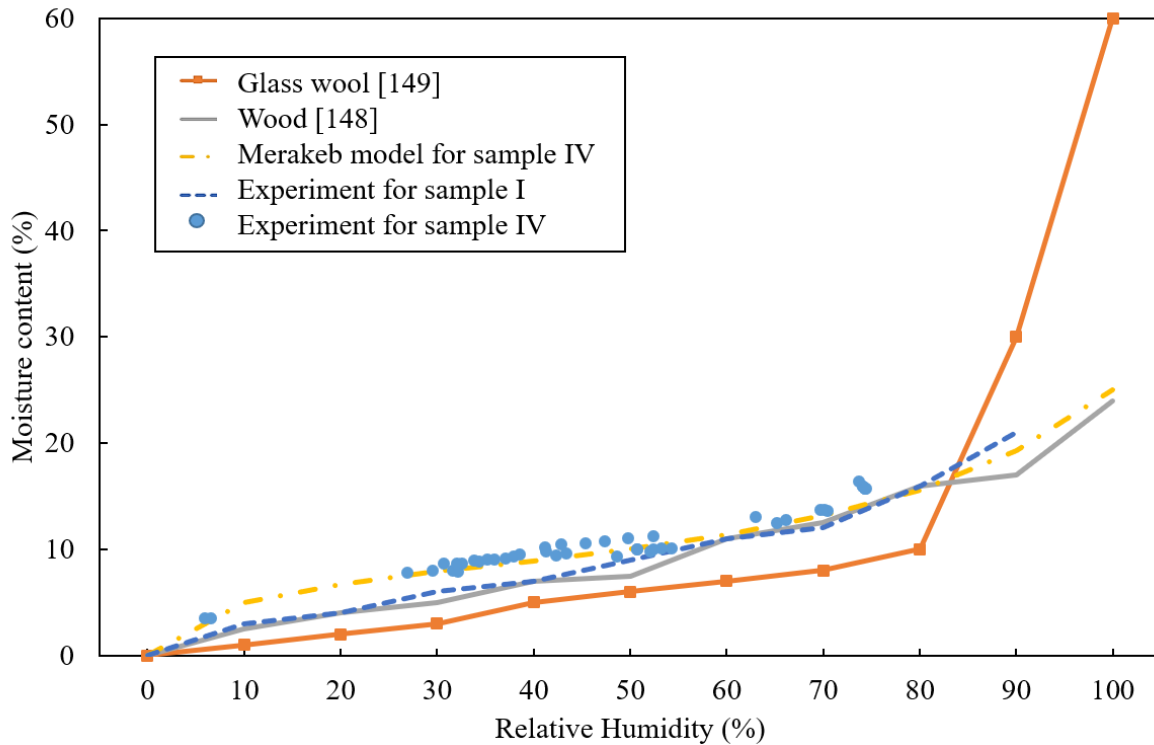


Figure 6.22: Comparison of the straw bale and fiber average sorption curves to the numerical model of Merakeb applied to straw, average sorption curve of wood [148], and average sorption curve of glass wool [149]

The second experiment concerning sample IV gave similar results as the previous ones. A comparison of the sorption isotherm curve according to the Merakeb *et al.* [130] model with that of the present experiment is presented in **Figure 6.22**. The sorption curve of the straw bale shows a hysteresis characteristic of a mesoporous material in which capillary condensation occurs. Water adsorption at 75% relative humidity of straw remains high (17 %) and seems to follow the trends of the numerical model with an RMSE of 2 %. A similar trend is observed for sample I as well. Results of samples I and IV are in good agreement, with an RMSE of 4.4 %. Straw and wood have similar sorption isotherm curves for all RH levels while glass wool has MC values lower by 48 % between 0 % and 80 % of RH, then it reaches 60 % MC at 100 % RH. The difference is due to the size and distribution of the pores.

6.3.2.2. Moisture buffer capacity

A material's ability to absorb or release moisture is referred to as moisture buffering capacity. It is a function of the permeability and the sorption capacity of the material. The moisture buffer value (MBV) is useful when designing a passive indoor climate or when studying the resistance of construction to interstitial condensation. The Nordtest is applied to five samples of type III having the same dimensions with a contact surface of 0.03 m². The initial weights of the samples are 1251.5 g, 1247 g, 1252.7 g, 1240.8 g, and 1070 g, respectively. These values are obtained after drying the straw for 24 h at 70 °C. The results shown in **Figure 6.23** were obtained for the first sample. It is noticed that three cycles are sufficient to obtain a constant weight.

Chapter 6. Experimental methods

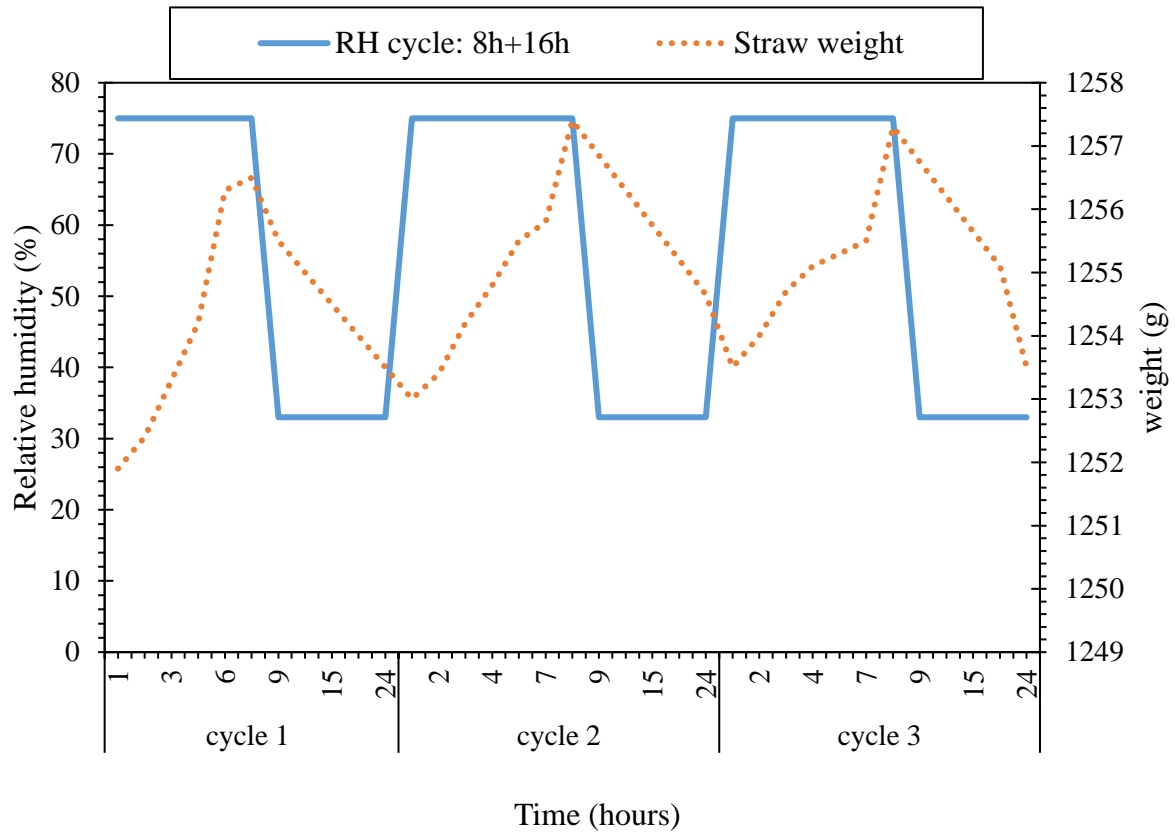


Figure 6.23: Relative humidity and weight of straw bale Type III (sample 1) variations during three cycles proposed by Nordtest

The calculated mean MBV of straw is about 3.07 g/(m².%RH). The MBV of all five samples during the three cycles is depicted in **Figure 6.24**. According to the MBV classification, straw fibers can be considered excellent to regulate the indoor RH since their buffering capacity is greater than 2 g/(m².%RH).

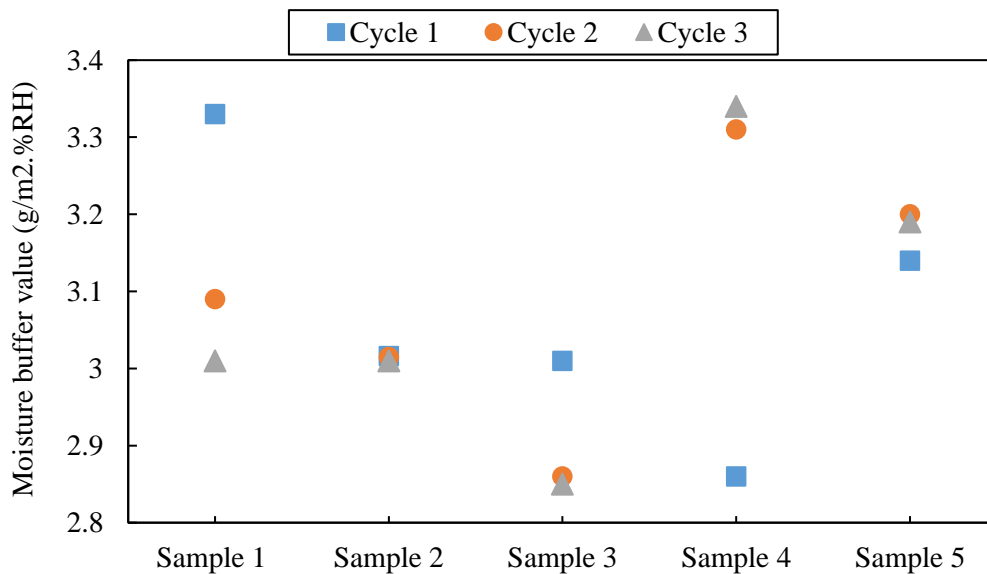


Figure 6.24: Average moisture buffer value variation according to the number of cycles and the different tested samples

Chapter 6. Experimental methods

6.3.2.3. Water vapor permeability

After drying the straw and maintaining its RH at 10 %, five samples of type III are exposed to 75 % RH, and vapor permeability values are calculated based on the difference in relative humidity. **Figure 6.25** depicts the water vapor permeability values and the water vapor diffusion resistance factor of the five samples (type III). It is noticed that the water vapor permeability of straw material ranges between 0.00036 g/m.h.Pa and 0.00057 g/m.h.Pa which means that this material is highly hygroscopic. This property was noticed also by [150]. Straw is able to absorb liquid water and water vapor from the air when exposed to a suitable source.

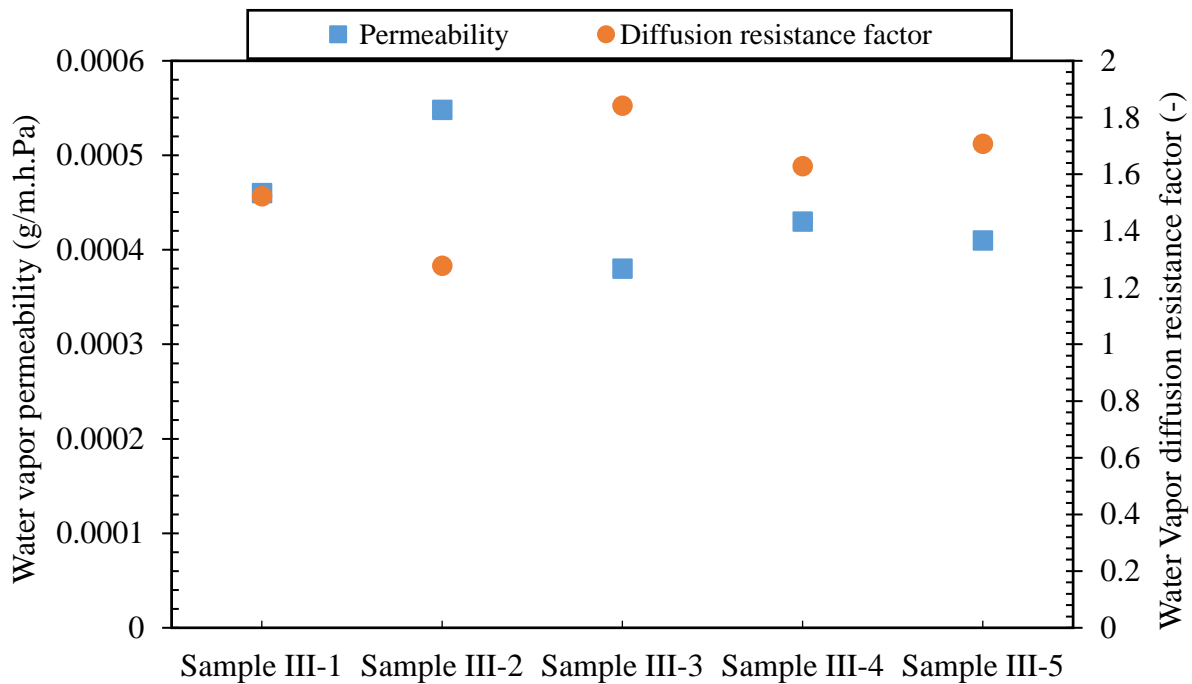


Figure 6.25: Water vapor permeability and diffusion resistance factor values of five straw samples of type III

The water vapor diffusion resistance coefficient was determined for straw bales in a wet state (between 10 % and 75 % relative humidity). **Figure 6.25** gives the vapor diffusion resistance factor calculated based on the vapor permeability factor. It can be noticed that the average value is about 1.58. This value is in accordance with RFCP [151] and similar to other types of fiber as mineral wool [152].

6.3.3. Thermal characterization

The thermal characterization of straw material is the main element of this section. The thermal properties of straw, in particular the thermal conductivity, determine the energy performance of the whole building. First, the thermal conductivity is analyzed for different affecting parameters such as temperature, relative humidity, density, and fiber orientation. Then the specific heat is measured as a function of the sample temperature. Both parameters allow the use of whole building simulation models with greater precision.

6.3.3.1. Thermal conductivity measurements

The thermal conductivity of three straw bales of density 80 kg/m³, 100 kg/m³, and 120 kg/m³ is measured by the transient-hot-wire method under various temperatures and RH. The experimental results are shown in **Figure 6.26** and **Figure 6.27**. The range of tested material temperatures and RH reflects the condition of building insulation materials in their actual environment. In the construction sector, both factors affect the ambient indoor temperature and RH of the building. In **Figure 6.26**, the majority of fibers are oriented perpendicularly to the heat flux. The thermal conductivity increases from a minimum

Chapter 6. Experimental methods

of 0.048 obtained at 15 °C and 15 % RH for a density of 80 kg/m³, to a maximum of 0.09 obtained at 55 °C and 95% RH for 120 kg/m³.

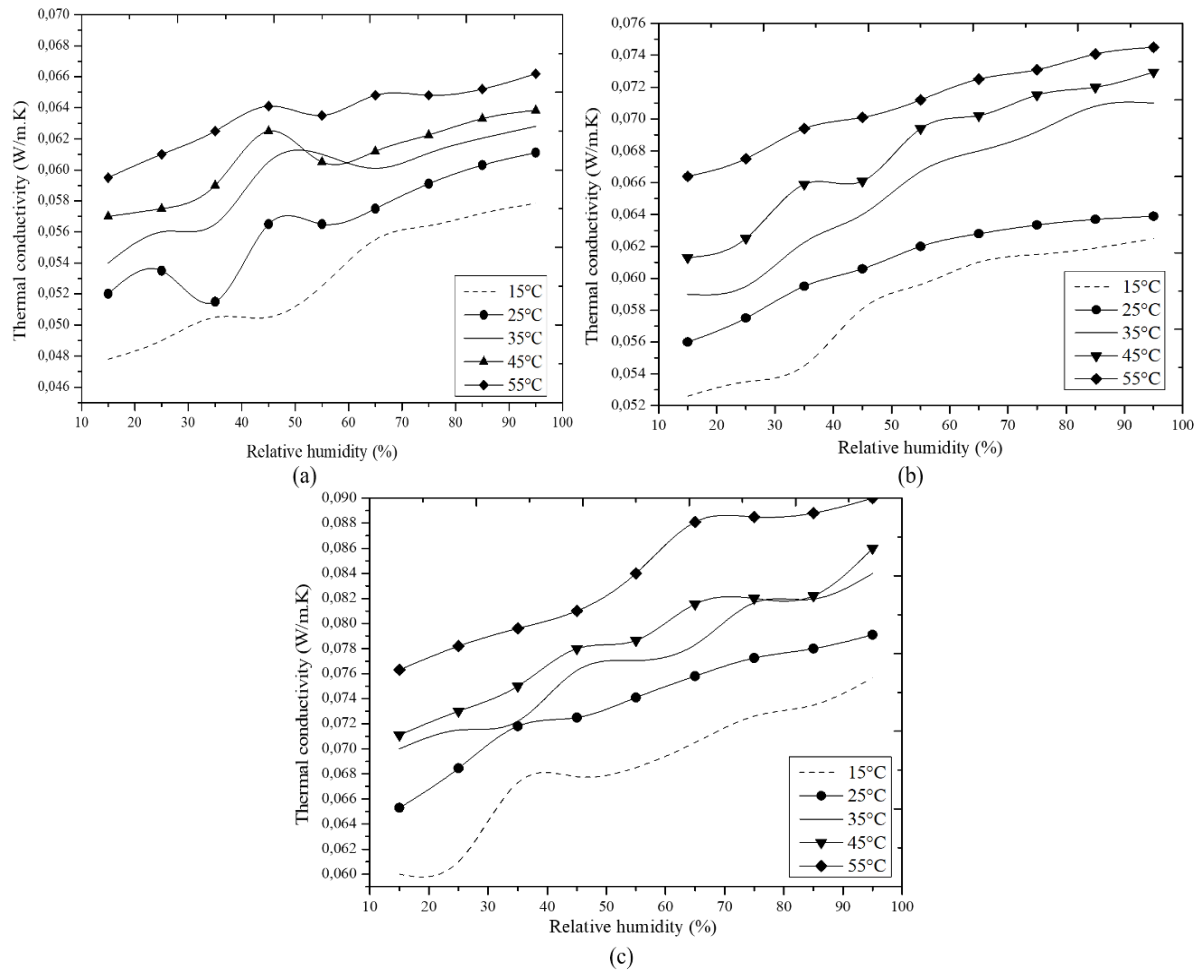


Figure 6.26: Thermal conductivity variation versus temperature and relative humidity for wheat straw bales having perpendicular fibers and density (a) 80 kg/m³, (b) 100 kg/m³, and (c) 120 kg/m³

Regarding the other investigated parameters, the thermal conductivity variation has almost the same curve trend, in perpendicular and parallel fibers' orientation. Temperature, humidity, and density all contribute to an increase in thermal conductivity, which causes the insulating characteristics to deteriorate. These factors are all related to the amount of air in the material. First, increasing the density reduces porosity, which reduces the air fraction and the insulating properties, resulting in an increase in thermal conductivity. Increasing the density by 40 kg/m³ through bale compression results in a 9% increase in thermal conductivity at a specific temperature and RH. Second, when the temperature rises, the kinetic energy of gas molecules rises accordingly, and the number of molecules colliding increases, thus increasing the thermal conductivity. During the experiment, it was noticed that a 10°C temperature elevation leads to a mean thermal conductivity elevation of 6 %. Third, high relative humidity reflects an increase in the quantity of water vapor in the air gaps of the bales and the water content in the material, which reduces the material's insulating properties. In each measurement, a 10 % increase in relative humidity leads to an increase in thermal conductivity by an average of 7 %.

When the majority of fibers are oriented parallel to the heat flux, the same trend emerges, as presented in **Figure 6.27**. The thermal conductivity increases from a minimum of 0.054 obtained at 15 °C and 15 % for a density of 80 kg/m³ to a maximum of 0.12 obtained at 55 °C and 95 % for 120 kg/m³ density. The perpendicular thermal conductivity is lower than the parallel by an average value of 16 %. The thermal paths through the fibers and the air explain this. In the perpendicular case, there is no direct path

Chapter 6. Experimental methods

for the heat to cross the material whereas in the parallel case, the direct path is through the fibers, which are less insulant than the air.

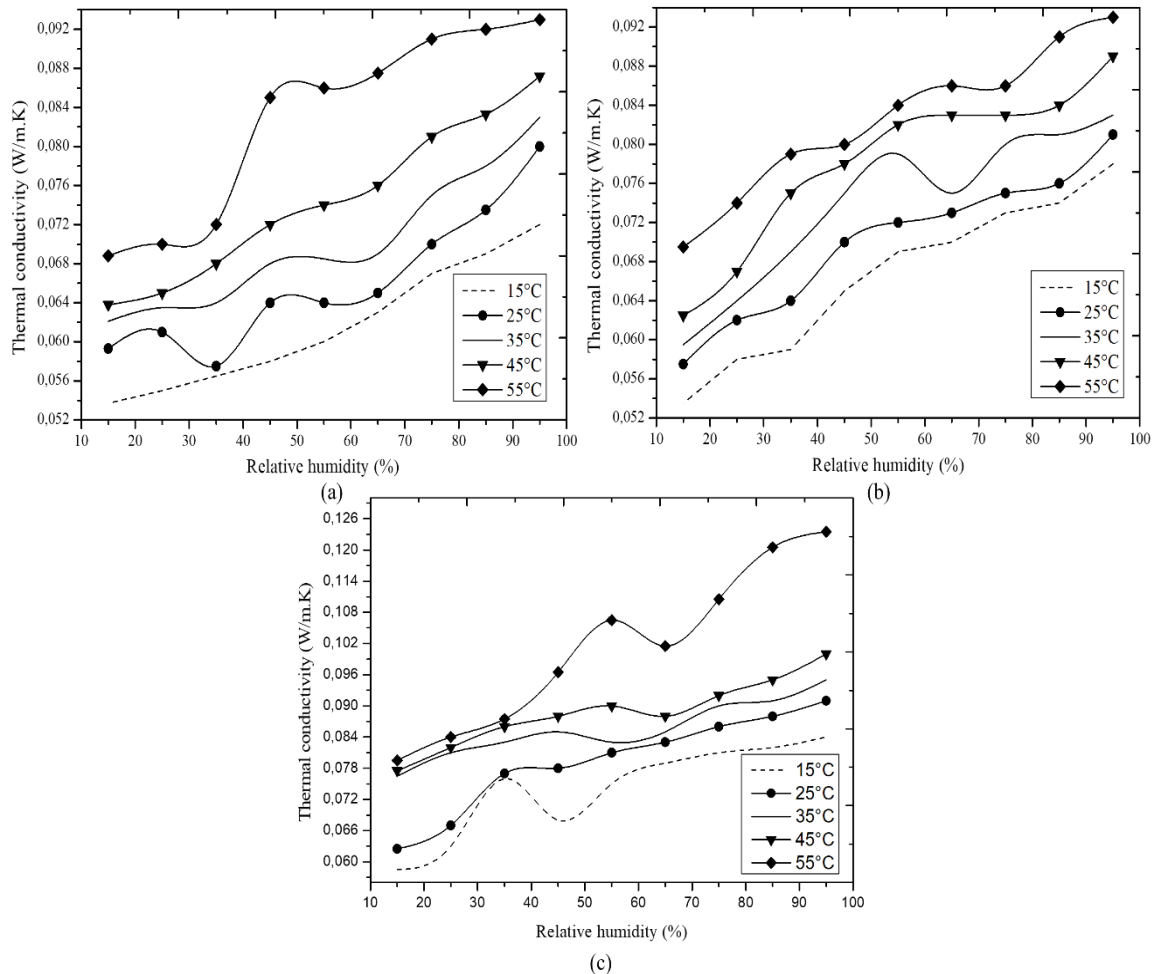


Figure 6.27: Thermal conductivity variations versus temperature and relative humidity for wheat straw bales having parallel fibers and density (a) 80 kg/m³, (b) 100 kg/m³, and (c) 120 kg/m³

6.3.3.2. Specific heat measurements

Specific heat capacity describes the ability of a material to store heat but also influences the non-stationary heat transfer. The heat spread slowly through the material when this parameter is high at constant density and conductivity. This is a key parameter, which contributes to the thermal mass of the wall and notably influences its decrement factor as well as its time lag.

Due to their low density, insulating materials typically contribute relatively little to the thermal mass of a wall. To investigate the specific heat of straw, a DSC is used to test type II samples of straw fibers across the temperature range from -10 °C to 40 °C. **Figure 6.28** shows the outcome of this characterization. Between -7 °C and 40 °C, the specific heat of straw fibers increases almost linearly with temperature from 1000 J/kg.K to 1600 J/kg.K. As the substance heats, the average kinetic energy of the molecules increases. The collisions impart enough energy to allow rotation to occur. The molecules' rotation then contributes to the internal energy and raises the specific heat.

In the temperature range of measurement, the researched materials' specific heat changes just a little. This temperature range is chosen to match the operating temperature of most buildings in temperate climates. It should be noted that the specific heat capacity is dependent on temperature and pressure but over a narrow temperature range, it is treated by building numerical simulation tools as independent of these two factors, especially for solid materials.

Chapter 6. Experimental methods

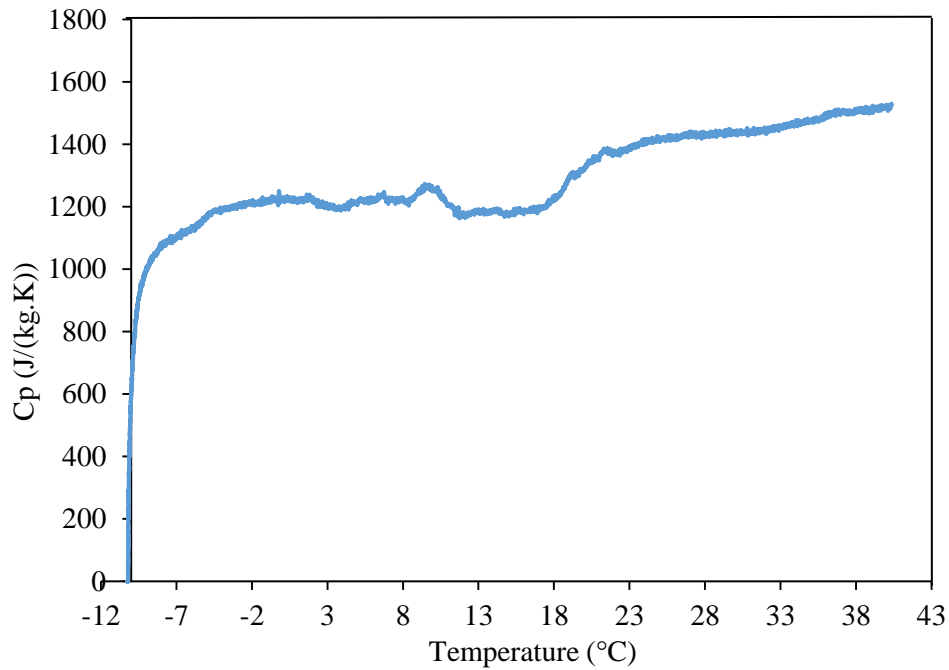


Figure 6.28: Specific heat variation of straw fibers using the DSC Calvet type

6.3.4. Hygric and thermal stability

This experiment is conducted for sample type IV to follow the temperature and RH variation inside the bale once subjected to specific exterior conditions. The cylindrical straw bale is tested under four different scenarios. For the first scenario, while maintaining a constant temperature, the RH of the climatic chamber is increased by 55 % after 21 hours. Between hours 25 and 45, the RH at the surface of the bale increases progressively from 45 % to 55 % while the RH inside of the bale is still low and reaches 35 %. The material takes 117 hours to stabilize its humidity and reach 55% RH. These results are depicted in **Figure 6.29**.

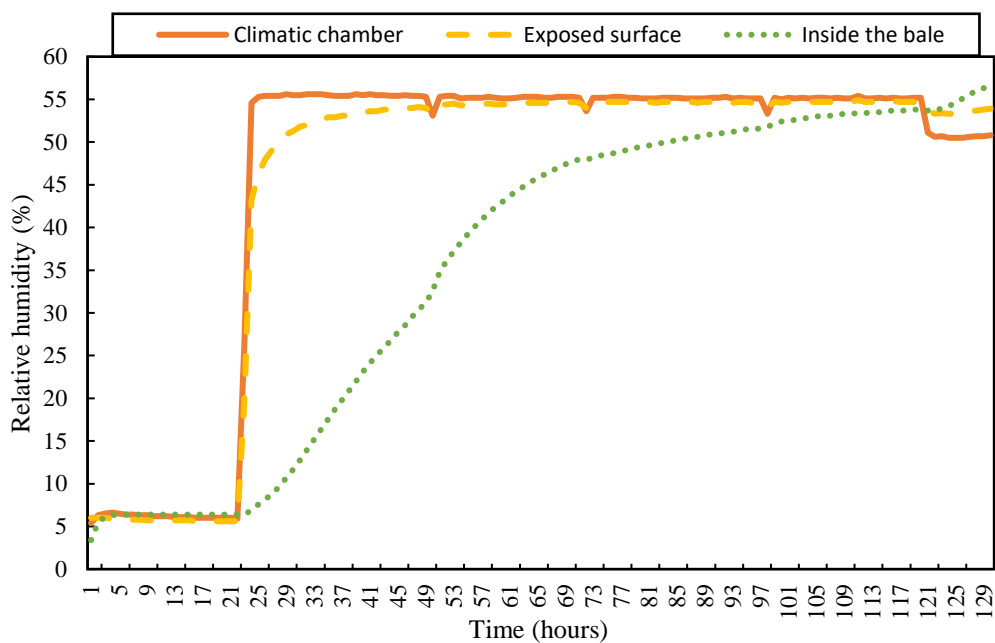


Figure 6.29: RH variations inside the climatic chamber, at the exposed surface, and inside the bale

Chapter 6. Experimental methods

In the second scenario, the RH surrounding the bale follows a sinusoidal function with a maximum value of about 80%, a minimum of about 30%, and a period of 12 hours as shown in **Figure 6.30**. These extreme values are not the same for the straw bale. The maximum and the minimum values reached at the surface differ from the exterior by +10% and -10%, respectively. Inside the bale, the RH decreases from 65% to 55% following the sinusoidal oscillation of the climatic chamber without time lag. The relative humidity behavior inside the straw is stable although there are large variations outside between 30 % and 80 % RH. It means that the moisture migration through the straw bale is very slow and that straw has the ability to dry during periods of low RH. This property helps prevent dryness problems.

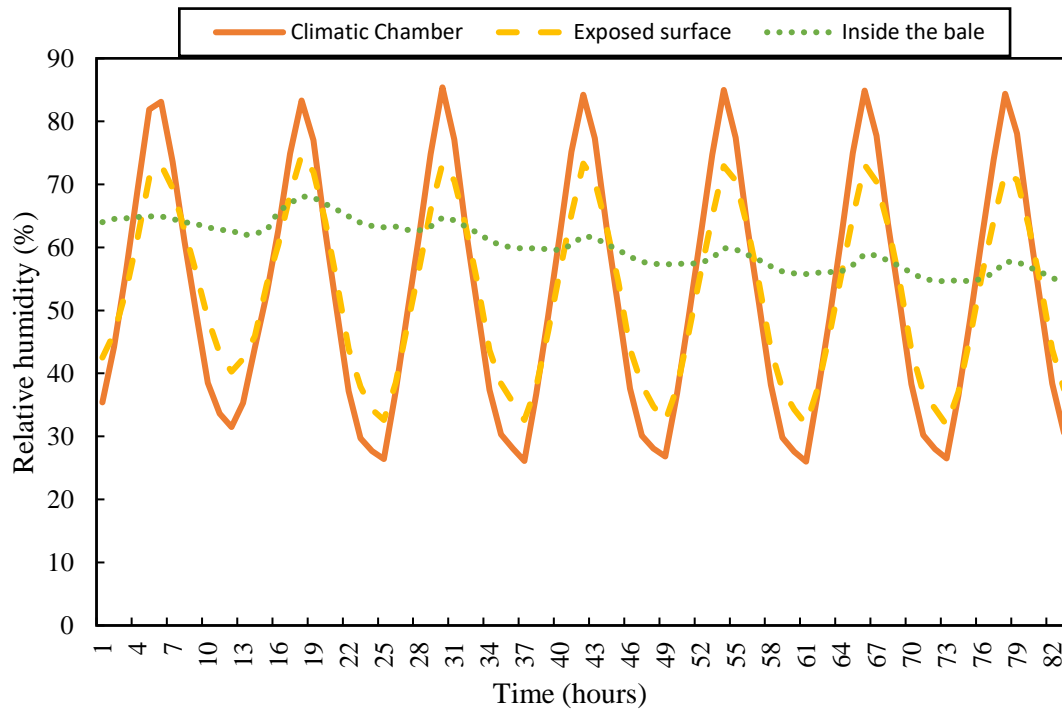


Figure 6.30: RH variations inside the climatic chamber, at the exposed surface, and inside the bale

Both scenarios prove the ability of the straw to exchange humidity with its surrounding. The responsible properties for this behavior are the moisture buffer capacity, which classifies the straw as excellent, and the sorption desorption characteristics of the material.

The temperature variations inside the bale are also investigated through two different scenarios while maintaining a constant relative humidity of 42 % for the third scenario and 60% for the last scenario. In the third scenario, the temperature varies periodically between 21°C and 23°C for a period of 24 hours, as presented in **Figure 6.31**. The time lag of temperature variation inside the base is estimated at 3.5 hours. In all cycles, the straw reaches the imposed temperature.

Chapter 6. Experimental methods

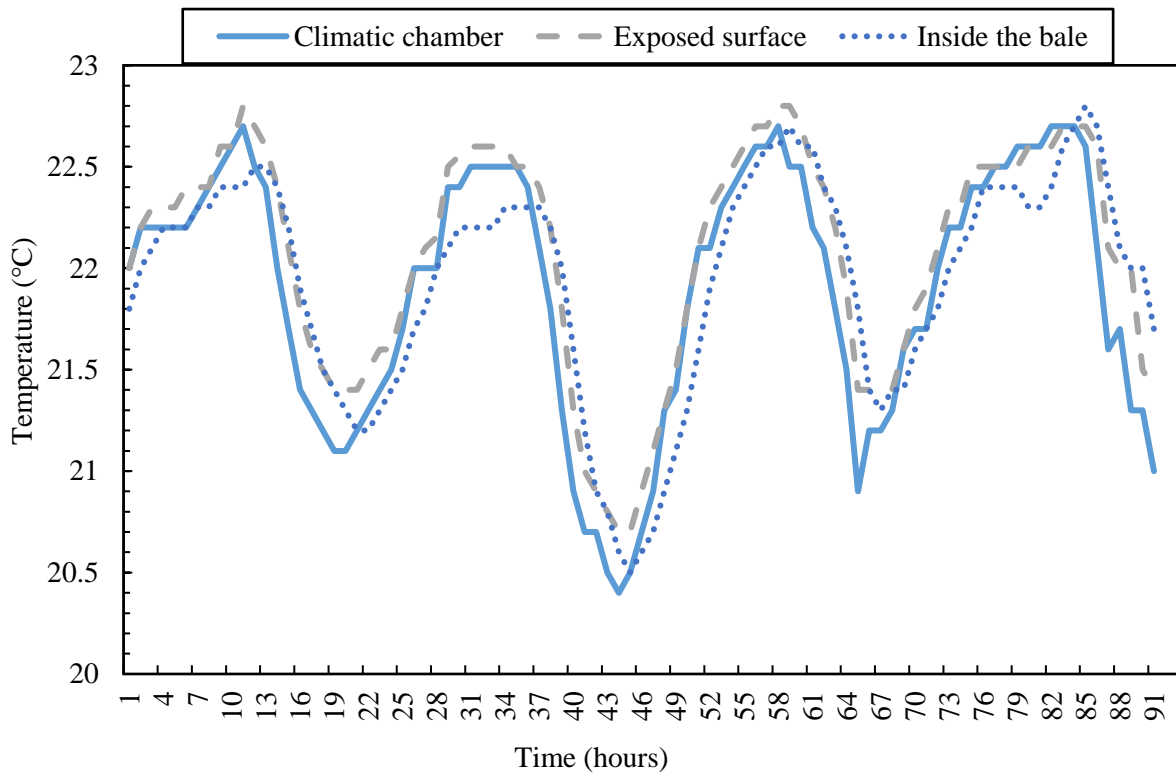


Figure 6.31: RH variations in the climatic chamber, inside the bale, and at the surface of the bale versus time

During the last scenario, the ambient temperature varied between -10°C and 35°C . Inside the bale at 18 cm from the exterior, the temperature takes about 6 hours to reach 22°C as shown in the first 30 hours in **Figure 6.32**. In the next 60 hours, the temperature inside the bale increases to attain 28°C despite the temperature stabilization in the chamber at 23°C . During the variation of the temperature, a 3-hour time lag is observed for the inside temperature. In all sensors' locations, the temperature has the same behavior but with different maximum and minimum values. The difference between the interior and exterior temperatures ranges from 3°C to 5°C .

Both temperature scenarios show that straw can smooth out the extreme external temperature peaks and provide better living conditions. This behavior is readily explained by the low thermal conductivity and diffusivity of the straw bales. Using additional layers of other materials like wood is likely to further increase the time lag.

Chapter 6. Experimental methods

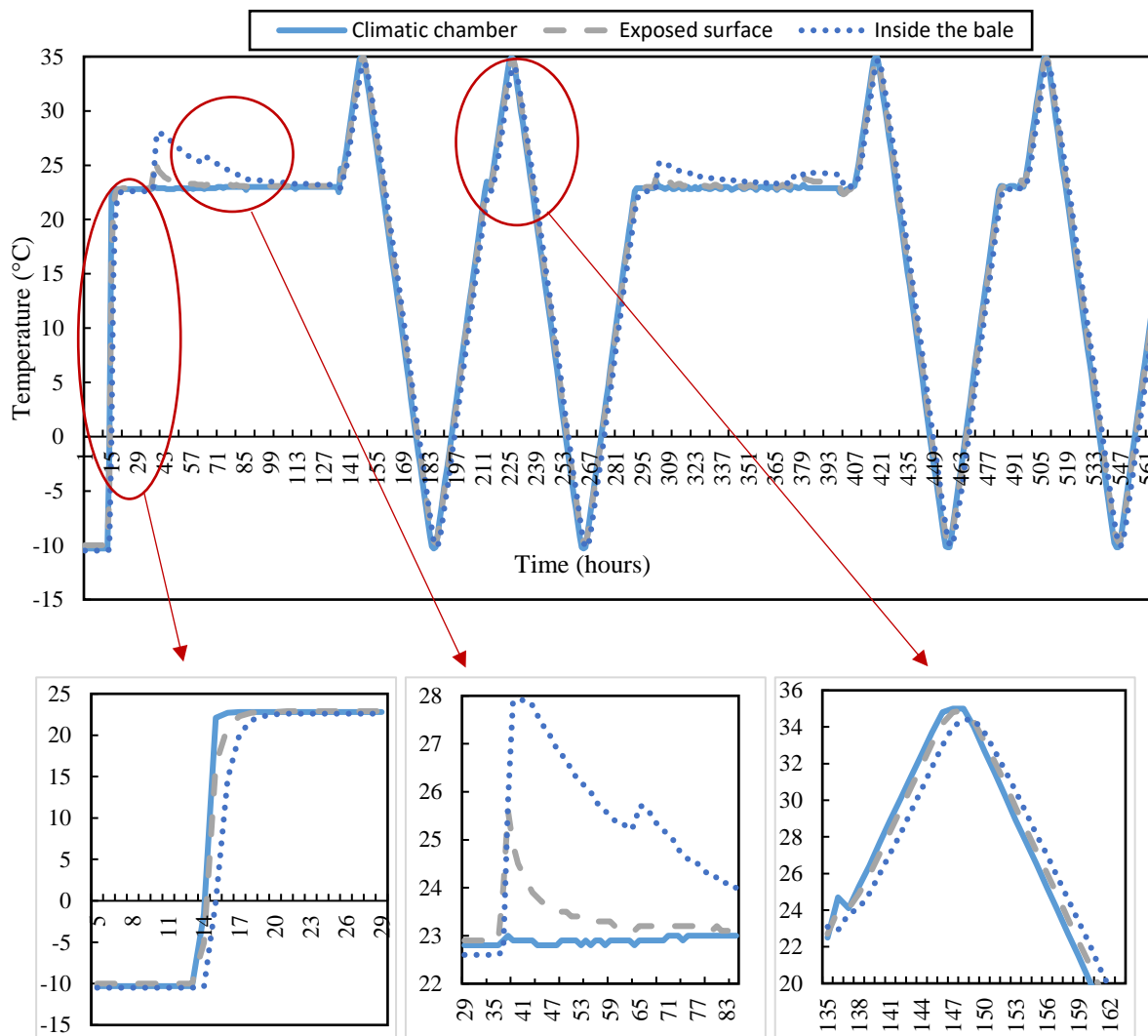


Figure 6.32: Temperature variations in the climatic chamber, inside the bale, and at the surface of the bale versus time

The characterization results presented in this chapter describe the main thermophysical properties of the straw collected from Allier, France. Five types of samples with different shapes and densities are tested to study their microstructure morphology, their hygric, and thermal properties. The microstructure of wheat fibers shows that the material is highly porous. The moisture buffer value and water diffusion resistance factor are found to be $3.07 \text{ g}/(\text{m}^2 \cdot \% \text{RH})$ and 1.58 respectively. These values show that the material can exchange humidity to regulate the indoor RH and maintain hygrothermal comfort. The heat capacity varies linearly between 1200 and $1500 \text{ J}/\text{kg} \cdot \text{K}$ for temperatures between $0 \text{ }^\circ\text{C}$ and $40 \text{ }^\circ\text{C}$. The thermal conductivity of straw bales varies between $0.048 \text{ W}/\text{m} \cdot \text{K}$ and $0.12 \text{ W}/\text{m} \cdot \text{K}$ for bales having a density between $80 \text{ kg}/\text{m}^3$ and $120 \text{ kg}/\text{m}^3$, temperature between $10 \text{ }^\circ\text{C}$ and $50 \text{ }^\circ\text{C}$, and RH between 10% and 90% . The variation of the thermal conductivity with several factors requires an expensive experimental campaign. Development of a mathematical model taking into account the dependence of the thermal conductivity on density, RH, T, and other factors may allow to efficiently provide accurate results. Such models predict thermal conductivity instead of measuring it.

7. Thermal conductivity numerical model

The properties of a straw bale are variable and mainly depend on its density, fibers orientation, chemical composition, average temperature and relative humidity. This chapter consists of designing a mathematical equation to predict the effective thermal conductivity of straw bales that can be applied to all straw types, submitted to different conditions, using the previous chapter's results. The first part describes the mathematical model which is based on heat transfer models in porous and fibrous materials. Then it is validated by the previous experimental study on thermal conductivity. At last, the model is used to study the impact of varying the cellulose content, bale density, temperature, relative humidity and fibers orientation, on the thermal conductivity.

Table of contents

7.1. Model description.....	78
7.1.1. Existing models.....	78
7.1.2. Solid and gas conduction.....	79
7.1.3. Radiative conduction.....	82
7.1.4. Effective thermal conductivity.....	83
7.2. Validation of the model.....	84
7.3. Parametric study.....	86
7.3.1. Effect of cellulose content.....	86
7.3.2. Effect of bale density.....	86
7.3.3. Effect of bale temperature.....	87
7.3.4. Effect of bale relative humidity.....	88
7.3.5. Effect of fibers' orientation.....	89

Chapter 7. Thermal conductivity numerical model

7.1. Model description

7.1.1. Existing models

The term "thermal conductivity" relates only to the transfer of heat by pure conduction. Since thermal insulators are frequently light and porous materials that serve as the location of heat exchanges that comprise conduction, radiation, and sometimes convection, conduction only cannot be consistently acknowledged. When heat transfer can only be conveyed by conduction, thermal conductivity is regarded as inherent to the material. Thermal conductivity is regarded as an effective attribute when radiation is added to the thermal transfer since it depends on several elements like surface emissivity.

Several previous studies investigated heat transfer models in porous and fibrous materials. He and Xie [153] and Xie *et al.* [154] developed an effective thermal conductivity model of silica aerogel composites based on their microstructure. The model considered the effect of the particles or fibers' size, temperature, mass fraction, and orientation. It was found that the thermal conductivity of the material increased as the mass fraction of the fibers and opacifiers increased. The material temperature highly affected its radiative conductivity, which caused the augmentation of the material's effective conductivity at high temperatures. The radiative conductivity was found to be also dependent on the fibers' diameter, with small diameters leading to a more insulating material. Wang *et al.* [155] predicted the effective thermal conductivity of natural fibers using the random generation-growth method and the energy transport equation. Their model involved the fibers' orientation, size, and volume fraction. The results indicated that orientation angles between 70° and 90° led to an isotropic effective thermal conductivity. This characteristic increased with the fiber volume fraction and the fiber length until reaching a constant value at a high length. Asako *et al.* [156] explained the variation of compressed wood radial effective thermal conductivity, using a microscopic 2D heat conduction model. It was concluded that the conductivity increased slightly with the density due to the effect of the air amount between the cell walls and in the cavities. Karamanos *et al.* [157] designed a mathematical model to determine the thermal conductivity of stone wool, based on microstructural and chemical characterization. Given the inorganic and fibrous nature of the material, the heat transfer model used in their study was considered a homogenous cylinder with infinite length. The performance of the stone wool depended highly on the air between fibers and its temperature. The variation of the temperature caused the variation of the total conductivity from 0.03 W/m.K at 0°C to 0.14 W/m.K at 1000 °C, due to the increase of the radiation and gas conduction. In addition, the same trend was observed when increasing the water content, that may cause damage to insulating materials. Xie *et al.* [158] discussed a model coupling heat conduction and radiation for porous and fibrous materials, using the finite volume and the discrete ordinate methods. The study focused on the thermal performance of randomly directionally distributed fibers, considering their length. It was found that the thermal conductivity decreased exponentially with the angle between heat flux direction and fiber orientation in their silica aerogel composite. Hoseini *et al.* [159] also investigated silica aerogel composites by proposing a new geometrical model for the material. The unit cell consisted of a cylindrical fiber surrounded by spherical aerogel, both suspended in the air. The material pores structure was the main factor influencing its thermal conductivity. The latter decreased when increasing the porosity of the material and slightly increased with increasing temperature. Most abovementioned studies investigated various composite materials different from straw, but having the same structure of cylindrical fibers filled with air and solid of different sizes and volume fractions.

Csanady *et al.* [160] conducted the only study that evaluated straw thermal conductivity and presented an analytical-empirical heat transfer model in straw fibers. The model takes into consideration the density and the fibers' composition. It is valid for barley and wheat straws having densities between 80 kg/m³ and 180 kg/m³. It was noticed that the only difference between these two types of straw is the internal gas thermal conductivity, which depends on the physical properties of the material. In spite of being the most important factors affecting thermal conductivity, the fibers' orientation, temperature, and RH were not included in their study. The present chapter aims to provide a heat transfer model in straw bales, in order to predict their effective thermal conductivity for a given density, temperature, and RH.

Chapter 7. Thermal conductivity numerical model

Straw bales are considered fibrous and porous materials. The presence of fibers in the bale has a significant impact on internal heat transmission. Fibers provide new solid conduction paths, which must be included in the conduction term and affect the radiative transfer in the composite due to its infrared extinction properties. At the same time, the gas conductivity is affected by the size, shape, and amount of pores. In the previous chapter, microscopic images showed that the diameter of the pores in a fiber varies from 5 μm to 45 μm and is spread randomly across the fiber envelope. In addition, the bale porosity ranges between 85% and 95% based on the compression ratio, with a gap dimension of 100 μm maximum. This means that only the microporous part appears in the gaseous conductivity equation and that the solid/gas conduction coupling can be neglected. For optically thick materials, even at short wavelengths, the coupling radiative/conductive (solid and gas) is insignificant. Thus, the heat transfer model for straw bales breaks down into a conductive contribution and a radiative contribution as denoted in equation (7.1).

$$k_{eff} = k_c + k_r \quad (7.1)$$

where k_{eff} is the effective thermal conductivity of the material, k_c the thermal conductivity taking into account the solid conduction of the fibers (k_f) and the gaseous conduction of the pores (k_g) and k_r the radiative conductivity.

Based on models used for the various composite materials described above, the present study improves the model of Csanady *et al.* [160] and extends it to all straw types under varied conditions by linking the straw morphological aspects with the heat transfer mechanisms. Then, the study is supplemented with a validation part demonstrating the effectiveness of the model when compared with experimental results taken from this our measurements and the literature.

7.1.2. Solid and gas conduction

7.1.2.1. Fibers thermal conductivity

Straw stems are composed of several sub-components such as lignin, cellulose, hemicellulose, ash, air, and other natural components [32]. To calculate the fiber thermal conductivity k_f , only the air, lignin and cellulose are considered since they have the highest amounts compared to the other components. The pores contained in the shell of straw stems are assumed to be disconnected to each other. Therefore, the calculation uses the series model which considers the solid conductivity k_s with volume fraction f_s , and the air conductivity k_{air} , as described by equation (7.2). Let $f_{cellulose}$ be the cellulose content in the solid part of the stem, $k_{cellulose}$ the thermal conductivity of cellulose, and k_{lignin} the thermal conductivity of lignin, the solid conductivity k_s is calculated as the volume weighted sum of cellulose and lignin conductivities, as described in equation (7.3). For this study, the thermal conductivity of cellulose is calculated by equation (7.4) and the thermal conductivity of lignin is taken at 1.83 W/(m.K), as provided respectively by Hurtado *et al.* [161] and Popescu [162].

$$k_f = \frac{k_s \cdot k_{air}}{f_s \cdot k_s + (1 - f_s) \cdot k_{air}} \quad (7.2)$$

$$k_s = f_{cellulose} \cdot k_{cellulose} + (1 - f_{cellulose}) \cdot k_{lignin} \quad (7.3)$$

$$k_{cellulose} = 0.0925 + 0.155 \times RH + 0.066 \times RH^{1.5} + 0.13 \times \exp(RH) \quad (7.4)$$

The thermal conductivity of the air is calculated by equation (7.5). The equation shows its relationship with the temperature, the static pressure P_s , the saturation water vapor pressure P_{sv} , and the relative humidity, as reported by Rasmussen [163].

Chapter 7. Thermal conductivity numerical model

$$k_{air} = \left(60.054 + 1.846T + 2.06 \times 10^{-6}T^2 + \left(40 \times RH \times \frac{P_{SV}}{P_S} \right) \right) 4,19 \times 10^{-5} \quad (7.5)$$

7.1.2.2. Gas conduction

Based on the gas tri-modal model and Knudsen value [164], the gaseous conductivity k_g in porous materials such as fibrous mats is the sum of the gaseous conductivities through the micropores (< 50 nm), mesopores (2-50 nm), macropores (> 50 nm), and through the internal cracks as shown in equation (7.6).

$$k_g = \frac{F\Pi_{meso}k_{air}}{1+2\xi \cdot \frac{l_f}{D_{meso}}} + \frac{\Pi_{macro}k_{air}}{1+2\xi \cdot \frac{l_f}{D_{macro}}} + \frac{\Pi_{micro}k_{air}}{1+2\xi \cdot \frac{l_f}{D_{micro}}} \quad (7.6)$$

The equation includes the mean diameter of the pores D , the pore volume fraction Π , the gas/solid coupling factor F , the air thermal conductivity k_{air} , the pressure dependent mean free path of the air molecules l_f calculated by equation (7.8), and the constant ξ determined by the accommodation and adiabatic coefficient of the air that depends on the ambient temperature [165,166].

The amount of air located between the fibers and inside the tubular hollow space at the center of the fibers is included in the gas conduction formula of this section, noting that the quantity present in the shell is excluded because it is already considered in section 7.1.2.1. The diameter of a fiber is found to be around 3176 μm in the microscopic analysis of section 6.18. Straw building regulations require bales compressed to obtain a density of 80 kg/m^3 to 140 kg/m^3 . As a result, the diameter of the fibers and the distance between them decrease to values in the 1000 μm range. Therefore, only the macroporous component appears in the gaseous conductivity formula expressed by equation (7.7).

$$k_g = \frac{\Pi_p \cdot k_{air}}{1+2 \cdot \xi \cdot \frac{l_f}{D}} \quad (7.7)$$

$$l_f = \frac{k_B T}{\sqrt{2} \pi d_g^2 P} \quad (7.8)$$

with k_B the Boltzmann constant, T the gas temperature, d_g the diameter of the gas molecules, and P the gas pressure.

The air contained in bales is considered stationary and constant ξ is taken as 1.5. The pore volume fraction (Π_p), considers the void inside and between the fibers. This coefficient is the ratio of the minimum to maximum heat path length, as represented in **Figure 7.1**. The maximum heat path leads to a minimum thermal conductivity while the minimum path means very low thermal resistance. In the first case, by assimilating each fiber to a cylinder, the length is equal to the fiber perimeter while in the second, it is equal to the epidermis thickness.

Chapter 7. Thermal conductivity numerical model

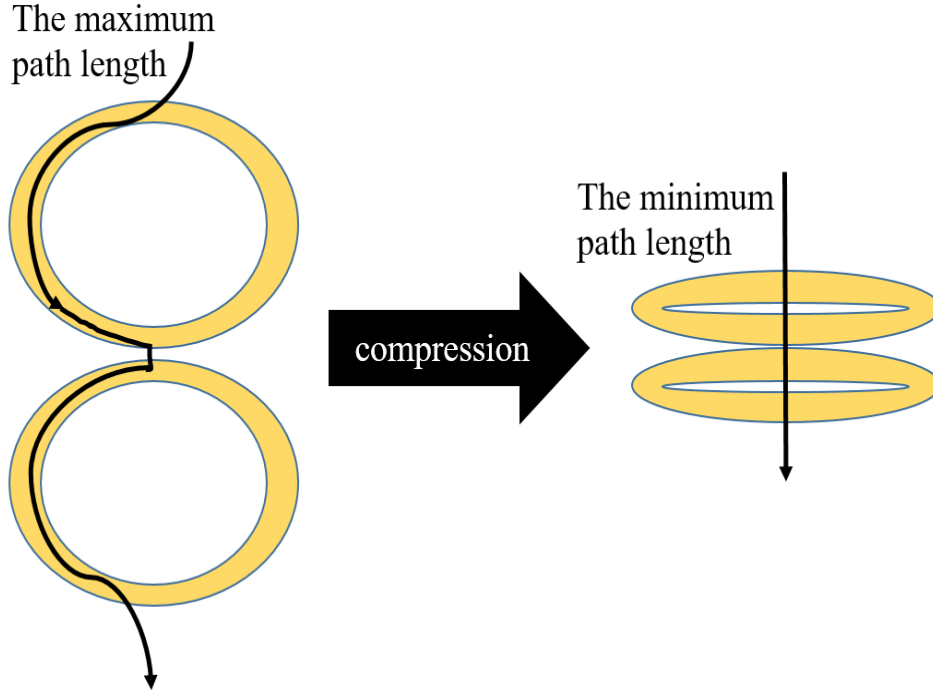


Figure 7.1: Schematic representation of the heat path in uncompressed and compressed straw fibers

7.1.2.3. Total conduction

Straw bales are groups of fibers piled up next to each other and compressed. The compression force determines the density of the material. Fibers in a bale can be parallel, perpendicular, or even oblique with respect to the heat flux. Let θ_n be the angle determining the orientation of the fibers relative to the heat flux direction as shown in **Figure 7.2**, C_n and N the fraction of fibers in a specific direction and the total number of orientations, respectively. k_c can be written as in equation (7.9) based on [158,167] and assuming it is a continuous function. **Figure 7.3** depicts the random fibers' distribution in a bale in terms of orientation, with the largest likelihood occurring at 90° orientation, according to Cotes *et al.* [43]. The fibers' orientation distribution C_n , a function of the angle θ_n , can be modeled by a Gaussian normal law with a distribution mean μ and a standard deviation σ . Thus, with this assumption, equation (7.9) leads to equation (7.10) with k_{par} and k_{ser} the parallel and series conductivities, which depend on the fiber volume fraction Π_f , the fibers' thermal conductivity k_f , and the gas thermal conductivity k_g as described in equation (7.11) and equation (7.12).

$$k_c = \int_0^N \sqrt{C_n^2 \cdot (k_{par}^2 \cdot \cos^2 \theta_n + k_{ser}^2 \cdot \sin^2 \theta_n)} d\theta_n \quad (7.9)$$

$$k_c = \int_0^{180} \sqrt{\left(10 \frac{e^{-0.5 \cdot \frac{(\theta_n - \mu)^2}{\sigma^2}}}{\sigma \sqrt{2 \cdot \pi}}\right)^2 \cdot (k_{par}^2 \cdot \cos^2 \theta_n + k_{ser}^2 \cdot \sin^2 \theta_n)} d\theta_n \quad (7.10)$$

$$k_{ser} = \left(\frac{\Pi_f}{k_f} + \frac{1 - \Pi_f}{k_g}\right)^{-1} \quad (7.11)$$

$$k_{par} = \Pi_f \cdot k_f + (1 - \Pi_f) \cdot k_g \quad (7.12)$$

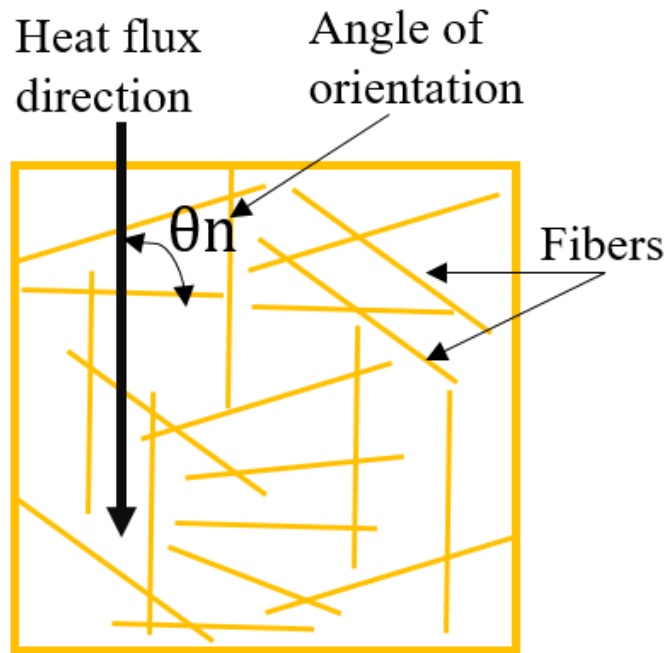


Figure 7.2: Schematic structure of straw bales having randomly oriented fibers.

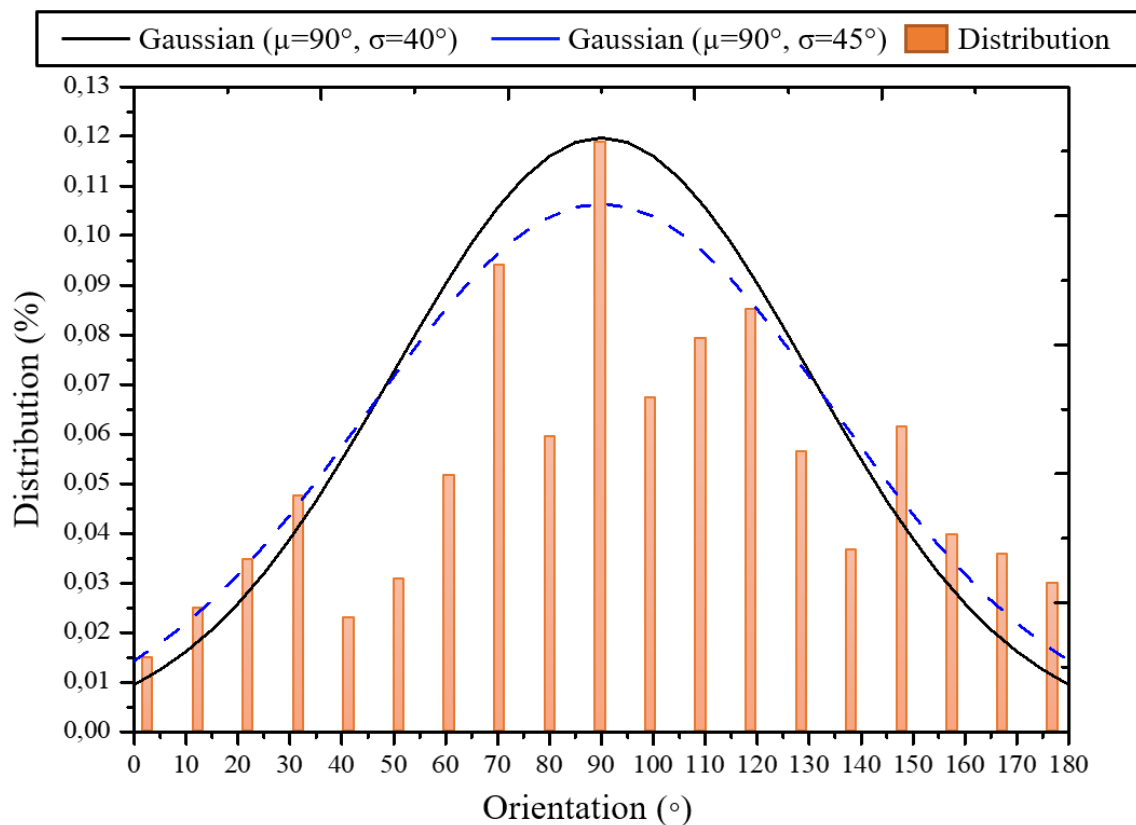


Figure 7.3: Gaussian normal laws of straw fibers' orientation distribution in a bale [43]

7.1.3. Radiative conductivity

The radiative conductivity is calculated by equation (7.13) using the standard Rosseland's method for an optically thick medium. The equation uses the Stephan-Boltzmann constant σ , the temperature T , the extinction coefficient a , the pores volume fraction Π_p , and the refraction index n that can be calculated

Chapter 7. Thermal conductivity numerical model

from the weighted volume average of the component's refraction indexes. For straw bales, n is 1 since the straw bales are about 90% porous.

$$k_r = \frac{16 \cdot \pi \cdot \sigma \cdot n^2 \cdot T^3}{3 \cdot a} \quad (7.13)$$

Pradhan *et al.* [168] and Fukushima and Hatfield [169] investigated the extinction coefficient of different types of straw. The results showed that wheat straw stem has an extinction coefficient of about 1754 m²/kg.

7.1.4. Effective thermal conductivity

Experimental results from the literature reveal that the effective thermal conductivity of straw bales changes depending on the straw type, density, temperature, RH, and fibers' orientation. Therefore, it is necessary to develop an empirical mathematical model that includes those variables in order to predict the value of effective thermal conductivity. In general, the effective thermal conductivity of a composite is determined by the constituents' properties, volume fraction, and microstructural organization [170]. In the mechanics of composite materials, effective properties prediction implies the introduction of a representative volume element (RVE). The RVE is a random volume in a material virtually generated and subjected to periodic boundary conditions. For the effective thermal conductivity calculation, the RVE of a straw bale is shown in **Figure 7.4**, where the proportion of each phase is representative on a microscopic scale. Heat transfer through the RVE includes a conduction component through the fibers and the gas, and a radiation component through the entire volume.

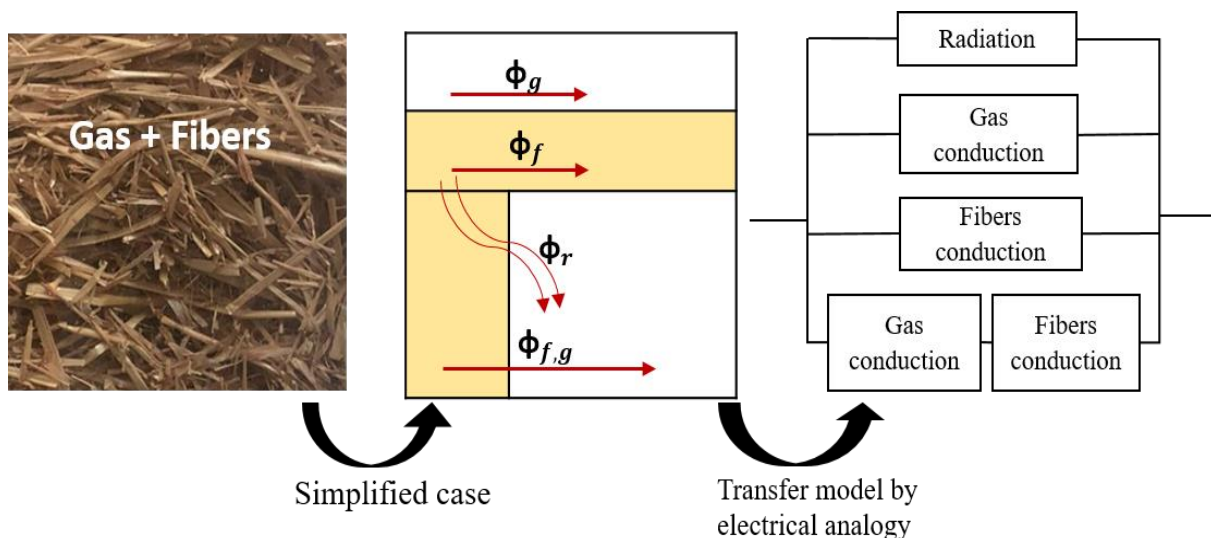


Figure 7.4: Representative volume element of a straw bale and its thermal electrical analogy model

Heat transport models in silicate-based solid fibers [157,158], porous and fibrous materials [155], and aerogel composites [159,171] are used to support the present model's rationale. The existing models are modified to consider the microstructure of the straw material. Csanady *et al.* [160] recently investigated wheat straw to develop a heat transfer model for straw-based structures. Fibers were supposed to be oriented perpendicular to the heat flow, although in reality, fibers have a wide range of orientations. Consequently, the present model introduces the fibers' angle of orientation as a variable. Additional parameters that influence the heat transfer such as bale density, temperature, and RH, are also introduced in the model.

In porous materials, four heat transfer modes are dominant: solid conduction, gas conduction, convection, and radiation. Inside straw materials, convection heat transfer can be neglected. This can be proved by calculating the Nusselt number Nu for straw pores, that have a diameter lower than 4 mm

Chapter 7. Thermal conductivity numerical model

[172]. Nu represents the ratio of the convection flux over the conduction flux. By assimilating straw fibers to cylinders, Nu can be calculated by equation (7.14) according to [173].

$$Nu = \left[0.6 + \frac{0.387 \times Ra^{\left(\frac{1}{6}\right)}}{\left[1 + (0.559 \times Pr)^{\left(\frac{9}{16}\right)} \right]^{\left(\frac{8}{27}\right)}} \right]^2 \quad (7.14)$$

with Rayleigh number Ra and Prandtl number Pr given by equation (7.15) and equation (7.16) that depend on air kinematic viscosity ν_{air} , air thermal diffusivity α_{air} , air thermal expansion coefficient β_{air} , the acceleration due to the gravity g , and the temperature difference ΔT across the fiber length l .

$$Ra = \frac{g \cdot \beta_{air} \cdot \Delta T \cdot l^3}{\nu_{air}} \times Pr \quad (7.15)$$

$$Pr = \frac{\nu_{air}}{\alpha_{air}} \quad (7.16)$$

Nu value is found to be lower than 1 for a ΔT_l lower than 5 °C and a fiber length lower than 15 cm, which is the case in this study. Thus, the convection is neglected compared to the conduction.

By analogy with the heat transfer models in porous and fibrous materials, the total heat flux ϕ_{total} crossing the RVE is the sum of the heat flux by conduction through the solid mater and the air ϕ_c , and the heat flux by radiation among the fibers and pores walls ϕ_r , as written in equation (7.17). By considering a temperature difference ΔT and by applying Fourier's law in an RVE of thickness Δx , equation (7.18) is obtained. Finally, the effective thermal conductivity of the material k_{eff} is obtained as the sum of the thermal conductivities corresponding to the conduction and radiation, respectively denoted k_c and k_r in equation (7.17). k_c is made of a solid conduction component through the matter composed of lignin and cellulose and a gas conduction component through the air, hereafter respectively denoted k_f and k_g . Importantly, the model assumes that there is no heat source inside the material, as can be the case during composting. Besides, the additional coupling between gas and solid conduction that can be found in heat transfer models of fibrous aerogel-based materials [174] is neglected here, due to the relatively large size of the straw fibers' pores.

$$\phi_{total} = \phi_c + \phi_r \quad (7.17)$$

$$\frac{\Delta T}{\Delta x} k_{eff} = \frac{\Delta T}{\Delta x} k_c + \frac{\Delta T}{\Delta x} k_r \quad (7.18)$$

7.2. Validation of the model

The model suggested in this work is designed to estimate the thermal conductivity of all types of straw bales under different conditions. The model is used to determine the thermal conductivity of bales of density 80 kg/m³, 100 kg/m³, and 120 kg/m³, RH between 15% and 95%, temperature between 15 °C and 45 °C, and mostly perpendicular fibers represented by a Gaussian law with a μ of 90° and a σ of 45°.

Chapter 7. Thermal conductivity numerical model

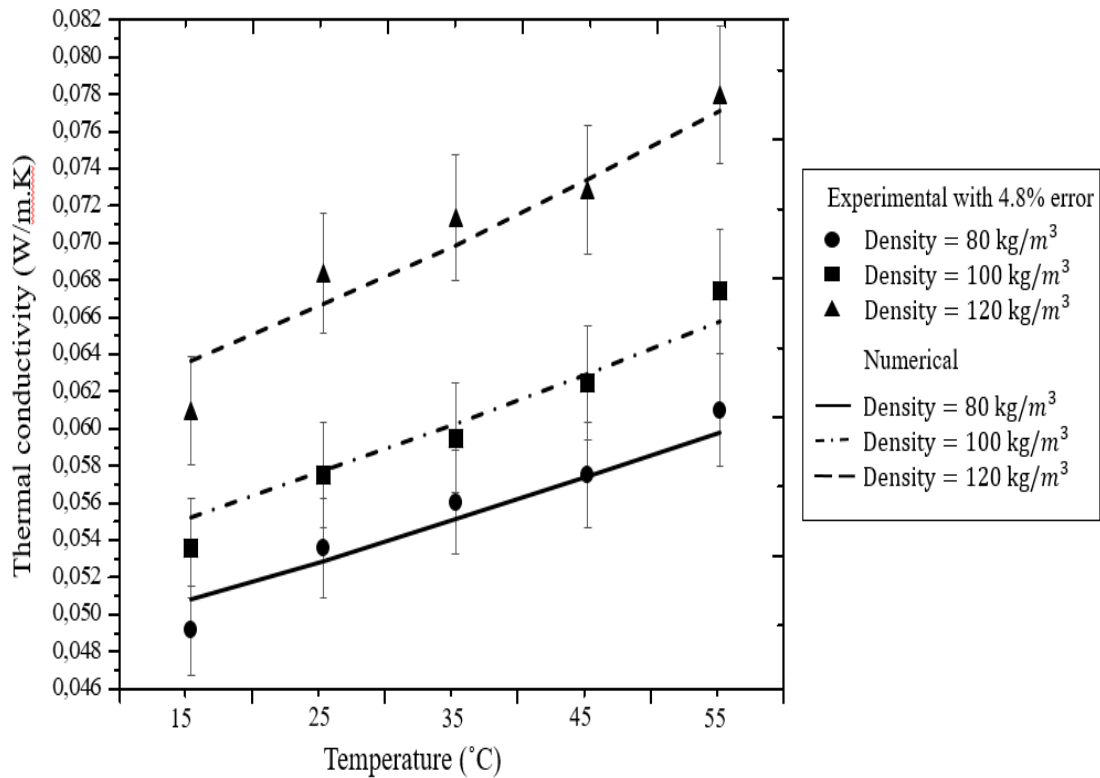


Figure 7.5: Comparison of the numerical and experimental thermal conductivity for bales having densities from 80 kg/m³ to 120 kg/m³ and temperature from 15 °C to 55 °C, at 25 % RH

To validate the mathematical model, these values are compared to the experimentally measured values reported in the previous section, as illustrated in **Figure 7.5** and **Figure 7.6**. The experimental measurement has a cumulated error of $\pm 4.8\%$ of the read value. As discovered during the experiment, the numerical thermal conductivity rises with temperature, RH, and bale's density. The evaluation of the numerical model shows that the trends and variations match the measured values. The quality of the prediction can be assessed by calculating the root mean square error (RMSE) and the scatter index (SI) that considers the measured parameter and its corresponding prediction. The RMSE is 0.0038 W/m.K, and the SI is 6 % (less than 10%), indicating that the model produces good results. In the following section, the validated numerical model is used to further discuss the effects of cellulose content, bale density, temperature, RH, and fiber orientation on the bale's effective thermal conductivity.

Chapter 7. Thermal conductivity numerical model

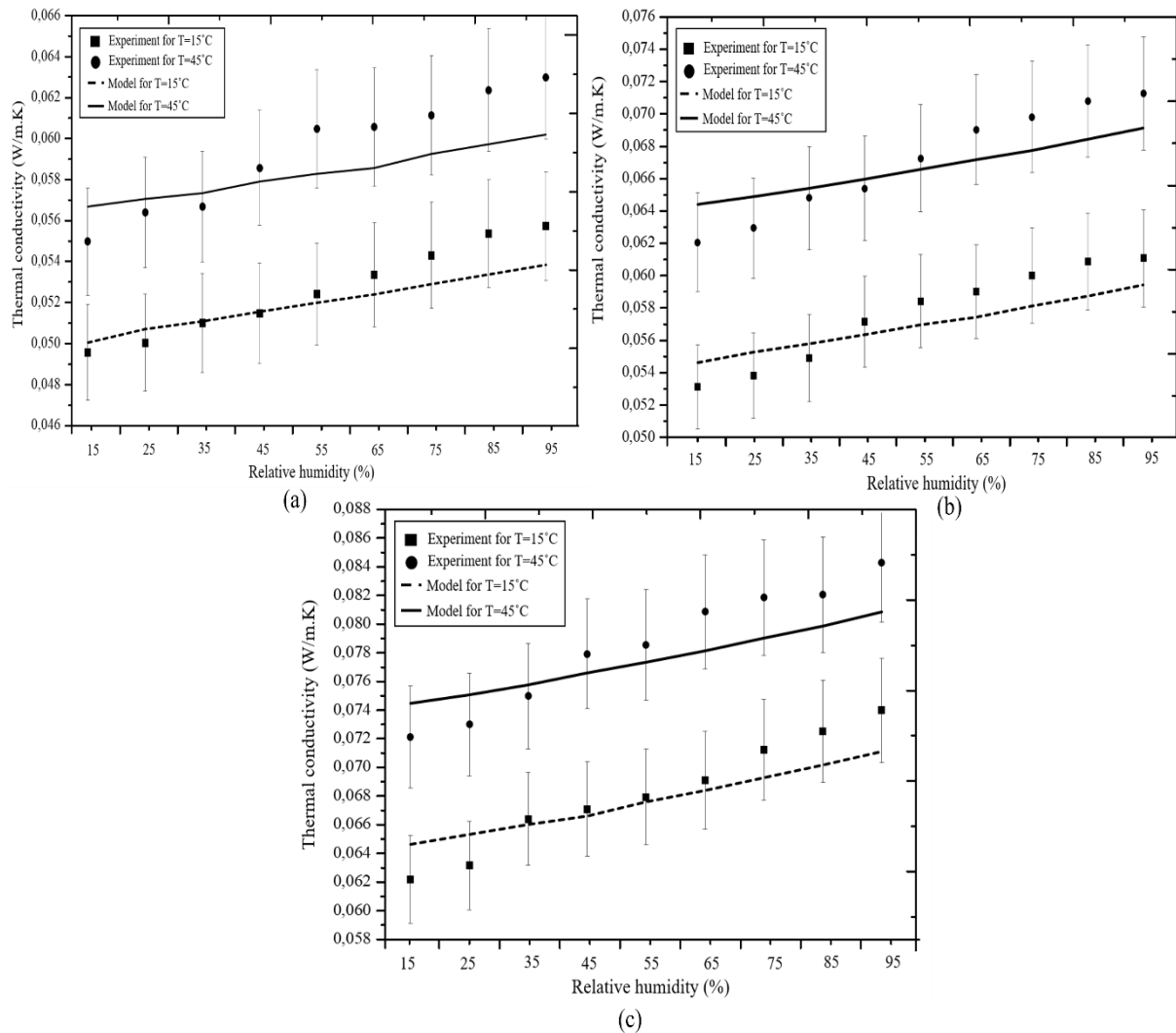


Figure 7.6: Numerical and experimental thermal conductivity variation versus RH for bales having density (a) 80 kg/m^3 , (b) 100 kg/m^3 and (c) 120 kg/m^3 , at 15 and 45 °C

7.3. Parametric study

7.3.1. Effect of cellulose content

Figure 7.7 presents the gas, solid, radiation, and effective thermal conductivity variations versus density and cellulose content, for a fixed temperature of 25 °C and relative humidity of 15 %. The study considers two bales having mostly perpendicular fibers. The first contains 48 % of cellulose and the second 38 % of cellulose. This 10 % difference in the chemical composition affects only the solid component and not the pores' microstructure. The gas conductivity and the radiation component are the same in both cases as they only depend on the air volume in the material. Fibers containing 38% cellulose have an effective thermal conductivity higher than the fibers that contain 48% cellulose by an average of 25%. This trend is readily explained by the insulation property of the cellulose that characterizes the solid part of the fibers, as described in equation (7.3). It can therefore be stated that an increase in cellulose content leads to a decrease in thermal effective conductivity. The cellulose content is directly related to the type of straw.

7.3.2. Effect of bale density

Figure 7.7 also shows the effect of the density on the gas, solid, radiation, and effective thermal conductivity at the same above-mentioned T and RH. The graphs of gas conductivity and radiation components decrease linearly as a function of bulk density, while the solid conductivity component increases as the bulk density increases, which is consistent with the predictions and experimental results.

Chapter 7. Thermal conductivity numerical model

Concerning the radiative component, despite a cubic function of the air amount that controls the total value, as indicated in equation (7.13), it has a very modest curvature at 25 °C. The solid thermal conductivity increases as the bulk density increases, indicating that the volume fraction of solids (less insulating than still air) in the natural composite is increased. Gas conduction varies contrary to solid conduction. This is because the amount of air, responsible for the gas conductivity, reduces with an increase in the bale density. This behavior is reflected in the gas conduction equation that includes the still air thermal conductivity taken as a constant value at a specific temperature. As a result, the linear curve's behavior is explained since the amount of air in gaps available for heat conduction decreases as the bulk density, and hence the number of solid components in bulk, rises. The increase in the solid conduction is higher than the decrease in the gas conduction, which causes an overall increase in the bale's effective thermal conductivity.

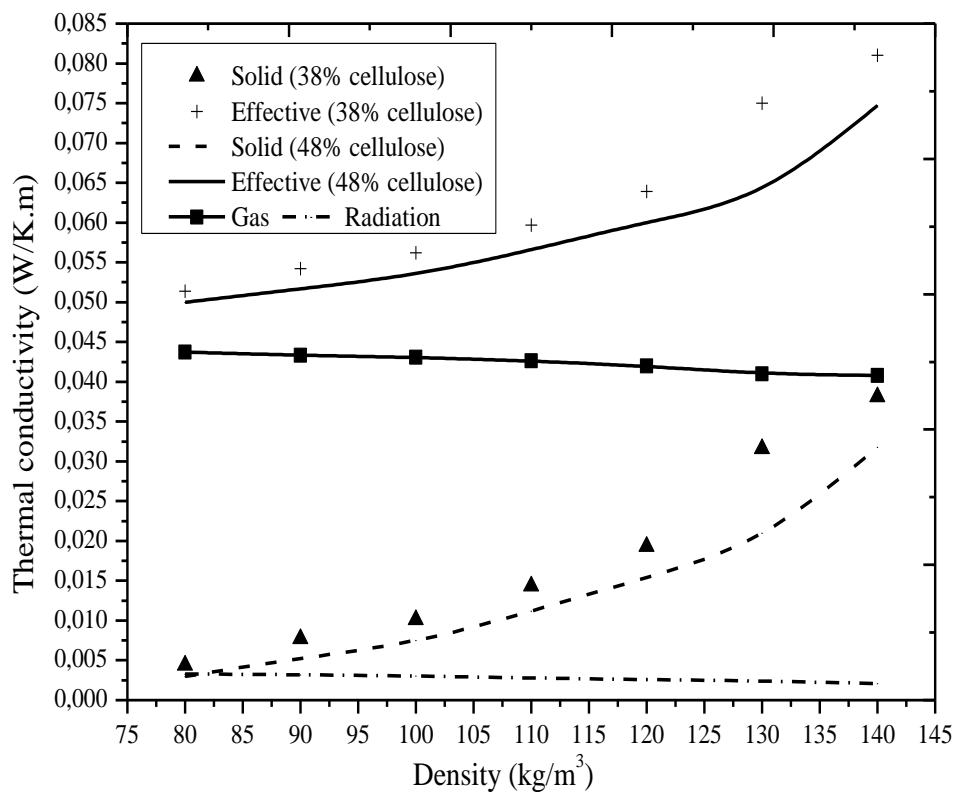


Figure 7.7: Solid, gas, radiation, and effective thermal conductivities versus density for two types of straw composed of 38 % and 48 % of cellulose

7.3.3. Effect of bale temperature

The temperature effect on the gas, fibers, radiation, and effective thermal conductivity is depicted in **Figure 7.8**. The density, RH, and cellulose content of the bale are considered 120 kg/m³, 10 %, and 38 %, respectively. Firstly, the fibers' conductivity does not vary with the temperature since the dominant component of k_s is $k_{cellulose}$, which is higher than k_{air} , and independent of the temperature variation. Secondly, the radiation conductivity slightly increases with the temperature since this component is dependent on the amount of gas and the temperature at order 3. Last, the gas conductivity increases by 12 % when the temperature changes from -10 °C to 30 °C, which causes an increase in the effective thermal conductivity by 9 %. Therefore, it can be stated that the bale's effective conductivity increases when the bale's temperature increases.

Chapter 7. Thermal conductivity numerical model

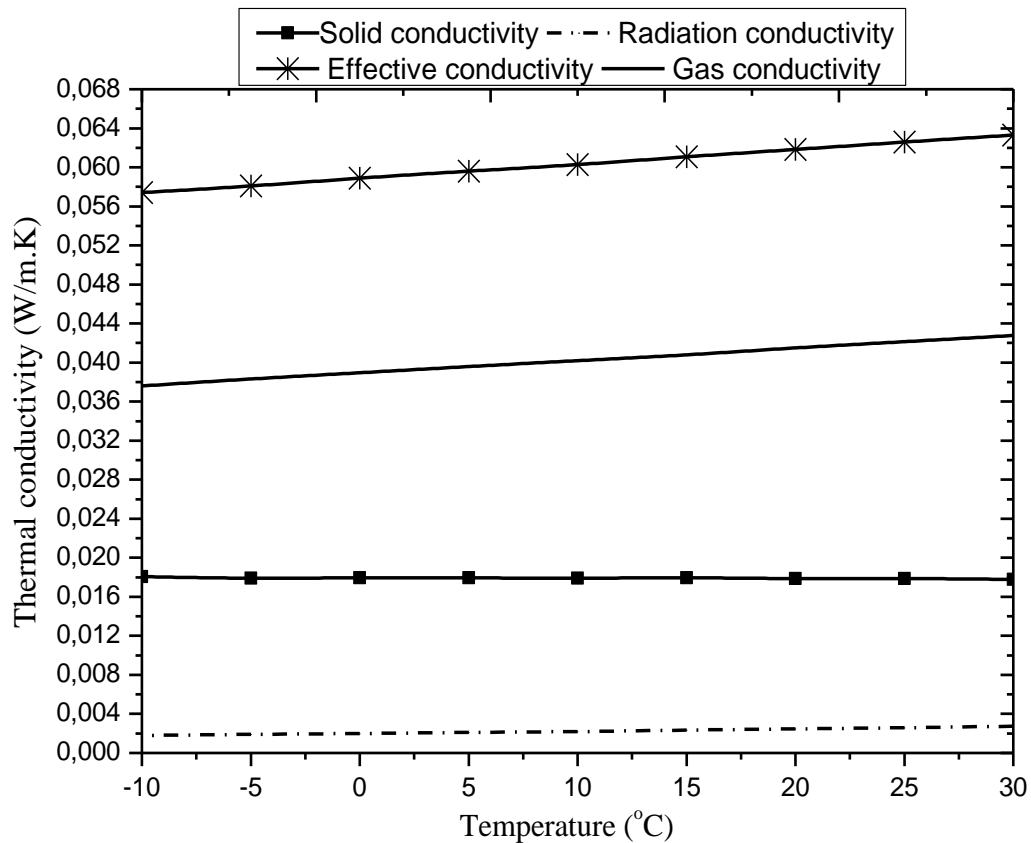


Figure 7.8: Solid, gas, radiation, and effective thermal conductivities versus temperature for a straw bale of RH 10 % and density 120 kg/m^3

7.3.4. Effect of bale relative humidity

The effect of relative humidity on the gas, solid radiation, and effective thermal conductivity is shown in **Figure 7.9**. The density, temperature, and cellulose content of the bale are considered 120 kg/m^3 , $20 \text{ }^\circ\text{C}$, and 38%, respectively. The effective thermal conductivity undergoes a linear growth with increasing RH from 0 % to 30 %. This growth is mainly caused by the increase in the fibers and gas conductivity. The water vapor enters the bale to fill the pores and changes the chemical composition of the fibers, which causes an increase in solid conductivity by 17%, gas conductivities by 4 %, and a decrease in radiative conductivity through the air by 3%. The curve of the gas conductivity is flat since the order of variation of the air thermal conductivity relative to the RH is about 10^{-4} .

Chapter 7. Thermal conductivity numerical model

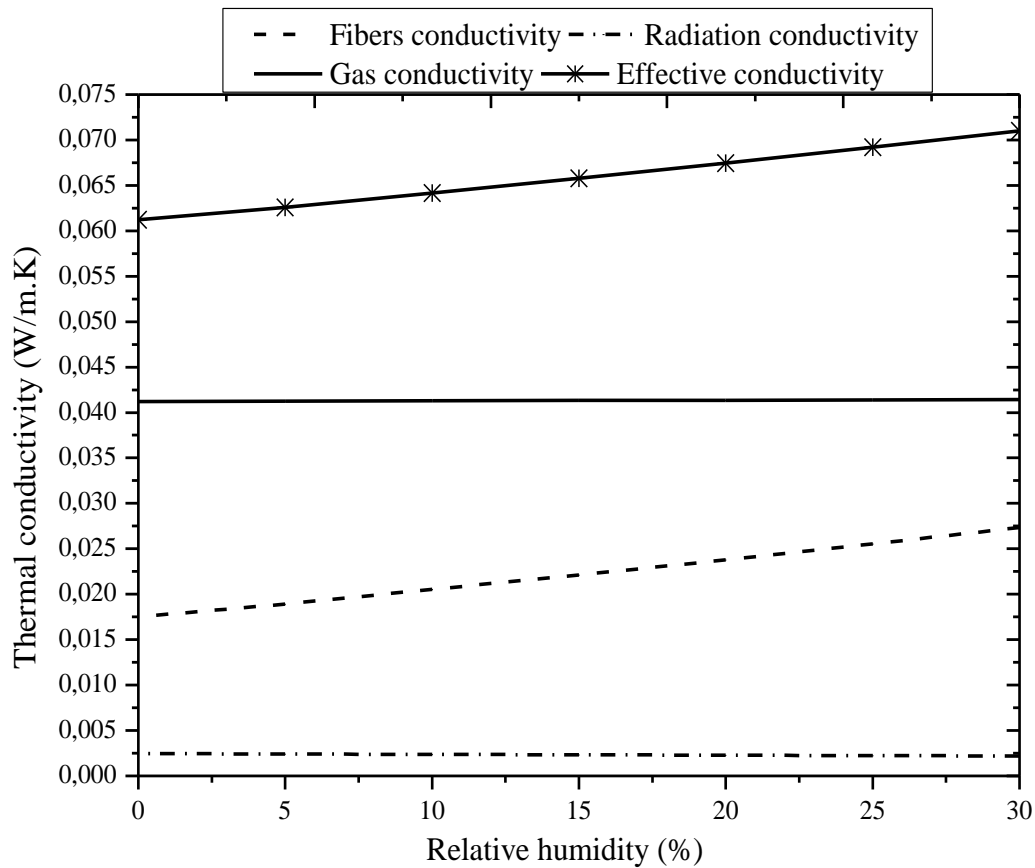


Figure 7.9: Solid, gas, radiation, and effective thermal conductivities versus RH for a straw bale of temperature 20 °C and density 120 kg/m³

7.3.5. Effect of fibers' orientation

The effective thermal conductivity model takes into consideration the orientation of the fibers as it is an important factor that causes its variation. The variation of the orientation is possible by varying the distribution mean μ and the standard deviation σ that determine the Gaussian normal law of fibers' orientation distribution. Straw bales contain fibers oriented in all directions but the distribution of these orientations shows a majority of fibers parallel or perpendicular to the heat flux. **Figure 7.10** compares the effective, solid, and gas thermal conductivity of two straw bales at 25°C and for RH varying from 0% to 30%. The cellulose content is 38% and the bale's density is taken at about 100 kg/m³. The first case is with mostly perpendicular fibers having $\mu = 90^\circ$ and $\sigma = 45^\circ$, while the second is with mostly parallel fibers with $\mu = 180^\circ$ and $\sigma = 45^\circ$. In both cases, as the RH rises, the radiation conductivity has a constant value of 0.003 W/m.K, and the gas conductivity increases slightly from 0.0426 W/m.K to 0.044 W/m.K. The constant radiation conductivity is explained by the constant density of the bale while the increase of the gas conductivity is explained by the higher thermal conductivity of water vapor compared to that of dry air. These parameters apply only in the gas phase, in which thermal conductivity does not depend on the fiber's orientation. The difference between the perpendicular and parallel cases is found to be in the solid conductivity. In the first case, it increases from 0.01 W/m.K to 0.02 W/m.K and in the second case from 0.023 W/m.K to 0.034 W/m.K. Solid conductivity augmentation leads to an increase in the effective thermal conductivity. As previously explained, the thermal conductivity of parallel fibers is higher than that of perpendicular fibers due to the difference in thermal paths. In the parallel case, there is a direct path for heat transfer through the solid part of the fibers, which increases the effective conductivity.

Chapter 7. Thermal conductivity numerical model

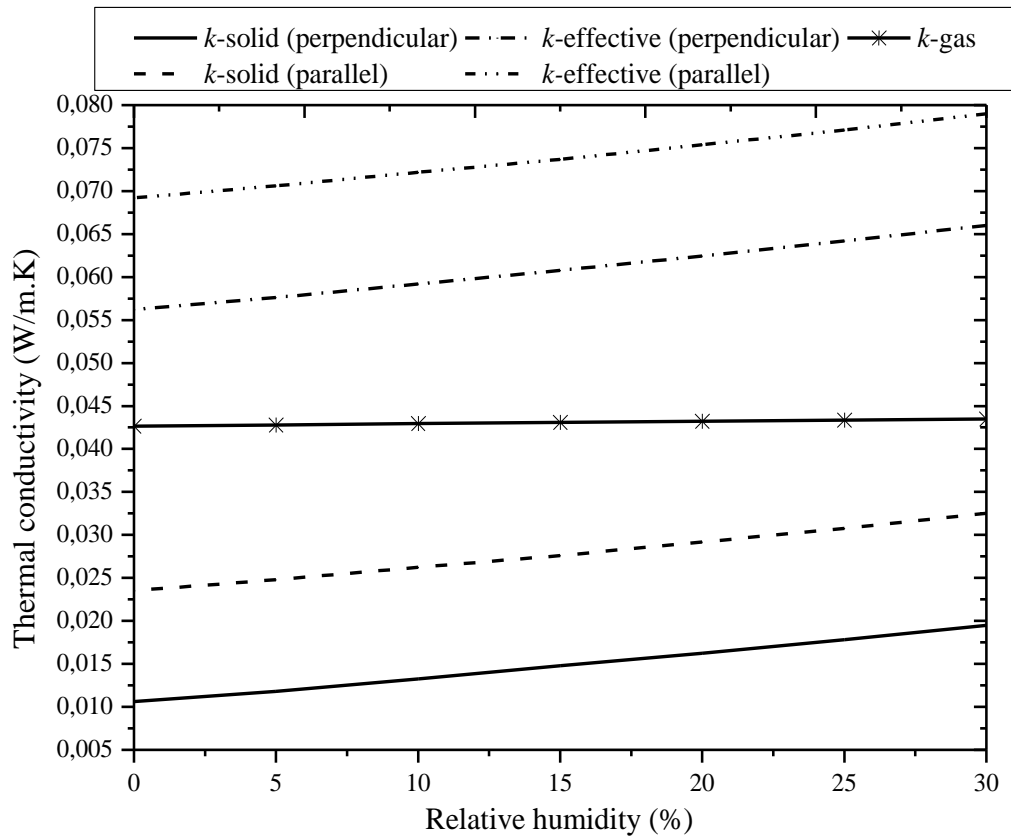


Figure 7.10: Solid, gas, and effective thermal conductivities versus RH for a straw bale at a temperature of 25 °C and density of 100 kg/m³ with fibers mostly perpendicular ($\mu=90^\circ$, $\sigma=45^\circ$) and mostly parallel ($\mu=180^\circ$, $\sigma=45^\circ$) to the heat flux.

The current chapter provides a mathematical equation that predicts the effective thermal conductivity of straw bales. The model is built from an observation of straw fibers' microstructure. It is then validated through experimental measurement of the thermal conductivity when varying the temperature, relative humidity, density, and the fibers' orientation. The microstructure and chemical composition of each part of a straw fiber, such as the nodes and the internodes, affect the heat transfer in the whole material. Fibers containing 38 % cellulose have an effective thermal conductivity higher than the fibers that contain 48 % cellulose by an average of 25%. The 10 % difference in the cellulose content affects only the solid component while the gas conductivity and the radiation component remain the same in both cases. Straw bale's effective conductivity increases with temperature by 9% due to the increase of the gas and radiation conductivity. Straw bale effective conductivity increases with the RH because of the increase in solid conductivity by 17%, gas conductivities by 4 %, and a decrease in radiative conductivity through the air by 3%. The thermal conductivity of wheat straw bales is highly affected by the fibers' orientation. The thermal conductivity of bales having perpendicular fibers is about 16 % lower than that of bales having parallel fibers. The proposed model allows the assessment of optimal thermal conductivity based on the main affecting factors. Such a study help reach a compromise between the fibers' chemical composition, density, RH, and orientation. The obtained results of this part will be used in the following parts to study their effect on the wall and building behavior.

Third part: Straw wall Characterization

8. Fire resistance test

This chapter examines the fire resistance of a novel type of straw bale wall covered by wood and mineral foam. The goal is to verify a 180-minute resistance. Firstly, the chapter describes the sample preparation and the thermocouples locations. Secondly, the fire resistance test is done according to Eurocode 8 by using a furnace and pyrometers. The experimental work is completed by the design of a numerical model of the heat transfer implemented on ABAQUS software. Both experimental and numerical results are compared in order to validate the numerical model. At the end, the main findings of the study are discussed.

Table of contents

8.1. Experimental work.....	93
8.1.1. Previous study.....	93
8.1.2. Sample preparation.....	93
8.1.3. Testing facilities.....	95
8.2. Experimental results.....	97
8.3. Numerical model.....	99
8.3.1. Modeling approach.....	100
8.3.2. Thermo-physical properties of materials.....	100
8.3.3. Boundary and initial conditions.....	101
8.4. Numerical results validation.....	102
8.5. Proposed solution.....	103

8.1. Experimental work

8.1.1. Previous study

One of the most serious risks that structures might encounter during their lifetime is fire. Testing for fire resistance is essential for building materials to evaluate how well the entire structure will withstand a fire. Typically, massive furnaces are used to test the fire resistance of walls, beams, etc. against a conventional temperature-time curve that rises from ambient to 1000 °C over 60 minutes [175]. This test is defined by the international standard ISO 834-1 since 1991 and is applied in Europe, Australia, and other countries [85]. This study focuses on the fire resistance of straw bale walls, which is mostly dependent on the entire wall assembly rather than just the main material used to build them. Because the flames cannot penetrate the straw bales, they serve as a second line of defense after the covering outer layers. Straw bales are distinguished by a density exceeding 100 kg/m³. Therefore, there is not enough free oxygen present to sustain the spread of flame. According to RFCP [151], straw bales are classified as a product having a very low contribution to a fire, a very little production of smoke, without producing blazing droplets (B-S1-d0). In the latest reviews [137,176], researchers highlighted the experiments achieved by studies on fire resistance straw bales walls. Wall *et al.* [84] looked at a straw-and-lime plastered wall's ability to resist fire. Before the plaster started to peel off from the bales, the wall survived the fire for 90 minutes. The test was carried out for a further 45 minutes, but only when the exposed area was completely charred and black. Therefore, it was assumed that the tested sample has a 135-minute fire rating surpassing the 30-minute threshold of the local UK regulation. A clay plastered straw bale wall passed a 30-minute fire test conducted by Andersen and Munch [177]. This fire spread rate exceeded their local Danish norm. In addition, Theis [91] mentioned an experimental study done by different researchers in Mexico to compare plastered and unplastered straw wall fire rates, based on the results of small scale ASTM E-119 fire tests. The unplastered wall resisted the fire for 30 minutes before the flames started penetrating the joint between bales while the plastered wall resisted for two hours. Džidić [85] also mentioned several experimental studies done in Austria, the Czech Republic, and the USA to show the fire resistance of straw walls. In the USA, a non-loadbearing straw bale wall covered by a 13 mm cement layer from both sides and having an area of 15.5 m² resisted the fire for 120 minutes [92]. In the Czech Republic, a loadbearing straw bale wall plastered on both sides and loaded with 12 kN/min resisted for 146 minutes as a maximum record while a straw wall covered by wood and loaded with 20 kN/min resisted for 66 minutes. Apte *et al.* [178] examined experimentally and numerically the fire behavior of rendered straw bales (with either lime or earth layer) when subjected to two different radiant heat flux: one of 30 kW/m² for 30 min and the other 50 kW/m² for 40 min. For both used renders, a fire started inside the bale at 50 kW/m² in about 10 days. This self-heating was modeled numerically and showed good agreement with the experimental results for the temperature inside the bale. The already obtained results concerning the performance of straw walls against fire do not include the layout proposed by the industrial partner Activ'Home. The current experiment is therefore necessary since the tested wall is different from the already investigated ones and will be tested for the first time.

8.1.2. Sample preparation

The tested wall is in the form of straw filled in a Laminated Veneer Lumber (LVL) box. The sample shown in **Figure 8.1**, has a length and height of 910 mm that correspond to the dimension of the oven's door. The wall mechanical resistance is ensured by a wood I-beam that separates two bales. The straw bales' dimensions are 860 mm × 360 mm × 460 mm with a density of 120 kg/m³ and a moisture content of 12%. These values respect the professional rules of straw construction [179]. The exterior and interior sides of the wall are covered with a 12.5 mm fermacell gypsum board. Only the surface exposed to the fire is covered by an additional 44 mm mineral foam layer. The materials are supplied and assembled by the industrial partner Activ'Home [121].

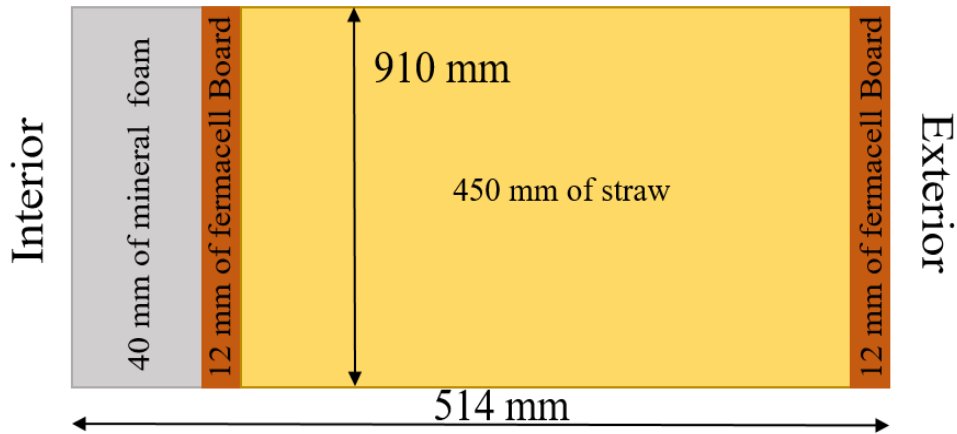


Figure 8.1: Side view of the sample showing its composition

The assemblage is done, first, by fixing the wooden LVL boards to the wood I-beam. LVL is a composite material made of layers of wood veneer laminated with an adhesive where the fibers are mostly oriented in the same direction. Secondly, the Fermacell panels and the mineral foam panel close the prepared frame from both sides as shown in **Figure 8.2 (1)**. Fire-resistant glue is used to assemble the four pieces of foam. As a final step, straw bales are compressed in a way to fill the whole box, and then an LVL board is added to isolate the straw from the exterior as shown in **Figure 8.2 (2)**. These steps are then followed by thermocouples fixation inside the wall at different locations. The full system is shown in **Figure 8.2 (3)**. The six sensors in the straw are inserted at 23 mm, 43 mm, 65 mm, 100 mm, 200 mm, and 300 mm from the mineral foam external surface.



Figure 8.2: Sample preparation steps and the thermocouple placement inside and on the surfaces of the wall

Chapter 8. Fire resistance test

8.1.3. Testing facilities

The fire resistance test is done by using a furnace equipped with 4 pyrometers, and 14 K-type thermocouples inserted in the tested straw wall. The oven is designed and manufactured in the workshops of IUT Clermont Auvergne by using 150 mm of Superwool Blanket and refractory bricks at the level of the chimney and the hearth as shown in **Figure 8.3**.

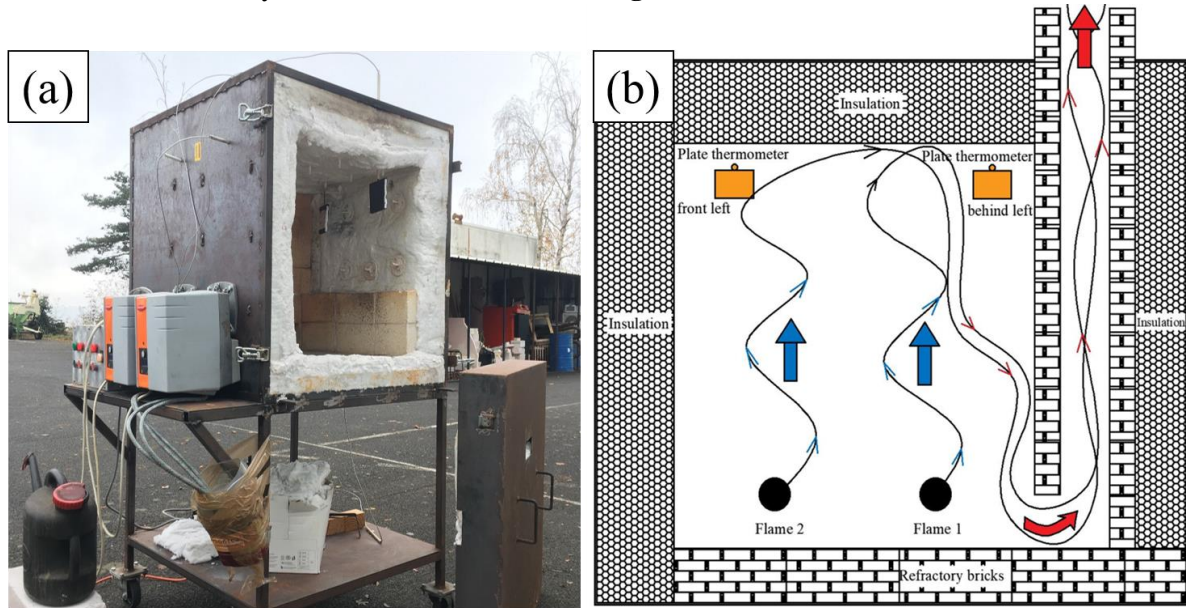


Figure 8.3: (a) furnace 1 m wide, 1 m deep, and 2 m high used for the experiment with two burners, (b) section sketch of furnace setup showing the flame and thermometer locations, and the smoke and heat path

The furnace is equipped with 2 fuel burners each having a power of 29 kW. The temperature in the furnace is measured by plate thermometers fixed at the 4 corners of the furnace. They are made of a folded steel plate base (nickel alloy strip 0.7 ± 0.1 mm thick), to which is fixed a sheathed K-type 1mm diameter thermocouple covered by an insulating material. The precision of these thermometers is about ± 6 °C while that of wall thermocouples is ± 0.5 °C. The thermocouples are distributed all over the investigated wall thickness. Thus, two sensors are placed on the exposed surface, three between the foam and the fermacell, one between the fermacell and the straw, six in the straw, one between straw and fermacell, and one on the non-exposed surface.

The test started by calibrating the burners inside the furnace to evaluate their capacity to reproduce the ISO-834 fire curve [175] according to EN-1363-1 2013 [180]. The calibration test was performed with an empty furnace and took 70 minutes in total. The comparison of the temperature inside the oven and the ISO-834 curve is represented in **Figure 8.4**. It is noticed that the temperature variations of the furnace followed properly the standard curve. The oscillations during the first 10 minutes are due to the turning on and off of the second burner. From minute 10, only one burner was sufficient to reproduce the ISO-834 curve.

After this calibration step, the test continued by hanging on the wall that is used as a door for the oven. To ensure the insulation on the boundaries between the wall and the furnace, a layer of super wool blanket was added on the edges, as seen in **Figure 8.5**. Then, the experiment began while observing the temperature variations in the furnace, the wall, and the exterior.

Chapter 8. Fire resistance test

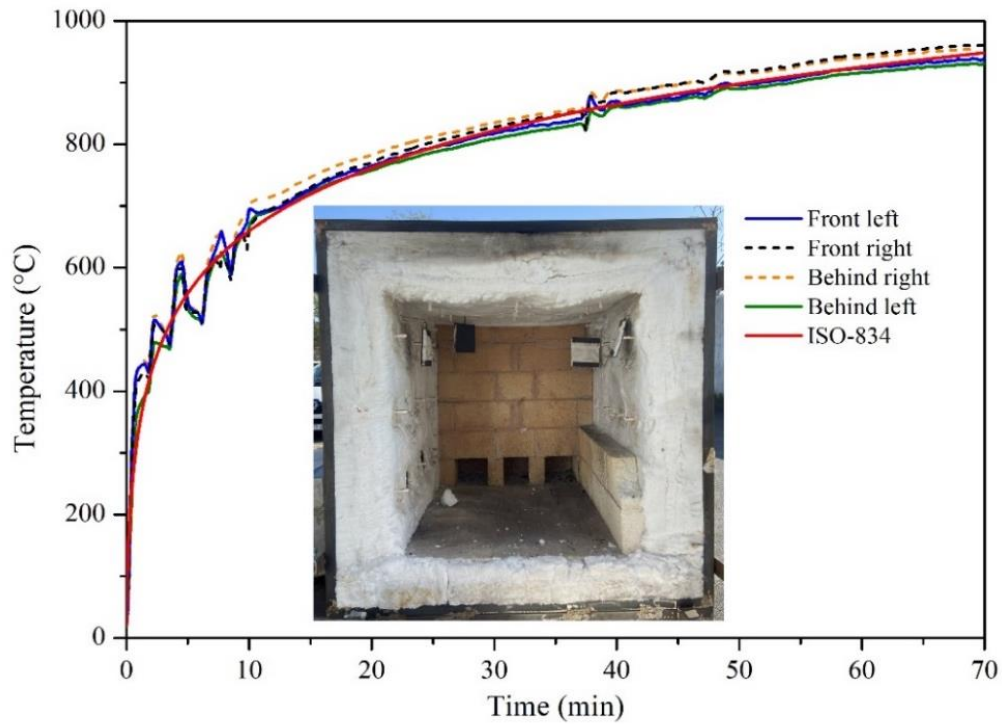


Figure 8.4: Temperature variation inside the furnace compared with ISO-834 curve



Figure 8.5: Installation of a straw wall. Insulation material is added at the edges between the wall and the furnace before starting the experiment

According to [85] a building component's performance against fire is classified by assigning a time limit in minutes that indicates how long the performance criteria are met during the test. The most important ratings include the load bearing capacity (R), the integrity (E), and the insulation (I). R denotes a building component's resistance to fire while supporting an external load. The element can be loaded in bending, such as the floor, or axially, such as the wall, and the rate of deformation should be measured in both

Chapter 8. Fire resistance test

cases. E represents a sample extracted from a building component that is exposed to fire on one side and can prevent flame passage through it. The requirements emphasize the observation of surface cracks, ignition, and flame on the exposed side. I describes how a sample with one exposed side can limit the temperature rise of the unexposed face. The same fire resistance ratings are used to classify the tested straw wall.

8.2. Experimental results

Visual observations of ignition indications such as burning, smoking, and cracking on the exterior surfaces, as well as temperature values at various locations in the wall, are used to study and analyze the performance of the sample against the fire. **Figure 8.6** and **Figure 8.7** depict the results of the test. The sample is classified as EI 180 which means that the wall exposed from one side prevents the fire from progressing to the other side. This classification is explained by the prevention of the flame passage to the unexposed surface and the absence of cracks with limited temperature rise on the unexposed surface.

Despite this performing result, the wall passed through many levels that threatened its mechanical stability and resistance. The first smoking indications were observed during the experiment at minute 77 between the mineral foam and the fermacell panel due to the fire seal paste that binds them. This finding is surprising given that the used paste is EI 180. As a result, the only reasonable explanation is that the paste was not applied correctly or in sufficient quantity. The deterioration of the fire seal paste in some locations allowed the fire to reach the fermacell and then the straw surface after 165 minutes when the smoke was seen. The heat capacity of the mineral foam, the fermacell, and the straw helped in preventing the total burning of the wall. Therefore, the goal of adding the mineral foam to the interior side of the wall is validated through this experiment since after 180 minutes the unexposed surface of the sample had a slight temperature increase to 60 °C.



Figure 8.6: Smoking indications on edges of the exposed face of the wall

Chapter 8. Fire resistance test

Regarding the temperature variation, the first temperature observations showed a progressive increase from 22°C to 50°C, between 40 mm and 75 mm from the fire at locations 3, 4, 5, 6, 7, and 8, after 10 minutes. At the end of the experiment, the maximum reached temperature was 750 °C for the same locations. Similar behavior was obtained after 40 minutes at locations 9 and 10 leading to stabilization at 100 °C between minutes 60 and 130 explained by a liquid to vapor phase change of the water contained in the straw bales. Afterward, the temperature increases until reaching a maximum temperature of 390°C for location 9 and 300 °C for location 10. Inside the bale, at location 11, the temperature remained at 28 °C for 100 minutes, and then it rose to reach 100 °C after 180 minutes. These values were similar at locations 12, 13, and 14. The low transfer of heat to the unexposed surface is explained by the high thickness, high thermal resistance, and low thermal diffusivity of the wall. In addition, it is important to mention that the initial presence of 15% of humidity in the straw prevented the temperature augmentation for a significant amount of time.

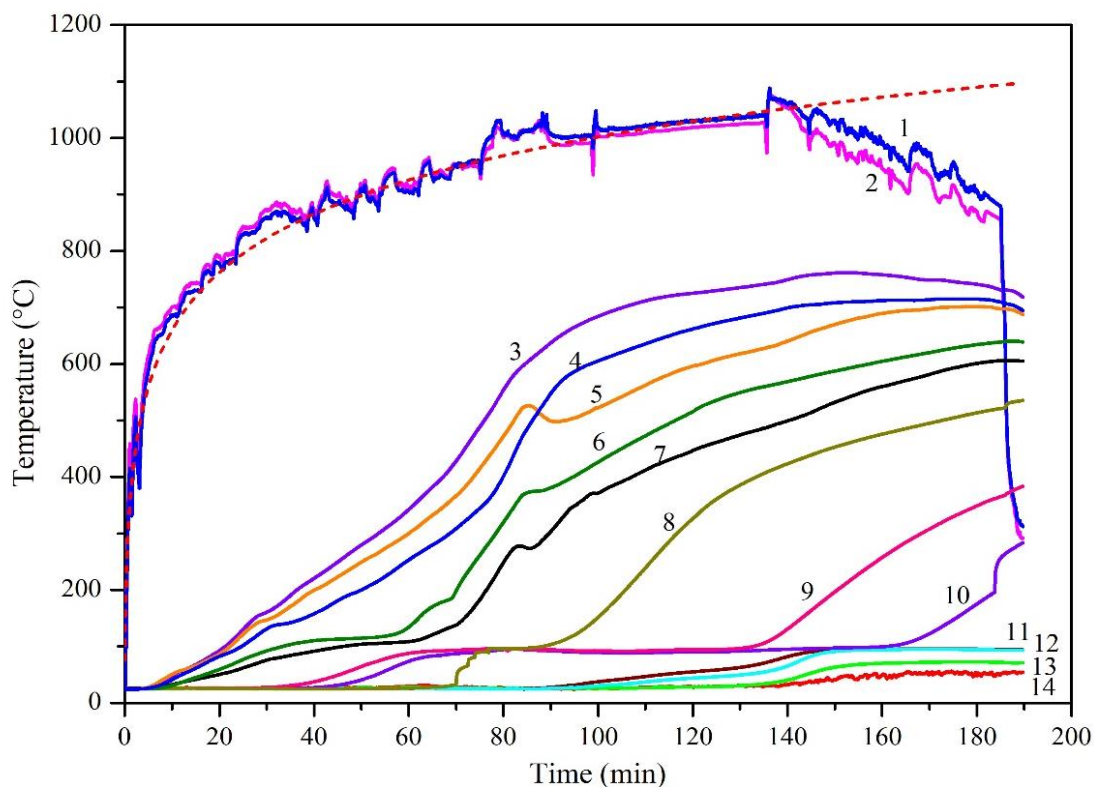


Figure 8.7: Transient temperature variation during the experiment at different locations in the wall

The furnace temperature followed the ISO-834 standard for 140 minutes, reached a maximum of 1088 °C, then started decreasing as seen at locations 1 and 2 that represent the sample surface, noting that the burners' power remains the same during the test. The temperature decrease in the furnace is explained by the fire penetration that caused the direct contact of the interior of the furnace and the fermacell having a lower temperature (500 °C). After 180 min, the burners are turned off and the experiment is stopped, the wall is taken down to inspect the exposed side as shown in **Figure 8.8**. The previous expectation is verified since a hole was formed in the fermacell which caused the combustion of the straw bale. As a result, about 36 % of the straw was damaged since the thickness diminished from 45 cm at the beginning to 29 cm at the end. The mineral foam which was in direct contact with the flame was damaged by about 50 %.

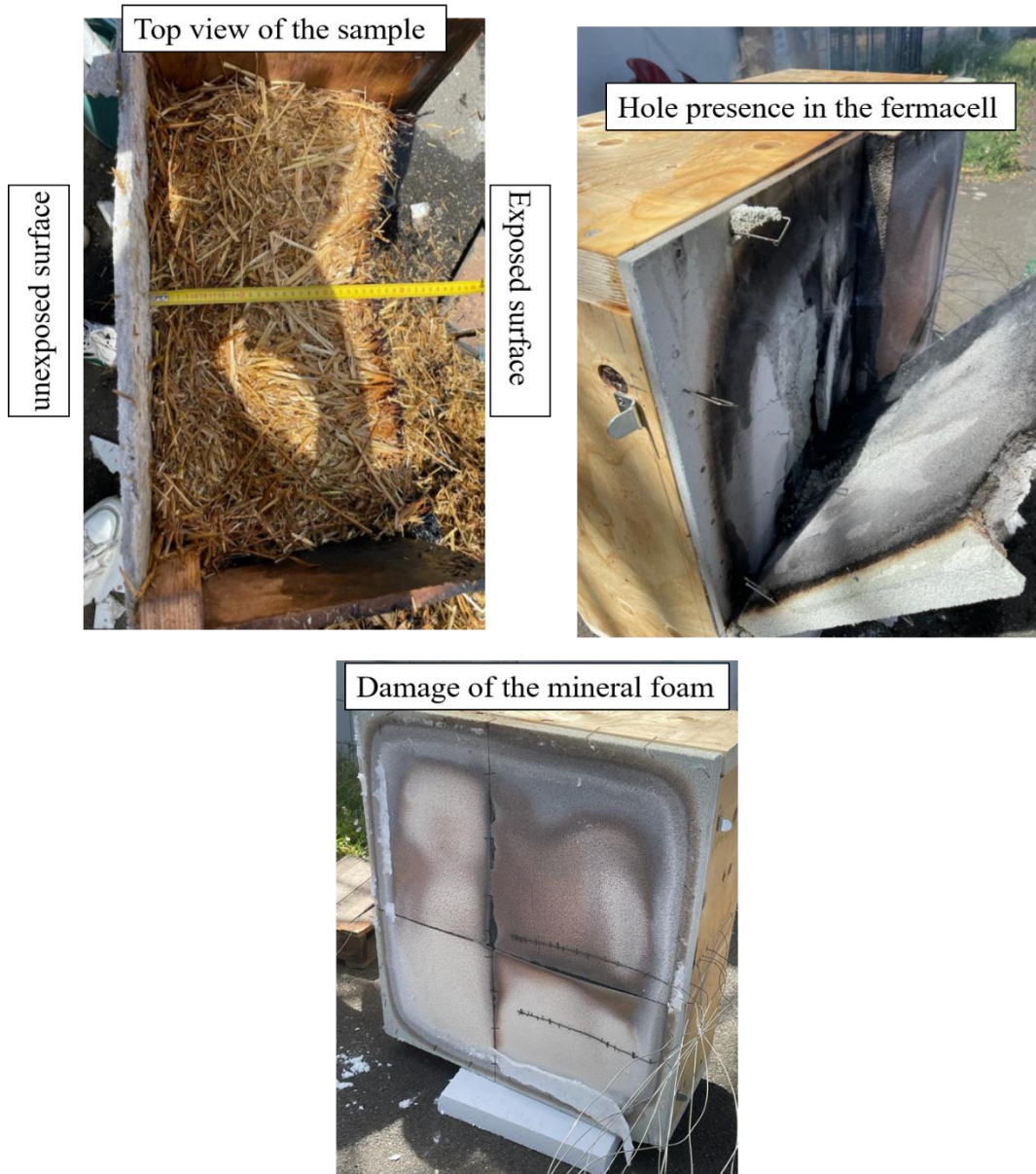


Figure 8.8: Post-fire sample aspect showing a hole in the fermacell that caused the straw to burn

During the tests, it was noticed that the presence of mineral foam delays the heating propagation to the straw. Thus, the wall succeeds in resisting the fire for more than 180 min. The main problem was the bad application of the fire seal paste which accelerate the process. It was not possible to repeat the experiment with the needed corrections.

8.3. Numerical model

The existing literature rarely presents numerical heat transfer models under fire for straw walls, which underlines the novelty and importance of such studies. This section examines numerically the fire resistance of a novel type of straw bale wall covered by wood and mineral foam by using Abaqus software. The study is based on several researches made for other materials. Hajiloo and Green [181] used Abaqus to evaluate and anticipate the stress in reinforced concrete slabs once subjected to fire. Gao *et al.* [182] built a finite element model in Abaqus to emulate reinforced concrete beams' behavior under fire. They concluded that the model produced more accurate findings when interfacial bonds between the reinforcing steel and the concrete were included in the model. Bamonte *et al.* [183] used Abaqus to carry out parametric research on the impact of boundary conditions and load levels on the structural

Chapter 8. Fire resistance test

behavior of reinforced concrete walls under fire. Their findings demonstrated that the amount and direction of the wall displacements during fire exposure are significantly influenced by the compressive load and boundary conditions. Kang *et al.* [184] examined how wall thickness affects the thermal behavior of reinforced concrete walls under fire, using Abaqus. For varied moisture conditions, they were able to forecast the temperature distribution over the thickness of the wall. These studies are used in this chapter to reproduce the experimental wall and propose a modified model that provides better results.

8.3.1. Modeling approach

The purpose of this section is to study the heat transfer behavior of two-dimensional (2D) straw walls numerically using Abaqus software [185]. Abaqus engineering software is suitable for computer simulations of heat transfer processes based on the finite elements method (FEM) that can predict the temperature distribution in a wall subjected to standard fire exposure.

Conduction, convection, and radiation are the three main heat transfer processes occurring over a wall that should be considered in the FE model. The net heat flux at the surfaces is the sum of convective heat flux (\dot{h}_c) and radiative heat flux (\dot{h}_r) as shown in equation (8.1), equation (8.2), and equation (8.3) defined by Eurocode 1 [186]. Eurocode 1 also implies the coefficient values of the exposed and unexposed surfaces.

$$\dot{h}_{\text{net}} = \dot{h}_c + \dot{h}_r \quad (8.1)$$

$$\dot{h}_c = \alpha_c \cdot (T_g - T_m) \quad (8.2)$$

$$\dot{h}_r = \phi_r \cdot \epsilon_m \cdot \epsilon_f \cdot \sigma \cdot (T_r^4 - T_m^4) \quad (8.3)$$

with ϵ_m the thermal emissivity of the materials equal to 0.8, ϵ_f the thermal emissivity of fire equal to 1, α_c the coefficient of convection on the exposed side is equal to 9 W/(m²·K) and on the unexposed side is equal to 4 W/(m²·K), σ the Stephan Boltzmann coefficient, T_g the temperature of the air inside the furnace, T_m the surface temperature of the material, T_r the radiation temperature of the fire environment, and ϕ_r a view factor that is usually taken as 1. In the case of fully engulfed objects, T_r is supposed to equal T_g .

Thermal FE models of walls are reliant on the material's thermal properties such as thermal conductivity, specific heat, and density variations with increasing temperature. The conduction effect is incorporated into the FE models by using thermal conductivity values at elevated temperatures.

The wood is considered orthotropic which means it has three planes of symmetry. A mesh size of 1 to 6 mm was used by several researchers for heat transfer analyses in timber, to ensure accuracy while saving computational time [187]. In this thermal model, the mesh size is set as 5 mm. It is assumed that all interfaces between wood and straw, straw and fermacell, fermacell, and foam are in perfect thermal contact (no contact resistance). Finite elements of type DC2D4 - linear heat transfer quadrilateral with 4 nodes available in the ABAQUS library are used, with normalized fire exposure time.

8.3.2. Thermo-physical properties of materials

The tested wall presented in **Figure 8.1** is modeled. It is composed of four elements that include the mineral foam layer, the fermacell layer on both sides, the wood box, and the straw. The seal paste between the mineral foam plates is modeled as a slot to represent the thermal bridge caused by its bad application. As previously mentioned, it is necessary to define the thermal conductivity, density, and specific heat capacity of each element.

At high temperatures, the variation of physical and thermal properties of wood with temperature was taken from the EN 1995-1-2 standards [188] as shown in **Figure 8.9**. The reported values of specific heat show a peak most often between 99 °C and 120 °C for wood. This accounts for the vaporization of

Chapter 8. Fire resistance test

water in the wood and is represented by a large increase in the energy required to facilitate this phase change from liquid to gas [189]. The wood thermal conductivity highly increases after reaching 600 °C and density decreases progressively from 600 kg/m³ to almost 0 kg/m³ due to the presence of cracks on the surface of the material already transformed into coal at 300 °C [190]. The same behavior is witnessed with straw material. However, the properties of straw at high temperature do not exist in the literature. Therefore, the model was calibrated to provide results closed to the experimental data. The straw's specific heat capacity is 1500 at a minimal temperature, from 0 to 70 °C. At a certain temperature, after 70 °C, the water will vaporize and the compressed bale will burn [191]. Therefore, the specific heat will increase to 10000 J/kg.K and decrease to attain 0 J/kg.K at 200 °C. These assumptions are taken after comparing the straw to the wood. For the other materials, constant values are considered due to lack of information. For the fermacell, the thermal conductivity, specific heat capacity and density are respectively 0.32 W/m.K, 1100 J/kg.K, and 1150 kg/m³ while for the foam, they are respectively 0.09 W/m.K, 1300 J/kg.K, and 300 kg/m³.

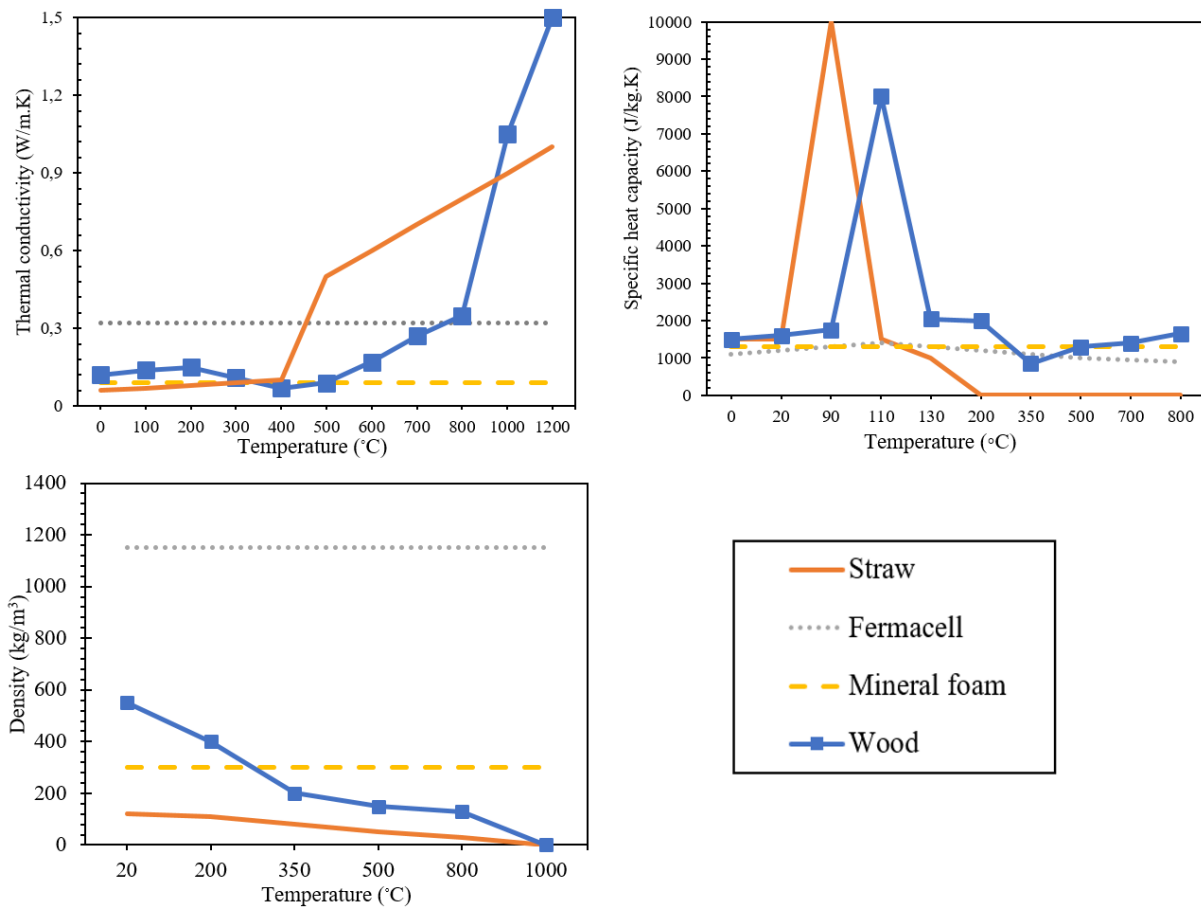


Figure 8.9: Thermal conductivity, specific heat capacity, and density variations with respect to the temperature of straw, fermacell, mineral foam, and wood

8.3.3. Boundary and initial conditions

The ISO-834 standard fire curve of the furnace is used as a boundary condition of the interior side of the tested wall as shown in **Figure 8.10**. This is assigned using the amplitude time-temperature curve. The interior and exterior convection coefficients are taken as 9 W/(m²·K) and 4 W/(m²·K), respectively. The radiation at the unexposed surface is neglected since the experiment is done in the morning and the shade. It is assumed that the layer's initial temperature is 20 °C. For the unexposed surfaces, the wood box and fermacell, the initial temperature is set at 20 °C which represents the temperature of the ambient environment at the beginning of the test.

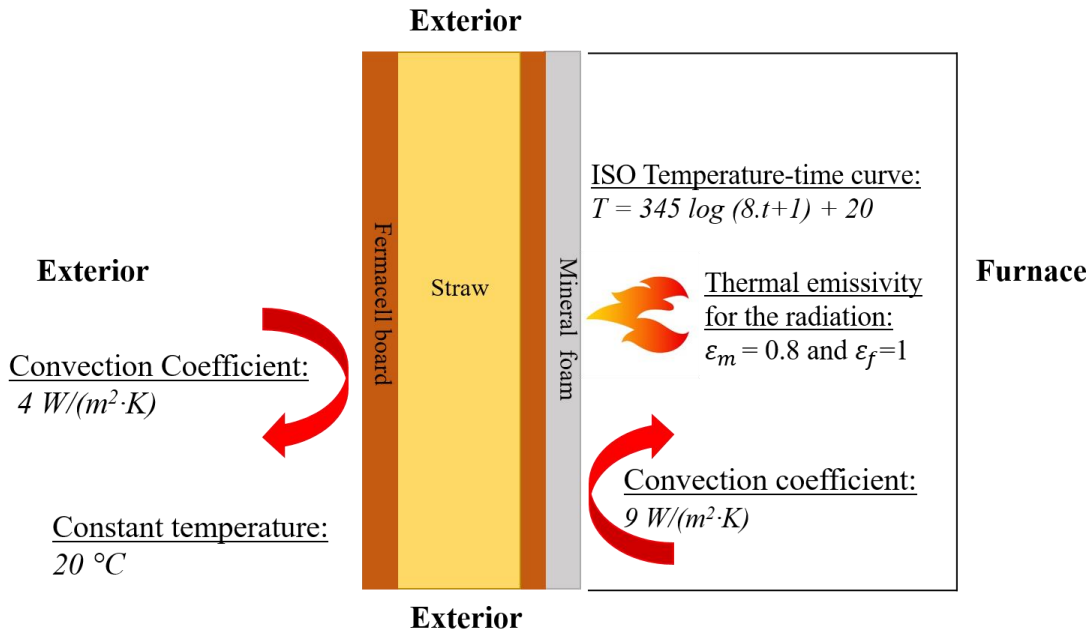


Figure 8.10: Boundary conditions at the interior and exterior sides of the test wall

8.4. Numerical results validation

Figure 8.11 compares the calculated and measured transient temperature values. The numerical and experimental temperature variations of the mineral foam surface are in good agreement. The root mean square error (RMSE) and the scatter index (SI) are respectively 24 °C and 3 %. The difference in temperature values at location 5, representing the fermacell surface, is due to the uncertainty in its properties. At this location, the RMSE and the SI are respectively 53 °C and 17 %. The RMSE at locations 6, 7, and 8 representing the inside of the bale is found to be respectively 36 °C, 31°C, and 44 °C, while the SI is found to be respectively 9 %, 8 %, and 12 %.

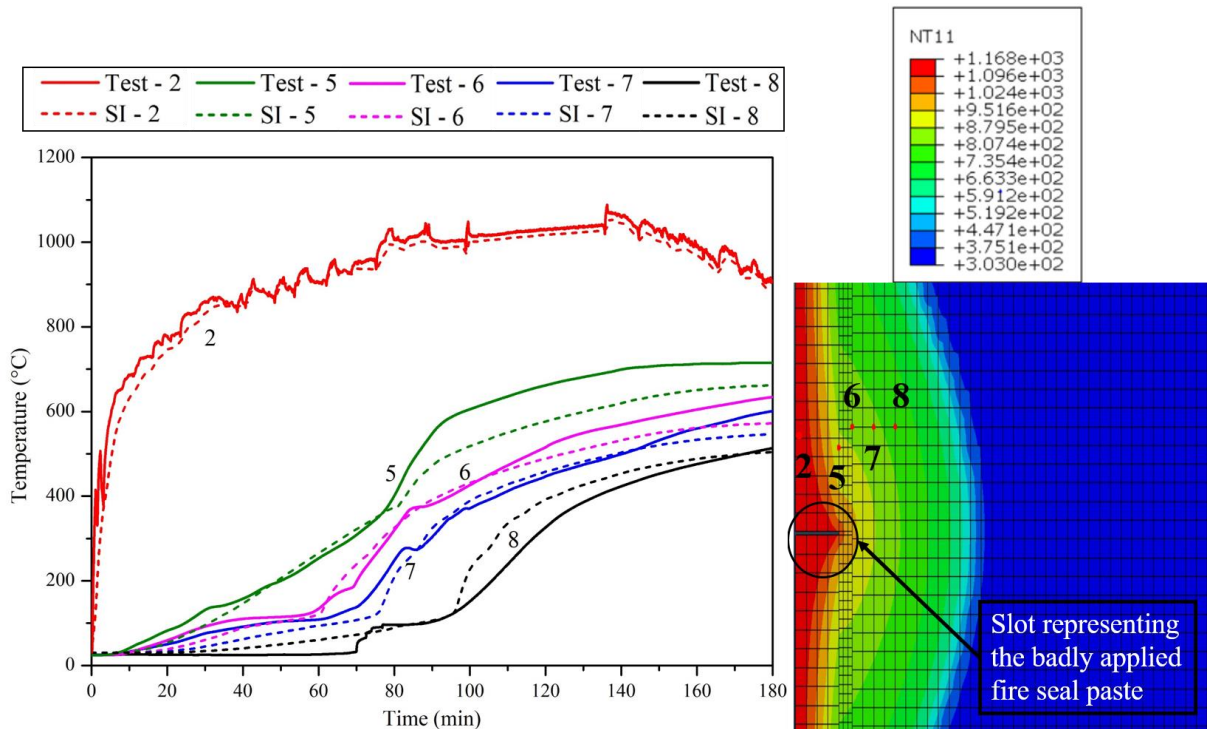


Figure 8.11: Comparison of the experimental (noted by test) and numerical (noted by SI) results at locations 2, 5, 6, 7, and 8

Chapter 8. Fire resistance test

The straw bale's maximum temperature is 600 °C, which ensures that the material is burned. The start point of the fire is the slot between the mineral foam layers representing the badly applied fire seal paste as can be seen in **Figure 8.11**. After reaching the fermacell, the fire spread in the straw bale. It can be noticed that the highest temperature values are obtained near the paste which validates the hole obtained at the end of the experiment (**Figure 8.8**).

8.5. Proposed solution

The numerical and experimental work shows the same behavior. The main problem that caused the straw burning is the seal paste that connects the foam four boards. To prove this statement a new model was made by replacing the foam four boards with only one board 910 mm wide and 910 mm long. **Figure 8.12** depicts the predicted temperature values. In the previous case, the maximal temperature at location 5 was 650 °C and the maximum inside the bale was 500 °C. In the new simulation, these values decrease to reach a maximum value of 500 °C and a maximum of 300 °C at the same locations, respectively. In addition, the fire does not spread into the wall and there was not a hole in the fermacell. Therefore, this wall should resist for more than 180 minutes.

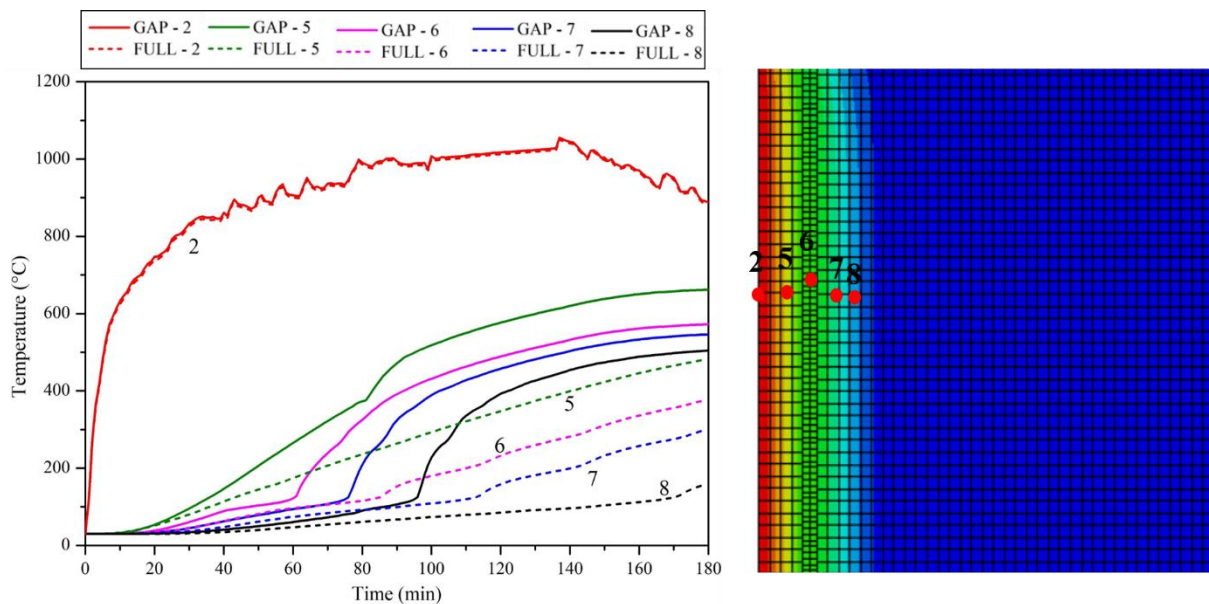


Figure 8.12: Comparison of the numerical results for the wall with (noted by GAP) and without (noted by FULL) fire seal paste

The main objective of this chapter is to study experimentally the fire resistance of a new type of straw envelope suggested by Activ'home. The experiment lasted 180 minutes without recording cracks or defects on the unexposed surface. At minute 77, smoking indications appeared between the mineral foam and the fermacell panel due to the fire seal paste that binds them. This is explained by the wrong application of the paste in some locations which allowed the fire to reach the fermacell and 16 cm of the straw bales. The unexposed surface temperature reached at the end of the test 60 °C. These indications determine an EI 180 classification for the whole envelope. In light of these findings, an Abaqus numerical model is proposed to reproduce the real case and test the model without adding fire seal paste. The new proposition prevents fire propagation in the straw bales.

9. Hygrothermal numerical study

The goal of this chapter is to assess the hygrothermal performance of multi-layered straw walls with different boundary conditions. The study consists of evaluating five typical straw-based wall assemblies, under a continental (Arkhangelsk, Russia) climate, a tropical climate (Brasilia, Brazil), a temperate Mediterranean climate (Nice, France), and a cold desert climate Xinjiang (China). Numerical models of the heat and moisture transfer through the walls using WUFI software are developed, calibrated, and validated through experimental results from the literature. The chosen evaluation criteria are the total water content, the drying rate, the condensation risk, the mold growth, the moisture quantity, the time lag, and the decrement factor. At the end of this chapter, solutions are proposed for detected problems in each climate. Depending on the climate, they mainly consist of increasing the thickness of a specific layer, adding a vapor retarder or installing an unventilated air layer.

Table of contents

9.1. Numerical modeling approach.....	105
9.2. Model validation.....	106
9.3. Case study.....	112
9.3.1. Materials properties.....	112
9.3.2. Wall configurations.....	112
9.3.3. Outdoor climates.....	114
9.3.4. Indoor climates.....	115
9.4. Hygrothermal criteria.....	116
9.5. Results and discussion.....	117
9.5.1. Total water content.....	117
9.5.2. Dryness rate.....	118
9.5.2. Condensation risk.....	119
9.5.3. Mold growth.....	120
9.5.4. ASHRAE criterion.....	121
9.5.5. Time lag and decrement factor.....	122
9.6. Proposed Solutions.....	123

Chapter 9. Hygrothermal numerical study

9.1. Numerical modeling approach

The physical model is that of multi-layer walls under transient boundary conditions. A numerical model based on WUFI software is used to predict the hygrothermal response of the walls under different weather conditions. WUFI-2D, developed by the Fraunhofer Institute for Building Physics in Germany, is a hygrothermal simulation program to analyze the heat and moisture transfer in 2D construction envelopes. The software introduces two moisture-flow driving forces: the liquid transport flux, which is affected by relative humidity, and the vapor diffusion flux, which is affected by vapor pressure. Conductive heat transfer, enthalpy flow, solar radiation (long and short waves), and surface diffusion (for the water motion) are all part of the used equations [192,193]. WUFI solves the temperature equation and the moisture equation iteratively, updating the storage and transport coefficients in each iteration to the new moisture and temperature fields until convergence is reached. The heat and moisture transfer equations are shown in equation (9.1) and equation (9.2), respectively.

$$\frac{\partial H}{\partial T} \cdot \frac{\partial T}{\partial t} = \nabla \cdot (\lambda \nabla T) + h_v \nabla \cdot (\delta_p \nabla \cdot (\phi P_{sat})) \quad (9.1)$$

$$\frac{\partial w}{\partial \phi} \cdot \frac{\partial \phi}{\partial t} = \nabla \cdot (D_\phi \nabla \phi + \delta_p \nabla \cdot (\phi P_{sat})) \quad (9.2)$$

where H , T , w and ϕ are the enthalpy, temperature, moisture content, and relative humidity, respectively. P_{sat} , λ , h_v , δ_p and D_ϕ stand for the saturation pressure, thermal conductivity, evaporation enthalpy of water, water vapor permeability, and liquid conduction coefficient, respectively.

The left side of equation (9.1) represents the heat storage while the terms on the right side are respectively the moisture-dependent thermal conductivity and vapor enthalpy flow. Water evaporation and latent heat absorption from one zone, followed by water diffusion into another zone to condense and release latent heat, are what cause heat to be transported via vapor enthalpy flow. The left side of equation (9.2) represents the moisture storage while the liquid diffusion and the vapor diffusion are given on the right side. Liquid transport through surface diffusion and capillary conduction due to a gradient of relative humidity shows a minor temperature dependence while the vapor diffusion is strongly affected by the temperature field since the saturation vapor pressure increases exponentially with temperature. WUFI solves these equations by using the finite volume technique and a fully implicit scheme for spatial and time discretization. The model input parameters include the wall geometry, the materials properties, the outdoor and indoor weather data, the initial temperature, and relative humidity conditions, and the calculation period.

The exterior and interior boundary conditions consider the convective and radiative heat exchanges of the internal and external surfaces, as well as their hygric transfer as shown in equation (9.3), equation (9.4), and equation (9.5).

$$q = \begin{cases} h_i(T_{si} - T_i) & \text{interior surface} \\ h_e(T_{se} - T_e) + \alpha_s \cdot G & \text{exterior surface} \end{cases} \quad (9.3)$$

$$g_v = \begin{cases} \beta_i P_{sat}(\phi_{si} T_{si} - \phi_i T_i) & \text{interior surface} \\ \beta_e P_{sat}(\phi_{se} T_{se} - \phi_e T_e) & \text{exterior surface} \end{cases} \quad (9.4)$$

$$g_{le} = \alpha_l \cdot R_{rain} \quad (9.5)$$

where q is the sensible heat flux density of the interior or exterior surface, T_{si} and T_{se} are respectively, the interior and exterior surface temperatures, T_i and T_e are respectively, the indoor and outdoor temperatures, h_i and h_e are respectively, the heat transfer coefficient of the interior and exterior surface

Chapter 9. Hygrothermal numerical study

including the effects of convection and long wavelength radiation, g_v is the water vapor flux density of the interior or exterior surface, β_i and β_e are respectively, the vapor transfer coefficient of the interior and exterior surfaces, φ_{si} and φ_{se} are respectively, the relative humidity of the interior and exterior surfaces, φ_i and φ_e are respectively, the indoor and outdoor relative humidity, α_s and α_l are respectively, the solar and liquid absorptance coefficients of the exterior surface, G is the global vertical radiation on the exterior surface and R_{rain} is the mass flow rate of rainwater on the exterior surface.

Several researchers used WUFI to assess the hygrothermal behavior of building exterior walls. Mesa and Arengi [13] validated their WUFI numerical model using experimental results from testing a straw bale wall in a climatic chamber. Kalamees and Venha [194] compared different programs, 1D-HAM, MATCH, and WUFI-2D with experimental results to compute the hygrothermal performance of timber-framed wall structures. Those comparisons gave similar results, which proved that WUFI is a useful tool to assess the moisture behavior of a wall. Delgado *et al.* [195] reviewed the coupled thermal and moisture transfer for 1D and multidimensional cases. They concluded that among fourteen hygrothermal modeling tools, the results of WUFI were found to be more precise in the quantitative computation of night-time cooling. Antretter *et al.* [196] validated a WUFI model by studying the hygrothermal performance of walls based on existing standards and guidelines such as ASHRAE 140-2007 [197].

The following section presents the numerical model validation, based on a straw wall experimentally studied by Douzane *et al.* [15].

9.2. Model validation

Douzane *et al.* [15] studied the hygric and thermal behavior of a two-story straw bale building with a total floor area of 188 m². The ground floor is composed of an open area and three rooms. The upper floor is divided into three bedrooms. The building's external walls' layout is shown in **Figure 9.1**. It is composed of 35 mm of exterior lime plaster, 440 mm of straw layer, 30 mm of an unventilated air layer, and 15 mm of plasterboard.

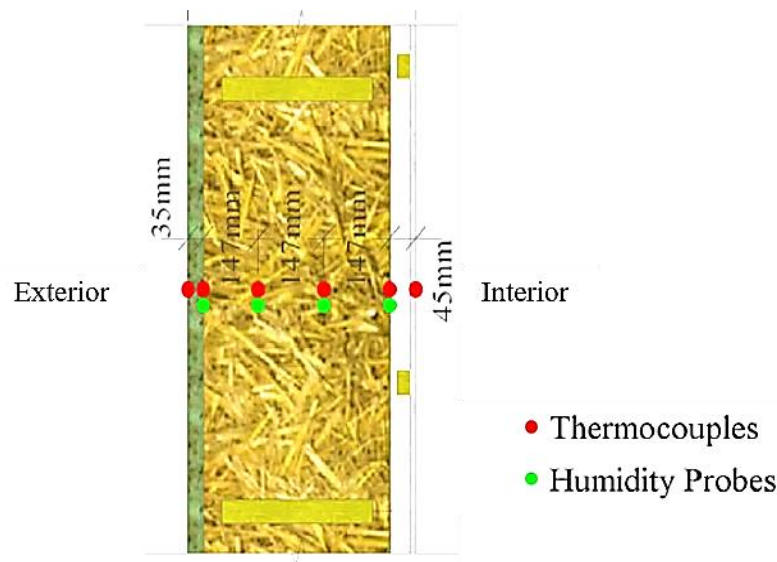


Figure 9.1: Location of thermocouples and humidity probes in the straw wall [15]

Straw hygrothermal properties are variable depending on the straw type, density, water content, relative humidity, wall thickness, and fibers' orientation. WUFI contains a large material database that distinguishes between basic hygrothermal values and hygrothermal functions. The parameters for the non-steady computation of the temperature fields at 20 °C and 20 % RH are the bulk density of the dry material, the specific heat capacity, and the thermal conductivity. For both hygroscopic and non-hygroscopic materials, basic hygric parameters such as the water vapor diffusion resistance factor and

Chapter 9. Hygrothermal numerical study

porosity must be provided. Other hygric properties include the thermal conductivity variation depending on the moisture content and the thermal conductivity based on temperature variations. The moisture storage function and the moisture-dependent liquid transport coefficient are needed for hygroscopic and capillary material simulation, respectively. The variations of each parameter must be entered to study their effect on the whole structure.

The thermophysical properties of lime plaster, unventilated air, and plasterboard taken from the WUFI database are provided in **Table 9.1**. Straw samples with dimensions $50 \times 50 \times 10 \text{ cm}^3$ and a density of 80 kg/m^3 were evaluated for thermal conductivity using a guarded hot plate apparatus after being oven-dried at $65 \text{ }^\circ\text{C}$. Experiments conducted by Douzane *et al.* [15] showed that for bale average temperature between $10 \text{ }^\circ\text{C}$ and $40 \text{ }^\circ\text{C}$, the thermal conductivity varied between 0.067 W/(m.K) and 0.088 W/(m.K) for horizontal fibers and between 0.046 W/(m.K) and 0.064 W/(m.K) for vertical fibers. The U-value of the experimental straw wall is therefore about $0.2 \text{ W/(m}^2\text{.K)}$.

Table 9.1: Straw buildings materials' basic properties extracted from WUFI materials database and literature at $20 \text{ }^\circ\text{C}$ and 20 \% RH

Material	Thermal conductivity (W/(m.K))	Density (kg/m ³)	Specific heat (J/(kg.K))	Porosity (m ³ /m ³)	Water vapor diffusion resistance factor (-)
Straw [15]	0.046-0.088	80	1200	0.9	1.3
Unventilated air gap (30 mm)	0.2	1.3	1000	0.99	0.32
Plasterboard	0.2	850	850	0.65	8.3
Lime plaster	0.7	1600	850	0.3	7

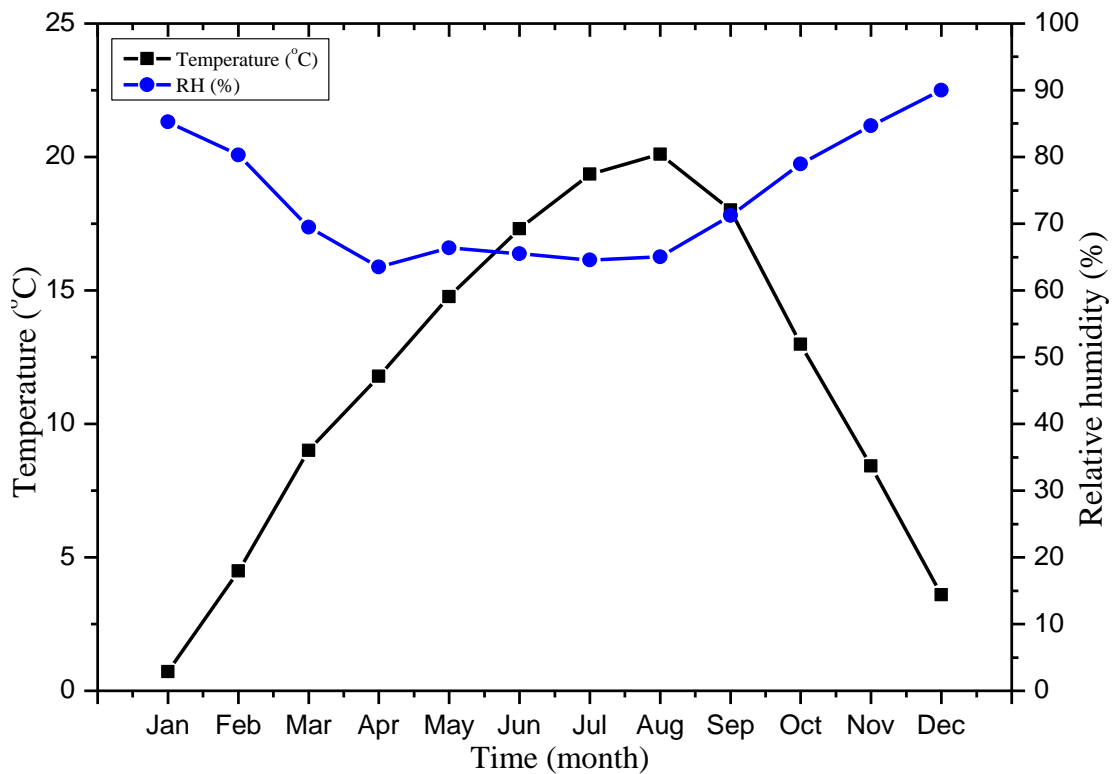


Figure 9.2: Monthly average outdoor temperature and relative humidity in the Picardy region

Chapter 9. Hygrothermal numerical study

The tested building is situated in the Picardy region, north of France. The Picardy climate is classified as temperate oceanic (Cfb) by the Köppen–Geiger classification [198]. The outdoor dry air temperature reaches 40 °C in summer and -10 °C in winter. **Figure 9.2** shows the monthly average outdoor temperature and RH in the test location. The outdoor RH ranges between 30 % in summer and 90 % in winter. The building's indoor temperature and RH were maintained between 20-25 °C and 40–60 % respectively, to ensure indoor thermal comfort. The authors measured the temperature and the RH at 38 different locations in the building using type-T thermocouples and HMP60 humidity probes. Inside a wall assembly, the distance between sensors was around 147 mm as shown in **Figure 9.1**. The experiment took place for 14 months between 25 May 2014 and 11 August 2015.

Figure 9.3 shows the experimental temperature and the RH variation of the outer and inner surfaces of the south-facing wall during the test period. The graph reveals the stability of the internal surface temperature at around 20 °C, even when the external surface temperature is very low or very high. The internal surface RH varies between 30 % and 60 % and does not depend on the large RH variation of the external face. The lower values of the inner surface RH can be explained by the heating of the building during winter, which increases the capacity of ambient air to store moisture without reaching saturation. Douzane *et al.* [15] concluded that the straw envelope could mitigate the outdoor temperature and moisture variations to preserve indoor comfort during the summer and winter periods.

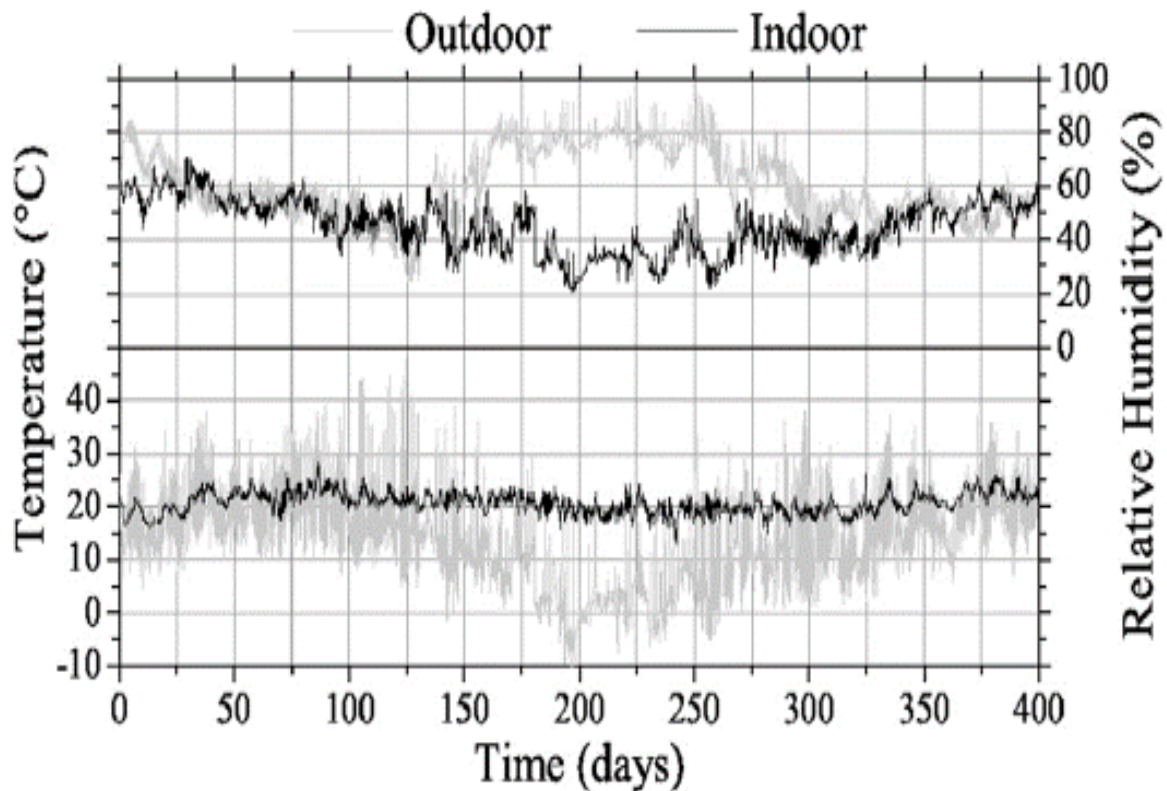


Figure 9.3: The variation of the inner and outer surfaces' temperature and RH [15]

The experimental data of [15] was used to calibrate and validate the numerical model by comparing the profile of the measured data to that of the simulated results for the internal and external surface temperatures and RH, over one year. Therefore, a WUFI model was set up using a geometry and weather data file similar to that of **Figure 9.1** and **Figure 9.2**, respectively. In the model, the interior surface's heat transfer coefficient was considered 8 W/m².K with a short wave radiation absorptivity of 0.2 and a longwave radiation emissivity of 0.9 because of its bright color. The heat transfer coefficient of the exterior surface was considered wind-dependent with a short-wave radiation absorptivity of 0.6 and longwave radiation emissivity of 0.9. Based on the initial exterior and interior air temperature and RH, the initial temperature was set at 20 °C for all materials, and the initial RH was set at 50 % for straw, wood boards, and plasterboards and 80 % for lime plasters.

Chapter 9. Hygrothermal numerical study

To obtain hygrothermal numerical results comparable to the experimental data, a calibration technique was required due to some experimental uncertainties. The simulation was replicated for different values of outer surface solar absorption, straw initial water content, and straw thermal conductivity, until reaching high accordance between the simulated and experimented surface temperature and RH variations. The straw thermal conductivity was finally set to 0.055 W/(m.K) at 20 °C and 20 % RH. The straw initial relative humidity was set at 40 %. The heat transfer coefficient of the interior surface was varied between 2 and 10 W/(m².K) and fixed at the end at 8 W/(m².K). The heat transfer coefficient of the exterior surface was varied between 10 and 20 W/(m².K) and fixed at the end at 17 W/(m².K). The vapor transfer coefficient of the interior and exterior surface are taken respectively as 25×10^{-9} kg/m².s.Pa and 75×10^{-9} kg/m².s.Pa. The straw sorption isotherm and thermal conductivity versus temperature and RH were collected from literature [15,36,43,48], as shown in **Figure 9.4**. These graphs provide information about the variation of the insulating property of the straw as a function of temperature and RH as well as the material's adsorption isotherm. High temperature and humidity affect negatively the thermal conductivity of the straw. The conductivity increases progressively with the temperature and reaches about 0.065 W/(m.K) at 45 °C. At the same time, the thermal conductivity increases with the RH until reaching 0.06 W/(m.K) at 80 % RH and then continues rising sharply to attain 0.12 W/(m.K) at 100 % RH. As for the moisture content variation, the graph shows its progressive raise while increasing the RH. This behavior demonstrates the high porosity of the straw.

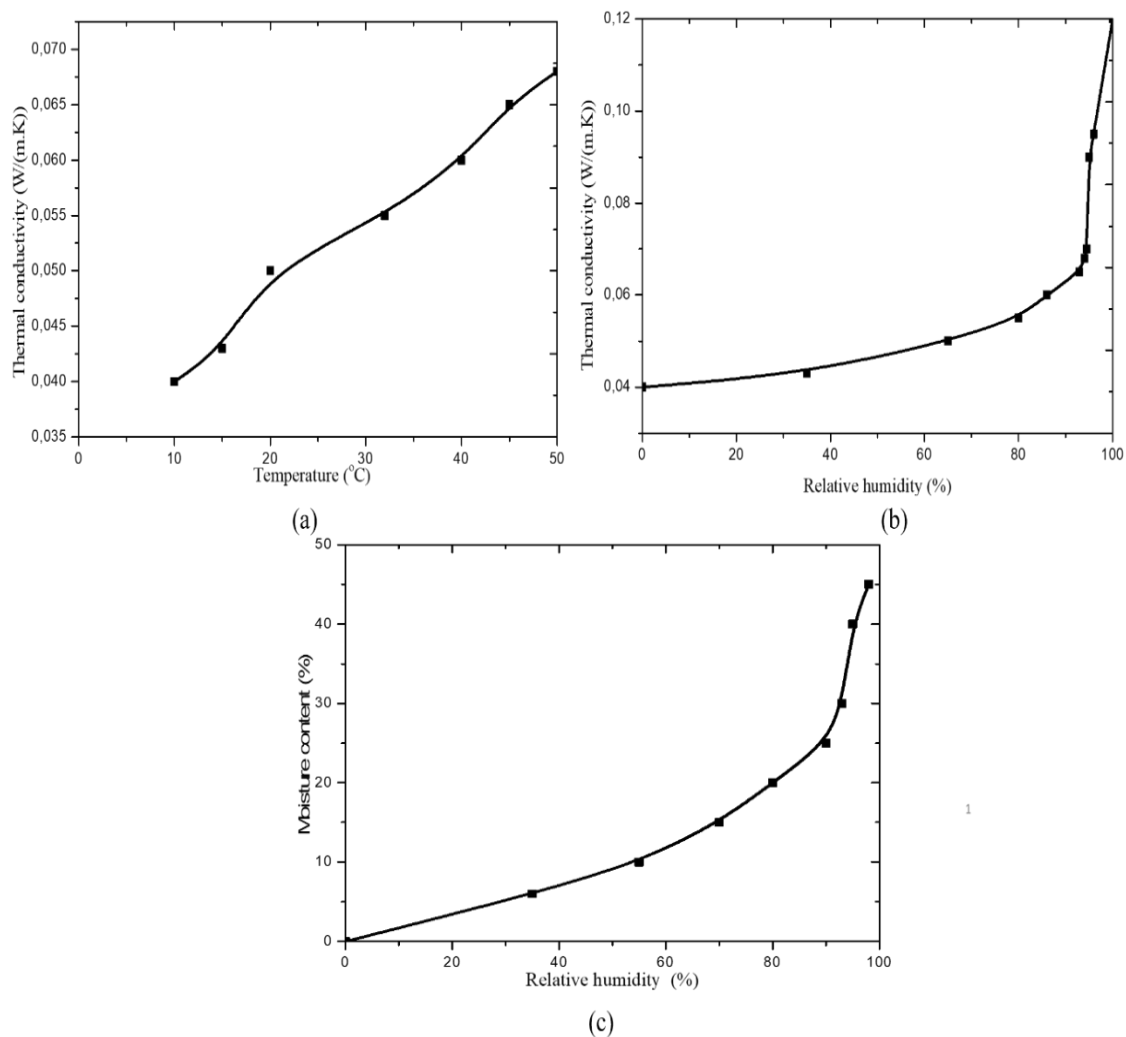


Figure 9.4: Straw material's hygrothermal functions showing the variation of thermal conductivity vs temperature (a), thermal conductivity vs relative humidity (b), and moisture content vs relative humidity (c) (based on [15,36,43,48])

Chapter 9. Hygrothermal numerical study

The weekly-averaged experimental and simulated results showing the temperature and the RH of the interior and exterior surfaces are represented in **Figure 9.5** and **Figure 9.6**, respectively. The WUFI model generates almost similar results as the experimental study of the straw building for the studied weather conditions. The peaks in the simulated case and the variation of values are close to the measured data. Regarding temperature, the plotted values are in good agreement with the measured values. The maximum obtained temperature for the exterior wall surface reaches 45 °C in the simulation results while it reaches about 43 °C in the experimental measurements. The minimum calculated temperature is about -14 °C while it is -10 °C in the experimental measurements. The interior surface temperature varies around 20 °C, which agrees with the experimental results.

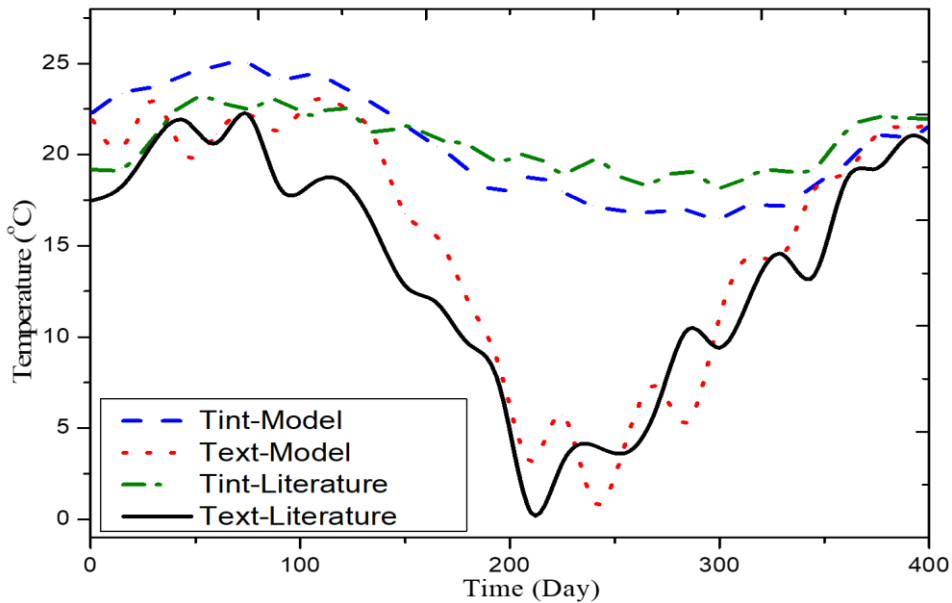


Figure 9.5: Comparison of the experimental and simulated weekly average temperature variations over one year for wall surfaces under Picardie weather conditions

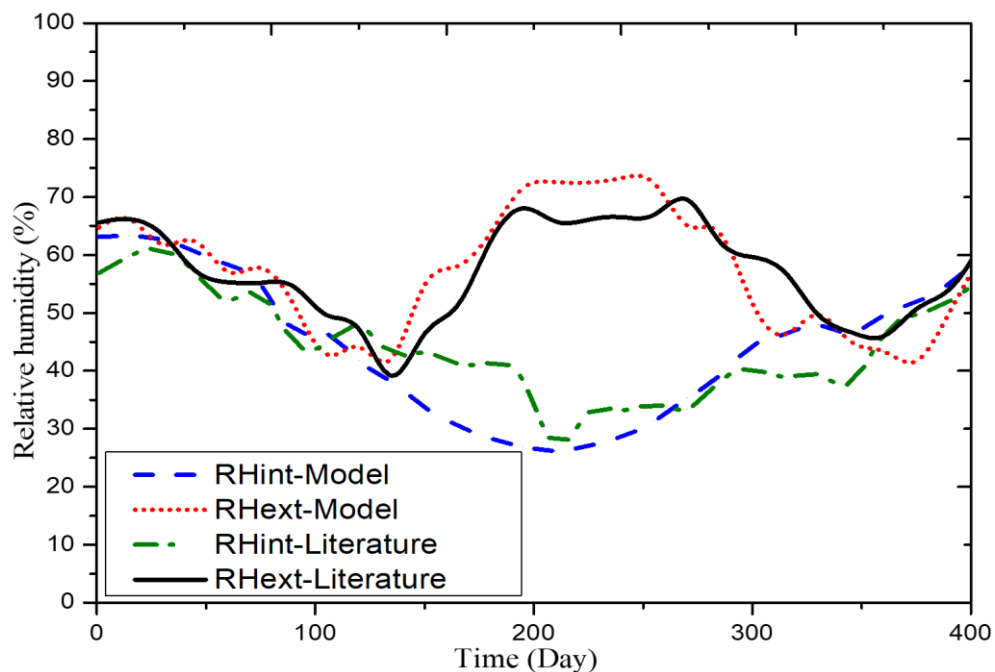


Figure 9.6: Comparison of the experimental and simulated weekly average RH variations over one year for wall surfaces under Picardie weather conditions

Chapter 9. Hygrothermal numerical study

Besides, the RH variation of the wall surfaces compares well to the experimental results. The initial value for RH considered in the numerical model (40 % for the straw and wood and 80 % for the lime plaster) can explain the differences in the interior surface RH variation. The behavior of the exterior surface RH is close to the in-situ measurements. The interior surface humidity varies between 35 % and 60 %, while the exterior surface humidity varies between 25 % and 85 %.

Douzane *et al.* [15] calculated the thermal inertia parameters based on the exterior and interior surface temperature variations for 24 hours to prove the mitigating effect of the straw-based wall against external variations and its beneficial impact on indoor thermal comfort. The time lag and the decrement factor are given in equation (3.1) and equation (3.2), respectively as given in [199].

The experimental results indicate a time lag of about 6 h and a decrement factor of about 0.09 while the numerical results provide a time lag of about 7 h and a decrement factor of about 0.066. **Figure 9.7** shows that the variation of the outdoor surface temperature barely affects the indoor surface temperature variation. For the numerical model, the difference between the maximum and the minimum of the external temperature was about 30 °C, which is close to the measured values. However, the temperature range of the internal surface is about 1.3 °C for the numerical model and up to 3 °C for the experimental measurements. The discrepancy between actual and modeled materials' characteristics and initial conditions can explain this difference. These results prove the thermal inertia of the straw bale wall that helps limit overheating in summer since the highest interior temperature is reached when the exterior temperature has decreased.

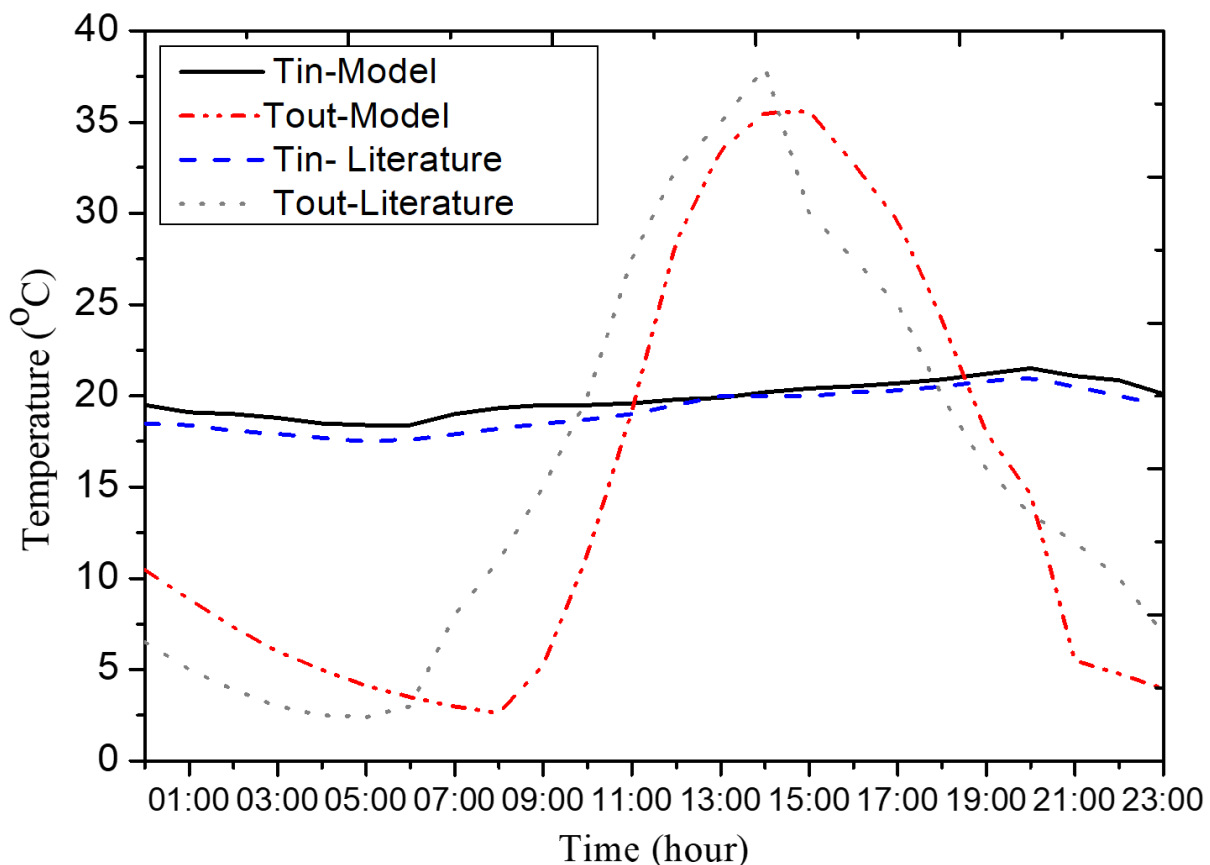


Figure 9.7: Variation of the interior and exterior surface temperature for the numerical model (WUFI) and the experiment [15] for 24 hours on 25 April 2010

The root mean square error (RMSE) and the percentage root mean square error (PRMSE) indicated in equation (9.6) and equation (9.7), respectively, are used to measure the agreement between experimental data (e_i) and simulated outcomes (s_i).

Chapter 9. Hygrothermal numerical study

$$RMSE = \sqrt{\frac{1}{n} \sum_{i=1}^n (s_i - e_i)^2} \quad (9.6)$$

$$PRMSE = \sqrt{\frac{1}{n} \sum_{i=1}^n \left(\frac{s_i - e_i}{e_i} \right)^2} \times 100 \quad (9.7)$$

The RSME and PRSME for the exterior surface temperature are 1.6 °C and 9 % respectively, while those for the interior surface temperature are 1 °C and 3.6 %, respectively. The RSME and PRSME of the exterior surface RH are 2 % and 3.5 % respectively, while those for the interior surface RH are 2.2 % and 4 %. These values quantitatively show a good agreement between the numerical model and the experiment. The numerical model is therefore used in the following section to investigate different wall configurations.

9.3. Case study

9.3.1. Materials properties

The principal layer in straw bale walls is the straw layer with a thickness varying from 360 mm to 440 mm. Straw bale walls are covered on both sides with cement or lime plaster and wood boards. All material properties including thermal conductivity, porosity, water vapor diffusion resistance factor, specific heat, and density are presented in **Table 9.2**. The layers' characteristics are taken from the WUFI database except for the straw. The straw characteristics are collected from different research works [15,36,43,48]. The straw hygrothermal functions for moisture storage and thermal conductivity versus temperature and RH are taken the same as in **Figure 9.4**.

Table 9.2: Straw buildings materials' basic properties extracted from WUFI materials database and literature at 20 °C and 20 % RH

Material	Thermal conductivity (W/(m.K))	Density (kg/m ³)	Specific heat (J/(kg.K))	Porosity (m ³ /m ³)	Water vapor diffusion resistance factor (-)
Cement plaster	1.2	2000	850	0.3	25
Hardwood board	0.13	650	1500	0.47	200
Wood wool	0.08	450	1500	0.55	9
Straw	0.055	120	1200	0.9	1.3
Unventilated air gap (30 mm)	0.2	1.3	1000	0.99	0.32
Unventilated air gap (50 mm)	0.28	1.3	1000	0.99	0.32






9.3.2. Wall configurations

The numerical model is applied to study five different wall structures under four different weather conditions. Straw construction is found in different forms and structures depending on the prevailing climate at the building's location.

Table 9.3 gives the most used wall structures in the actual straw construction sector.

Chapter 9. Hygrothermal numerical study

Table 9.3: Different layers composition of five considered cases

Exterior layer-----Interior layer								
Cases	Layer 1	Layer 2	Layer 3	Layer 4	Layer 5	Layer 6	Layer 7	Layer 8
Case 1 [3] 	Cement plaster 20mm	Straw 360mm	Cement plaster 20mm	-	-	-	-	-
Case 2 [85] 	Hardwood 30mm	Straw 360mm	Hardwood 30mm	-	-	-	-	-
Case 3 [15] 	Cement plaster 35mm	Straw 440mm	Unventilated air gap 30mm	Hardwood 15mm	-	-	-	-
Case 4 [105] 	Hard- wood 40mm	Unventilated air gap 30mm	Cement plaster 20mm	Straw 360mm	Cement plaster 20mm	-	-	-
Case 5 [121] 	Cement plaster 10mm	Wood wool 40mm	Hardwood 18mm	Straw 360mm	Hardwood 10mm	Unventilated air gap 50mm	Hardwood 30mm	Cement plaster 15mm

In the first wall structure, a 20 mm thick cement layer covers the straw from both sides and gives a total wall thickness of around 400 mm. Cement plaster is used as a surface finish to protect the straw from fire, rot, and fungus, even though this material increases the carbon footprint of the wall [200]. In the second case, 30 mm hardwood boards cover the straw layer on both sides, thus yielding a wall assembly thickness of 420 mm. Hardwood boards are used to protect the straw layer, increase thermal performance, and reduce the environmental impact of the wall in the condition that the wood source is sustainably exploited [201,202]. In the two following cases, an unventilated air layer is added at different positions to increase the insulation property of the wall, reduce the mass transfer, and provide space for electrical cables and pipework. The thickness of the straw is different in those two cases, as well as the total wall thickness, which is 520 mm and 470 mm in case 3 and case 4, respectively. Those two walls

Chapter 9. Hygrothermal numerical study

can show the effect of the straw thickness and the air layer on the hygrothermal properties of the whole structure. In the last case, a wood wool layer is added to increase the thermal resistance of the wall. The total thickness of the structure is 533 mm. The latter assembly was recently proposed by French contractors [121] to increase thermal comfort in straw buildings.

Parameters such as solar radiation, the driving rain intensity and direction, and the structure orientation affect the hygrothermal behavior of the wall. It is important to study the worst-case scenario of an envelope exposed to the highest hygrothermal stress. Therefore, all walls in the present study are north-oriented, since the generally higher driving rain intensity and lower solar radiation in that direction increase the occurrence probability of drying problems.

9.3.3. Outdoor climates

Four climates were chosen according to their extremely different temperature and humidity profiles, as reported by the Köppen–Geiger classification [198], and according to local cereal availability. The cost and the environmental impact of the construction caused by the material transportation from the manufacturing location to the site of work are thus minimized. The USA, China, Russia, Brazil, and some European countries have the highest annual cereal production [203]. Therefore, the cities chosen in this study are Nice-France, Xinjiang-China, Arkhangelsk-Russia, and Brasilia-Brazil. **Table 9.4** describes the main weather characteristics of the selected cities as well as their longitude, latitude, and elevation. Tropical, dry, temperate, and continental climates were considered to test the ability of straw walls to stabilize the variation of interior temperature and relative humidity.

Not all these areas experienced growth in straw construction. In the Russian region, construction with straw bales was started in 1996 by foreign organizations as an experimental environmental village. This type of construction has since been developed in Belarus, Ukraine, and Russia [204,205]. In the Brazilian construction field, straw buildings were first utilized in the 1970s, but their use declined in 2009 and is not widely used today [206]. Straw buildings appeared in China's construction industry in 1998. More than 600 straw structures have been constructed in China since then [207]. In France, more than 4000 buildings are constructed from wheat straw bales [208]. Straw bale construction attracts growing interest in the industrial sector, regarding its sustainability, its practicality, and its reduced construction time.

Table 9.4: Köppen–Geiger Climate classification for the four chosen cities

City, Country Climate	Location	Description
Brasilia, Brazil Aw	Longitude= 47.93 west Latitude= 15.78 south Height=1160 m Time zone= -3	<ul style="list-style-type: none"> • Tropical wet and dry or savanna climate • Dry winter • Average temperature about 18°C
Xinjiang, China BWk	Longitude= 89.2 east Latitude= 42.93 north Height=35 m Time zone= +8	<ul style="list-style-type: none"> • Cold desert climate • Average temperature below 18°C • At least one month has a temperature below 0°C
Nice, France Csa	Longitude= 7.2 east Latitude= 43.65 north Height=10 m Time zone=+1	<ul style="list-style-type: none"> • Temperate and Mediterranean climate • Precipitation in winter, dry and hot summer • Average temperature above 22 °C
Arkhangelsk, Russia Dfc	Longitude= 40.47 east Latitude= 64.53 north Height=13 m Time zone= +4	<ul style="list-style-type: none"> • Subarctic continental climate • No dry season and cold summer • Maximum average temperature 10 °C

Chapter 9. Hygrothermal numerical study

Figure 9.8 presents the outdoor temperature and RH of each climate. The figure shows remarkable differences between the cities' temperature and RH variations. In Brasilia, the maximum temperature is generally reached in September, the warmest month of the year with a monthly average temperature of about 21.5 °C. The minimum average temperature reaches about 18 °C in the coldest month, July. The average RH varies between 40 % and 88 %, respectively in September and in December. It should be noted that December is the wettest month while July is the driest one. In Xinjiang, the warm season is from May to September when the maximum weekly average temperature reaches about 33 °C with a low RH of about 30 %. The cold season is from November to January when the monthly average temperature reaches -12 °C with a high RH of about 80 %. The wettest month in Xinjiang is January and the driest is July. In Nice, the warmest month is August with a maximum weekly average temperature of about 25 °C and an RH reaching about 75 %. The coolest month is December with a minimum average temperature of about 6 °C where the RH reaches about 50 %. In general, the wettest month in Nice is November and the driest month is July. In Arkhangelsk, the extreme weekly average temperatures are about 17 °C and -17 °C, respectively in July the hottest month, and January the coldest month. The humidity varies between 60 % and 90 % for the same months. The wettest month is February and the driest one is August. The weather data files are extracted from the EnergyPlus weather library [48].

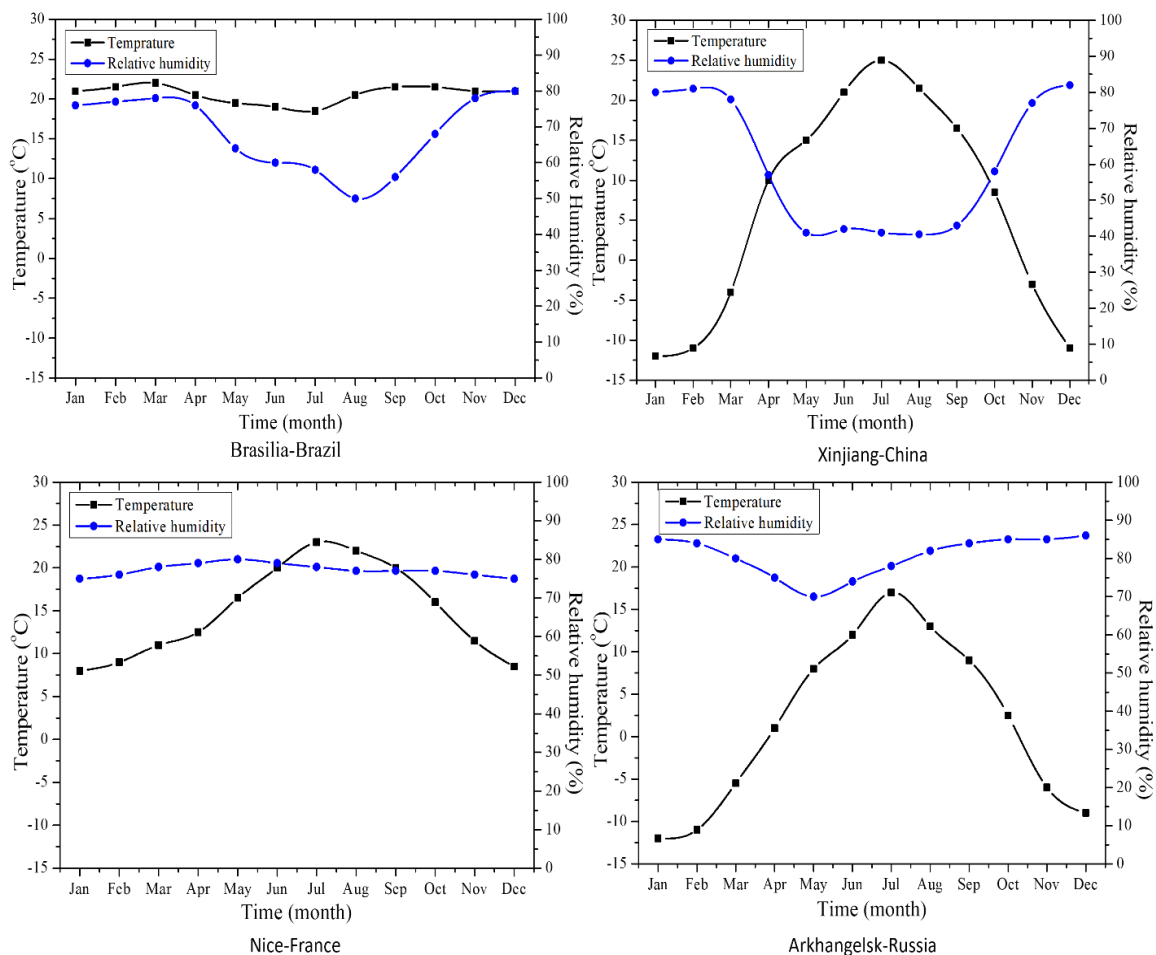


Figure 9.8: Monthly average outdoor temperature and relative humidity in Brasilia-Brazil, Xinjiang-China, Nice-France, and Arkhangelsk-Russia over one year

9.3.4. Indoor climates

The simulated sinusoidal functions used for the indoor temperature and the humidity are respectively given in equation (9.8) and equation (9.9).

Chapter 9. Hygrothermal numerical study

$$T = 2.5 \sin(t - c) + 21.5 \quad (9.8)$$

$$RH = 10 \sin(t - h) + 50 \quad (9.9)$$

where t is the time (month), c and h are constants that depend on the climate characteristics of the considered region, as shown in **Table 9.5**. The resulting temperature and RH graphs are plotted in **Figure 9.9**. The indoor dry air temperature ranges from 19 °C (winter) to 24 °C (summer) while the indoor RH varies between 30 % (winter) and 60 % (summer). These variations are based on ASHRAE-55 [209] and EN 13779 [210] which recommend a winter temperature of 19 °C to 24 °C with a relative humidity of 30-40 %, and a summer temperature of 23 °C to 26 °C with a relative humidity of 50-60 %.

Table 9.5: c and h values used in equation (9.8) and equation (9.9) for each country

Country	c	h
Brazil	2.57	-2
China	1.57	-1.57
Nice	2	0.57
Russia	1.57	-2.57

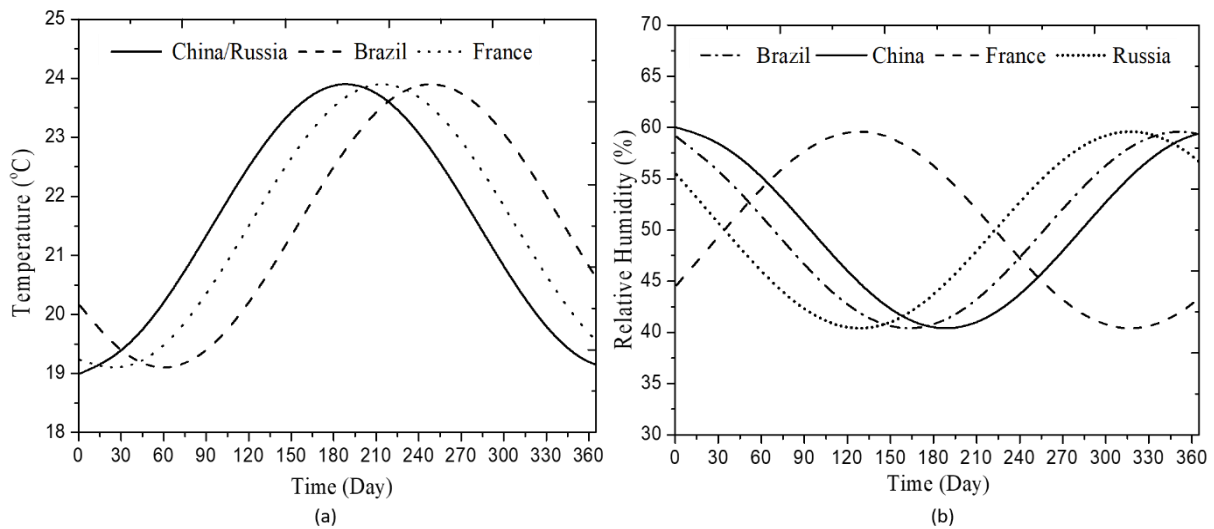


Figure 9.9: Annual variation of the indoor dry air temperature (a) and the indoor air relative humidity (b)

9.4. Hygrothermal criteria

In the present study, the thermal evaluation uses the time lag and the decrement factor, as presented in equation (3.1) and equation (3.2), to detect respectively the time that takes a heatwave to cross the wall and the decreasing amplitude ratio. The hygric evaluation uses the following criteria:

- **Total water content (TWC):** This criterion indicates whether the wall tends to accumulate moisture or dry over the surveyed period. This can be evaluated by comparing the initial and the final moisture content. The wall passes this criterion if the final content is lower than the initial content. The initial trend of the total water content strongly depends on the initial conditions. This is why the simulations are carried out over four consecutive years so that the wall reaches a steady state, independent of the initial conditions.
- **Dryness rate (DR):** a higher dryness rate means a faster ability to dry out. The DR calculates the difference between the final and initial moisture content.
- **Condensation risk (CR):** On the indoor surface, the condensation risk appears if the material temperature is lower than the indoor dew point temperature [211]; this risk is greater if this

Chapter 9. Hygrothermal numerical study

situation appears for a long time. For each wall, the percentage of time the surface temperature falls below the dew point is determined. Within the wall, the CR appears when the calculated vapor pressure is equal to or higher than the saturated vapor pressure.

- **Mold growth (MG):** In the walls, the inner surface and the interfaces between the layers are likely to develop mold depending on the hygrothermal conditions. Beyond aesthetic considerations, the substances produced and emitted by mold can threaten the health of the occupants. To analyze the risk of mold development, WUFI compares the hygrothermal conditions of surfaces (Isopleths) with the conditions necessary for mold development. Mold can grow when the hygrothermal conditions of a wall reach a particular threshold. This limit known as the lowest isopleth for mold (LIM) is based on humidity, temperature, exposure period, and material properties. The criterion consists of plotting the RH of a material versus the temperature at a certain time. As a result, if the conditions (RH and T) remain over the LIM for an extended period, the building material will be prone to grow mold. For building materials, two limitations LIM 1 and LIM 2 are of interest. The first is for products created from biodegradable materials, while the second is for non-biodegradable materials.
- **ASHRAE criterion (ASH):** In 2006, ASHRAE published a standard concerning the criteria for the sizing of building walls with respect to humidity. The ASHRAE criterion was created to prevent moisture problems in envelope assemblies by limiting the amount of moisture in buildings [52]. The standard can be applied to all materials and surfaces except for the external layers. To avoid mold development after 30 days with an average surface temperature between 5 °C and 41°C, the standard demands a time-averaged surface RH of less than 80 %.

Those criteria have been used by several authors [212–214] to assess the hygrothermal performance of walls. Based on WUFI results, they are utilized to analyze the behavior of five typical straw wall assemblies in the next section. Through these findings' moisture concerns are predicted for all cases under various boundary circumstances.

9.5. Results and discussion

The five cases of straw walls proposed in **Table 9.2** are considered to find the optimum assembly depending on the four chosen locations around the world. Knowing that the initial condition in WUFI can be modified according to each material, the RH and the temperature of the straw and the wood were respectively considered equal to 50 % and 20 °C, while for the other material they were set to 80 % and 20 °C. In all cases, the wall was oriented to the north where the solar radiation is low and the driving rains are high. The WUFI outputs show the variation of the water content, the relative humidity, and the temperature of each layer with respect to time. The analysis of the walls' behavior is based on WUFI outputs and the defined hygrothermal criteria. The objective of the simulations is to detect risks of condensation, problems of dryness, and mold growth for each climate, to choose the optimal wall design for each area, or to propose novel wall layouts.

9.5.1. Total water content

Excessive moisture content in straw and hygroscopic building materials leads to bio-deterioration, mold, and decay damages in the whole structure. **Figure 9.10** compares the day-averaged total water content variation for wall cases three, four, and five under the Arkhangelsk-Russia and Brasilia-Brazil climates over four years. The graphs depict different outcomes depending on the studied cases. The worst scenario is 4-R, in which the water content gradually rises from 15% to 55 % over 1200 days because of the wall's over-saturation during the winter and the incapacity to dry out during the cold subarctic summer. This problem is caused by the air layer on the exterior side of the wall. This type of wall has difficulties rejecting all the absorbed moisture because of the humidity stored in the air layer. An oscillating behavior, which may be explained by moisture adsorption-desorption over the winter and summer periods, accompanies this increasing tendency. The TWC increases from 15 % to 20 % during the first oscillation in 4-R, then drops to 17 % during the summer period, then progressively climbs to 55 % after three winter-summer cycles. In 4-B, the TWC decreases progressively (with winter-summer oscillations) from 18 % to 8 % which means that the wall is drying out during summer. Cases

Chapter 9. Hygrothermal numerical study

3-B and 3-R, on the other hand, show quasi-periodic graphs which means that dynamic equilibrium is reached due to the higher straw thickness of about 440 mm. The cited walls show similar oscillations during each winter-summer phase (for Brasilia-Brazil, the first winter period is situated between the 200th and the 400th day of simulation), but the maximum TWC remains different due to the different weather conditions. The maximum value in case 5-B is about 20 %, before starting to decrease as the construction is drying out. The minimal value in summer for the same case is about 15 % and during the next years, the dynamic equilibrium is reached. This behavior is explained by the presence of layers such as wood wool, which has low vapor permeability.

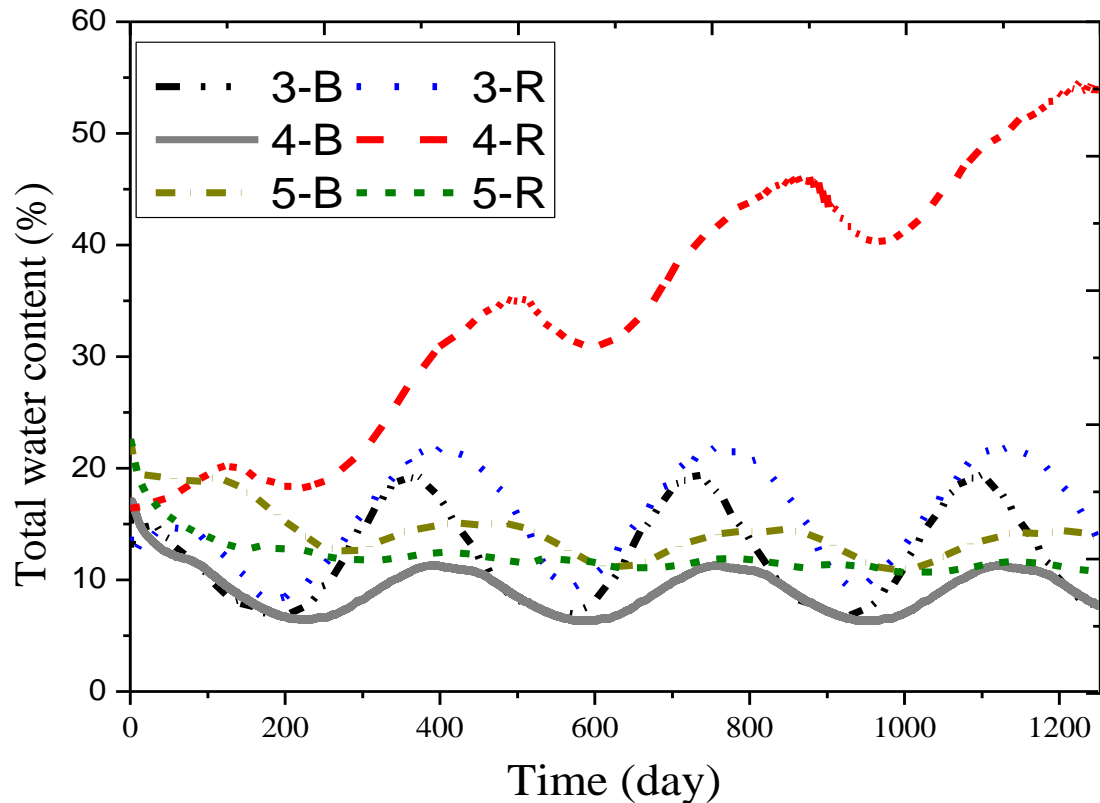


Figure 9.10: Day-averaged total water content variation for cases three, four, and five over four years under R- the Arkhangelsk-Russia weather and B- the Brasilia-Brazil weather

The WC variation of case 5-R does not match with the previous cases since the curve is flat and there are no oscillations. The TWC keeps decreasing from about 20 % to 10 % over four years. This behavior is mainly due to the high-water vapor diffusion resistance factor of the hardwood layer covering both sides of the straw layer, thus reducing moisture transfer to and from the straw.

Therefore, the current criterion shows that all the walls can dry out except in some cases in specific weather. The problem was noticed in the first, second, and fourth cases for Arkhangelsk-Russia. This can be related to the subarctic Russian weather, which is characterized by a very cold winter with temperatures that reach $-30\text{ }^{\circ}\text{C}$, and RH that reaches 90 %. The increasing trend of the TWC factor may cause moisture problems, which are studied by calculating the dryness rate.

9.5.2. Dryness rate

The dryness rate (DR) rate is the difference between the initial water content (TWC_i) and the final water content (TWC_f) divided by the initial water content over four years as shown in equation (9.10). **Figure 9.11** presents the DR for all wall configurations and all considered climates.

$$DR = \frac{TWC_i - TWC_f}{TWC_i} \times 100 \tag{9.10}$$

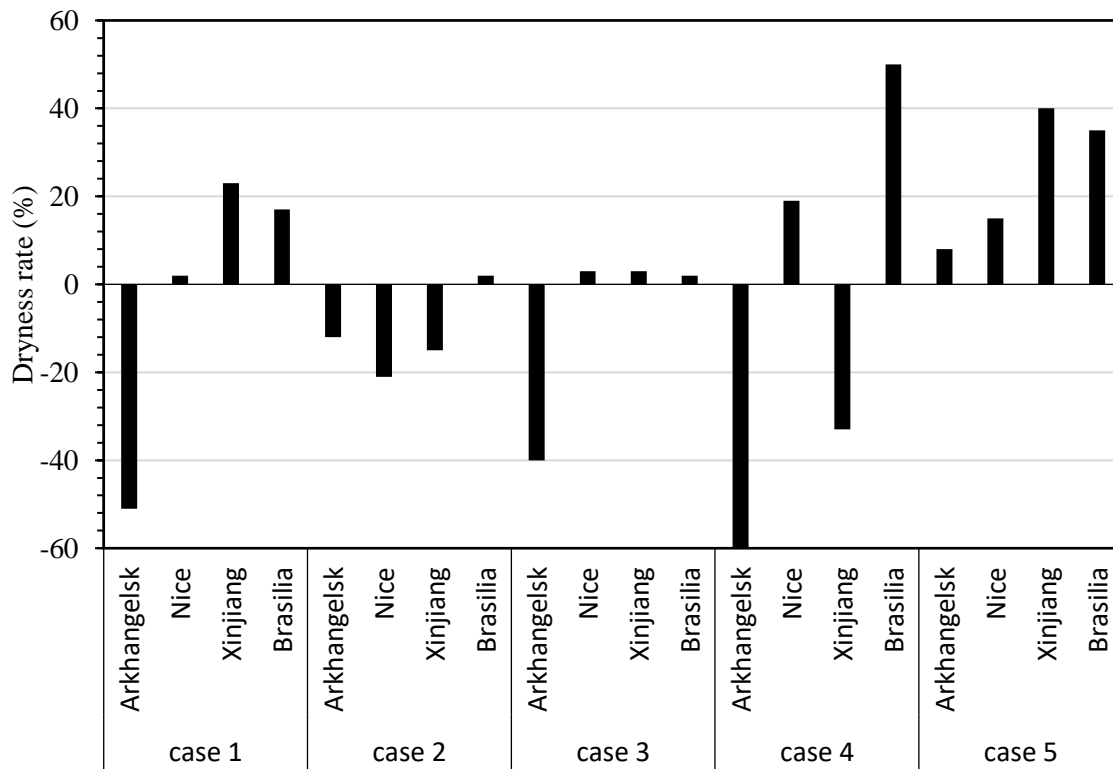


Figure 9.11: Dryness rate of all cases in all climate conditions for four years

Negative rates mean that the wall absorbs the humidity and the moisture over the years while positive rates mean that the wall rejects progressively the humidity during the studied period. Not surprisingly, for all weather conditions in case 5, the rates are positive. This type of wall configuration provides high thermal insulation, which helps to raise the average temperature in the wall, and therefore delays saturation. It should be noted that temperature controls the water vapor movement by limiting the maximum saturation water vapor pressure. If the saturation pressure is low (in cold weather) then the drying rate will decrease because of the low difference between the saturation pressure and the water vapor pressure. Case 4 has a higher DR than case 5 for the tropical Brazilian weather condition due to the influence of the outer air gap in hot climates. In case 4 for the subarctic continental Russian weather condition, the lowest DR is likewise found due to the influence of the outer air gap in cold climates. It can be seen that the air gap is beneficial in hot climate cases and is a drawback in cold climate cases. The third wall, which is made of a 440 mm straw layer, has a negative DR for the subarctic continental Russian weather (-40 %) and roughly 3 % for all other weather. It can be explained by the porous nature of the straw, which allows humidity to pass through until its saturation in cold weather. The different results between case 1 and case 2 are due to the higher water diffusion resistance factor and thickness of the hardwood layer.

Therefore, the type of the covering materials and their thickness explain the obtained results since the exterior insulation material improves the dryness of the wall, in indoor conditions, and outdoor weather [213]. In addition, the damaging effect of mold growth and moisture presence can be reduced by minimizing the condensation risk (CR) of the surfaces.

9.5.3. Condensation risk

Figure 9.12 indicates the percentage of time when the CR occurs in the considered walls. Results show that the maximum risk of surface condensation, about 60 %, occurs in all structures for the Russian

Chapter 9. Hygrothermal numerical study

weather and that the minimum CR, about 0 % to 5 %, occurs in all cases for tropical Brazilian weather. The CR is explained by the direct contact of the wall with the cold environment that leads to low indoor surface temperatures, or by the high RH in the wall. This fact is clear since Arkhangelsk-Russia has a maximum outdoor temperature and RH of about 30 °C and 100 % respectively, and a minimum outdoor temperature and RH of about -30 °C and 23 %, while Brasilia-Brazil has a maximum temperature and RH of about 32 °C and 90 % and a minimum temperature and RH of about 11 °C and 20 %. In addition, the exterior insulation in the building envelope affects the CR as the lowest values are obtained for case 5 for all climates. The layers of wood wool, hardwood, cement plaster, and air gap contribute to the wall's thermal insulation. These layers assist in raising the temperature of the interior layers and surfaces above the dew point temperature of the room to prevent the condensation risk, especially during the winter.

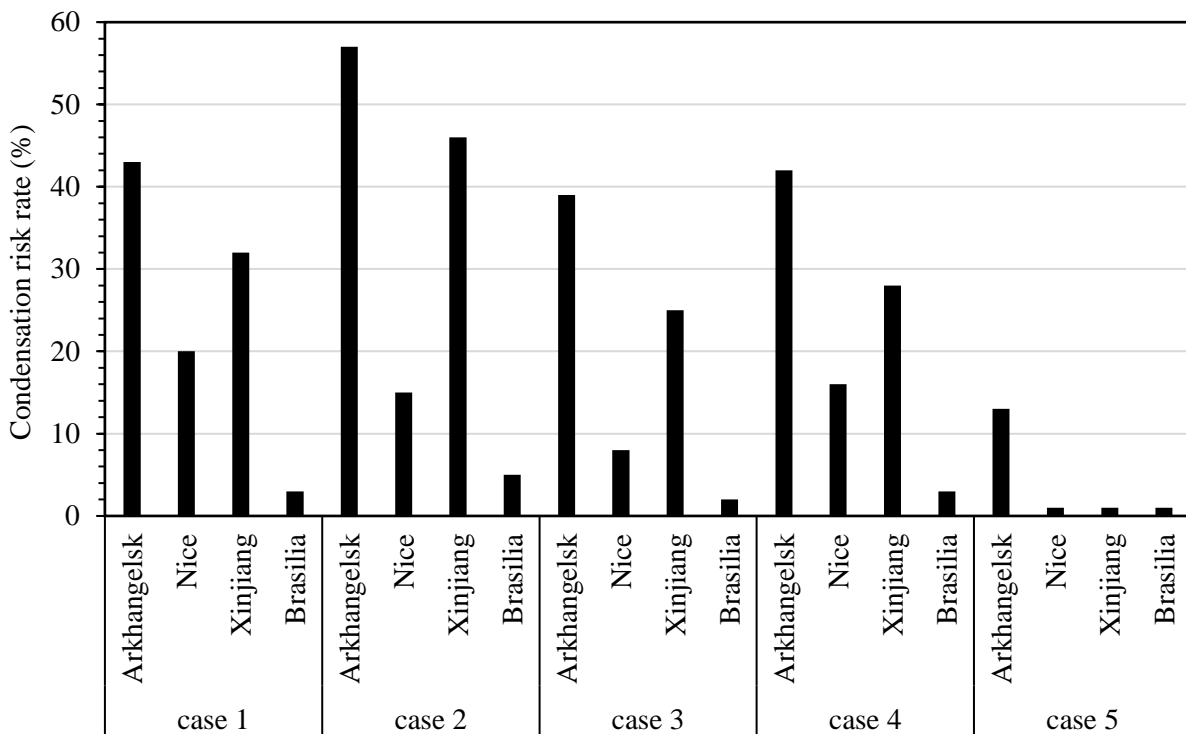


Figure 9.12: Time percentage where the condensation might occur for all cases over four years

9.5.4. Mold growth

The decisive parameters for mold growth are humidity and temperature. WUFI generates the isopleth graphs that show the hygrothermal condition of a wall based on its humidity and temperature. As an example, **Figure 9.13** compares the isopleth graphs of the last two cases under the subarctic continental Russian climate conditions (4-R and 5-R). Both cases correspond to minimal dryness rates as shown in **Figure 9.11**. In case 4, the hygrothermal conditions at the interior surface cross both Lim 1 and Lim 2 curves while in case 5, they stay below the curves. Consequently, mold growth problems will occur in case 4. For the other cases, results show a risk of mold growth only for the first case under the subarctic continental Russian climate conditions.

Furthermore, a risk of composting can occur when the moisture levels are high at not low enough temperatures. Among all simulated cases, the first and fourth cases present a risk of composting the straw layer in the Russian weather only. The temperature and average RH of the straw layer respectively reach 15°C and 85% for case 1 and 20°C and 90% for case 4 (see **Figure 9.13**).

Chapter 9. Hygrothermal numerical study

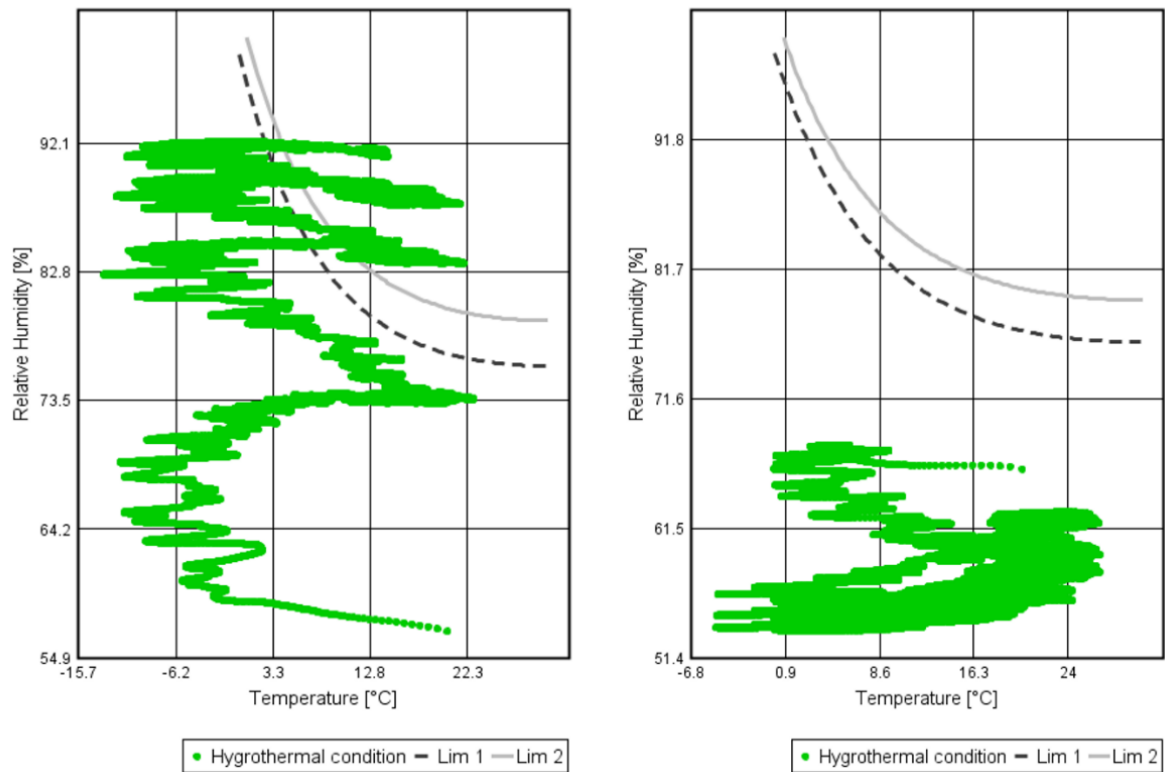


Figure 9.13: Isopleth for case 4 (left) and case 5 (right) tested with Arkhangelsk-Russia climate condition

9.5.5. ASHRAE criterion

Table 9.6 summarizes the results of the ASHRAE criterion once applied to the selected cases. It was observed that the ASH criterion is not respected 30 %, 17 %, 28 %, 73 %, and 2 % of the time respectively in cases one, two, three, four, and five for Arkhangelsk-Russia where the RH surpasses the 80 % limit and reaches 85 % after four years. The high risk in the subarctic continental Russian weather only, in all cases, is explained by the exterior and interior conditions that affect the humidity of the exterior and interior layers. In that climate, the first four wall configurations are not able to dry out, as seen in Figure 11. For the same reasons as explained for the DR criterion, these walls have high relative humidity. The variation of the average RH inside the wall in case 3-R over 100 days is presented in **Figure 9.14**. The thickness of the straw layer plays an important role in regulating the humidity of the whole structure. The RH decreases from 80 % to 30 %. The air and the hardwood layers also participate in moderating the humidity fluctuations by preventing the indoor air humidity to penetrate the wall.

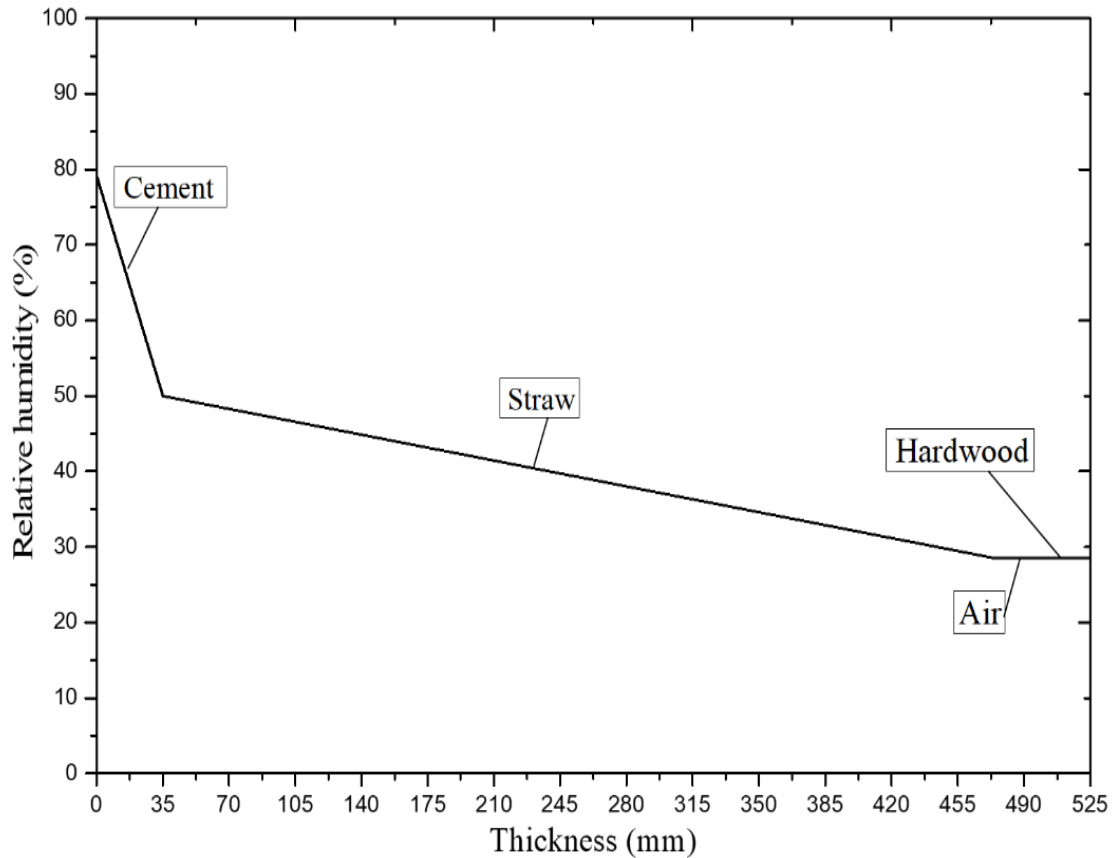


Figure 9.14: Relative humidity distribution inside the wall (3-R) through all the layers during 100 days in winter

Table 9.6: Computed results from the straw walls cases regarding the ASHRAE standard (ASH)

ASH criterion	Case 1	Case 2	Case 3	Case 4	Case 5
Arkhangelsk -Russia	Risk (30 %)	Risk (17 %)	Risk (28 %)	Risk (73 %)	Risk (2 %)
Nice-France	No risk	No risk	Risk (2 %)	No risk	No risk
Xinjiang-China	No risk	No risk	No risk	No risk	No risk
Brasilia-Brazil	No risk	No risk	No risk	No risk	No risk

9.5.6. Time lag and decrement factor

Those two important parameters of wall thermal inertia are calculated based on equation (3.1) and equation (3.2) for all of the wall configurations. It is known that the material's thermal diffusivity and thickness especially affect the time lag and the decrement factor. To obtain a low decrement factor and high time lag, the thermal diffusivity of a wall should be decreased by reducing the thermal diffusivity of its layers, while the wall thickness should be increased. Results in **Table 9.7** show that the first and the second wall have the same time lag but different decrement factors. The second wall has a higher decrement factor because the hardwood has a higher thermal diffusivity than the cement layer. In addition, the third case shows better values than the fourth case due to the straw layer thickness that provides lower thermal diffusivity. The different layers used in the last case, such as wood wool,

Chapter 9. Hygrothermal numerical study

hardwood, and cement layer, reinforce the thermal mass of the wall. Therefore, the fifth case obtains the highest time lag of about 8 hours and 30 minutes and the lowest decrement factor of value 0.05.

Table 9.7: Computed results from the straw walls cases regarding time lag and decrement factor

	Case 1	Case 2	Case 3	Case 4	Case 5
$\phi(h)$	6h30	6h30	7h30	7h	8h30
$f(-)$	0.06	0.07	0.055	0.065	0.05

9.6. Proposed Solutions

The hygrothermal problems can be solved using several measures such as increasing the straw thickness, adding a vapor retarder layer, adding an unventilated air layer, and controlling the indoor conditions. A higher thickness of straw may have a good effect since it reinforces the wall permeability and its thermal resistance. To confirm this hypothesis, a new case (3-R/360) is simulated corresponding to case 3 with a reduced straw thickness of 360 mm. The results are illustrated in **Figure 9.15**. Whereas the total water content reached a permanent regime in case 3 under the subarctic continental Russian climate (3-R in **Figure 9.10**), it is increasing consistently for the new 3-R/360 case over 4 years. Besides, high indoor RH has a critical impact on the behavior of straw-based envelopes. For example, case 5-R passed the TWC criterion under normal indoor conditions (40 % - 60 % RH) (**Figure 9.10**). However, this behavior changes when increasing the indoor RH to 60 % in winter and 90 % in summer. Under these new indoor conditions, **Figure 9.15** shows that the WC of case 5-R increases over four years without attaining equilibrium.

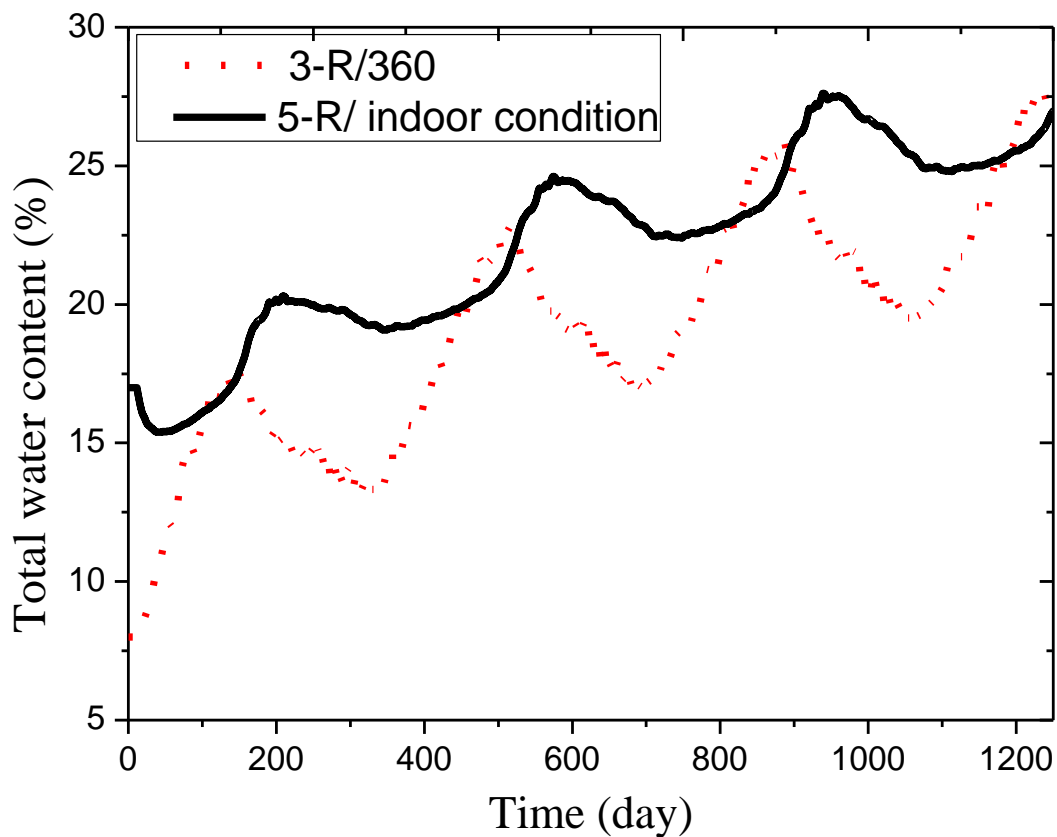


Figure 9.15: Daily total water content of case 3 (3-R/360) with a straw thickness of about 36 cm and case 5 (5-R) under high indoor relative humidity in Arkhangelsk-Russia for four years

Chapter 9. Hygrothermal numerical study

The use of a material that retards the transmission of water vapor is an adequate solution to eliminate the risk of mold growth. For example, by adding a vapor retarder layer behind the interior plaster in 4-R, the dryness rate increases and the hygrothermal conditions stay below the limiting curves as can be seen in **Figure 9.16**. The same result is reached by increasing the straw thickness to 440 mm in the 4-R case.

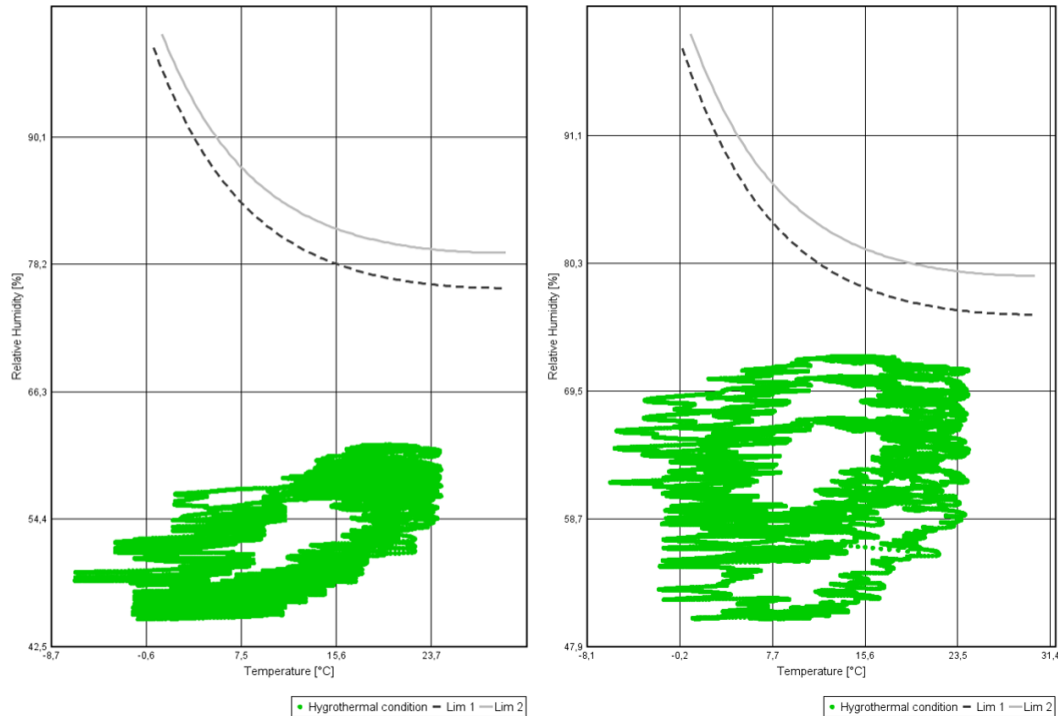


Figure 9.16: Isoleth for case 4 with vapor retarder layer (left) and with high straw thickness layer (right) tested with Arkhangelsk-Russia climate condition

Composting may be prevented in cases 1-R and 4-R by using an exterior ventilated rain screen and a lime layer on both sides of the straw wall. **Figure 9.17** depicts the impact of these layers through the isopleth of case 1-R. The maximum RH drops from roughly 90 % to 54 %. Furthermore, the dryness rate increased from -50 % to -5 %. These findings show that the wall's durability related to the condensation and composting risks is improved, especially during the winter. The ventilated rain screen reduces water and humidity infiltration from the outside, while the lime layer enhances the permeability of the wall, which allows for quick drying out.

Chapter 9. Hygrothermal numerical study

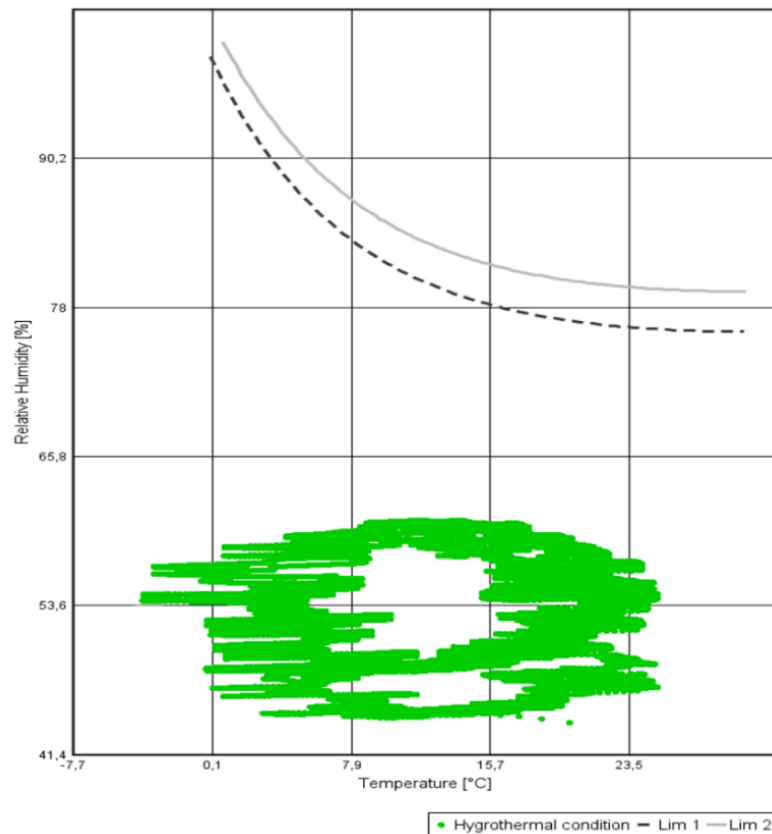


Figure 9.17: The isopleth for case 1-R with ventilated rain screen and lime layer

The condensation risk and the ASH failure in case 2-R can be avoided by adding an unventilated air layer or an insulating material at the exterior side of the straw layer. The gap between the hardwood and the straw reinforces the exterior insulation and helps to increase the interior surface temperature. In this way, the condensation risk decreases from 60 % (case 2 under Russian climates in **Figure 9.12**) to 11 %. At the same time, the ASH criterion is respected during the whole period since the risk is reduced from 17 % (case 2 under subarctic continental Russian climates in **Table 9.6**) to 2 %. It is demonstrated through these additional simulations that the application of a solution to meet one particular hygrothermal criterion can solve problems on other criteria at the same time.

Straw construction spreads worldwide regarding its wide economic and environmental advantages. Despite its promising characteristics, it may include moisture and condensation risks leading to health, mechanical stability, and lifetime durability problems. Interior and exterior humidity, driving rain, ground moisture, and leakage can all generate moisture in straw walls. For this reason, the current chapter studies the hygrothermal behavior of various straw wall compositions numerically. From the obtained results, some problems are detected for all wall configurations under the subarctic continental climate weather of Arkhangelsk, Russia. Such cold and wet climate weather with a high level of air RH are prone to cause serious moisture issues [215]. Cold weather generates low surface temperatures that are close to the dew point temperature, which increases the condensation risk even for moderate indoor RH levels. The difference between the saturation pressure and the water vapor pressure is also reduced, which leads to condensation risks within the wall. This can explain the high condensation risk of the four first cases, which can reach 80 % of the simulated time, particularly for the subarctic continental Russian and cold desert Chinese weather. This problem can be avoided by reinforcing the exterior insulation. The climate condition in Arkhangelsk-Russia also explains the lower dryness rate when

Chapter 9. Hygrothermal numerical study

compared to the other simulated climates. This study aimed to associate each climate with the optimum wall composition from a hygric and thermal point of view. It was noticed that hygrothermal issues occurred mainly in cold or/and humid weather. The first, second, and fourth wall configurations have similar behavior and can be used in temperate-Mediterranean (Csa) and savanna (Aw) climates such as Nice and Brazilia. The third wall shows good thermal properties and can be used in cold desert climates (BWk) such as Xinjiang. The last wall did not present hygrothermal problems and mold growth in all climates with normal indoor conditions and can be used in all climates, including the subarctic continental climates (Dfc) such as Arkhangelsk. The presence of the wood wool as exterior insulation and the interior air layer in case five prevented hygric issues. For this reason, it has better performance under all conditions.

Fourth part: Building characterization

10. Experimental straw building's thermal performance

The experimental work on a building scale is detailed in this chapter. The objective is to investigate how the straw building reacts to weather variations. T/RH sensors are inserted in the test building's walls and indoor space, and a weather station is set up three meters from the north wall. The building is in free floating condition, meaning the indoor conditions are free to fluctuate without any mechanical cooling, heating and ventilating devices. The outcome is then evaluated using criteria of thermal and hygienic comfort. These criteria are crucial in the construction industry not only for the welfare of people but also to forecast the energy load the mechanical equipment should supply for.

Table of contents

10.1. Experimental setup.....	129
10.1.1. Description of the tested building.....	129
10.1.2. Building instrumentation.....	130
10.1.3. Sensors positioning.....	131
10.2. Methodology and assessment criteria.....	132
10.2.1. Evaluating the hygrothermal performance of the envelopes.....	132
10.2.2. Evaluating the indoor thermal comfort.....	132
10.2.3. Evaluating the indoor hygrothermal comfort.....	133
10.3. Experimental results.....	133
10.3.1. Thermal and hygric performance of the envelopes.....	133
10.3.2. Indoor thermal comfort.....	136
10.3.3. Indoor hygrothermal comfort.....	137

10.1. Experimental setup

10.1.1. Description of the tested building

The experimental campaign uses a building located in Reugny (03190), France. The building, shown in **Figure 10.1**, was built in 2019 and represents a typical French house. It has a living area of 120 m² spread over two levels with a height of 2.6 m for each level. The first floor consists of an entrance hall, a pantry, an open kitchen, a dining area, and a living room. The second floor consists of three bedrooms and a bathroom. The ground floor rests on steel piles to avoid any contact of the wood-straw elements with the natural ground and to provide stability to the structure. The building is equipped with insulated double-glazed windows and doors on the south and north walls for a total area of 18 m². The double glazing has a U-value of 1.2 W/ m².K and a g-value of 0.57 [216]. The main entrance door has a U-value of 0.9 W/ m².K and acoustic resistance of 35 dB [216]. The building is not equipped with an HVAC system to control the indoor temperature, RH, and ventilation to study indoor comfort.



Figure 10.1: Experimental straw building located in Reugny, France

The studied building is constructed using the prefabricated method. The prefabricated envelopes are customized according to the CAD plans of the building to correspond to the different openings and dimensions of the floors. The industrial partner Activ'home manufactures seven types of prefabricated modules with a fixed height of 3 m, a fixed thickness of 54 cm, and a variable length from 4.9 m to 7.8 m with an increment of 0.48 m. Exterior walls, roofs, and floors have the same composition. The straw wall shown in **Figure 10.2** is composed, from outside to inside, of an exterior plaster composed of a 1.5 cm thick cement layer and 2 cm thick wood board, a 4 cm thick wood wool layer, a 36 cm thick straw layer, a 10 cm fermacell board, a 60 cm unventilated air layer and an interior plaster composed of a 13 cm thick gypsum board. The wall U-value is about 0.137 W/ m².K.

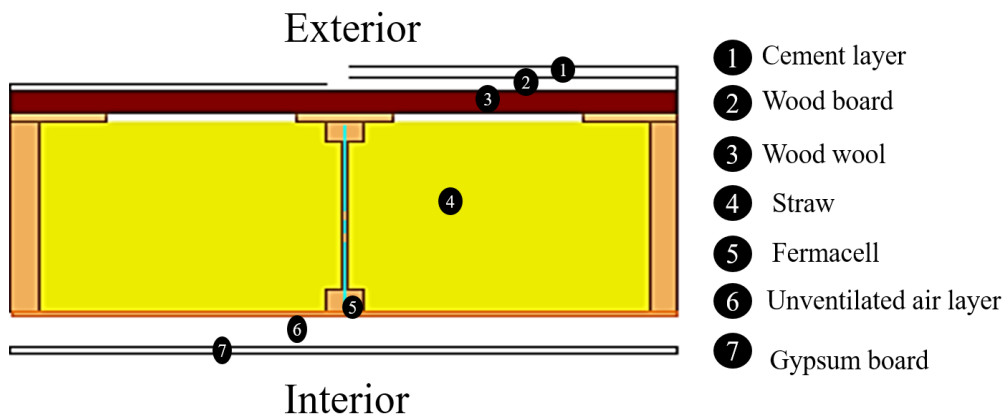


Figure 10.2: Composition of the straw wall used in the experimental building

Chapter 10. Experimental straw building's thermal performance

10.1.2. Building instrumentation

In order to monitor the performance of the whole system, the building and the walls are instrumented with temperature sensors, humidity sensors, presence detectors, and a weather station to measure the exterior conditions. The details of each sensor and the measured quantities are given below.

10.1.2.1. Weather station

A weather station is installed about three meters away from the building's north wall to measure the outdoor weather conditions. It is a Vantage Pro 2 Plus- 6162EU - Davis instrument [217] equipped with dry-bulb air temperature and RH sensors, which are protected from solar radiation and wind. The temperature range is -40°C to $+65^{\circ}\text{C}$ with $\pm 0.3^{\circ}\text{C}$ accuracy while the RH range is 1 % to 100 % with an accuracy of $\pm 2\%$. The weather station is also equipped with a wind vane anemometer to measure wind speed and direction that range from 3 to 290 km/h and 0° to 360° with an accuracy of ± 3 km/h and ± 3 degrees, respectively. The horizontal (short wave radiation) [218] and vertical (long wave radiation) [217] global solar radiation ranging from 0 to 1800 W/m^2 are measured by a pyranometer with a $\pm 1\text{ W/m}^2$ accuracy. In addition, accumulated rain ranging from 0 to 999.8 mm in 24h with an accuracy of 0.2 mm is measured daily by a rain gauge. The data is recorded every minute over two years.

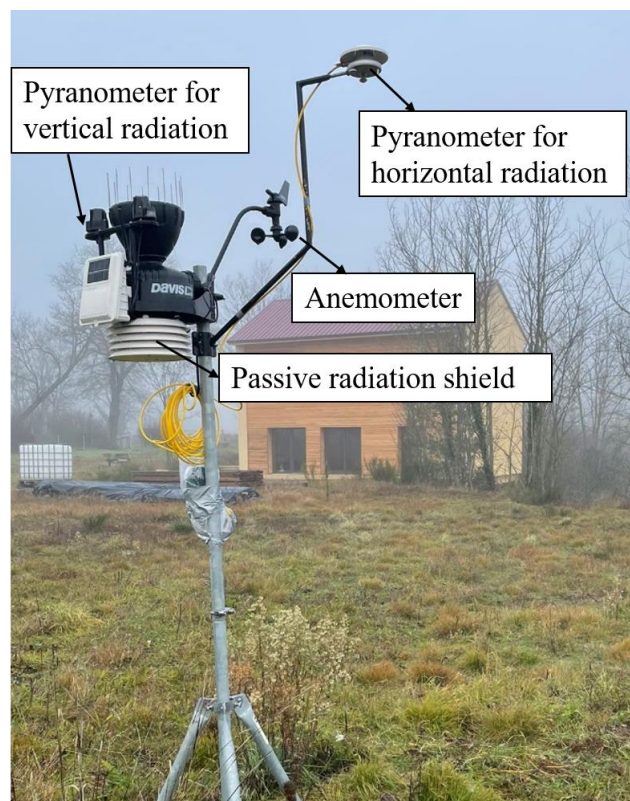


Figure 10.3: Weather station installation at six meters away from the experimental building

10.1.2.2. Temperature and relative humidity sensors

The T/RH sensors used to measure these parameters at different locations in the building and the walls are presented in **Figure 10.4**. The walls' interior and exterior surface temperature and RH values are measured using HYT 939 Digital humidity and temperature sensors [219]. The temperature measurement range is between -40°C and $+125^{\circ}\text{C}$ with an error of $\pm 0.3^{\circ}\text{C}$. The RH measurement range is between 0 % and 100 % with an error of $\pm 1.8\%$. The exterior surfaces are highly affected by solar radiation which may lead to measuring errors. Therefore, the sensors are integrated into the outer surfaces to be well covered and protected. Indoor air temperature and relative humidity are measured with a NodOn EnOcean RH/T sensor with an accuracy of $\pm 1^{\circ}\text{C}$ for temperature and $\pm 3\%$ for RH [220]. The indoor motion is detected with PIR motion sensors that detect at distances up to 5 m [221]. It should be noted that the indoor temperature and RH are not controlled. Thus, these parameters are free-floating during summer and winter. Measurements in Free-Floating are mostly carried out in order to study indoor comfort.

Chapter 10. Experimental straw building's thermal performance

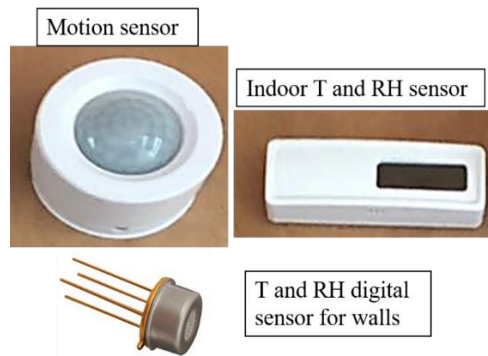


Figure 10.4: Motion sensor, T and RH sensors installed in the walls

10.1.3. Sensors positioning

Eleven lines of sensors are installed on certain walls and floors of the experimental building. They are located on the floor of the second floor, in the walls of the first and second floors at 1 m from each floor ground for the first floor and at 2 m for the second, as shown in **Figure 10.5**. Each location is composed of three T/RH measurement points at three depths in the element wood-straw: 3 cm from the inside of the straw volume, in the center, and 3cm from the outside. This variety of locations is done to check the uniformity of the values through the envelopes and to detect any measurement anomaly. The indoor T/RH and motion sensors are located on the east wall at 1.8 m from the floor of each level.

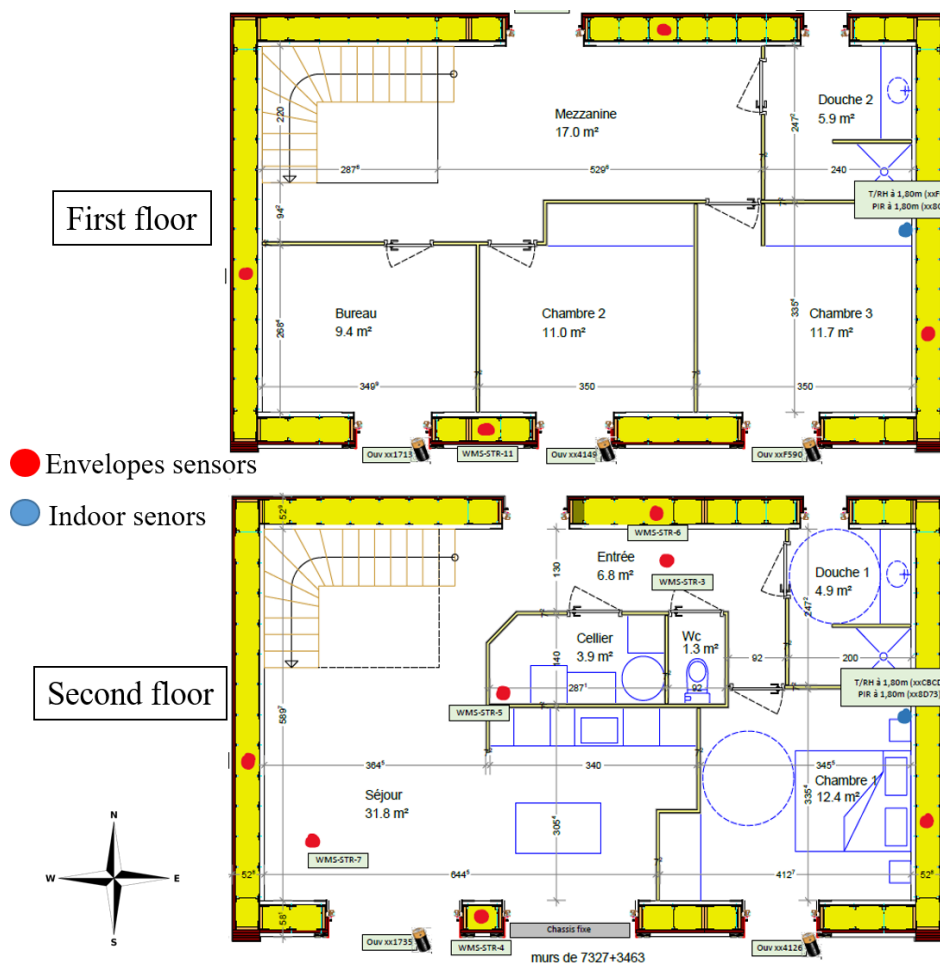


Figure 10.5: Drawing plan of the building with the location of the sensors (red and blue)

Chapter 10. Experimental straw building's thermal performance

10.2. Methodology and assessment criteria

The purpose of the experimental measurement campaign is to study the effect of straw envelopes on the indoor behavior of the building. The performance of the insulation system is evaluated by criteria that include thermal and hygric comfort.

10.2.1. Evaluating the hygrothermal performance of the envelopes

To assess the hygrothermal performance of straw bale walls, temperature, and relative humidity were measured on the internal and external sides of the south-, north-, east- and west- facing walls. In this section, only the south and north-facing walls are presented since they show the worst cases in terms of solar radiation on the south and wind and driven rain on the north. This assessment studies the evolution of the superficial T and RH on the internal side of the walls, as a function of changing boundary conditions on their external side. It gives experimental access to wall thermal inertia properties such as the time lag and the decrement factor based on equation (3.1) and equation (3.2).

10.2.2. Evaluating the indoor thermal comfort

Thermal comfort is an important concept to consider when designing a building. In particular, summer comfort is one of the three major requirements of the French Environmental Regulation for Buildings RE 2020. The first assessment of the test building's thermal comfort is done by calculating the thermal comfort index (TCI). The index determines the number of degree-hours spent beyond the comfort zone and depends on the measurement period. Thus, the criterion is calculated as the average difference between the operating and the comfort temperatures of the zone, as described in equation (10.1).

$$TCI = \frac{\sum |T_{op} - T_{comf}|}{\sum dt} \cdot dt \quad (10.1)$$

where T_{op} is the operative temperature calculated using the indoor air temperature and the surface temperature of the walls [222] and T_{comf} the recommended comfort temperature in the tested zone. It corresponds approximately to a comfort temperature range of 20-26°C during the winter and summer periods as recommended in the EN 15251 norm.

According to Brotas and Nicol [223], overheating is already a problem in different climates across Europe. This problem is occurring during the summer in buildings that are well insulated to improve their thermal performance in the winter. Thus, to assess overheating problems, the second considered assessment criterion calculates a comfort temperature based on the outdoor temperature as recommended by CIBSE TM53 guidelines [224]. This standard distinguishes between free-running and mechanically ventilated buildings, each with its own set of acceptable temperature ranges. Several categories are defined by the standard, category I being recommended in case of very sensitive occupants, category II for new buildings, category III for existing buildings, and category IV for building used during a limited part of the year. In this study, as the building is new, the used limits are those indicated by category II with a suggested acceptable temperature range of $\pm 3^\circ\text{C}$. Thus, the comfort temperature is calculated by equation (10.2). In addition, ASHRAE standard 55 [209] uses an adaptive comfort model based on the mean monthly outdoor temperature (T_{out}) to examine the indoor thermal comfort. The comfort temperature is presented by equation (10.3) that corresponds to 90 % acceptability limits.

$$T_{comf} = 0.33 \times T_{op} + 18.8 \pm 3 \quad (10.2)$$

$$T_{comf} = 0.31 \times T_{out} + 17.8 \pm 2.5 \quad (10.3)$$

Chapter 10. Experimental straw building's thermal performance

10.2.3. Evaluating the indoor hygrothermal comfort

The concept of comfort cannot be limited to temperature only. It is commonly accepted that relative humidity has a significant impact on feeling comfortable. ASHRAE 55 [209] recommends an indoor RH between 30% and 60%. Thus, the period when the indoor RH exceeds the limits is estimated as a preliminary evaluation of the risk of hygric discomfort.

The second assessment combines the temperature and RH effects on comfort by using Fauconnier's [225] model, later used in straw buildings by Douzane *et al.* [15]. This model defines a hygrothermal comfort range, characterizing the couple (temperature; humidity) as shown in **Figure 10.6**. This zone is defined by four T/RH points. The first accepts a limit of 45 % at 18°C, the second 35 % at 26 °C, the third 80 % at 18°C, and the fourth 50 % at 26 °C.

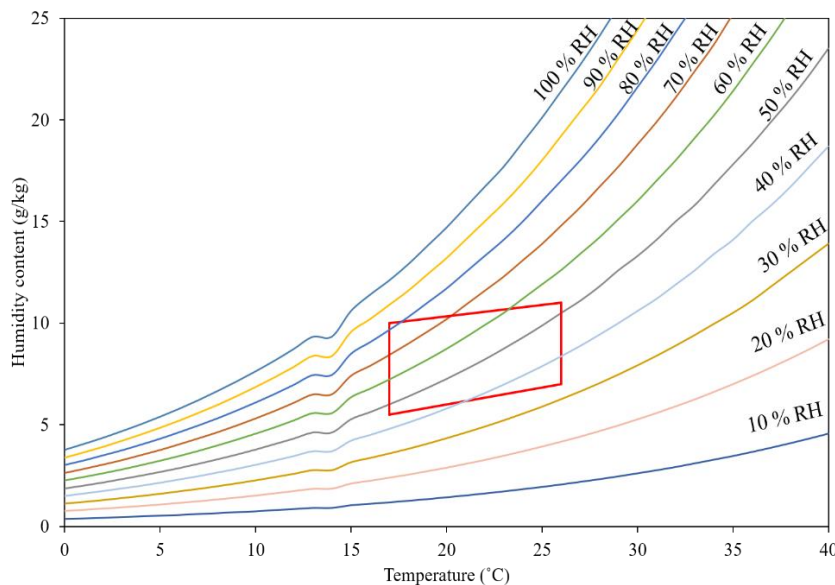


Figure 10.6: Fauconnier's model showing the hygrothermal comfort zone based on the temperature and RH combination

10.3. Experimental results

10.3.1. Thermal and hygric performance of the envelopes

Figure 10.7 displays the variations of the indoor and outdoor air temperature and RH during one year starting on August 1st. The daily average indoor temperature on the second floor ranged throughout the year between 5 °C and 30 °C, whereas the seasonal variations in the daily outdoor average temperature were between -3 °C and 28 °C. The insulation property of the straw is proved by the indoor and outdoor air temperature difference during the winter since the walls had the ability to increase the minimal outdoor temperatures by 25 % and up to 15°C. For the relative humidity values, despite the significant values of the outside RH, the indoor relative humidity (RH) is relatively steady. The daily average indoor RH on the second floor ranged throughout the year between 36% and 56 %, whereas the seasonal variations in the daily outdoor average RH were between 44 % and 90 %. The wall has the ability to decrease the indoor RH by 53 % and up to 37 % RH. This behavior is due to the combined moisture buffer properties of the straw and wood layers.

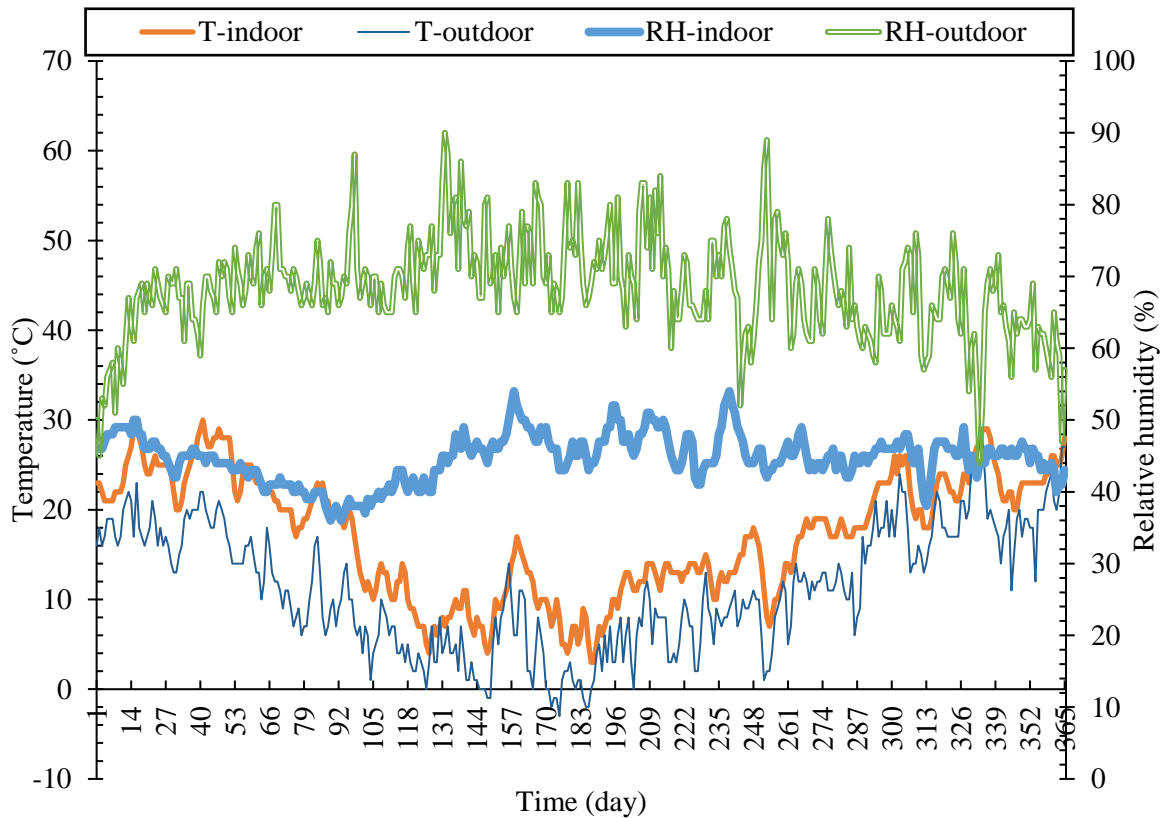


Figure 10.7: Comparison of the daily outdoor air (weather station) and indoor (on the second floor) temperature and relative humidity

Figure 10.8 represents the interior and exterior surface temperature and RH of the north and south facing walls on the second floor. The results show that the wood-straw wall controls the external peaks of RH and temperature to offer better indoor comfort. The external RH of the north face increased from 58 % on the first of August to reach a maximum value of 70 % on the first of February. On the internal face, it started at 46% RH and the maximum attained RH was 55 % at the end of February. The same trend is obtained for the south face but with a maximum external RH of about 60-65 % during the winter season. The 5 % difference between the north and the south is explained by the rain that causes moisture absorption with lower sunlight and thus increases the RH according to the sorption isotherm curve of the straw and the covering materials. A decrease of approximately 10 % occurred on day 90. It can be explained by the natural ventilation of the building caused by workers entering the building. This period of ventilation led to drier ambient air.

Chapter 10. Experimental straw building's thermal performance

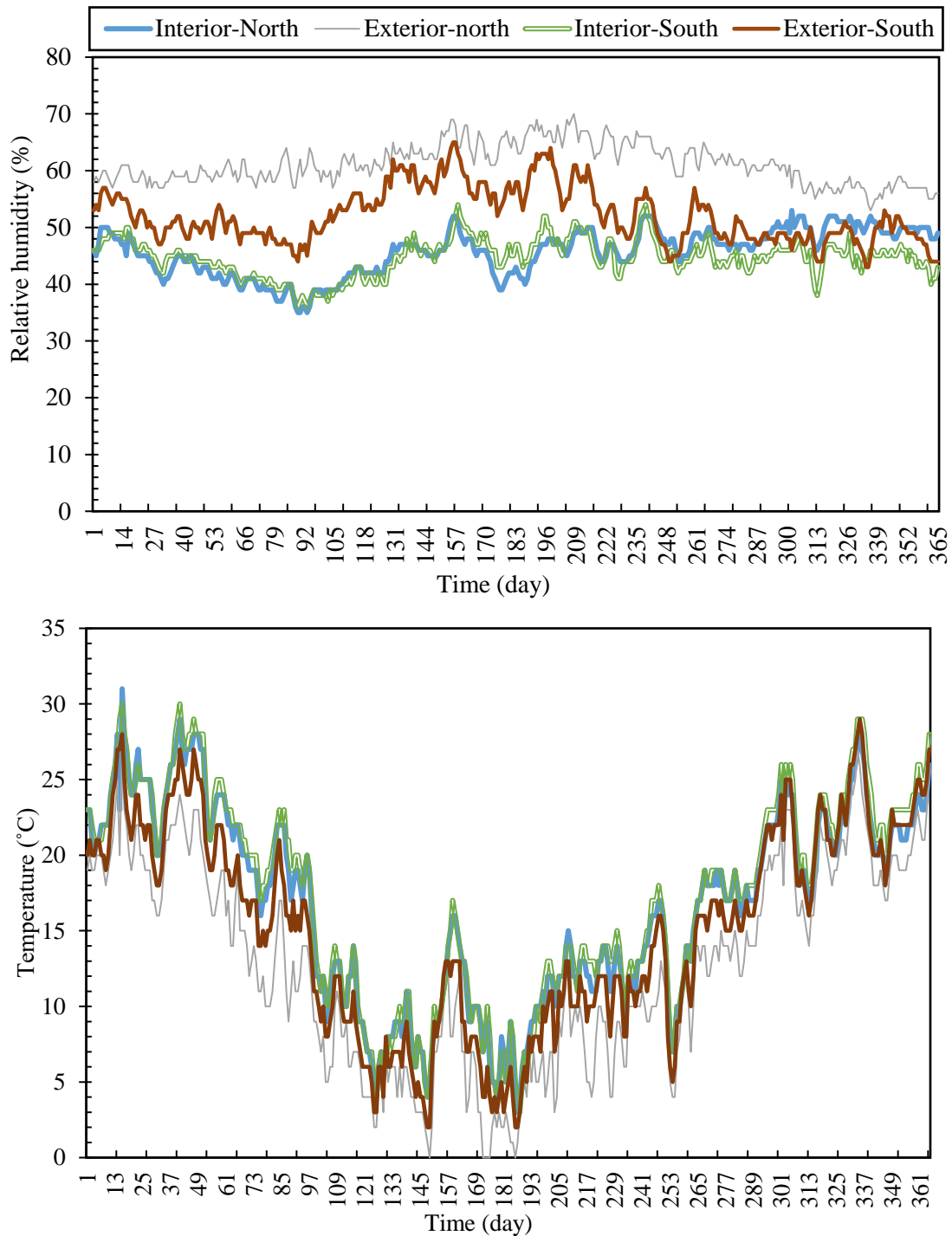


Figure 10.8: RH and temperature daily variation of the internal and external surfaces of the north and south facing walls on the second floor of the test building

The internal and external surface temperature curves followed the indoor temperature curve. The external temperature decreased from 30 °C to 0 °C while the internal decreased from 30 °C to 5 °C. The south and north wall internal and external surface temperature values were close, with a difference of 3 °C and 7 °C, respectively, due to more solar radiation in the south. In February and March, the external surface temperature attained a daily average minimum of -3 °C which was barely noticeable on the internal side of the wall, with a gap of 8 °C despite the absence of a heating system. Similarly, when the external surface temperature reached 30 °C in August the internal surface temperature was 25 °C without any ventilation or cooling. The time lag of the test wall is found to be 9 hours with a decrement factor

Chapter 10. Experimental straw building's thermal performance

of 0.16. These values indicate heat storage in the envelope during the day. On one side, this cuts down on the amount of time needed for cooling during the hot period and heating during the cold period. The wall releases the stored heat 9 hours after having the maximal temperature which increases the indoor temperature by 16 %.

Both parameters show a positive disposition concerning indoor comfort with a possibly minimal time of heating during the winter. For the summer period, overheating may occur on specific days, since the gap between the surfaces and indoor temperature was not large. These two points are studied in detail in the next sections.

10.3.2. Indoor thermal comfort

The average TCI on the first floor is found to be 1.5 °C in summer and 4 °C in winter while on the second floor it is found to be 2 °C in summer and 6 °C in winter. This difference between the first and second floors is caused by the stack effect of the building that will affect the indoor operative temperature and relative humidity. **Figure 10.9** represents the variation of the indoor operative temperature and the minimum and maximum comfort temperatures of different standards over one year from August 1 to July 31.

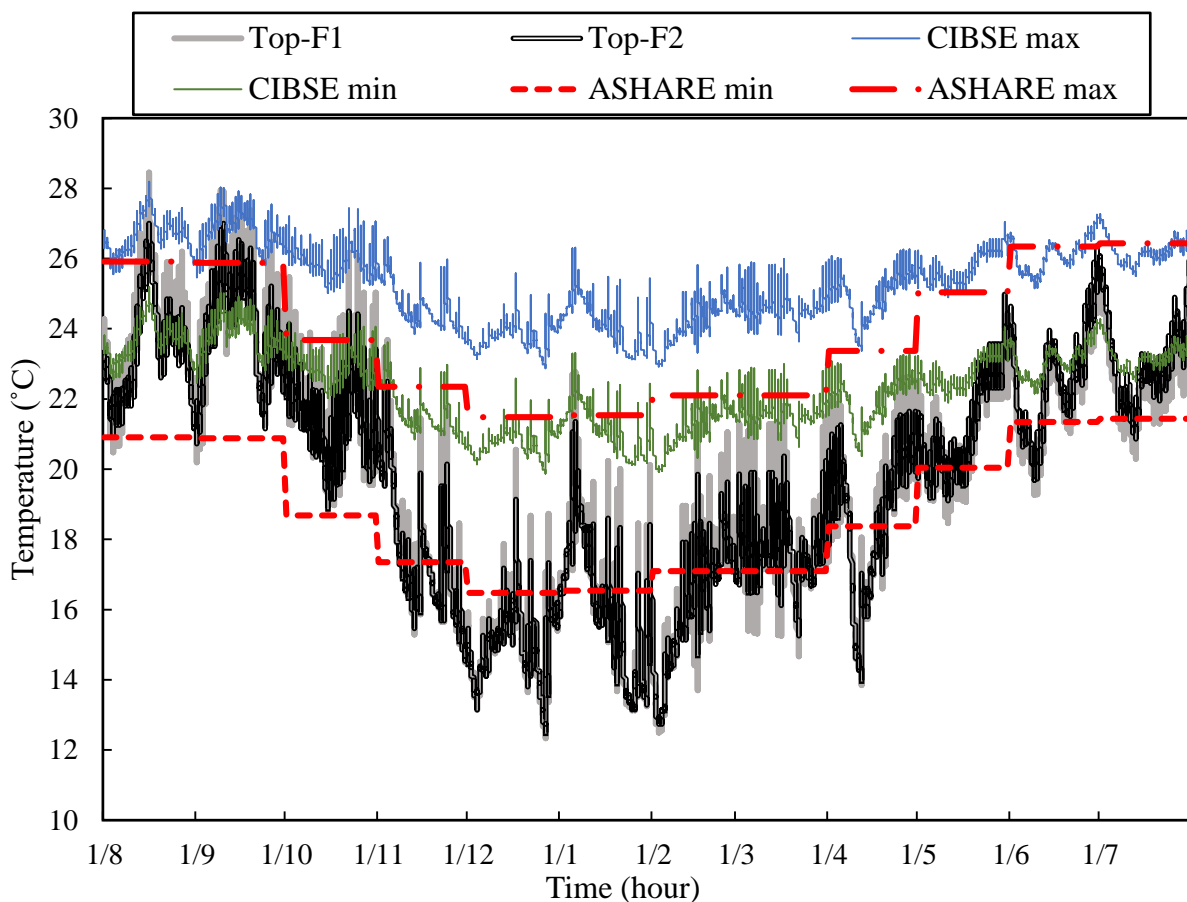


Figure 10.9: Comparison between the operative temperature of the first floor (F1), the second floor (F2), the CIBSE and ASHRAE maximum and minimum acceptable temperature over one year from August 1 to July 31

The indoor operative temperature decreases when the outdoor temperature decreases. Note that during the winter, the monthly average exterior temperature attains 3.2 °C and in summer it reaches 20 °C. It can be noticed that, compared to the CIBSE limits, the tested straw wall does not ensure indoor thermal comfort from November to March, and a heating system is required to decrease the TCI index. The situation is much better in summer (between July and September) when a little overheating may occur. The application of ASHRAE limits presents the same situation during summer, where there is no

Chapter 10. Experimental straw building's thermal performance

requirement for a cooling system, while in winter different results are obtained. The indoor operative temperature exceeds the limits 31 % of the time. Therefore, it can be concluded that the indoor operative temperature is acceptable based on the outdoor monthly average temperature.

10.3.3. Indoor hygrothermal comfort

Figure 10.10 reproduces the indoor RH on both floors. It can be noticed that ASHRAE RH limits are respected all the time except for some days in August, February, and March. The impact of wall sorption on indoor air relative humidity has been demonstrated experimentally. In winter, the indoor air RH values are greater than in summer due to the low indoor temperature and high outdoor RH which can cause hygrothermal issues in the wall. These results are not sufficient and cannot decide whether indoor comfort is reached or not.

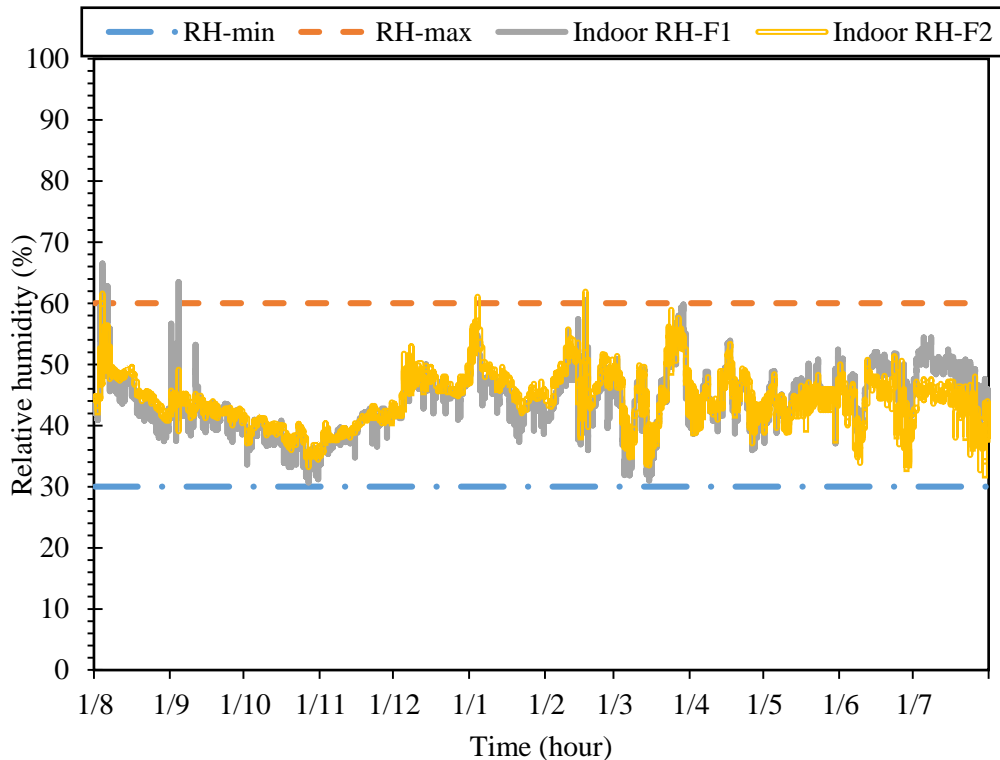


Figure 10.10: Indoor RH variations at the first (F1) and second floors (F2) with reference to the maximum and minimum RH recommended by ASHRAE 55 over one year from August 2020 to July 2021

The psychrometric chart for average daily operative temperature, RH, and the hygrothermal comfort zone is shown in **Figure 10.11**. It can be seen that the indoor T_{op} and RH are outside the comfort zone 62 % of the time during one year. The hygrothermal discomfort is caused by the high temperature values (25 °C – 30 °C) during summer and low temperature (10 °C – 15 °C) during winter at RH levels between 30 % and 60 %.

Chapter 10. Experimental straw building’s thermal performance

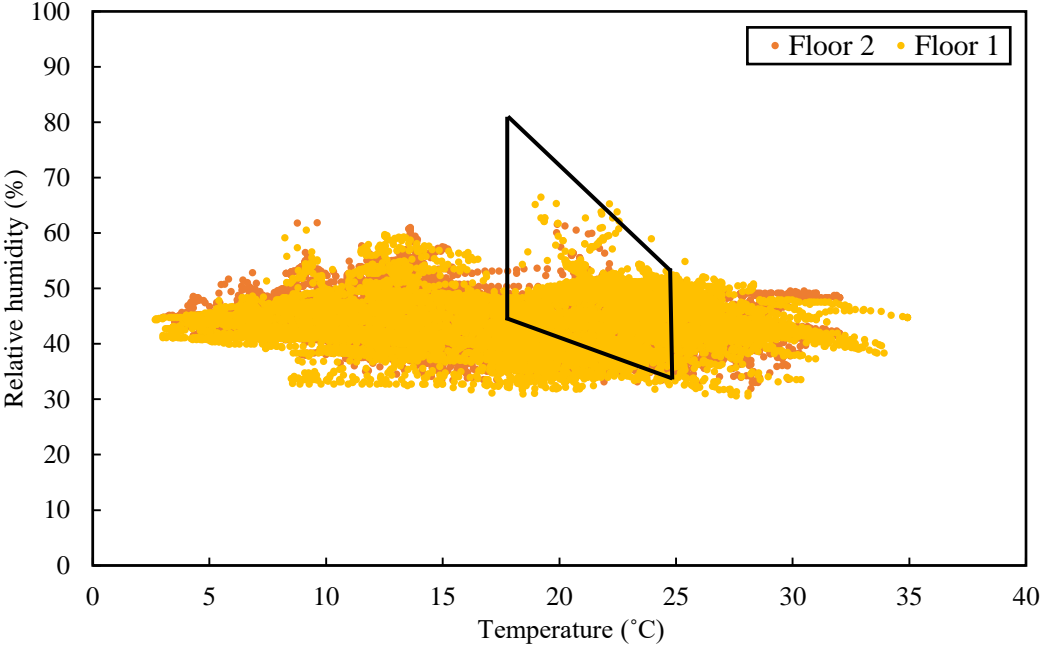


Figure 10.11: T_{op} and RH values of the indoor air of the first and second floors with respect to the hygrothermal comfort zone defined by Fauconnier’s model

The experimental work consisted of measuring the indoor air temperature of a free-floating straw building to assess indoor hygrothermal comfort. During the winter, the difference between the indoor and outdoor air temperature is found to be +25 % while in summer this difference decreased to attain +2 %. The indoor air RH ranged between 30 % and 60 % all over the year while the outdoor RH ranged between 45 % and 90 %. Straw walls proved their high thermal resistance and their ability to exchange humidity with their surroundings. The indoor air operative temperature and relative humidity were outside the hygrothermal zone 46 % of the time. To avoid discomfort, it is necessary to assist the indoor temperature and RH with a mechanical HVAC system. The following chapter studies the thermal comfort and the heating and cooling demand of several straw buildings under different climates, using EnergyPlus software.

11. Numerical study of thermal and energetic performance of straw buildings

EnergyPlus software is used to study the energetic and thermal performance of different straw buildings under several climates. First, the software is described to assess its functionality and capability. The model is validated by using data from the experimental building detailed in the previous chapter. Next, a sensitivity analysis determines the factors affecting most the thermal behavior of the test building. The model is then applied for the different straw wall structures and weathers already used in chapter 9, with two internal gains scenarios. The objective is to show the net need for heating and cooling in each case and to find the best fitted weather for each building type, while considering the results of chapter 9. In addition, the indoor comfort is investigated based on the indoor temperature and relative humidity during summer and winter periods.

Table of contents

11.1. General description of EnergyPlus.....	140
11.1.1. Thermal and hygric transfer through the walls.....	140
11.1.2. Indoor thermal and hygric balance.....	141
11.2. Model description and validation.....	141
11.3. Sensitivity analysis.....	145
11.4. Case study description.....	148
11.5. Numerical results.....	149
11.5.1. Thermal comfort.....	149
11.5.2. Hygrothermal comfort.....	151
11.5.3. Energy consumption.....	152

11.1. General description of EnergyPlus

The rules concerning the requirements on building envelope's thermal behavior have become increasingly restrictive. The heat loss through the envelopes is the main problem of the whole building's energy consumption and indoor comfort. Therefore, it is important to examine the energetic performance and the thermal comfort of straw buildings in different climates by using different straw envelopes. This study is done numerically by using EnergyPlus (EP) software.

EP is a thermal and energy analysis simulation program for buildings developed by the DOE (Department Of Energy, United States) to carry out studies concerning energy consumption and indoor comfort [226]. It simulates heat transfer through walls, soil, and air. The thermal loads allowing for simultaneous calculation of radiant and convective effects in the interior and exterior surface at each time step are based on the heat balance solution. The solar calculations are advanced since EP can calculate the amount of beam radiation falling on each surface. It gives the possibility to simulate the internal gains, the building equipment, occupancy, and lighting to detect the appropriate scenario for the studied building. The software makes it possible to estimate the net energy requirement of the building, the final energy consumption of many HVAC systems, and the primary energy load. Several comfort models are integrated into the software such as Fanger's model (PMV and PPD) and the adaptive model (ASHRAE 55 and EN 1521).

Since EP is a simulation engine with no user-friendly graphical interface, the geometry of the building is modeled using the software Google Sketchup. Then it is imported to EP using the interface Open Studio plug-in for Google Sketch. The building is divided into thermal zones of a single temperature. A thermal zone can include several rooms, provided that they have similar internal loads (occupation, equipment, scenario ...) and also similar external charges (solar radiation and shadows, and therefore the orientation of the walls).

11.1.1. Thermal and hygric transfer through the walls

EnergyPlus predicts the hygrothermal transfer through the envelopes by using four calculation algorithms, combined heat and moisture transfer (HAMT), Effective moisture penetration depth (EMPD), Conduction by transfer functions, and Conduction by finite differences. Researchers [227] compared these algorithms and found that the HAMT model is the most efficient for predicting the hygrothermal behavior of a building.

The HAMT algorithm is a coupled, one-dimensional, heat and moisture transfer model simulating the simultaneous transport and storage of heat and moisture in surfaces from and to both interior and exterior environments. Through composite building walls, HAMT may also provide temperature and moisture profiles and assist in locating places with high surface humidity. Equation (11.1) and equation (11.2) are derived from heat and moisture balance equations to describe a theoretical model for the transfer of heat and moisture through a material (Künzel [192]). The three terms in equation (11.1) describe the storage, transport, and generation of heat respectively. The three terms in equation (11.2) describe the storage of moisture, the transport of liquid moisture, and the transport of vapor respectively. Equation (11.3) calculates the vapor diffusion coefficient in the air (δ) which is used in the third term of both equations. The heat storage capacity ($\frac{\partial H}{\partial T}$) depends on the moisture content w of the material through the equation (11.4). The moisture content of the material w and the vapor diffusion resistance factor μ depends on the relative humidity inside the material. The parameters $\frac{\partial w}{\partial \phi}$, k^w and D^w are also moisture dependent parameters.

$$\frac{\partial H}{\partial T} \frac{\partial T}{\partial t} = \frac{\partial}{\partial x} \left(k^w \frac{\partial T}{\partial x} \right) + h_v \frac{\partial}{\partial x} \left(\frac{\delta}{\mu} \frac{\partial T}{\partial x} \right) \quad (11.1)$$

$$\frac{\partial w}{\partial \phi} \frac{\partial \phi}{\partial t} = \frac{\partial}{\partial x} \left(D^w \frac{\partial w}{\partial \phi} \frac{\partial \phi}{\partial x} \right) + \frac{\partial}{\partial x} \left(\frac{\delta}{\mu} \frac{\partial T}{\partial x} \right) \quad (11.2)$$

Chapter 11. Numerical study of thermal and energetic performance of straw buildings

$$\delta = \frac{(2 \times 10^{-7} \times (T + 273.15)^{0.81})}{P_{\text{ambient}}} \quad (11.3)$$

$$\frac{\partial H}{\partial T} = C \cdot \rho + c^w \cdot w \quad (11.4)$$

with H the heat storage capacity, T the temperature, φ the relative humidity, w the moisture content, k^w the moisture content-dependent thermal conductivity, D^w the moisture content-dependent liquid transport coefficient, δ water diffusion coefficient of the air, μ vapor diffusion resistance dependent on the moisture content, P_{ambient} the ambient air pressure, C the specific heat capacity of the dry material, ρ the material's dry density, and c^w the specific heat of the water.

11.1.2. Indoor thermal and hygric balance

The heat and moisture balance of the air in a zone is described in equation (11.5) and equation (11.6), respectively. These equations calculate the indoor temperature and RH responsible for indoor comfort. In addition, indoor conditions are used to predict building energy consumption.

$$\rho \cdot C_p \cdot V \frac{dT_i}{dt} = \sum_j A_j \cdot h_j (T_j - T_i) + n \cdot \rho \cdot C_p \cdot V \cdot (T_{out} - T_i) + \dot{Q}_{in} + \dot{Q}_{HVAC} \quad (11.5)$$

$$V \frac{dv_i}{dt} = M_{in} + M_{HVAC} + \sum_j A_j g_{in,j} + nV(v_{out} - v_i) \quad (11.6)$$

where $\rho \cdot C_p \cdot V \frac{dT_z}{dt}$ is the energy stored in the air of the zone, ρ the density of air, C_p the heat capacity of the air, V the volume of the room, t the time, A_j the envelope surface area, h_j the heat transfer coefficient, T_j the surface temperature, T_i the indoor temperature, T_{out} the exterior air temperature, $\dot{m}_{inf} + \dot{m}_{vent}$ the air mass flow rate due to infiltrations and ventilation, \dot{Q}_{in} the internal convective charges (equipment, occupants), \dot{Q}_{HVAC} the power released by the energy systems to regulate room temperature, v_i the vapor content of the interior air, v_{out} the vapor content of the exterior air, $g_{in,j}$ the moisture flux into the room, n the air change rate, M_{in} the internal moisture gain, M_{HVAC} the moisture gains or loss due to the HVAC system.

11.2. Model description and validation

In the previous chapter, a straw building having a living area of 120 m² located in Reugny, France, was studied to show its indoor comfort quality. The exterior walls, floor, and roof are composed of exterior plaster, wood wool, straw, wood, unventilated air, and interior plaster. This same building is used to validate the EP model. The validation is based on comparing the indoor and walls temperature and RH variations based on the exterior conditions measured by the weather station as shown in **Figure 11.1**.

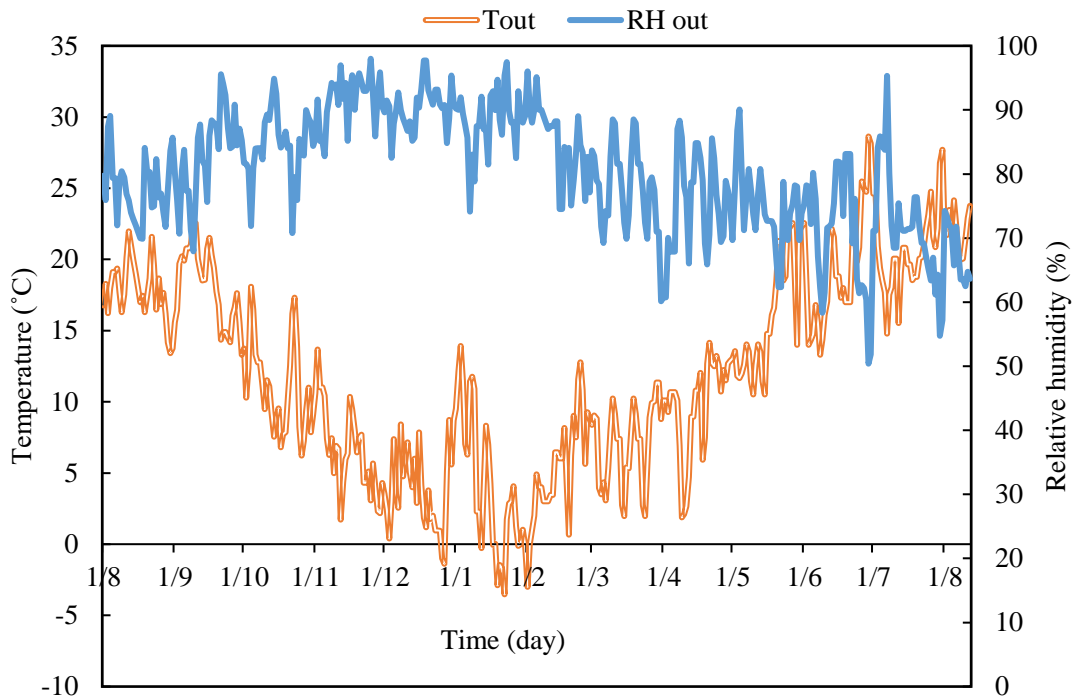


Figure 11.1: Daily outdoor air temperature (T_{out}) and relative humidity (RH_{out}) at Reugny obtained for one year from August 1 to July 31

Figure 11.2 shows the geometry of the modeled house done by using Sketchup. The two floors are free-floating without any internal gain and each one is considered as one zone to decrease the simulation time. The inputs include the materials' properties, and the inside and outside convection.

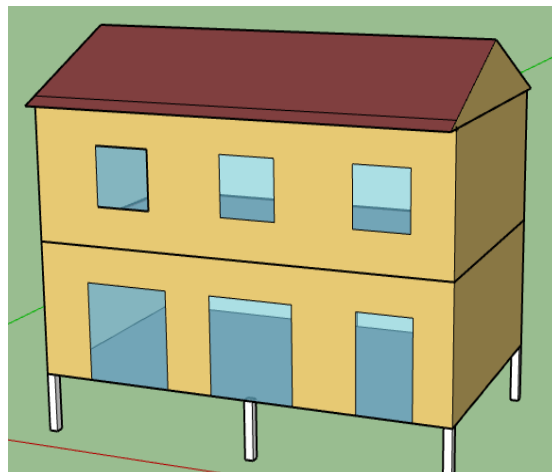


Figure 11.2: Test building geometry using Sketchup and EnergyPlus plugins

Table 11.1 represents the material properties that compose the test wall. Straw characteristics are extracted from the experimental work of this study while the other materials characteristics are extracted from literature. The HAMT model necessitates additional information concerning the properties of the materials such as the sorption isotherm and the moisture content-dependent thermal conductivity that are respectively extracted from **Figure 6.21** and **Figure 6.26 (c)**. For the other materials, these curves are not added and the calculation is based on **Table 11.1** values. The inside and outside convection vary according to TARP and DOE-2 algorithms defined in equation (11.7) and equation (11.8). The internal

Chapter 11. Numerical study of thermal and energetic performance of straw buildings

and external vapor coefficient values are 2×10^{-8} kg/Pa.s.m² and 6.25×10^{-8} kg/Pa.s.m² respectively, chosen based on [228,229].

$$h_{inside} = 2.5 \cdot R_f \cdot \frac{PV_z}{A} + h_n \quad (11.7)$$

$$h_{outside} = R_f \cdot ((h_n^2 + 10.6 \cdot (V_z)^{1.78})^{0.5} - h_n) + h_n \quad (11.8)$$

$$h_n = \begin{cases} 1.31 \cdot (T_{air} - T_{surface})^{0.3} & \text{if } T_{air} - T_{surface} = 0 \\ \frac{9.48 \cdot (T_{air} - T_{surface})^{0.3}}{7.28 - \cos\gamma} & \text{if } T_{air} - T_{surface} < 0 \\ \frac{1.81 \cdot (T_{air} - T_{surface})^{0.3}}{1.38 + \cos\gamma} & \text{if } T_{air} - T_{surface} > 0 \end{cases} \quad (11.9)$$

With h_n the natural convective heat transfer coefficient calculated according to equation (11.9), R_f a constant that designates the roughness of the surface, V_z the wind speed, γ the surface tilt angle, P the surface perimeter, T_{air} the indoor or outdoor air temperature, and $T_{surface}$ the surface temperature.

Table 11.1: Materials hygric and thermo-physical properties at 20°C

	Thermal conductivity (W/m.K)	Density (kg/m ³)	Specific heat (J/kg.K)	Porosity (-)	Water vapor diffusion factor (-)	Initial water content ratio (kg/kg)
Straw	0.06	120	1500	0.9	1.5	0.2
Wood wool	0.08	450	1500	0.55	8	0.2
Wood board	0.13	650	1500	0.47	12	0.2
Unventilated air	0.028	1.3	1000	0.99	0.32	0.6
Cement layer	1.2	2000	850	0.2	25	0.5
Fermacell Gypsum board	0.32	1250	850	0.4	7	0.5

Figure 11.3 and **Figure 11.4** depict the experimental and numerical results of the indoor air and the internal surface temperature and RH. The findings are in good agreement. For the walls, the RMSE for the average temperature and relative humidity is 1.5 °C and 5.8 %, which corresponds to a scatter index of 9.5 % and 8.4 %, respectively. For the indoor air, the RMSE for the average temperature and relative humidity is respectively 1.8 °C and 3.6 %, which corresponds to a scatter index of 6 % and 9.2 %. The main discrepancies are found for the second-floor south wall internal RH. They may be explained by errors in two factors: the sorption isotherms and the initial moisture content of the used materials that affect the walls RH and then the indoor air RH.

Chapter 11. Numerical study of thermal and energetic performance of straw buildings

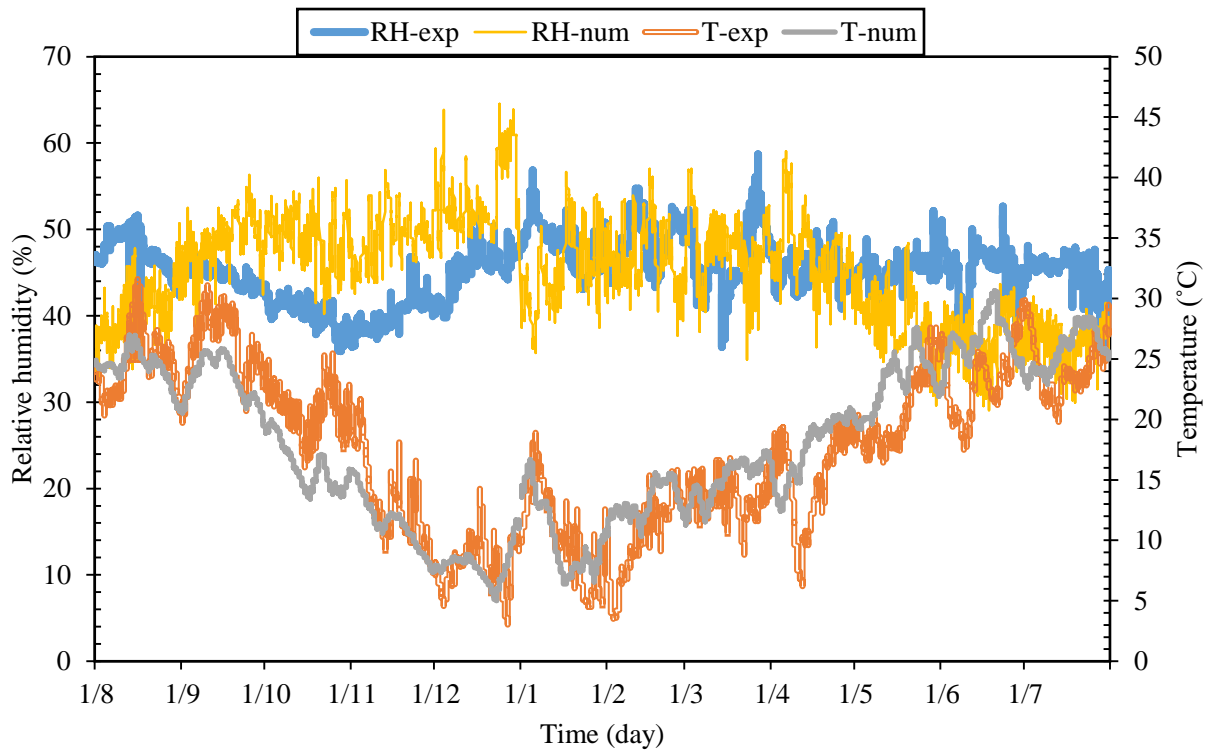


Figure 11.3: Comparison of numerical and experimental findings for the south internal surface temperature and the relative humidity on the second floor from August 1 to July 31

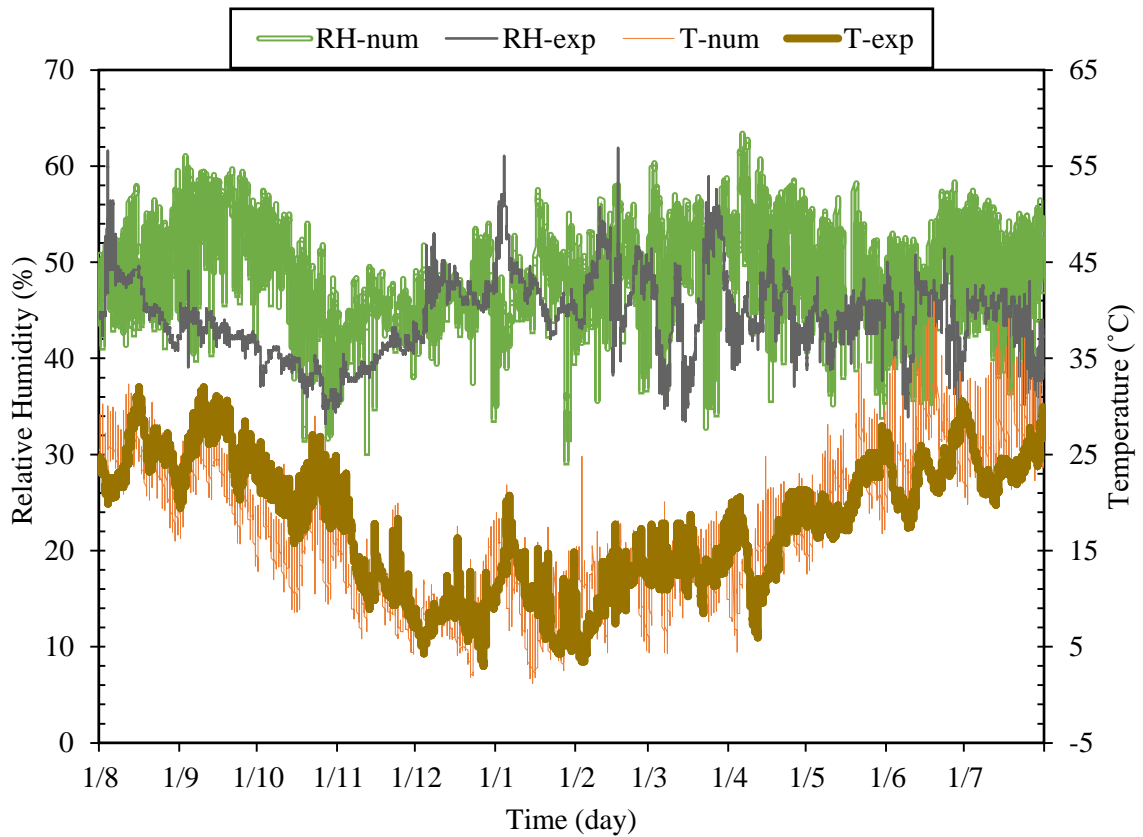


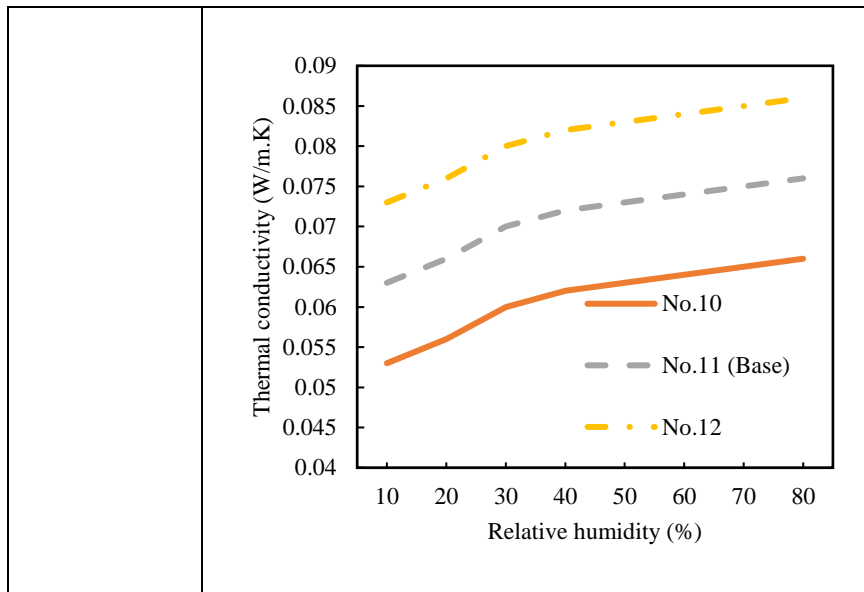
Figure 11.4: Comparison of the numerical and experimental findings for the indoor air temperature and the relative humidity on the second floor from August 1 to July 31

11.3. Sensitivity analysis

Sensitivity analysis is a type of analysis to test the quality of a model that relies on the input uncertainty that may affect the output uncertainty. This type of study is important since straw has a variety of characteristics that may depend on temperature, RH, plant growth conditions, chemical composition, etc. These parameters could not be all studied due to a lack of time. Thus, the selected input parameters include the straw sorption isotherm, thermal conductivity (dependent on RH), density, and initial moisture content as shown in **Table 11.2**, with the base case being a straw bale of density 120 kg/m³, the initial water content of 25%, and the same average sorption isotherm and moisture-dependent thermal conductivity as those experimentally described in Section 6.3, **Figure 6.22**, **Figure 6.26** and **Figure 6.27**. To model the variability in the sorption isotherm, two cases are created by shifting the moisture content values of the base case by + 3 % MC and - 3 % MC respectively. The same is done for the RH-dependent thermal conductivity, where the base case value is either increased by 0.01 W/mK or decreased by 0.01 W/mK. The studied output parameters are the indoor air temperature and RH. The used model is Sobol’s indices or variance-based sensitivity analysis (VB-SA) since it is simple to implement and it is popular [230,231]. The VB-SA ranks the input factors based on their effect on the output variance. The analysis is done by calculating a quantity S_i corresponding to the fraction of the output variance attributed to each input alone. This quantity is known as the first-order index.

Table 11.2: Studied inputs values (No. 2, 6, 8, and 11 present the experimental case)

Input variable	case	Values
Density	No. 1	100 kg/m ³
	No. 2 (Base)	120 kg/m ³
	No. 3	140 kg/m ³
Initial water content	No. 4	5 %
	No. 5	15 %
	No. 6 (Base)	25 %
Average sorption isotherm		
Thermal conductivity vs RH		



The indices presented in **Figure 11.5** show that the thermal conductivity variations have a higher effect on the indoor air temperature and that the isotherms variations have a higher effect on the indoor air RH. The second most affecting parameter is the sorption isotherm. These two inputs are important in a HAMT model and should be chosen carefully to obtain exact results. For a better analysis, the combination of the input must be studied since, for example, the density affects the thermal conductivity values.

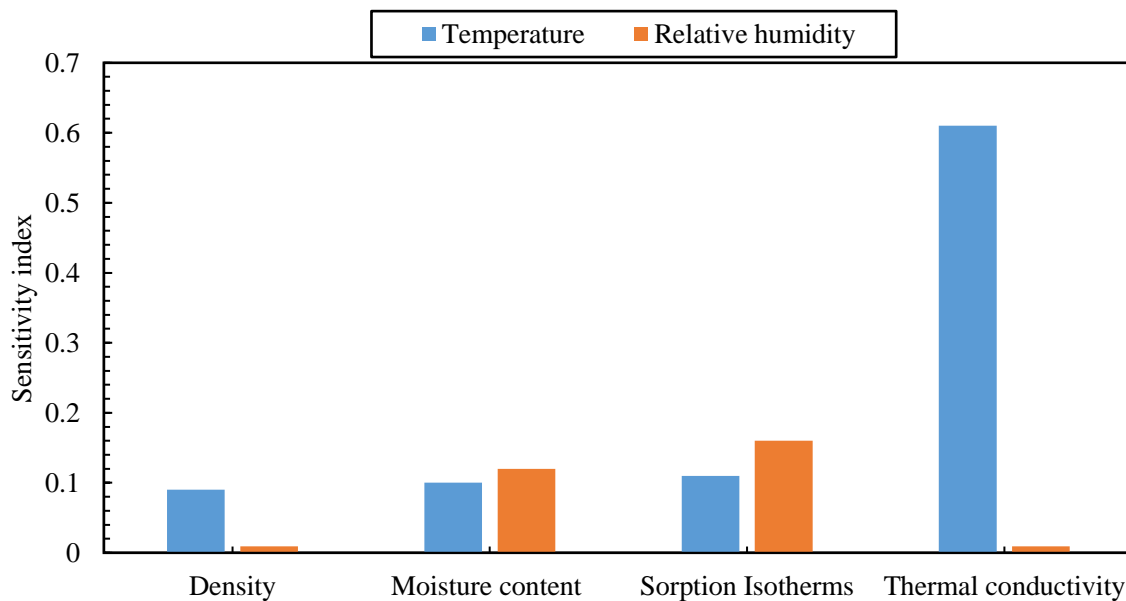


Figure 11.5: First order sensitivity index of the four variable inputs on the indoor air temperature and relative humidity

Figure 11.6, Figure 11.7, Figure 11.8, and Figure 11.9 display the indoor air temperature and RH of the base and the modified cases. It shows that modeled indoor temperature varies up to $\pm 2^\circ\text{C}$ when the straw density varies by 20 kg/m^3 . The moisture content variation by 10% affects the indoor temperature and RH, respectively, by 1°C and 5%. The sorption isotherms curves of straw affect the indoor temperature by $\pm 1.5^\circ\text{C}$ and the RH by $\pm 4\%$. The indoor temperature increases by up to 4°C when increasing the thermal conductivity of straw by 0.01 W/m.K with respect to its relative humidity.

Chapter 11. Numerical study of thermal and energetic performance of straw buildings

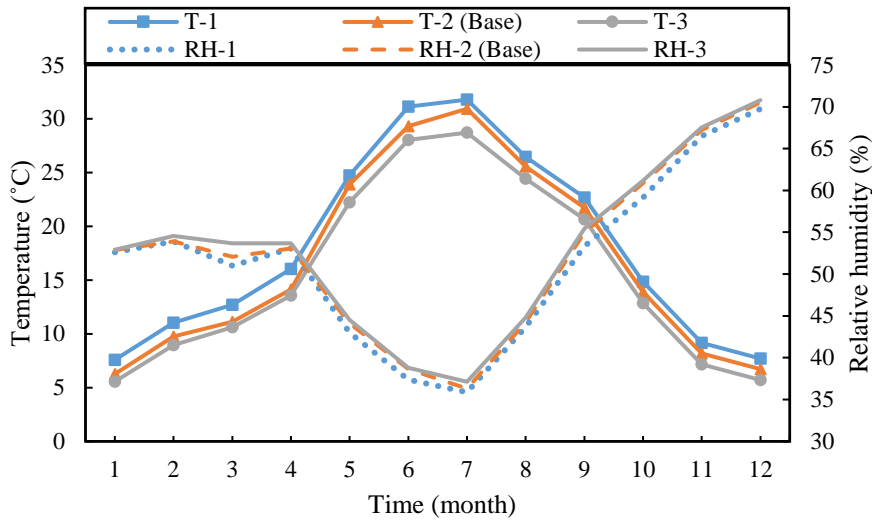


Figure 11.6: Monthly average indoor air temperature and relative humidity variations by varying the density (1, 2, and 3 are the case number)

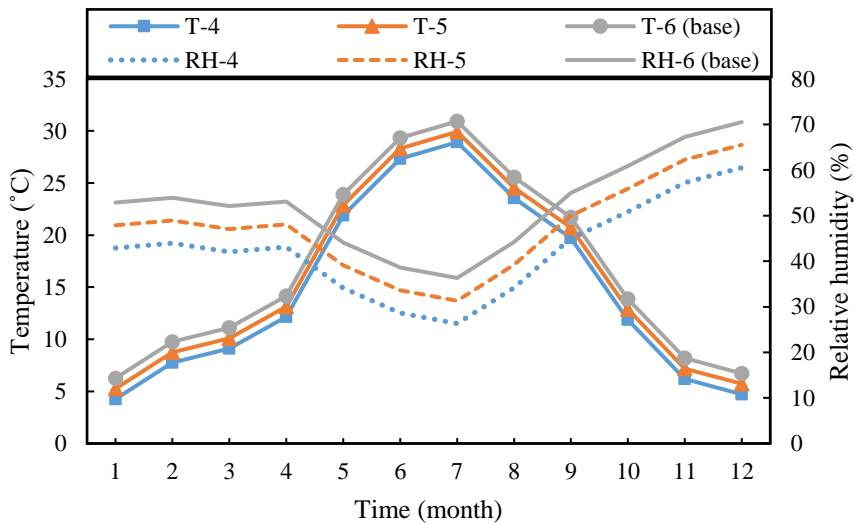


Figure 11.7: Monthly average indoor air temperature and relative humidity variations by varying the moisture content (4, 5, and 6 are the case number)

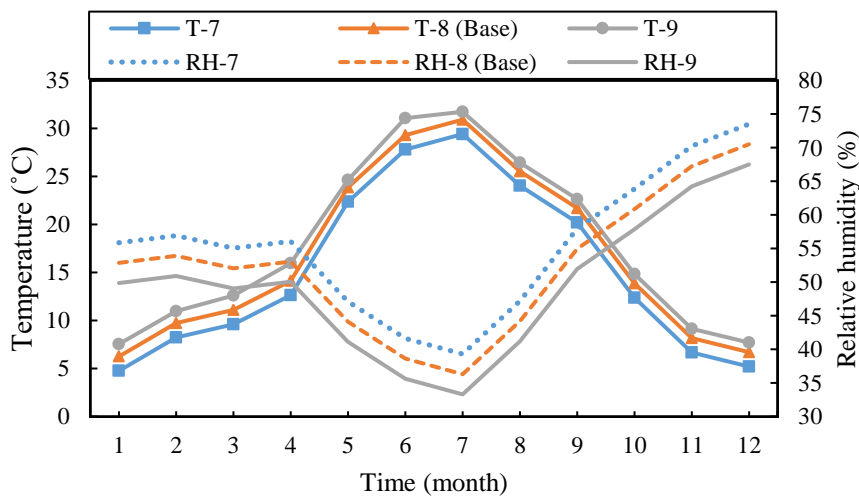


Figure 11.8: Monthly average indoor air temperature and relative humidity variations by varying the sorption isotherms curve (7, 8, and 9 are the case number)

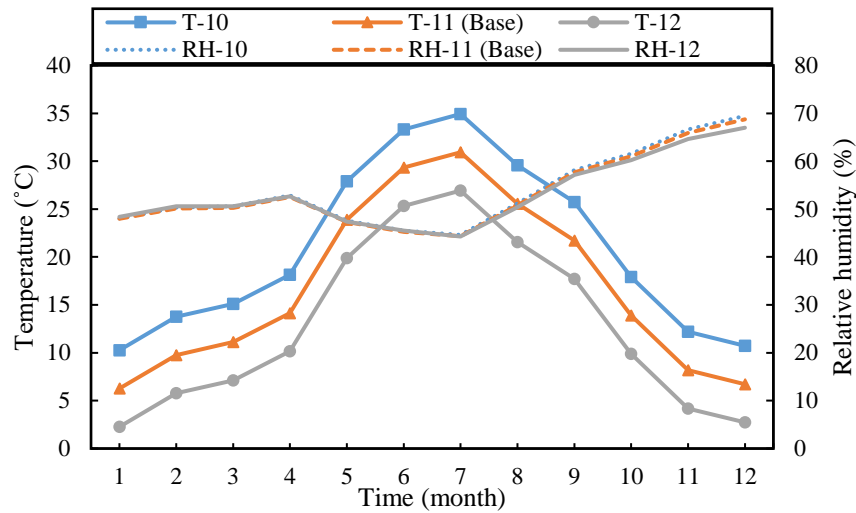


Figure 11.9: Monthly average indoor air temperature and relative humidity variations by varying the thermal conductivity dependent RH curve (10, 11, and 12 are the case number)

11.4. Case study description

The purpose of this section is to study the test building under several climates and wall compositions given respectively in **Figure 9.8** and

Table 9.3. A sixth case is added to these five cases to compare with a standard brick wall used in Europe [232]. The wall is composed of a 0.4 cm of exterior layer (tensile membrane), 1.5 cm of air cavity, 5 cm of wood wool, 1.5 cm of cement plaster, 15 cm of brick, 4 cm of unventilated air, 11 cm of brick, 1.5 cm cement plaster. The properties of the brick are extracted from Coticos [232] and Abbood *et al.* [233]. The comparison of straw walls to this conventional wall helps in determining their efficiency.

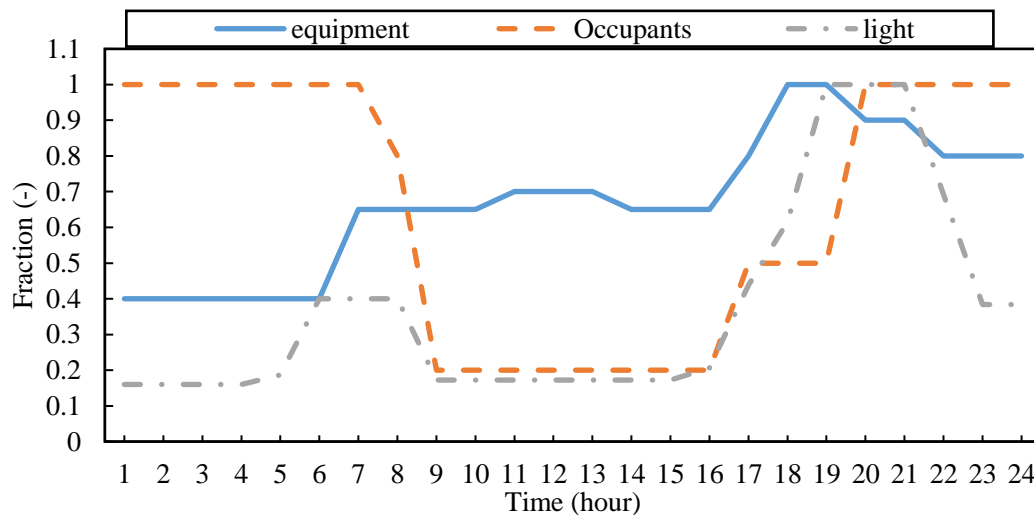


Figure 11.10: Equipment, occupants, and light schedule during 24 hours

In this chapter, the hygrothermal and the energetic performance of each case are studied by using Faucounnier’s model and by calculating the total energy consumed, respectively. To study indoor comfort the building should be free floating while for the energetic study, internal gains should be considered. Therefore, for all the proposed cases, the internal heat gains include 120 W per person for a four-person occupancy, 4 W/m² for lighting, and 4 W/m² for electrical equipment. The nominal thermal loads are also modulated with the schedule given in **Figure 11.10**. An air change rate of 0.8 vol/h is used for modeling natural ventilation and infiltration. The temperature set points are 19°C for heating and 24°C for cooling. The temperature range is maintained by an energy system, thus providing the net

energy requirement of the apartment. To get the final energy requirement, a COP of 0.8 is used for the heating system and a COP of 3 is used for the cooling system.

11.5. Numerical results

11.5.1. Thermal comfort

Figure 11.11, Figure 11.12, Figure 11.13, and Figure 11.14 show the indoor operative temperature variation of the different cases under the Brazilian, Chinese, French and Russian weather, respectively.

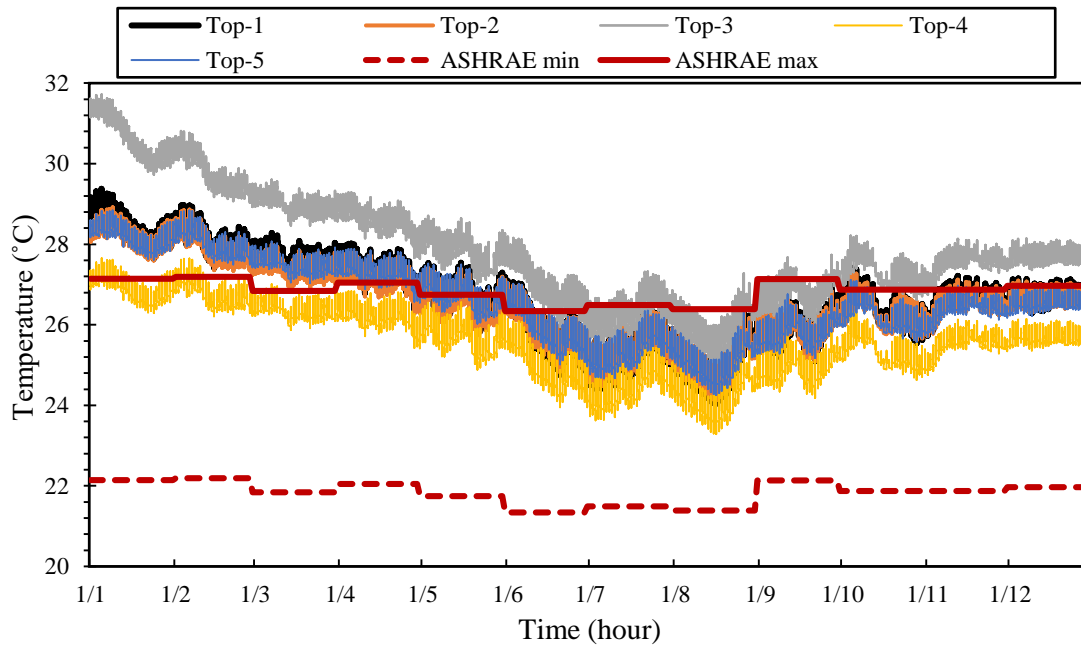


Figure 11.11: Comparison of the indoor operative temperature of cases 1 (Top-1), 2 (Top-2), 3 (Top-3), 4 (Top-4), 5 (Top-5), and ASHRAE maximum and minimum limits under the Brazilian climate over one year from January 1 to December 31

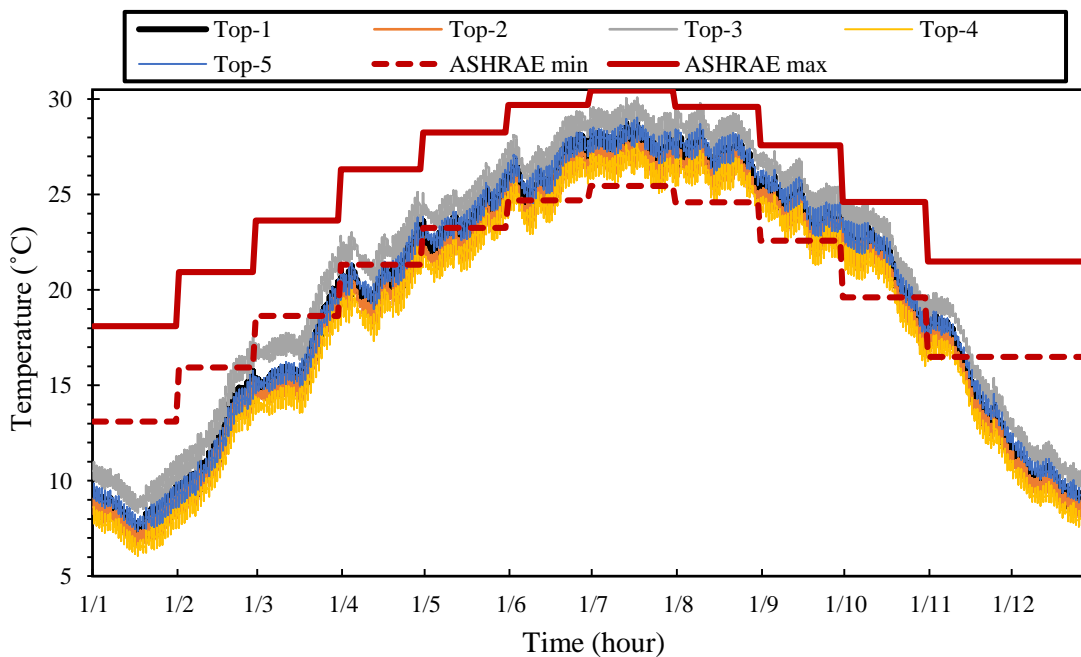


Figure 11.12: Comparison of the indoor operative temperature of cases 1 (Top-1), 2 (Top-2), 3 (Top-3), 4 (Top-4), 5 (Top-5), and ASHRAE maximum and minimum limits under the Chinese climate over one year from January 1 to December 31

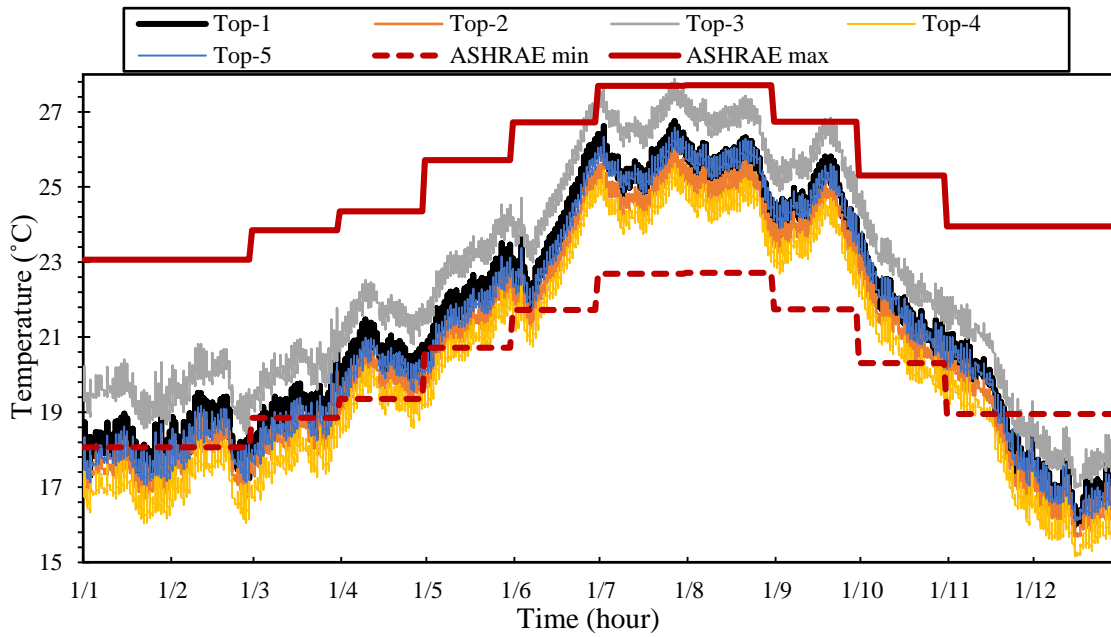


Figure 11.13: Comparison of the indoor operative temperature of cases 1 (Top-1), 2 (Top-2), 3 (Top-3), 4 (Top-4), 5 (Top-5), and ASHRAE maximum and minimum limits under the French climate over one year from January 1 to December 31

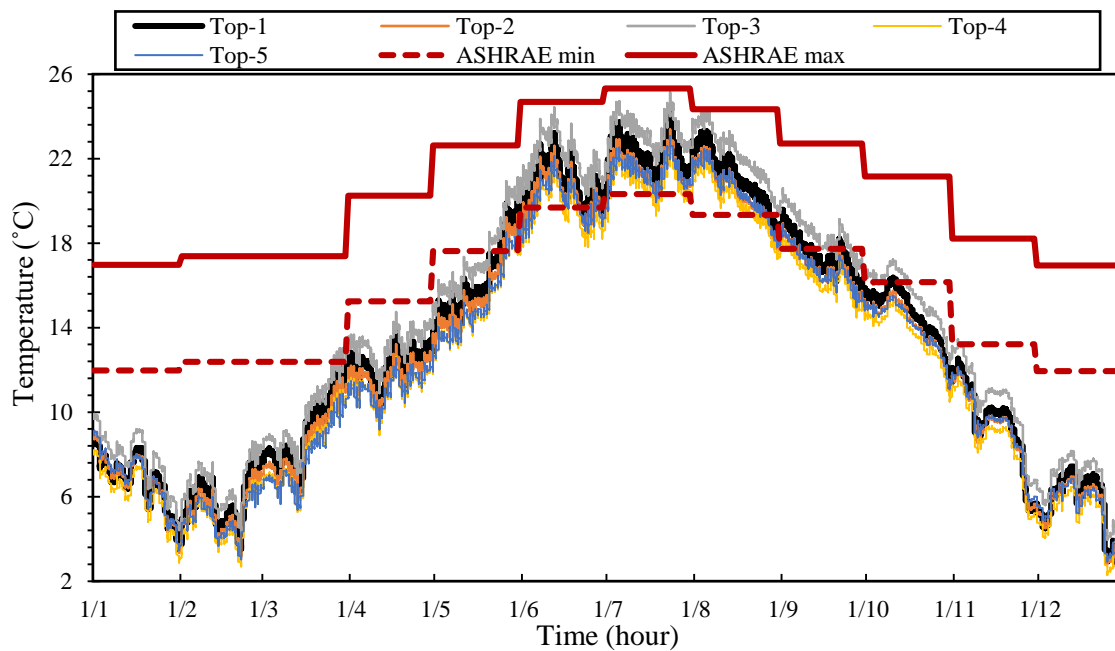


Figure 11.14: Comparison of the indoor operative temperature of cases 1 (Top-1), 2 (Top-2), 3 (Top-3), 4 (Top-4), 5 (Top-5), and ASHRAE maximum and minimum limits under the Russian climate over one year from January 1 to December 31

Cases 1, 2, and 5 in the Brazilian weather meet the ASHRAE limits 60 %, 64 %, and 61 % of the time, respectively. Case 3 has the worst indoor operative temperature, which only adheres to the limits for 20 % of the time. This case suggests overheating issues during the hot season, particularly from January to March. Case 4 has the best indoor operative temperature, which stays within limits for 96 % of the time. Cases 1, 2, and 5 in the Chinese weather meet the ASHRAE limits 49 %, 42 %, and 52 % of the time, respectively. Case 4 has the lowest indoor operative temperature, which adheres to the limits for 37 % of the time. Case 3 has the best indoor operative temperature, which stays within limits for 64 % of the

Chapter 11. Numerical study of thermal and energetic performance of straw buildings

time. During the hot season, all cases are free of the risk of overheating. The main issue occurs during the cold season (November to June) when the indoor operative temperature is low. Cases 1, 2, 4, and 5 in the French weather meet the ASHRAE limits for 76 %, 65 %, 51 %, and 71 % of the time, respectively. The issue is discovered between December and March. Case 3 has the best indoor operative temperature, which stays within limits for 88 % of the time throughout the year except in November and December. Cases 1, 2, 3, 4, and 5 in Russian weather meet the ASHRAE limits for 28 %, 23 %, 39 %, 18 %, and 23 % of the time, respectively. The indoor operative temperature is respected only during the hot period between April and September. For the rest of the year, the temperature remains low due to the low exterior temperature.

11.5.2. Hygrothermal comfort

In the absence of an HVAC system, it is necessary to ensure the indoor comfort of the occupants during summer and winter. The tested straw walls and the conventional wall have different thermal resistances which are 6.41 m².K/W for the first case, 6.15 m².K/W for the second, 7.87 m².K/W for the third, 6.71 m².K/W for the fourth, 7.46 m².K/W for the fifth and 2.5 m².K/W for the sixth (the conventional wall). In addition, as shown in chapter 9, the envelopes have different hygric properties that affect indoor comfort. **Figure 11.15** compares the indoor hygrothermal comfort based on the indoor air temperature and RH.

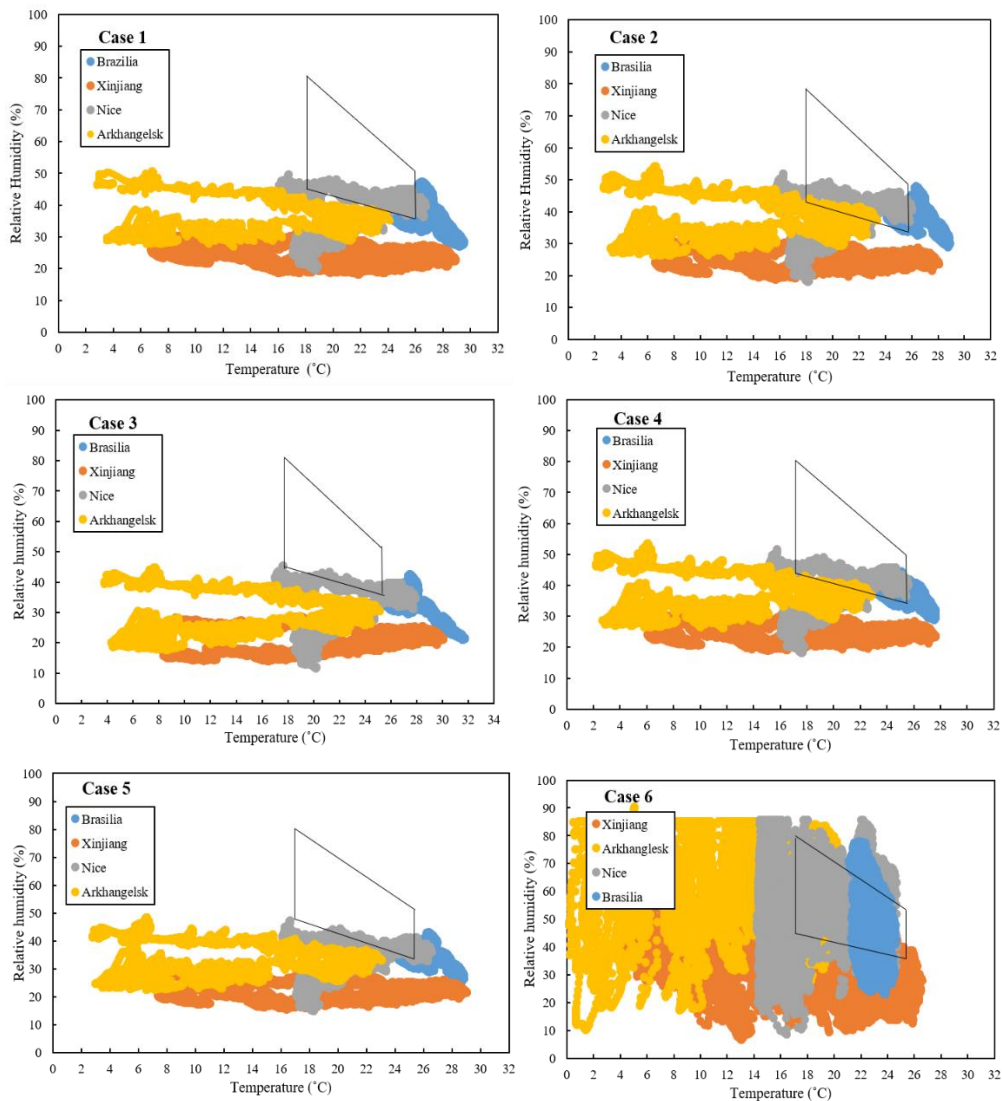


Figure 11.15: Hygrothermal indoor comfort of the six cases under Brasilia, Xinjiang, Nice, and Arkhangelsk weather

Chapter 11. Numerical study of thermal and energetic performance of straw buildings

The conventional wall ensures hygrothermal comfort 80% of the time in Brasilia, 5 % in Xinjiang, 45% in Nice, and 11% in Arkhangelsk. For all straw wall cases, indoor comfort is not ensured under the Chinese weather due to the high outdoor RH of 85 % during winter with an average temperature of -10 °C and low RH of 40 % during summer with an average temperature of 25 °C. The low temperature during winter causes low indoor air temperature showing the inefficiency of the walls' thermal resistance, while the low RH during summer causes a low indoor air RH. These problems can be solved by adding internal sources of humidity such as plants [234]. For the Russian weather, hygrothermal indoor comfort is ensured 18 % of the time in case 1, 22 % in case 2, 4 % in case 3, 20 % in case 4, and 7 % in case 5. The problem is related to the low indoor temperature and RH values over the year. It should be noted that almost all cases exceed ASH limits which indicates high RH in the walls. This can be explained by the interior layers that prevent humidity diffusion toward the inside. For the Brazilian weather, hygrothermal indoor comfort is ensured 26 % of the time in case 1, 28 % in case 2, 1 % in case 3, 44 % in case 4, and 6 % in case 5. This type of envelope under high outdoor temperatures causes overheating as found in cases 3 and 5. In addition, the indoor RH is found to be low due to the interior layers. For the French weather, hygrothermal indoor comfort is ensured 48 % of the time in case 1, 59 % in case 2, 25 % in case 3, 55 % in case 4, and 40 % in case 5. The lowest comfort time of case 3 is due to the low indoor RH between February and August. The comparison of the straw buildings and the conventional buildings shows that straw constructions are not suitable for hot weather like that of Brasilia. In addition, straw building improved on average by 10 % the indoor hygrothermal comfort in cold weather like that of Arkhangelsk, Russia.

11.5.3. Energy consumption

The simulation results of the net energy requirement necessary for comfort are presented in **Figure 11.16**. Two cases can be distinguished according to the simulated climate. For a tropical (Aw) climate, the share of cooling demand is predominant between September and February. During the other months, indoor comfort is ensured without an HVAC system. For subarctic (Dfc), mediterranean (Csa), and arid (BWk) climates, the share of heating demand is predominant during the winter period of each country.

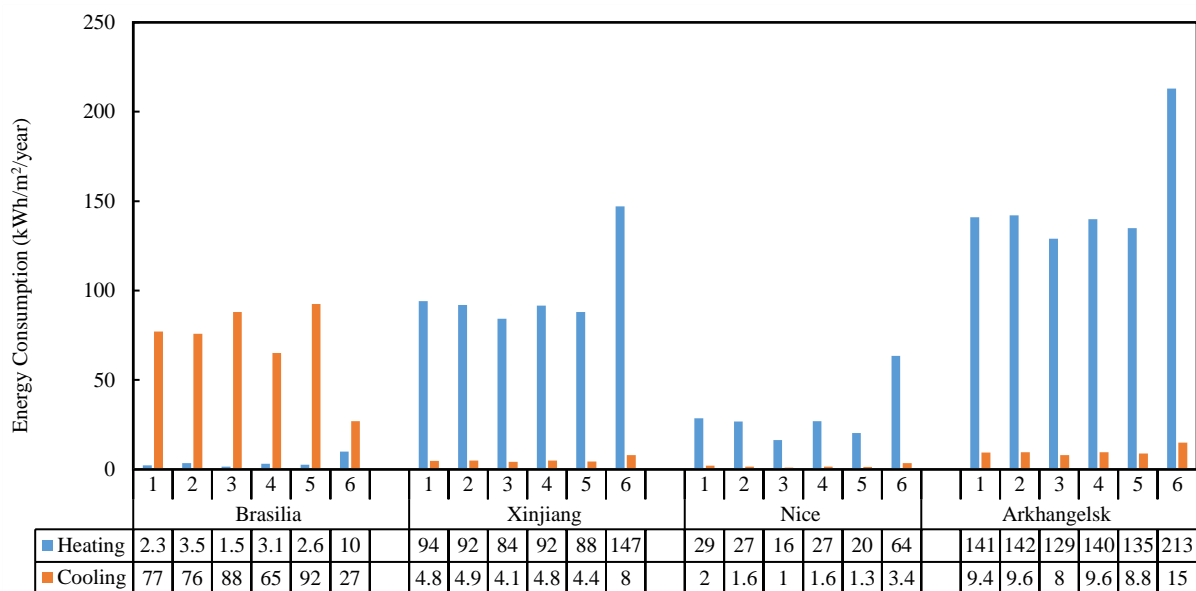


Figure 11.16: Simulation results of the annual heating and cooling energy consumption for all cases based on the weather and the wall composition

All straw cases have a low heating demand of 1.5 to 3.5 kWh/m² and high cooling demand of 65 to 92 kWh/m² in Brazilian weather. Case 3 has the lowest heating demand, which is 85 % lower than Case 6. Case 4 has the lowest cooling demand, which is 58 % higher than Case 6. In China, all straw cases have a low cooling demand of 4.1 to 4.9 kWh/m² and high heating demand of 84 to 94 kWh/m². Case 3 has

Chapter 11. Numerical study of thermal and energetic performance of straw buildings

the lowest heating and cooling demand, which is 42 % and 48 % less than case 6. Due to its low thermal resistance, Case 1 has the highest heating demand of the straw cases. In the French climate, all straw cases have a low cooling demand of 1 to 2 kWh/m² and low heating demand of 16 to 29 kWh/m². Case 3 has the lowest heating and cooling demand, which is 75 % and 70 % less than case 6. All straw cases have a low cooling demand of 8 to 9.6 kWh/m² and high heating demand of 129 to 142 kWh/m² in Russian weather. Similar to previous weather, case 3 has the lowest heating and cooling demand, which is 39 % and 46 % lower than case 6. The comparison of the straw buildings with the brick building shows an improvement in all weather except in Brasilia where the cooling load increases by 30 % for straw buildings. This can be explained by the high thermal resistance of straw walls which is suitable in cold weather and the lower thermal resistance of the insulated brick wall which suits hot weather.

The aim of this study was to associate each climate with the optimum wall composition from an energetic and hygrothermal point of view based on indoor temperature and relative humidity. It was noticed through the results that straw walls are good insulators and can decrease the heating demand by more than 30 % compared with conventional walls. Mainly the indoor comfort issues occurred in the cold and humid weather. The first, second, and fourth cases have similar behavior and can be used in Csa and Aw climates such as Nice and Brasilia. The third and fifth cases show higher thermal resistance and can be used in BWk climates such as Xinjiang and Dfc climates such as Arkhangelsk. Although to avoid hygric issues in the walls, case 3 should be only used in BWk climates.

12. Environmental and economic study

In this chapter, the environmental and economic aspects are each assessed separately for the test building and the case studies already defined in chapter 9. Environmentally, the carbon emissions are calculated according to the materials quantity and their carbon emission factor. Economically, the life cycle cost and the payback period are calculated according to the materials, heating and cooling prices in each country. The objective of the study is to compare the calculated parameters in each case and to re-associate them to the appropriate weather while considering the results of chapter 9 and chapter 11. The results showed that, in all studied climates, the environmental performance of the building is improved by replacing standard materials such as brick and cement with bio materials such as straw and wood. From an economic point of view, straw buildings are not cost-effective at current energy and investment prices in Brazil (Aw) and Russia (Dfc).

Table of contents

12.1. Previous studies.....	155
12.2. Environmental assessment.....	155
12.2. Economic assessment.....	158

Chapter 12. Economic and environmental study

12.1. Previous studies

The investigation of the thermal and energy performance of the test building needs to be completed by an environmental and economic assessment. Previous Life Cycle Assessment (LCA) studies showed that straw is more environmentally friendly than conventional thermal insulating materials [235,236]. It was shown that bales extracted from extensively (without the use of advanced agricultural tools) cultivated pastures have an ecosystem quality impact higher by 20 times than that of bales from intensive crop production. This factor affects the LCA of the whole building. Yin *et al.* [236] found that the energy efficiency of buildings improved by applying straw walls in all Chinese climatic regions. Alcorn & Donn [110] compared the LCA of straw buildings with that of standard buildings and noticed a CO₂ emission reduction of 15 % and an annual energy consumption reduction of 11 %. Interestingly, the reduction in CO₂ emissions was almost the same as the total emission reduction from applying energy-minimizing technologies, excluding onsite renewable energy generation. Studies on the economic analysis based on life cycle costs and payback periods for straw buildings are found to be missing in the literature. Therefore, this chapter performs such analyses on the cases proposed in Chapter 9 (**Table 9.3** and **Table 9.4**), to compare the cases according to their environmental impact and economic cost. Each envelope is supposed to be incorporated into a building similar to the test building.

12.2. Environmental assessment

In France, new buildings are subjected to the RE2020 carbon indicator threshold which stresses the importance of an environmental assessment of straw buildings. The straw envelope fabrication, the transport, and the worksite cause CO₂ emissions (CE) that need to be calculated according to equation (12.1) used by Alcorn and Donn [110] and Syngros *et al.* [237] to predict the whole building's CO₂ emissions. To establish an assessment that is suitable for comparison, the functional unit of the building's carbon emission is taken as the equivalent of carbon emission per unit of building area (kg of CO₂/m²).

$$CE = \frac{\sum(\text{quantity} \times \text{CO}_2 \text{ emission factor})}{\text{Surface area}} \quad (12.1)$$

The carbon emissions of building materials are calculated by resources and energy input. The data in the project budget statement or final account statement is converted to obtain the quantity of the material used in the building. The carbon emissions due to material transportation are calculated based on the transportation distance and the energy consumption of the vehicle. The calculation differs between the cases, depending on the site location. The carbon emissions during construction mainly come from on-site mechanical equipment, including fuel equipment and electrical equipment. The calculation is the same for all climates. Despite the importance of the transportation and construction process emissions, they are not considered in this study, as Li *et al.* [238] found that they account for no more than 3 % of the total emissions.

Table 12.1 collects the materials' average CO₂ emission factor due to the production process, electricity, and natural gas demand. Electricity and natural gas CO₂ emission factors are multiplied by the heating and cooling demand already obtained in chapter 11, to calculate the annual heating and cooling emissions. Bio-based materials, as opposed to conventional construction materials, absorb CO₂ as they develop through photosynthesis and store it in the structure. Straw and wood absorb CO₂ and create stable compounds like cellulose, hemicellulose, and lignin that can store CO₂, minimizing the greenhouse impact. The carbon neutral coefficient (CNC) is calculated by equation (12.2) that evaluates the carbon reduction effect of wood-straw materials compared to the total carbon emissions due to their production (TCP) [239].

$$CNC = \frac{3.67 \cdot \sum m_{\text{CO}_2}}{TCP} \quad (12.2)$$

Chapter 12. Economic and environmental study

Table 12.1: CO₂ emission factor of the used construction materials, electricity, and natural gas

	Average CO ₂ emission factor
Straw bale [240]	50 kg of CO ₂ /tons
Cement [241]	1670 kg of CO ₂ /m ³
Timber [242]	159 kg of CO ₂ /m ³
Wood wool [243]	7.4 kg of CO ₂ /m ³
Plasterboard [244]	1.4 kg of CO ₂ /m ²
Brick [245]	30 kg of CO ₂ /m ²
Double glazing [246]	76 kg of CO ₂ /m ²
Electricity [247]	0.27 kg of CO ₂ /kWh
Natural gas [247]	0.2 kg of CO ₂ /kWh

Table 12.2 shows the total emissions obtained due to the materials production and the building operation using an HVAC system. Results show that case 6 (standard brick building) has the highest materials carbon emission at 253.51 kg of CO₂/m². The use of brick in case 6 causes 35 % of the total emissions. The second highest carbon emissions due to materials production are obtained in case 4 at 209.26 kg of CO₂/m². This case is highly affected by the exterior plaster emissions that account for 75 % of the total emissions. Case 2 has the lowest value at 111.85 kg of CO₂/m² due to the low emissions of wood and straw. Case 5 total emissions are similar to case 4 because of the use of exterior and interior plaster and the quantity of wood. Wood wool has a very low impact of 1 % on the total emissions in cases 5 and case 6. It is noticed that the cement layer is the main cause of increasing the total emission of straw buildings. In addition, comparing Case 2 to Case 6 shows that straw buildings can decrease carbon emissions by 44 % compared to standard brick buildings.

Table 12.2: Results showing the total CO₂ emission due to the materials production process, the carbon neutral coefficient, and the net carbon emissions of the building

Cases	Materials production emissions (kg of CO ₂ /m ²)	CNC	Net carbon emissions of the materials (kg of CO ₂ /m ²)
1	190.7	0.12	151.8
2	118.85	0.59	-124.6
3	158.56	0.22	61.5
4	209.26	0.27	34.6
5	207.37	0.25	35.2
6	253.51	0.005	248.5

Chapter 12. Economic and environmental study

Biomass materials such as straw bales, wood wool, and timber, have carbon sequestration effect, which reduces the total carbon emissions of the building. Wheat straw and wood contain 40 % and 50 % of carbon respectively [248,249]. The amount of stored CO₂ in the material is used to calculate the net carbon emissions by subtracting it from the materials' production emissions. The carbon storage of straw bales only is between 45.8 kg of CO₂/m² in case 3 and 36.7 kg of CO₂/m² in the other cases. The carbon storage of wood reaches 38.4 kg of CO₂/m² in case 1 and 243 kg of CO₂/m² in case 2. The wood cases have higher values because they include the quantity used for the structure of the whole building. Thus, the net embodied carbon emission calculated by the total emissions minus the stored carbon of biomass materials decreases by 20 % in case 1, 205 % in case 2, 61 % in case 3, 83 % in case 4, and case 5, and 2 % in case 6. The higher net carbon emissions value is then obtained in case 1 which includes the largest quantity of cement. The carbon storage of the cases affects directly the carbon reduction effect. To classify the cases according to the net carbon emissions caused by the materials, it is noticed that case 2 is the best while cases 4 and 5 come as the second-best compositions.

The CNC in case 6 is only 0.005 with only wood wool as a bio-material. The higher CNC is in case 2 at 0.59 because it is highly based on straw bales and wood. For cases 3, 4, and 5, the CNC is about 0.25 while for case 1 it is 0.12. Straw buildings' CNC values indicate that the building has a carbon neutrality effect depending on the covering materials and that straw reduces the carbon emissions per unit area of the building.

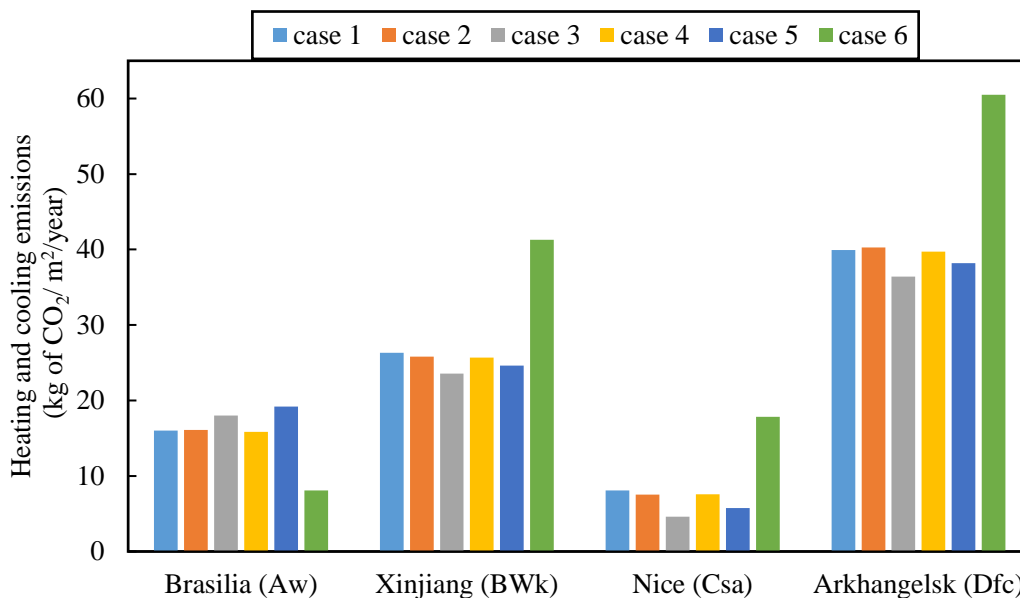


Figure 12.1: Heating and cooling annual CO₂ emissions of the studied cases

The previous results change when considering the carbon emissions caused by the heating and cooling of the building each year. This part depends on the climate region that indicates the building heating and cooling demand determined in chapter 11. **Figure 12.1** presents the annual emissions of each case due to the heating and cooling. The first two cases have similar annual emissions of about 16 kg of CO₂/m², 26 kg of CO₂/m², 8 kg of CO₂/m², and 40 kg of CO₂/m², respectively under the Brazilian, Chinese, French, and Russian weather. For tropical climate (Aw), case 6 has the lowest carbon emissions due to its lowest cooling demand per year. For cold desert climates (BWk), Mediterranean climate (Csa), and subarctic continental (Dfc), straw building cases have lower emissions than the brick case by an average of 36 %. It can be concluded that straw buildings are not environmentally efficient in tropical weather. In addition, cases 5 and 3 can be associated with subarctic and Mediterranean weather, respectively. Cases 1, 2, and 4 should be used in cold desert weather.

Chapter 12. Economic and environmental study

12.3. Economic assessment

In this section, the same methodology as that of Ibrahim *et al.* [250] and Souayfane *et al.* [251] is used to carry out the economic assessment of straw buildings. The life cycle cost (LCC) and the payback period (PP) are calculated according to equation (12.3) and equation (12.4), respectively.

$$LCC = IC + PWF \cdot EC \quad (12.3)$$

$$PP = \frac{IC}{ESC} \quad (12.4)$$

with IC the initial cost for implementing the considered wall (materials prices, installation, labor cost), EC the annual energy cost required to maintain the indoor comfort, calculated by equation (12.5), PWF the present worth factor calculated by equation (12.6), and ESC the annual savings on energy costs including the savings on lighting costs. It is calculated by comparing the annual total energy cost of straw cases to that of brick cases.

$$EC = \frac{Q_h}{\eta} \cdot C_g + \frac{Q_c}{COP} \cdot C_e \quad (12.5)$$

$$PWF = \frac{1 - (1 + r_d)^{-N_l}}{r_d} \quad (12.6)$$

where Q_h , Q_c , C_g , C_e , η , COP , r_d , and N_l respectively stand for the annual heating load, annual cooling load, natural gas cost, cost of electricity, heating system efficiency, coefficient of performance of the cooling system, discount rate, and lifetime. N is assumed to be 50 years.

The initial investment cost is calculated for the material and installation costs while the installation cost of the HVAC systems and other design costs were not considered since their values are assumed to be the same for all the cases. For the same reason, only the energy costs were considered annual costs. In each country different electricity costs, natural gas prices, and labor costs are considered as summarized in **Table 12.3**. The prices represent the final total cost including tax and grid costs. The prices of the used materials are summarized in **Table 12.4**.

Table 12.3: Gas price, electricity price, discount rate, and present worth factor in four countries

	Gas price (\$/kWh) [252]	Electricity price (\$/kWh) [253]	Discount rate (%) [254]	PWF
Brazil	0.189	0.198	13.2	7.56
China	0.1	0.079	3.7	22.6
Russia	0.009	0.078	9.5	10.4
France	0.099	0.184	0.05	49.3

Table 12.4: Materials average price

Material	Average prices
Wheat straw [255]	120 \$/ton

Chapter 12. Economic and environmental study

Concrete [256]	120 \$/m ³
Timber [257]	400 \$/m ³
Wood wool [258]	80 \$/m ³
Plasterboard [259]	18 \$/m ²
Double glazing [256]	400 \$/m ²
Brick [260]	250 \$/m ²

In most projects, labor costs represent approximately 25-35% of the total project costs [261]. The labor cost is estimated in each country between these two values (lower income countries have lower labor costs). Although the prices change according to the location, the material costs were assumed to be unvaried but later multiplied by the labor cost. The heating system is a natural gas boiler with an efficiency of 90 % and the COP of cooling systems is taken as 3.

The lighting price is accounted for within the total life-cycle cost, when the artificial lighting is needed, and when its value is significant compared to heating and cooling loads prices. The European Lighting Standard EN12464-1 [262], requires an illuminance of 200-500 lux depending on the working level in the zone. Using a LED lamp, the illuminance of 300-500 lux corresponds to a power of 3.333 W/m² - 5.555 W/m² respectively. Accordingly, the calculated total annual lighting load is 15 kWh/m²/year.

The life cycle cost is evaluated for all straw wall cases and the brick wall case, and the recommendation for each climate from an economic point of view will be discussed. **Table 12.5** shows the materials price for the six cases under four different climates. The straw buildings' total materials price is found to be lower than that of the standard buildings by about 45 %. Case 1 and case 5 have the prices of the lowest and highest materials, respectively, since in the first case the walls are composed of straw and cement with a wooden structure while in the fifth case hardwood boards are added, which increases the quantity of timber. The replacement of the cement plaster with wood boards in case 2 increases the total materials price by 34.6 % while in case 3, the replacement of cement plaster with wood boards on one side only increases the total price by 30 %. The added hardwood boards in case 4 increase the total price by 31.6 %.

Table 12.5: Materials total price of the studied cases

Cases	1	2	3	4	5	6
Materials total price (\$/m ²)	151.0	231.0	216.3	221.0	279.3	615.0

The annual energy cost depends highly on the electricity and natural gas prices of the considered country. Russia has the lowest energy prices which lead to the lowest energy cost despite the high heating and cooling demand calculated previously. The total energy cost of all cases is presented in **Figure 12.2**. The low heating and cooling demand in Nice gives low energy cost that is nevertheless higher than Russia by 51 % to 59 %, depending on the case. In Xinjiang, the cost is higher than in the French and Russian cases for two reasons, the annual heating demand and the kWh price. The cooling demand in Brazil increases the annual cooling cost by more than 70 % for straw buildings. Last, the brick building has an annual energy cost higher than the straw in all cases except the Brazilian case due to the cooling demand.

Chapter 12. Economic and environmental study

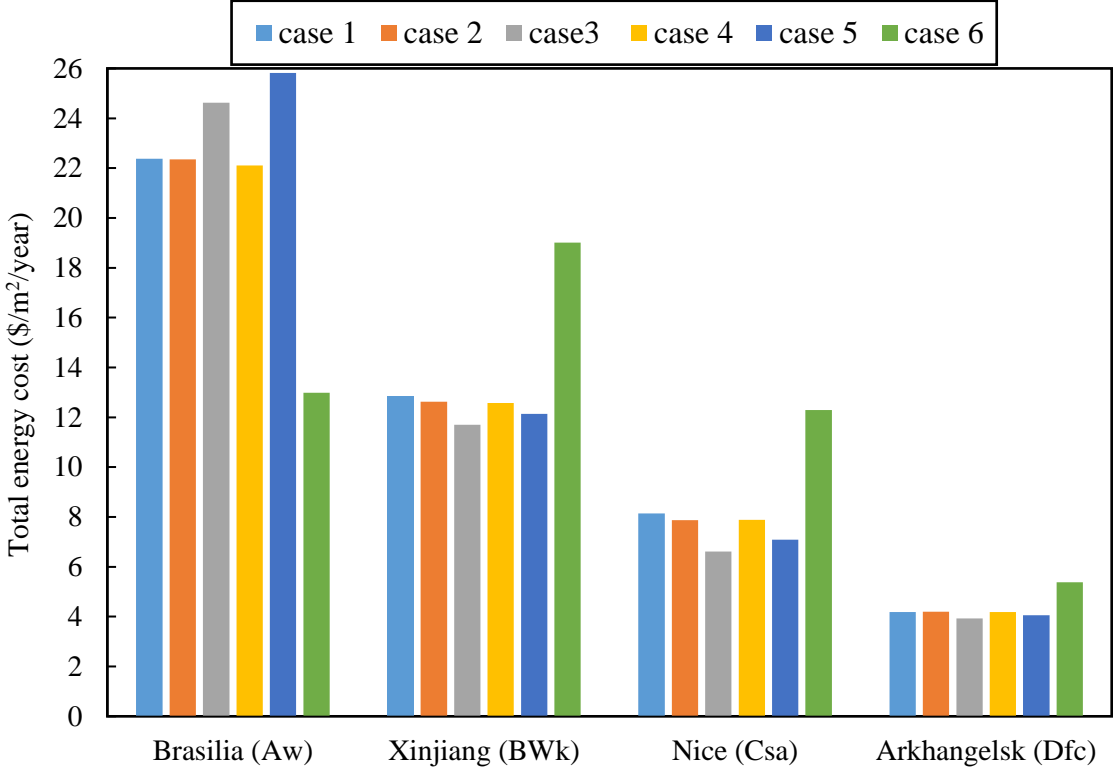


Figure 12.2: Total energy cost of the different cases

Figure 12.3 and **Figure 12.4** depict, respectively, the initial cost and life cycle cost of straw and brick buildings in the chosen countries. The initial cost of all wall types hardly varies with the countries, since it is affected by the materials' total price by 75 %, which is the same in all countries. However, each nation has a different life cycle cost that takes both the IC and EC into account. The energy cost affects the life cycle cost by 9 %, 38 %, 45 %, and 26 %, respectively in Russia, China, France, and Brazil. The used covering materials do not help in suppressing the heating demand of the buildings and increase the total materials price. Case 1 has the lowest LCC of 518.5 \$/m², 687.2 \$/m², 632 \$/m², and 396.4 \$/m², respectively, in Brazil, France, China, Russia. Case 5 has the higher straw building LCC, which is still lower than that of the brick building (case 6) by an average of 30 %. It is concluded that straw buildings save money in the initial cost in all countries and energy costs except in hot and tropical climates (Aw).

Chapter 12. Economic and environmental study

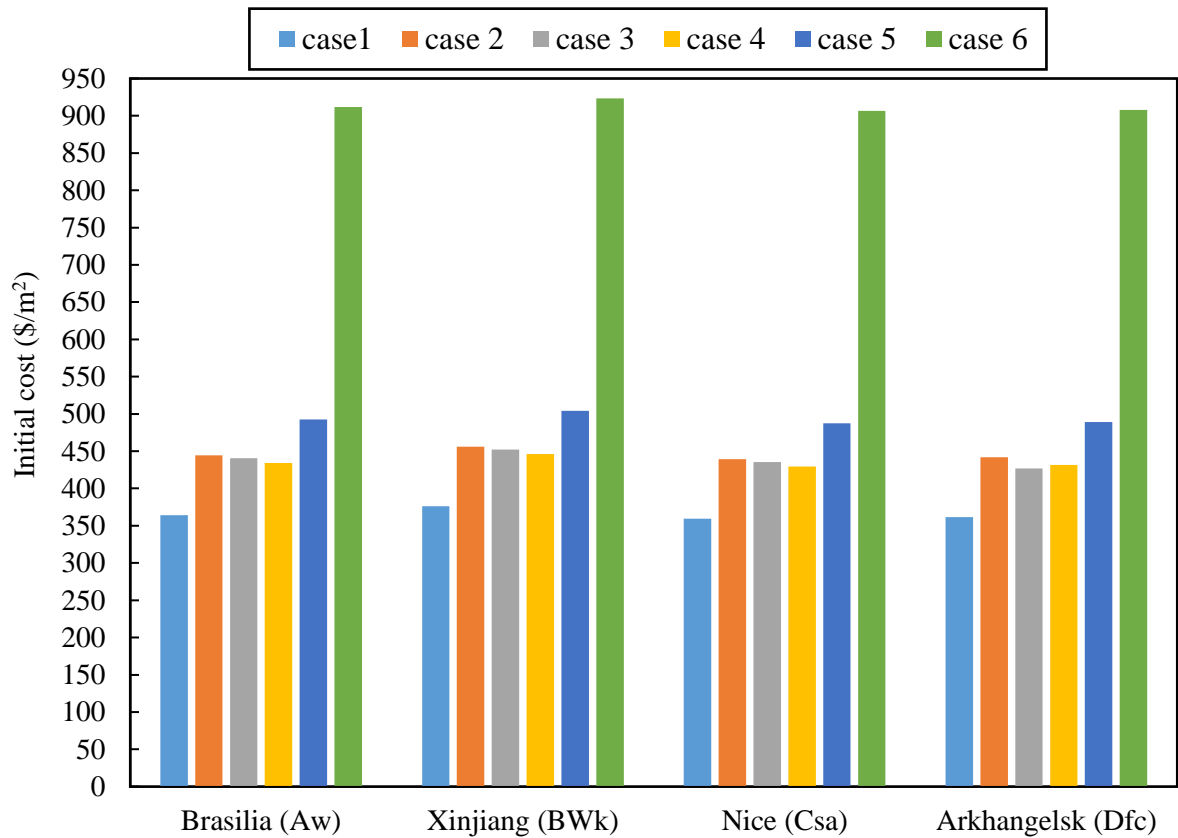


Figure 12.3: Initial cost of the studied cases

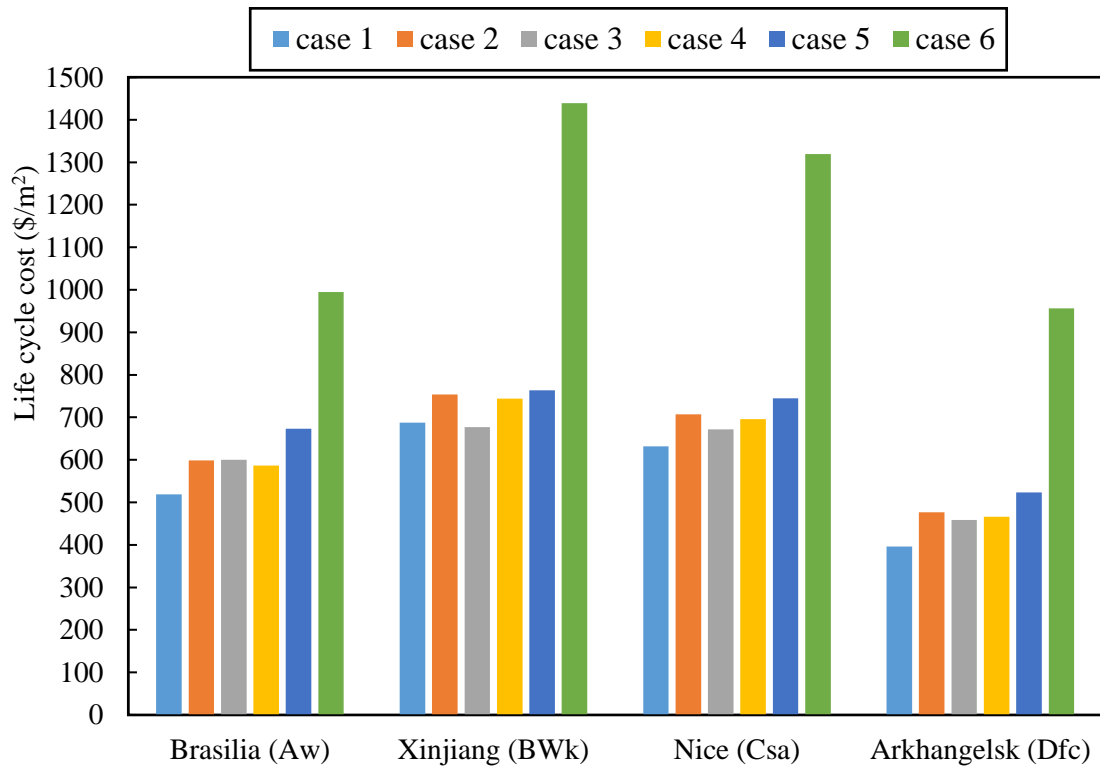


Figure 12.4: Life cycle cost of the studied cases

Chapter 12. Economic and environmental study

Table 12.6 summarizes the payback period of straw buildings by calculating the energy savings according to the energy consumption differences between brick and straw buildings. Results show that straw buildings need lots of years to pay back the initial cost. The average payback period is 47 years, 32 years, and 187 years, respectively in cold desertic, mediterranean, and subarctic weather. In tropical weather, the use of straw is not profitable as the payback period is negative which means in the five cases the energy consumption of brick buildings is lower than that of straw buildings.

Table 12.6: Payback period of straw buildings

cases	Payback period (year)			
	Brasilia	Xinjiang	Nice	Arkhangelsk
1	negative	45.4	29.1	168.9
2	negative	51.6	34.4	206.8
3	negative	39.8	29.8	161.9
4	negative	50.6	33.3	197.0
5	negative	48.5	35.5	201.4

In this chapter, the environmental and economic analysis of the application of different straw walls on a typical building envelope was investigated under different climates. The results showed that, in all studied climates, the environmental performance of the building is improved by replacing standard materials such as brick and cement with bio-materials such as straw and wood. From an economic point of view, straw buildings are not cost-effective at current energy and investment prices in Brazil (Aw) and Russia (Dfc). Thus, to associate each climate to the appropriate envelope at the lowest cost and moderate environmental impact, case 1 should be used in a tropical climate (Aw), case 2 in a cold desert climate (Bwk), case 3 in a mediterranean climate (Csa), and case 4 and 5 in subarctic continental climate (Dfc).

13. Straw building's mechanical performance

This chapter investigates the mechanical resistance of straw buildings confronted to seismic solicitations and hazardous loads. The study is numerical and done by using ROBOT structural analysis software. In the first section, the case study is described, which is the experimental building and the numerical model is detailed. The following section shows the loads applied on each element of the structure. The solicitations include snow, wind and seismic loads. As a result, the most stressed beams, panels, piles and braces are selected and compared to the stress that can be supported. Finally, the whole building deformation is studied according to the Eurocode 8.

Table of contents

13.1. Case study description.....	164
13.2. Numerical model of the structure.....	164
13.2.1 Geometry.....	165
13.2.2. Dead loads.....	166
13.2.3. Imposed loads.....	167
13.2.4. Climatic loads: snow and wind.....	168
13.2.5. Seismic acceleration.....	169
13.2.6. Loads combinations.....	170
13.2.7. Mesh.....	170
13.3. Results.....	171
13.3.1. Foundation resistance	171
13.3.2. Panels resistance.....	171
13.3.3. Seismic analysis.....	172

Chapter 13. Straw building mechanical performance

13.1. Case study description

The objective of this chapter is to study the mechanical behavior of wood-straw buildings located in regions of seismic and climatic hazards. The scientific literature still does not include such a study. Yet, this step is essential in any construction project in order to ensure the safety of future occupants and the durability of the house in the face of such extreme conditions. Thus, this study may introduce new questions concerning the use of straw buildings in geologically critical areas.

The studied building is constructed following the prefabricated technique used by the Industry partner Activ'home. The prefabricated walls are custom-assembled in the factory according to the plans of each house to correspond to the different openings and dimensions of the floors. The first step consists in assembling the various wooden parts which later form the wooden frame which will have to sustain all building specific and climatic loads. The second step consists of filling the wooden frames with straw with a high density using a press, to guarantee good thermal insulation and fire resistance. The filling of the wooden frames is automated with a press that can fill up to 30 m² of prefabricated panel per hour. The third step consists of transporting the prefabricated walls and floors and then assembling them on-site.

In this chapter, the modeled house is supposed located in the mountainous French region of Isola (06420), at an altitude of 1500 m. It is an area of average seismicity, with significant snow and wind loads. The building is intended for residential use with a living area of 120 m². The construction comprises two floors with a floor over a crawl space and a roof.

13.2. Numerical model of the structure

The structural analysis characterizes the influence of external loads such as permanent and climate loads on the various elements (sections, and frame assembly) that compose the entire structure. Several analysis tools can provide finite element modeling of cellular beams and plate design in 3D structures. The structural analysis requires the determination of structural loads, geometry, support conditions, and materials properties. The results of such a study include support reactions, stresses, and displacements that should respect certain criteria to avoid failure. The material mechanics' approach or strength of materials, the elasticity theory approach (used in the field of continuum mechanics), and the finite elements approach are the three main approaches to the analysis. The first two are analytical formulations that mostly use simple linear elastic models, resulting in closed-form solutions that can often be solved by hand. The finite element method is a numerical method for solving differential equations generated by mechanics theory. The finite-element method is heavily reliant on computer processing power and is better suited to structures of arbitrary size and complexity.

These analysis approaches are all tools in Building Information Modeling (BIM). BIM is a design concept that allows for complex data collection, processing, and analysis at each stage of the design process and helps avoid design collisions. It supports the exchange of information throughout the life cycle of a building, from conception to demolition, passing through feasibility studies, construction, operation, and maintenance. It applies to all of the actors and stakeholders in a construction project: architects, economists, research institutes, businesses, and so on.

In the construction industry, BIM tools are used in the early stages of design to exchange building information and to create sustainable designs. Basic models are created with appropriate BIM software and exported to BIM integrated software for various analyses. BIM contains a wealth of information on these models, allowing for efficient, cost-effective, and feasible building design. Automated construction systems are widely used in architecture, engineering, and construction, as well as in facilities management, to maximize the potential of building information models for sustainable and efficient building design.

Several researchers [263,264] studied BIM tools such as Robot structural analysis software, Lira SAPR software, and SCAD software. Robot structural analysis is chosen in this chapter since it allows to

Chapter 13. Straw building mechanical performance

achieve structural calculations by using finite element analysis while considering wind, snow, and seismic loads.

13.2.1. Geometry

The structure is modeled as described in **Figure 13.1**. For the foundations, the building rests on piles driven into the ground to avoid any contact of the wood-straw elements with the soil. In the numerical model, the foundation is taken as piles embedded at the base while assuming the slope of the soil as negligible. These piles are composed of 100 mm I-section beams shown in **Figure 13.2**.

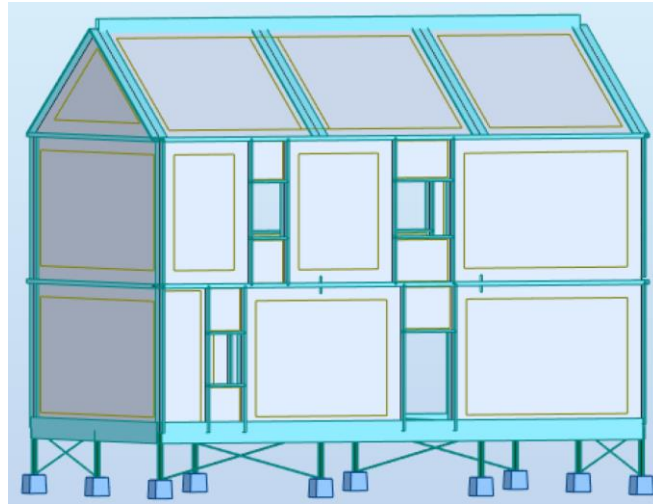


Figure 13.1: Straw-wood building modeled in RSA (Robot Structural Analysis) software

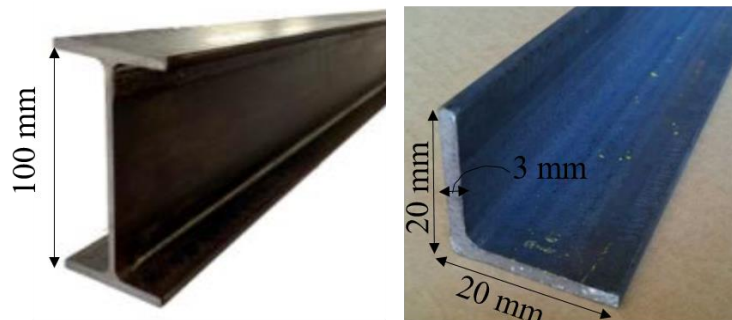


Figure 13.2: I-section steel beams (left) and angle steel (right) profiles

For better stability in case of horizontal forces such as wind or earthquakes, braced frames are added on each side of the piling building to block its displacement. These bracing frames, presented in **Figure 13.2**, are modeled as 20 mm x 3 mm S 235 equal angle steel (see Appendix A2). The piles and braces then take up the wood beams which constitute the base of the building as a wood box foundation. The foundation is then covered by the prefabricated wood-straw floor. The walls are placed on the peripheral wooden base that has a section of 16 cm x 45 cm. They are modeled on RSA software by a rectangular profile of glued laminated wood GL24h.

For the modeling of the floor, a new thickness is created in Robot which corresponds to a honeycomb floor with a stiffener in one direction represented in **Figure 13.3**. The dimensions are chosen based on the real case with h , $h1$, $h2$, $a1$, and $a2$ equal respectively to 42.5 cm, 4 cm, 2 cm, 47.5 cm, and 3.5 cm. The “Automatic direction” option in ROBOT allows automatically arranging the stiffeners in the right direction depending on whether it is a wall (Z direction) or a floor (X or Y direction).

Chapter 13. Straw building mechanical performance

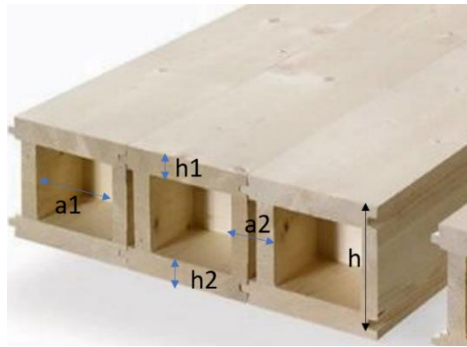


Figure 13.3: Honeycomb with stiffener panel dimension annotation

The upper and lower timber runners constituting the frame of the wall are not modeled in the same dimensions as the stringers. Thus, they are taken within a section of $36 \text{ cm} \times 9 \text{ cm}$. The used wood type is the glued-laminated timber of GL24 type, which has the characteristics described in Appendix A2. The straw bales are not considered a loadbearing material since they only offer an insulation role. Their presence affects only the weight of the building from a mechanical point of view. In the end, the roof is modeled with trusses made of wood-straw panels and purlins, identical to those used for the stringers.

In this section, the bracing forces taken up by the walls are calculated by using two methods recommended by Eurocode 5 concerning wood panel bracing inspection. The bracing forces in a wood frame panel are carried by the connecting elements of the plywood plate to the wood studs. In this study, the bracing panels are assembled to the uprights by means of staples. Under these conditions, the assembly's resistance should be tested in accordance with Eurocode 5.

The panels composing the walls are made of a 10 mm thick plate on one side and a 40 mm thick plate on the other. For the 10 mm thick plates, the staples used in the assembly step have a length of 40 mm while for 40 mm thick plates, the staples have a length of 64 mm. These two types are studied by calculating their strength. Figure 13.4 presents the dimensions of the staples. All the dimensions are calculated in Appendix A3.

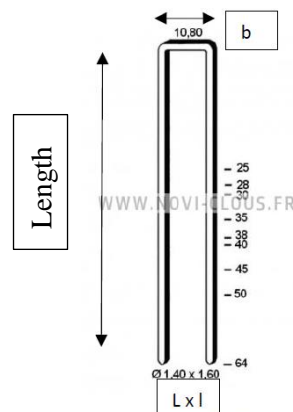


Figure 13.4: Staples dimension annotation [265]

The bracing of the walls parallel to wind loads is studied to check the structure's mechanical resistance to wind. The bracing resistance is calculated by equation (A3.1) and found to be 41 kN. This value is compared to the load exerted by the wind on the south wall which is about 15 kN. It can be deduced that the bracing resistance of the panels can largely support the forces related to the wind of the structure.

13.2.2. Dead loads

The density of straw bales is 120 kg/m^3 with a weight of 14 kg each. The whole prefabricated panel's dead weight is estimated at around 100 kg/m^2 . This weight is multiplied by the

Chapter 13. Straw building mechanical performance

acceleration of gravity to obtain a self-weight of about 0.98 kN/m². The linear load is then obtained by multiplying the self-weight by their height. **Figure 13.5** gives the applied dead loads with a surface load of 1kN/m² for each floor and a linear load of 3.10 kN/m for each wall. These loads are also applied to the roof space since its weight is not negligible.

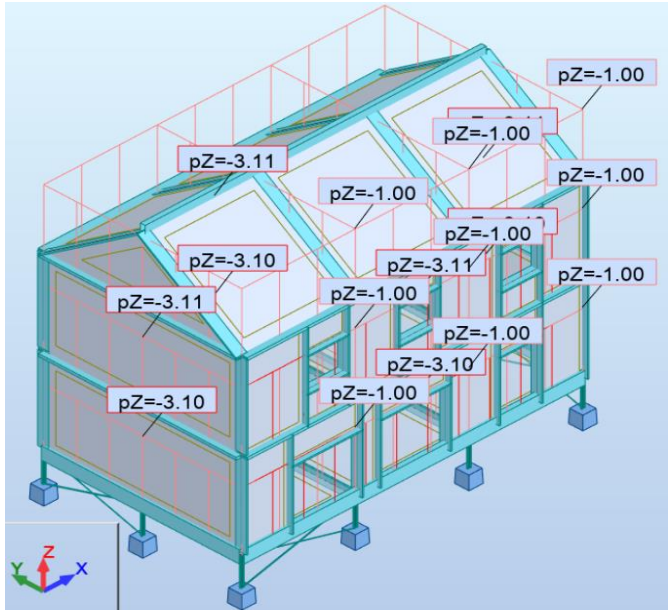


Figure 13.5: Surface and linear dead loads applied to the whole structure

13.2.3. Imposed loads

Eurocode 1 defines actions and provides guidelines for the structural design of buildings and civil engineering projects, including geotechnical considerations [266]. To categorize a structure, the considered elements include the weights of construction materials, stored materials, and the whole construction. Based on **Table 13.1**, the test building is rated in category A for housing and residential constructions that have a load between 1.5 and 2 kN/m² for floors.

Table 13.1: Eurocode 1 load categories for different areas [266]

Loaded area category		Surface Load [kN/m ²]	Load [kN]
A: Residential	Floors	1.5 to 2	2 to 3
	Stairs	2 to 4	2 to 4
	Balconies	2.5 to 4	2 to 3
B: Office		2 to 3	1.5 to 4.5
C: Meeting surface (except areas of categories A, B, and D)	C1: with tables	2 to 3	3 to 4
	C2: with fixed seats	3 to 4	2.5 to 4
	C3: with no obstacles to the movement of people	3 to 5	4 to 7
	C4: allowing physical activities	4.5 to 5	3.5 to 7
	C5: to accommodate large crowds	5 to 7.5	3.5 to 4.5
D: Commercial space	D1: regular commerce	4 to 5	3.5 to 4
	D2: department stores	4 to 5	3.5 to 7

The studied building has very little permanent storage space such as a library and is unlikely to accommodate a large number of people. For this reason, the applied surface load is taken as 1.5 kN/m² for each living floor of the building. These charges, shown in **Figure 13.6**, do not apply to the roof as it remains inaccessible.

Chapter 13. Straw building mechanical performance

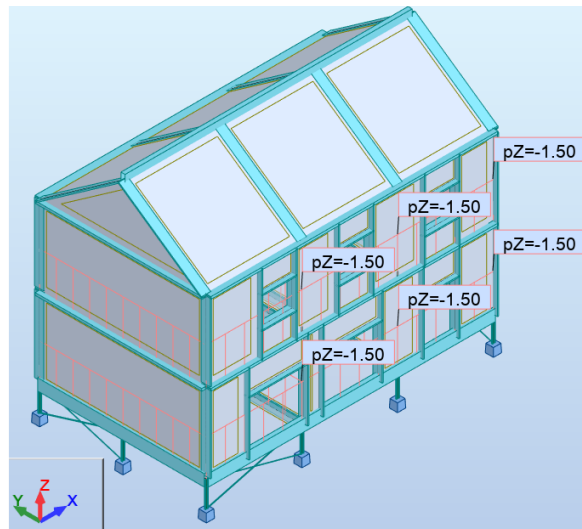


Figure 13.6: Imposed loads applied to the living spaces

13.2.4. Climatic loads: snow and wind

To estimate the building resistance while adding climatic loads such as snow and wind loads, the structure is supposed located in a mountainous region at an altitude of 1500 m. According to Part 3 of Eurocode 1, the location is ranked in the C1 category (appendix A4), which gives a characteristic snow load value of 0.65 kN/m^2 . This load should be adapted with a correction coefficient considering the altitude of the location. Thus, the final snow load is found about 3.45 kN/m^2 (calculated by equation A4.1). To study the worst-case scenario, it is assumed that the snow is prevented from sliding and that the exposure and thermal conditions of the roof are normal. Finally, the obtained case, shown in **Figure 13.7**, presents an unintentional situation with a load of 6.9 kN/m^2 obtained by multiplying 3.45 kN/m^2 by factors representing the considered situation.

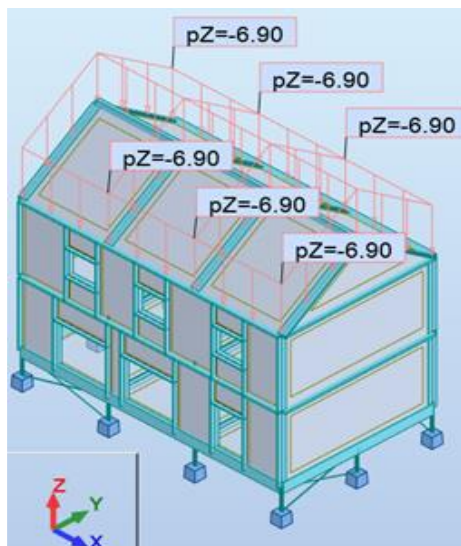


Figure 13.7: Snow load applied to the roof

Section 4 of Eurocode 1 deals with wind loads that may affect the structure during a year. Based on the location of the building (appendix A5), category IIIa determining a land case is chosen, since the building is assumed located in the countryside. The Eurocode imposes equations that consider the height of the structure, the wind average speed, the peak dynamic pressure, etc. The height of the building is 9.5 m. The wind orientation coefficient according to the French national appendix is 0.85, which corresponds to a south wind. However, to achieve a more unfavorable calculation, the Eurocode recommends a value of 1. The relative altitude between the construction and the natural ground is taken

Chapter 13. Straw building mechanical performance

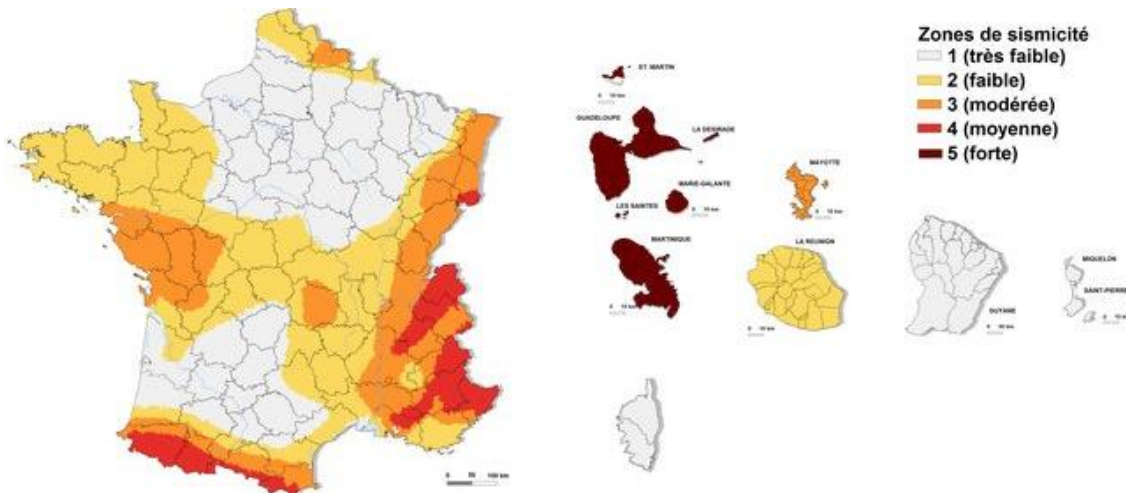


Figure 13.9: French seismic zonation map [268]

Table 13.2: Eurocode 8 requirements for different building types to resist the horizontal acceleration

	I: buildings without human activity	II: residential buildings	III: building with 3000 occupants
Zone 1	No requirements	No requirements	No requirements
Zone 2			0.7 m/s ²
Zone 3		1.1 m/s ²	1.1 m/s ²
Zone 4		1.6 m/s ²	1.6 m/s ²
Zone 5		3 m/s ²	3 m/s ²

13.2.6. Loads combinations

After having applied all the loads that the building may undergo, it is necessary to carry out combinations of these forces with different weightings defined in Eurocode 0. In this study, three combinations described in equation (13.1), equation (13.2), and equation (13.3) are chosen, the first two are for a durable and transient situation and the third one is for an accidental situation. In all three combinations, snow is the dominant parameter.

$$\text{Comb 1} = 1.35.DL + 1.5.SL + 0.9.WL + 1.05.IL \quad (13.1)$$

$$\text{Comb 2} = 1.35.DL + 1.5.W + 1.05.SL + 1.05.IL \quad (13.2)$$

$$\text{Comb 3} = DL + 0.5.IL + S_{acc} + 0.2.WL \quad (13.3)$$

where DL represents the dead loads, IL the imposed loads, SL the snow loads without multiplying it by coefficients representing the tested situation, WL the wind loads, and S_{acc} the accidental snow load after multiplying it by factors representing the tested situation.

13.2.7. Mesh

A simple mesh generation by Coons method [269] is selected to build a finite element mesh. Coons method is for 3D surface meshing, used for quadrilateral or triangular contours that can be divided into the same number of segments. For better reliability of element calculation, the used mesh is composed of equilateral triangles and squares with a side length of 1 m in order to cover all areas of the 3D model. To have the most regular possible mesh, the panels have been cut so that they are all rectangular as shown in **Figure 13.10**. Therefore, the mesh by finite elements is mainly of square type.

Chapter 13. Straw building mechanical performance

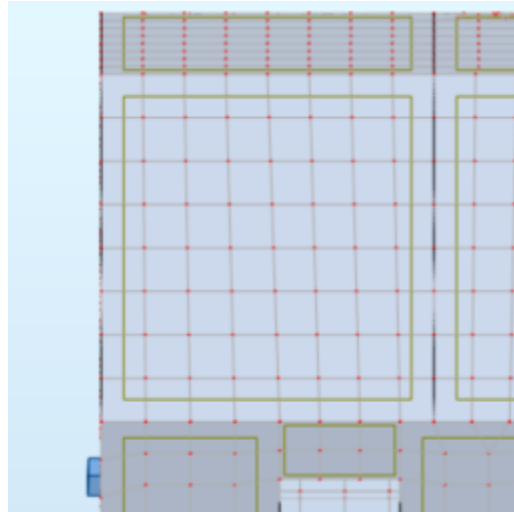


Figure 13.10: Mesh of the panels

13.3. Results

This section investigates the moments, shear forces, responses, and deflections after adding wind, snow, imposed, and dead loads to the test building. The results show the resistance of each element including the foundation and the walls. In the end, the structure behavior is presented after adding seismic horizontal load.

13.3.1. Foundation resistance

The bracing frames are found to be affected highly by horizontal forces such as wind. This ensures their important role in resisting lateral forces. The bracing frames that connect the piles diagonally work in tension in order to prevent the piles from collapsing. The maximum stress observed on a wind load case is only 10 MPa. This value is very small compared to the yield strength of the steel S235 (235 MPa), which indicates a good lateral force resistance. For the piles, the most affected case is obtained by applying the Comb 1 case with the snow loads as the dominant variable action. The maximum stress calculated for this load case is 146 MPa which can also be supported by the S 235 steel profiles. For the wood box, the maximum stress applied is 2.75 MPa obtained for the Comb 1 case. This value is verified for a GL24h glued laminated timber element that can support stress up to 19.2 MPa. The assumptions made for the bracing frames and the piles are therefore acceptable for the dimensioning of the building. They show the stability of the structure in the face of permanent and climatic stresses.

13.3.2. Panels resistance

To assess the panels' resistance, the Von Mises criterion is used since it accounts for traction, compression, and shear force components, to provide an isotropic level of shear force that is constant in all directions. To remain within the elastic range of the material, the equivalent constraint must be less than the plastic constraint. **Figure 13.11** represents the maps of the unfavorable cases to show the maximum stressed panels. It is noted that the maximum values of the stresses remain quite low compared to the resistance of the materials used for the construction. The I-beams which are elements of the panels made of GL24h glued laminated timber have a compressive and bending strength of 24 MPa. The test shows that the maximum applied stress is about 5 MPa which is smaller than the allowable stress. Therefore, it is considered that the combinations involving snow loads (Comb 1 and 3) do not threaten the structure.

Chapter 13. Straw building mechanical performance

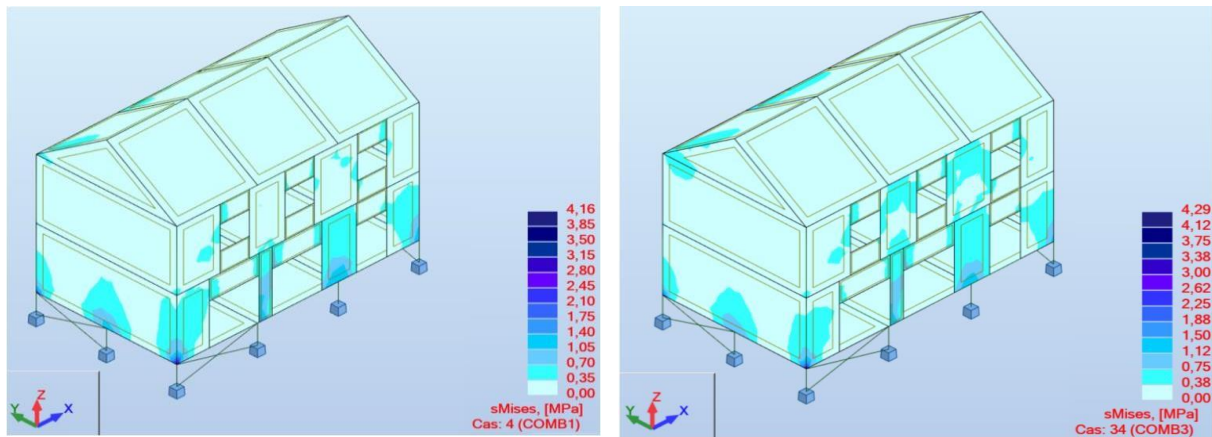


Figure 13.11: Panels stresses map based on Von Mises criterion for Comb 1 (left) and Comb 3 (Right)

13.3.3. Seismic analysis

The building is studied under a seismic load with a horizontal acceleration of 1.6 m/s^2 . The knowledge of the structure period is necessary to determine the elastic response spectrum defined as the peak response (displacement, velocity, or acceleration) of a series of oscillators that are forced into motion by the same base vibration. The elastic spectrum response for this case is presented in **Figure 13.12**. The numerical natural period of the modeled wood-straw building is 0.16 seconds. That period is between the lower limit of the period for the constant spectral acceleration branch (0.15 s) and the upper limit of the period for the constant spectral acceleration branch (0.4 s). Thus, the structure is considered rigid and capable of withstanding an earthquake with 1.6 m/s^2 horizontal acceleration.

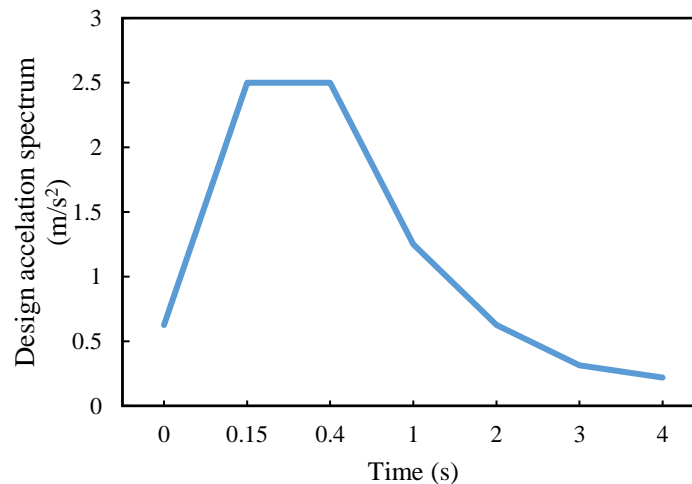


Figure 13.12: Recommended type 1 elastic spectrum response applicable for ground from type A

In the buildings sector, the design and construction of secure and safe buildings are the primary goals for stakeholders. The mechanical resistance of straw buildings is studied numerically under climatic loads and seismic acceleration. Results show that the test building of chapter 11 is able to support snow and wind load of 6.9 kN/m^2 and 0.65 kN/m^2 , respectively. In addition, the building resisted the applied horizontal seismic acceleration of 1.6 m/s^2 . Its natural period was lower than the upper limit period by more than four times which verifies the Eurocode criterion ($T_{\text{natural-period}} \leq 4 \times T_{\text{upper-limit}}$). Thus, it can be concluded that straw building is safe and can resist moderate earthquakes and severe climatic loads.

General conclusion and perspectives

The objectives of the thesis work were to provide scientific answers to the questions that still prevent the dissemination of straw bale buildings. Such questions are related to the indoor hygrothermal comfort, energy consumption, environmental benefit, profitability, and mechanical and fire resistance of straw buildings.

First, a multiscale (straw fiber-bale-wall-building) literature review is conducted from chapters 1 to 5 to define the gaps in the existing knowledge. Straw is an agricultural coproduct formed following grain harvesting of various varieties of wheat, barley, oats, and others. In many applications, natural organic fibers are becoming viable alternatives to synthetic fibers. As shown by the review, few studies had been done on the characterization of such material. The experiments described in chapter 6 respond to this lack. The experimental study includes the microstructure characterization, the measurement of the moisture buffer value, the water vapor permeability, the adsorption/desorption curves, the thermal conductivity, and the specific heat capacity.

Chapter 7 deals with heat transfer in straw bales. The literature includes a limited number of models as only one study was found for straw bales. Natural fibers have good thermal properties because they contain cellulose and have a low environmental impact due to their limited gray energy and greenhouse gas emissions. In the building construction application, natural composites may be used for their thermal insulation characteristics, which depend on several factors such as T, RH, and others. For this reason, this chapter provides a mathematical equation that predicts the effective thermal conductivity of straw bales as a function of temperature, relative humidity, cellulose and lignin content, fibers' orientation, and density. The model is built from the microstructure characterization and validated through the experimental measurements of the thermal conductivity carried out in the previous chapter.

Chapter 8 deals with the fire resistance of a new type of straw wall proposed by Activ'home, the industrial partner of this thesis. A mineral foam layer is added to the interior side in a way to protect the straw-wood structure that is already covered by fermacell boards on both sides. The experiment is done by using a 1 m³ furnace equipped with thermometers and reproducing the ISO-834 fire curve. The goal of the study is to test a 180 min resistance to fire. Then, a numerical model is designed using ABAQUS software. The model is validated using experimental data.

Despite the promising characteristics of the straw material, it may include moisture and condensation risks leading to health, stability, and durability problems. Interior and exterior temperature and humidity, driving rains, ground moisture, and leakage can all generate moisture in the straw walls. For this reason, chapter 9 studies numerically the hygrothermal behavior of various multilayered straw wall compositions by using WUFI software. The validation of the model is done by the comparison of the data to results found in the literature. This study associates each climate with the optimum wall composition from a hygric and thermal point of view.

Chapter 10 begins the investigation at the building scale. Straw bales are used to build an experimental building following the prefabricated method. The executor of the building is the industrial partner. The goal is to assess the indoor comfort of the straw building during summer and winter. In addition, this chapter helps in validating the already obtained characteristics of straw walls.

Chapter 11 examines the thermal and energy consumption of straw buildings under different climate conditions and wall compositions. To that end, an EnergyPlus model is built and validated using the experimental data of the previous chapter. The model is then used to associate each climate and the appropriate wall composition from the viewpoints of hygrothermal comfort of energy consumption. In addition, the chapter investigates the sensitivity of the indoor air temperature and RH to variations in the density, thermal conductivity, initial moisture content, and sorption isotherms of the straw material.

Chapter 12 is about the economic and environmental assessment of the different straw buildings under different weather. The environmental assessment is based on the calculation of the carbon emissions of each case. The calculation includes the materials' net carbon emissions and the emissions generated by the heating and cooling loads of each case. Economically, the life cycle cost and the payback period are calculated according to the materials, heating, and cooling prices in each country.

Chapter 13 investigates the mechanical resistance of straw buildings. The objective here is to study the mechanical behavior of the experimental building in the face of seismic and climatic hazards. The work is done numerically by using a Robot software structural analysis model. This step is essential before any construction in order to ensure the safety of future occupants and the durability of the house in the face of extreme conditions.

Results and perspectives

1- Material scale

Main contributions:

The microstructure and chemical composition of each part of a straw fiber, such as the nodes and the internodes, affect the heat transfer in the whole material. The microscope images of wheat straw show that the pores' diameter varies randomly from 5 μm to 45 μm and the external surface (epidermis) thickness is about 100 μm . The studied straw material showed an average thermal conductivity of about 0.07 W/m.K. This parameter is found to be dependent on the chemical composition, temperature, relative humidity, density, and the fibers' orientation relative to the heat flux. Among all the tested parameters, the one most affecting the bale's effective conductivity is the fiber orientation. The minimum value was found about 0.048 W/m.K for perpendicular fibers at 15 °C and 15 % RH for wheat bales having a density of about 80 kg/m³. The maximum was about 0.12 W/m.K for parallel fibers at 55 °C and 95 % for wheat bales having a density of about 120 kg/m³. The thermal conductivity of bales having perpendicular fibers is about 16 % lower than that of bales having parallel fibers. Straw bale's effective conductivity was found to increase with temperature. At 25 % RH, the measured thermal conductivity of a bale of density 120 kg/m³ with perpendicular fibers varied from 0.061 W/m.K to 0.076 W/m.K for a temperature variation from 15 °C to 55 °C. Straw bale effective conductivity increases also with the RH. At 25 °C, the measured thermal conductivity of a bale of density 120 kg/m³ with perpendicular fibers varied from 0.063 W/m.K to 0.078 W/m.K for an RH variation from 15 % to 95 %. In addition, the straw bale's effective conductivity increases with density. At 25 °C and 15 % RH, the measured thermal conductivity of a bale with perpendicular fibers varied from 0.052 W/m.K to 0.066 W/m.K for a density variation from 80 kg/m³ to 120 kg/m³. These trends are also obtained in parallel by the proposed numerical model that predicts the effective thermal conductivity by considering the fibers' orientation, volume fraction and cellulose content, bale density, temperature, and RH. The model shows that the gas conduction in the bale and the radiation component decrease linearly with density, while the solid conduction increases exponentially.

The hygric characterization results show that the moisture buffer value and water diffusion resistance factor of an 83 kg/m³ straw bale are 3.07 g/(m².%RH) and 1.58 respectively. The sorption curve of straw fibers in a 120 kg/m³ density bale corresponds to an IUPAC - II H3 pattern, which means a macroporous material. The obtained values show that the material can exchange humidity and gas to regulate the indoor RH and maintain hygrothermal comfort.

Limitations and perspectives:

The material characterization study was limited to samples having small dimensions based on the tests' requirements. The results may have slightly varied if a whole bale was tested. In addition, the mathematical model of thermal conductivity was limited to lignin, cellulose, and moisture. Other chemical components that may affect the thermal conductivity were not considered. To complete the study, future work may include a comparison of different types of straws such as rice, oat, and barley.

This comparison would help standardize the properties of each type. The proposed numerical model allows the assessment of optimal thermal conductivity based on the main affecting factors. Such a study helps reach a compromise between the fibers' chemical composition, density, RH, and orientation. Future numerical models may include the effect of fiber's length and of cracks that may occur in the solid component. The same work might be repeated to obtain a model of the effective specific heat and sorption hysteresis formulation for straw materials, based on their microstructure and as a function of their density, temperature, humidity, fibers orientation, etc. These models are important in estimating the thermal and hygric characteristics of a specific type of straw bale under specific conditions, without having to carry out tedious and long experimental tasks. In the end, such models will increase the accuracy of the thermal and energy simulation of constructions including this type of materials in their envelope.

2- Wall scale

Main contributions:

The tested wall had the ability to resist the fire for 180 min without recording cracks or defects on the unexposed surfaces. During the experiment, smoking indications appeared between mineral foam and the fermacell panel due to the fire seal paste's wrong application. These indications determine an EI 180 classification for the whole envelope. In light of these findings, an Abaqus numerical model is proposed to reproduce the real case and test the model without adding fire seal paste. The new proposition prevents fire propagation in the straw bales and improves the previous results.

In terms of condensation risk and mold growth, it is found that straw walls with cement or wood covering best fit in tropical and temperate climates, coated straw walls with additional air layers in dry climates, and insulated straw walls are recommended in continental climates. The simulated results show that the first and fourth investigated wall structures (cases) present mold growth and composting risks for the subarctic continental climate only. Both dryness rate and mold growth problems can be avoided by adding a vapor retarder layer or by increasing the straw thickness. The composting risk can be prevented by adding an exterior ventilated rain screen and a lime layer on both sides of the straw wall. In the third case, under all the climates except Arkhangelsk-Russia, the total water content is stable and the RH is lower than 80 % over four years, thanks to the air layer on the interior side and the high thickness of the straw. These results are different for the 3-R case because of the interior insulation and the low interior surface temperature. The interior layers in 4-R, 4-C, 3-C and 5-R cases lead the interior surface temperature to decrease, thus reducing the drying capability of the building envelope. The thermal inertia was assessed by comparing the time lag and the decrement factor of each wall. The time lag of the first two cases was 6 hours and 30 minutes while for cases three and four, it was 7 hours. The last case having in its structure multiple wood layers, a wood wool layer, and a straw layer, had the highest time lag of about 8 hours and 30 minutes. All cases show a low decrement factor varying between 0.05 and 0.07. Such results show that walls with the highest thickness and lowest thermal diffusivity feature higher time lags and lower decrement factors. Therefore, to prevent problems, the first, second and fourth wall configurations have similar behavior and can be used in temperate-Mediterranean (Csa) and savanna (Aw) climates such as Nice and Brazilia. The third case shows good thermal properties and can be used in cold desert climates (BWk) such as Xinjiang. The last case did not present hygrothermal and mold growth problems in all climates with normal indoor conditions and can be everywhere, including in subarctic continental climates (Dfc) such as Arkhangelsk. The presence of the wood wool as exterior insulation and the interior air layer in case five prevent hygric issues. For this reason, it has better performance under all conditions.

Limitations and perspectives:

The glue used during the fire resistance test was rated EI 180 meaning a fire resistance time higher than 180 minutes. However, experiments showed the destruction of the glue. Therefore, new experiments should investigate the already tested wall by ensuring a correct application of the glue. The Abaqus numerical model considered a constant external convection coefficient as recommended by Eurocode 8. More accurate models may consider variable coefficients based on the temperature difference between the external surface and the surrounding air. Additional fire resistance testing that will take into account the type of straw, its chemical composition, the density of straw bales, the composition and design of various kits made of straw bales, and even extensive tests that are not just performed on individual building elements but also on entire structures to assess the effects of other building elements to fire. A full study should be done to examine the driving rain effect on the hygrothermal property of the five chosen straw walls. It will be interesting to vary the thickness of straw bales in the wall in order to choose the optimal thickness according to its hygrothermal properties. Straw should be also studied as an exterior insulation material for standard walls under different climates to show the effect of straw on the wall temperature and relative humidity. Mechanically, straw walls need to be tested to measure their tensile and shear capacities.

3- Building scale

Main contributions:

The study at the straw bale scale underlined a variety of properties that can affect the building's thermal and mechanical performance. As a result, experimental work is done on a wood straw building in Reugny, France, by measuring the temperature and relative humidity in indoor and outdoor environments and walls. It is noticed that the indoor air temperature is higher than the outdoor by about 25 % and that the indoor air RH is lower by 42 %. The internal and external surface temperature also differs by 5 °C and the RH by 10 % all over the year. The indoor temperature and RH are inside Fauconnier's hygrothermal comfort zone 54 % of the time without the need for an HVAC system, and the thermal comfort index is 2 °C during summer and 6 °C during winter. The measured time lag and decrement factor for the building walls are 9 hours and 0.16, respectively.

Using the EnergyPlus model, the calculation of the Sobol sensitivity index shows that the indoor air temperature is mostly influenced by the straw layer's thermal conductivity, while the indoor RH mostly depends on the straw's sorption isotherm. Concerning indoor thermal comfort, in tropical climates (Aw) climates, case 3 has the worst indoor operational temperature, which only adheres to the ASHRAE limits for 20 % of the time. Case 4 has the lowest indoor operative temperature in cold desert BWk, Mediterranean (Csa), and subarctic continental climates (Dfc), which adheres to the limits for 37 %, 51 %, and 18 % of the time, respectively. The main problem occurs during the cold period for almost all cases. All straw cases do not ensure the hygrothermal comfort in cold desert climate (Bwk) due to the high outdoor RH of 85 % with an average temperature of -10 °C during winter, and low RH of 40 % with an average temperature of 25 °C during summer. In subarctic continental climates (Dfc), case 3 records the worst results with a 4 % of indoor hygrothermal comfort. The other cases ensure comfort by an average of only 19 % of the time. The problem is related to the low indoor temperature and RH values over the year. In tropical climates (Aw) climates, hygrothermal indoor comfort is ensured 1 % of the time in case 3. This type of envelope causes overheating under high outdoor temperatures. In the Mediterranean climates (Csa), the lowest comfort time of case 3 with a percentage of 25 % is due to the low indoor RH between February and August. The comparison of the straw buildings and the conventional buildings shows that the investigated straw constructions are not suitable for hot weather. In addition, straw building improved on average by 10 % the indoor hygrothermal comfort in cold weather. The energy study proves that straw walls are good insulators and can decrease the heating demand by more than 30 %, depending on the wall configuration. The straw wall composition type does not affect the heating and cooling loads, while the exterior conditions affect highly energy consumption. In addition, it is noticed that wood-straw buildings are not recommended in tropical Aw climates since

they increase the cooling demand which makes cost savings impossible, compared to standard buildings. The net carbon emissions of straw buildings vary from -124.6 kg of CO₂ to 151.8 kg of CO₂ per habitable surface area depending on the covering materials. Cement plasters increase the building's net carbon emissions while the use of wood decreases the emissions due to its carbon sequestration effect. Materials needed to build straw buildings are cheaper than for standard brick buildings by more than 30 %. The energy costs to meet the heating and cooling loads affect the life cycle cost by 26 %, 45 %, 38 %, and 9 %, respectively, in Brazil (Aw), France (Csa), China (Bwk), and Russia (Dfc). To conclude, straw buildings using case 1 wall configuration are suggested in tropical climates (Aw), but with modifications that could reduce the cooling demand, case 2 in cold desert climates (Bwk), case 3 in Mediterranean climates (Csa), while cases 4 and 5 are suggested in subarctic continental climates (Dfc). Regarding the mechanical stability of that modeled straw, the building withstood a horizontal seismic acceleration of 1.6 m/s², a wind load of 0.65 m/s, and a snow load of 6.9 kN/m².

Limitations and perspectives:

The current sensitivity analysis considers the effect of each parameter, taken separately, on the indoor temperature and T and RH. Future studies should consider the cross influence of the parameters as, for example, the bales' density affects their thermal conductivity. The numerical study focused on the effect of the exterior climate on indoor comfort in a residential building. However, it would be interesting to study the same cases under different indoor scenarios and for different building types. The indoor comfort of standard buildings maybe studied by adding straw as exterior insulation or by varying the thickness of straw as a solution in some climates such as tropical weather. Such cases should be completed by calculating the energy cost savings after insulating the building and determining the payback period. Mechanically, the building should be tested at different locations that may include additional loads such as vertical seismic acceleration. Similarly, the three main straw building construction methods have not been fully investigated in terms of their inherent benefits and limitations from the hygrothermal and mechanical perspectives. For example, it is still unclear which, among the load-bearing, infill, and prefabricated method, delivers the highest thermal comfort, energy savings, and seismic resistance depending on the building location and its scenarios of occupation and operation. Regarding the environmental assessment, in the case of the wide dissemination of straw bale construction, more work will have to be devoted to the impact of heavy trucks shipping straw material or prefabricated straw walls close to the building sites. In this regard, the use of train or ship transport might be an environmentally friendly alternative. Last, the thermal impact of straw buildings on the urban micro climate might be examined using adapted experimental and numerical tools.

Reference

- [1] Énergie dans les bâtiments - Ministère de la transition écologique et solidaire, (2017). <https://www.ecologique-solidaire.gouv.fr/energie-dans-batiments>.
- [2] M.J. González, J. García Navarro, Assessment of the decrease of CO₂ emissions in the construction field through the selection of materials: Practical case study of three houses of low environmental impact, *Build. Environ.* 41 (2006) 902–909. <https://doi.org/10.1016/j.buildenv.2005.04.006>.
- [3] L. Arnaud, C. La Rosa, F. Sallet, Mechanical behaviour of straw construction following the GREB technique, in: *Non-Conventional Mater. Technol. (NOCMAT)*, ResearchGate, Bath, UK, 2009: pp. 1–8.
- [4] D. Sietske Boschma, I. Kees, W. Kwant, Rice and wheat straw Potential feedstocks for the Biobased Economy, Netherland, 2013. www.wageningenur.nl/fbr.
- [5] B. Kretschmer, B. Allen, K. Hart, Mobilising cereal straw in the EU to feed advanced biofuel, London Office, 2012. <http://enrd.ec.europa.eu/pictures/rdp/F037A3EA-C0D0-7FC5-D02C-D29280D12CCF.JPG>.
- [6] Safer, France: The leading agricultural country in the EU, *Terres d'Europe*. (n.d.). <http://www.terresdeurope.net/en/france-agriculture-leading-country-europe.asp>.
- [7] M. Desriers, L'agriculture française depuis cinquante ans : des petites exploitations familiales aux droits à paiement unique, 2007th ed., *L'agriculture, nouveaux défis*, 2007. <http://agreste.agriculture.gouv.fr/IMG/pdf/AGRIFRA07c-2.pdf>.
- [8] R. Edwards, M. Šúri, T.A. Huld, J.F. Dallemand, GIS-based assessment of cereal straw energy resource in the European Union, *Biomass Energy, Ind. Clim. Prot.* (2005) 17–21. <https://doi.org/10.1108/QMR-06-2016-0055>.
- [9] Les agricultures régionales françaises, *Inst. Des Territ.* (2017). <https://institutdesterritoires.com/2017/09/04/les-agricultures-regionales-francaises/>.
- [10] SCM Lejeune, La construction en paille: construire en paille, construire l'avenir, *Reseau Fr. La Constr. Paille SCM Lejeune*. (2015). www.rfcp.fr.
- [11] RFCP, L'âge de paille, retour sur trois périodes marquantes de la construction paille., *Historique/RFCP*. (n.d.). <https://rfcp.fr/historique/>.
- [12] P. Walker, A. Thomson, D. Maskell, Straw bale construction, in: *Nonconv. Vernac. Constr. Mater.*, Elsevier, 2016: pp. 127–155. <https://doi.org/10.1016/b978-0-08-100038-0.00006-8>.
- [13] A. Mesa, A. Arengi, Hygrothermal behaviour of straw bale walls: experimental tests and numerical analyses, *Sustain. Build.* 4 (2019) 10. <https://doi.org/10.1051/sbuild/2019003>.
- [14] T. Ashour, H. Georg, W. Wu, Performance of straw bale wall: A case of study, *Energy Build.* 43 (2011) 1960–1967. <https://doi.org/10.1016/j.enbuild.2011.04.001>.
- [15] O. Douzane, G. Promis, J.M. Roucoult, A.D. Tran Le, T. Langlet, Hygrothermal performance of a straw bale building: In situ and laboratory investigations, *J. Build. Eng.* 8 (2016) 91–98. <https://doi.org/10.1016/j.jobbe.2016.10.002>.
- [16] M. Amin, B.A. Tayeh, I. saad Agwa, Investigating the mechanical and microstructure properties of fibre-reinforced lightweight concrete under elevated temperatures, *Case Stud. Constr. Mater.* 13 (2020). <https://doi.org/10.1016/J.CSCM.2020.E00459>.
- [17] I.S. Agwa, O.M. Omar, B.A. Tayeh, B.A. Abdelsalam, Effects of using rice straw and cotton stalk ashes on the properties of lightweight self-compacting concrete, *Constr. Build. Mater.* 235 (2020) 117541. <https://doi.org/10.1016/J.CONBUILDMAT.2019.117541>.
- [18] M. Saad, I.S. Agwa, B.A. Abdelsalam, M. Amin, Improving the brittle behavior of high strength

- concrete using banana and palm leaf sheath fibers, (2020). <https://doi.org/10.1080/15376494.2020.1780352>.
- [19] A.M. Heniegal, M.A. Ramadan, A. Naguib, I.S. Agwa, Study on properties of clay brick incorporating sludge of water treatment plant and agriculture waste, *Case Stud. Constr. Mater.* 13 (2020) e00397. <https://doi.org/10.1016/J.CSCM.2020.E00397>.
- [20] D. Chandramohan, & K. Marimuthu, A Review On Natural Fibers, *Int. J. Recent Res. Appl. Stud.* 8 (2011). www.arpapress.com/Volumes/Vol8Issue2/IJRRAS_8_2_09.pdf.
- [21] N. Doroudgarian, High Performance Bio-based Composites: Mechanical and Environmental Durability, *Universitat politecnica de Catalunya*, 2016.
- [22] A.K. Mohanty, M. Misra, L.T. Drzal, Sustainable Bio-Composites from renewable resources: Opportunities and challenges in the green materials world, *J. Polym. Environ.* 10 (2002) 19–26. <https://doi.org/10.1023/A:1021013921916>.
- [23] A. Laborel-Préneron, J.E. Aubert, C. Magniont, C. Tribout, A. Bertron, Plant aggregates and fibers in earth construction materials: A Review, *Constr. Build. Mater. J.* (2016) 719–734. <https://doi.org/10.1037//0033-2909.126.1.78>.
- [24] A. Laborel-préneron, J. Aubert, Characterization of Barley Straw, Hemp Shiv and Corn Cob as Resources for Bioaggregate Based Building Materials, *Waste and Biomass Valorization.* 9 (2018) 1095–1112. <https://doi.org/10.1007/s12649-017-9895-z>.
- [25] M. Bouasker, N. Belayachi, D. Hoxha, M. Al-Mukhtar, Physical Characterization of Natural Straw Fibers as Aggregates for Construction Materials Applications, *Materials (Basel).* 7 (2014) 3034–3048. <https://doi.org/10.3390/ma7043034>.
- [26] A. Kurniati, H. Darmokoesoemo, N.N.T. Puspaningsih, Scanning Electron Microscope Analysis of Rice Straw Degradation by a Treatment with α -L-arabinofuranosidase, *Procedia Chem.* 18 (2016) 63–68. <https://doi.org/10.1016/J.PROCHE.2016.01.011>.
- [27] S. Halvarsson, H. Edlund, M. Norgren, Wheat Straw As Raw Material for Manufacture of Straw (Mdf), *BioResources.* 5 (2010) 1215–1231. <https://doi.org/10.15376/biores.5.2.1215-1231>.
- [28] T. Ashour, W. Wu, Using barley straw as building material, in: S. Elfson (Ed.), *Barley Prod. Cultiv. Uses*, Nova Science Publishers, Inc., 2011.
- [29] Alpha cellulose - CAMEO, (2016). http://cameo.mfa.org/wiki/Alpha_cellulose.
- [30] D. Wang, Basic Lignin Chemistry, (n.d.). <http://web.nchu.edu.tw/pweb/users/taiwanfir/lesson/10476.pdf>.
- [31] Comité National des Coproduits ADEME, Co-produits riches en ligno-cellulose, Paille de céréale, Fiche 1, n.d. <https://librairie.ademe.fr/>.
- [32] I. Plazonić, Ž. Barbarić-Mikočević, A. Antonović, Chemical Composition of Straw as an Alternative Material to Wood Raw Material in Fibre Isolation, *Drv. Ind.* 67 (2016) 119–125. <https://doi.org/10.5552/drind.2016.1446>.
- [33] Nutritional Requirements of Plants | Boundless Biology | | Course Hero, (n.d.). <https://www.coursehero.com/study-guides/boundless-biology/nutritional-requirements-of-plants/> (accessed June 8, 2022).
- [34] F. Nicholson, D. Kindred, A. Bhogal, S. Roques, J. Kerley, S. Twining, T. Brassington, P. Gladders, H. Balshaw, S. Cook, S. Ellis, Straw incorporation review, *HGCA.* (2014). <https://doi.org/10.13140/RG.2.1.2364.2721>.
- [35] W.E. Johns, K.A. Niazi, Effect of pH and Buffering Capacity of Wood on The Gelation Time of Urea-Formaldehyde Resin, *Wood Fiber Sci.* (1981) 255–263.

<https://wfs.swst.org/index.php/wfs/article/view/1988> (accessed October 22, 2021).

- [36] X. Yin, M. Lawrence, D. Maskell, M. Ansell, Comparative micro-structure and sorption isotherms of rice straw and wheat straw, *Energy Build.* 173 (2018) 11–18. <https://doi.org/10.1016/j.enbuild.2018.04.033>.
- [37] S. Liuzzi, C. Rubino, F. Martellotta, P. Stefanizzi, C. Casavola, G. Pappaletta, Characterization of biomass-based materials for building applications: The case of straw and olive tree waste, *Ind. Crops Prod.* 147 (2020) 112229. <https://doi.org/10.1016/J.INDCROP.2020.112229>.
- [38] K.S.W. Sing, D.H. Everett, R.A.W. Haul, L. Moscou, R.A. Pierotti, J. Rouquerol, T. Siemieniewska, Reporting physisorption data for gas/solid systems with special reference to the determination of surface area and porosity, *Pure Appl. Chem.* 57 (1985) 603–619. <https://doi.org/10.1351/PAC198557040603/MACHINEREADABLECITATION/RIS>.
- [39] R. Wimmer, H. Hohensinner, L. Janisch, M. Drack, Building with renewable raw materials, *Berichte Aus Energie- Und Umweltforsch.* (2002). www.NachhaltigWirtschaften.at.
- [40] K.C. Watts, K.I. Wilkie, K. Tompson, J. Corson, Thermal and mechanical properties of straw bales as they relate to a straw house, *Can. Soc. Agric. Eng.* (1995). https://www.researchgate.net/publication/284418271_Thermal_and_mechanical_properties_of_straw_bales_as_they_relate_to_a_straw_house.
- [41] J. McCabe, The thermal resistivity of straw bale construction, (1993). <https://studylib.net/doc/8455783/the-thermal-resistivity-of-sb-construction>.
- [42] Wimmer Robert, Hohensinner Hannes, Janisch Luise, Drack Manfred, *Wandsysteme aus nachwachsenden Rohstoffen Wirtschaftsbezogene Grundlagenstudie*, 2001. www.hausderzukunft.at.
- [43] J.-P. Costes, A. Evrard, B. Biot, G. Keutgen, A. Daras, S. Dubois, F. Lebeau, L. Courard, Thermal conductivity of straw bales: full size measurements considering the direction of the heat flow, *Buildings.* 7 (2017). <https://doi.org/10.3390/buildings7010011>.
- [44] J. Wihan, Humidity in straw bale walls and its effect on the decomposition of straw, University of East London School of Computing and Technology Londbridge Road, 2007. https://www.enertech.fr/pdf/45/humidite_murs_paille.pdf.
- [45] A. Louis, A. Evrard, B. Biot, L. Courard, F. Lebeau, De l'expérimentation à la modélisation des propriétés hygrothermiques de parois isolées en paille, *Ann. Du Batim. Des Trav. Publics.* (2013) 34–40. <https://docplayer.fr/22293188-De-l-experimentation-a-la-modelisation-des-proprietes-hygrothermiques-de-parois-isolees-en-paille.html>.
- [46] A. Romano, A. Bras, S. Grammatiko, S. Wylie, P. Kot, A. Shaw, On the development of self-controlled bio-based panels for building's thermal management, in: *Eur. Conf. Compos. Mater.*, 2018: p. 8. https://www.researchgate.net/publication/325539191_On_the_development_of_self-controlled_bio-based_panels_for_building's_thermal_management.
- [47] J. Vejelienė, Processed straw as effective thermal insulation for building envelope constructions, *Eng. Struct. Technol.* 4 (2012) 96–103. <https://journals.vgtu.lt/index.php/EST/article/view/4715/4037>.
- [48] K.A. Sabapathy, S. Gedupudi, Straw bale based constructions: Measurement of effective thermal transport properties, *Constr. Build. Mater.* 198 (2019) 182–194. <https://doi.org/10.1016/j.conbuildmat.2018.11.256>.
- [49] T. Ashour, The use of renewable agricultural by-products as building materials, Faculty of agriculture, Moshtohor Zagazig University Benha Branch, 2003. <https://doi.org/10.13140/RG.2.1.2887.7285>.

- [50] A. Shea, K. Wall, P. Walker, Evaluation of the thermal performance of an innovative prefabricated natural plant fibre building system, *Build. Serv. Eng. Res. Technol.* 34 (2013) 369–380. <https://doi.org/10.1177/0143624412450023>.
- [51] M. Palumbo, A.M. Lacasta, N. Holcroft, A. Shea, P. Walker, Determination of hygrothermal parameters of experimental and commercial bio-based insulation materials, *Constr. Build. Mater.* 124 (2016) 269–275. <https://doi.org/10.1016/J.CONBUILDMAT.2016.07.106>.
- [52] O. Douzane, G. Promis, J.M. Roucoult, A.D. Tran Le, T. Langlet, Hygrothermal performance of a straw bale building: In situ and laboratory investigations, *J. Build. Eng.* 8 (2016) 91–98. <https://doi.org/10.1016/j.jobe.2016.10.002>.
- [53] CEC/ATI, Thermal Performance (ATI-20227), Fresno, California, USA: California Energy Commission, n.d. <https://www.archtest.com/>.
- [54] A. Beck, U. Heinemann, M. Reidinger, J. Fricke, Thermal Transport in Straw Insulation, *J. Therm. Envel. Build. Sci.* 27 (2004) 227–234. <https://doi.org/10.1177/1097196304039831>.
- [55] Utilisation de la paille en parois de maisons individuelles a ossature bois, (2004). <https://docplayer.fr/60439589-Utilisation-de-la-paille-en-parois-de-maisons-individuelles-a-ossature-bois.html>.
- [56] FASBA, Thermal performance: Strawbale building, *Res. Dev.* 2003-2009. (2009). <https://fasba.de/category/nachrichten-fasba/>.
- [57] K. Wei, C. Lv, M. Chen, X. Zhou, Z. Dai, D. Shen, Development and performance evaluation of a new thermal insulation material from rice straw using high frequency hot-pressing, *Energy Build.* 87 (2015) 116–122. <https://doi.org/10.1016/j.enbuild.2014.11.026>.
- [58] L. Conti, M. Barbari, M. Monti, Steady-State thermal properties of rectangular straw-bales (RSB) for building, *Buildings.* 6 (2016) 44. <https://doi.org/10.3390/buildings6040044>.
- [59] R. Gallegos-Ortega, T. Magaña-Guzmán, J.A. Reyes-López, M.S. Romero-Hernández, Thermal behavior of a straw bale building from data obtained in situ: A case in Northwestern México, *Build. Environ.* 124 (2017) 336–341. <https://doi.org/10.1016/j.buildenv.2017.08.015>.
- [60] F. D'Alessandro, F. Bianchi, G. Baldinelli, A. Rotili, S. Schiavoni, Straw bale constructions: Laboratory, in field and numerical assessment of energy and environmental performance, *J. Build. Eng.* 11 (2017) 56–68. <https://doi.org/10.1016/j.jobe.2017.03.012>.
- [61] S. Cascone, G. Evola, A. Gagliano, G. Sciuto, C.B. Parisi, Laboratory and in-situ measurements for thermal and acoustic performance of straw bales, *Sustainability.* 11 (2019). <https://doi.org/10.3390/su11205592>.
- [62] B. Marques, A. Tadeu, J. Almeida, J. António, J. de Brito, Characterisation of sustainable building walls made from rice straw bales, *J. Build. Eng.* 28 (2020). <https://doi.org/10.1016/j.jobe.2019.101041>.
- [63] S. Goodhew, R. Griffiths, Sustainable earth walls to meet the building regulations, *Energy Build.* 37 (2005) 451–459. <https://doi.org/10.1016/J.ENBUILD.2004.08.005>.
- [64] A. Chaussinand, J.L. Scartezzini, V. Nik, Straw bale: A waste from agriculture, a new construction material for sustainable buildings, *Energy Procedia.* 78 (2015) 297–302. <https://doi.org/10.1016/j.egypro.2015.11.646>.
- [65] C. Atkinson, Energy Assessment of a Straw Bale Building, University of East London, 2008. <https://fr.scribd.com/document/258350643/19-Energy-Assessment-of-a-Straw-Bale-Building-1>.
- [66] M. Gedeon, Materion performance alloys technical tidbits Thermal diffusivity and effusivity, 2018. <https://materion.com/-/media/files/alloy/newsletters/technical-tidbits/issue-no-111->

thermal-diffusivity-and-effusivity.pdf (accessed May 20, 2019).

- [67] Build desk, Vapour resistances and μ -values, (2002).
- [68] BS EN 12086 : 2013 | Thermal insulating products for building applications- Determination of water vapour transmission properties, BSI Standa, European committee for standardization, 2013. https://infostore.saiglobal.com/en-us/Standards/EN-12086-2013-343326_SAIG_CEN_CEN_785965/.
- [69] M. Labat, C. Magniont, N. Oudhof, J.E. Aubert, From the experimental characterization of the hygrothermal properties of straw-clay mixtures to the numerical assessment of their buffering potential, *Build. Environ.* 97 (2016) 69–81. <https://doi.org/10.1016/j.buildenv.2015.12.004>.
- [70] EN 12086:2013 - Thermal insulating products for building applications - Determination of water vapour transmission properties, (n.d.). <https://standards.iteh.ai/catalog/standards/cen/a7981453-bb3c-4dc3-8b42-71cd0f2ab52e/en-12086-2013> (accessed August 22, 2022).
- [71] P. Konečný, J. Teslík, M. Hamala, Mechanical and Physical Properties of Straw Bales, *Adv. Mater. Res.* 649 (2013) 250–253. <https://doi.org/10.4028/www.scientific.net/amr.649.250>.
- [72] G. Forêt, C. Hamelin, M. Olivier, M. LA Olivier BOTTE DE PAILLE, M. Porteur, F. Gilles, H. Cédric, O. Myriam, La boîte de paille, materiau porteur, *ECOBAT Sci.* (2013). <https://hal-enpc.archives-ouvertes.fr/hal-00940081>.
- [73] T. Ashour, A. Bahnasawey, W. Wu, Compressive Strength of Fibre Reinforced Earth Plasters for Straw Bale Buildings, *Aust. J. Agric. Eng.* 1 (2010) 86–92. <https://search.informit.com.au/documentSummary;dn=633149344967656;res=IELENG>.
- [74] S. Goodhew, J. Carfrae, P. De Wilde, Briefing: Challenges related to straw bale construction, *Proc. Inst. Civ. Eng. - Eng. Sustain.* 163 (2010) 185–189. <https://doi.org/10.1680/ensu.2010.163.4.185>.
- [75] S. Vardy, C. Macdougall, Compressive testing and analysis of plastered straw bales, *J. Green Build.* 1 (2016) 65–78. <https://doi.org/10.4324/9781315657455>.
- [76] A. Thomson, P. Walker, Durability characteristics of straw bales in building envelopes, *Constr. Build. Mater.* 68 (2014) 135–141. <https://doi.org/10.1016/J.CONBUILDMAT.2014.06.041>.
- [77] J. Robinson, H.K. Aoun, M. Davison, Determining Moisture Levels in Straw Bale Construction, *Procedia Eng.* 171 (2017) 1526–1534. <https://doi.org/10.1016/J.PROENG.2017.01.390>.
- [78] K.A. Sabapathy, S. Gedupudi, In situ thermal characterization of rice straw envelope of an outdoor test room, *J. Build. Eng.* 33 (2021) 101416. <https://doi.org/10.1016/J.JOBE.2020.101416>.
- [79] C. Rye, C. Scott, The spab research report 1. U-value report, 2012. www.spab.org.uk.
- [80] Barbara, Information guide to straw bale building, for self builders and the construction industry, Amaz. Nails. (2001). <http://baubiologie.at/download/strawbaleguide.pdf>.
- [81] I. Guillen, A. Uris, H. Estelles, J. Llinares, A. Llopis, On the sound insulation of masonry wall façades, *Build. Environ.* 43 (2008) 523–529. <https://doi.org/10.1016/j.buildenv.2007.01.010>.
- [82] A. Trabelsi, Z. Kammoun, Experimental evaluation of acoustic characteristics of straw walls, *Can. Acoust.* 46 (2018) 49–56. <https://jcaa.caa-aca.ca/index.php/jcaa/article/view/3185>.
- [83] R. Dalmeijer, Straw-bale Sound Isolation and Acoustics - TLS #53, Last Straw J. (2013). <https://thelaststraw.org/strawbale-sound-isolation-acoustics/>.
- [84] K. Wall, P. Walker, C. Gross, C. White, T. Mander, Development and testing of a prototype straw bale house, *Http://Dx.Doi.Org/10.1680/Coma.11.00003.* 165 (2015) 377–384.

<https://doi.org/10.1680/COMA.11.00003>.

- [85] S. Džidić, Fire resistance of the straw bale walls, in: 5th Int. Conf. Contemp. Achiev. Civ. Eng. 21. April 2017., Subotica, Serbia, 2017. <https://doi.org/10.14415/konferencijagfs2017.044>.
- [86] FCBA, Rapport de classement de la reaction au feu conformément à l'EN 13501-1:2007, (2012). https://rfcp.fr/wp-content/uploads/fichiers/Rapport_Classement_Feu_Mars_2012.pdf.
- [87] Ecobati, Classement feu - Euroclasse, (n.d.). <https://www.ecobati.com/fr/a-propos/services/conseils/lexique/classement-feu>.
- [88] Pole des Laboratoires Bois, Rapport d'essai reaction au feu, (2010) 6. https://rfcp.fr/wp-content/uploads/fichiers/allumabilite_Rapport_FEU.pdf.
- [89] E. Janowska-renkas, A. Król, S. Pochwała, D. Pałubski, M. Adamska, I. Klementowski, The fire resistance and heat conductivity of natural construction material based on straw and numerical simulation of building energy demand, *Energies* 2022, Vol. 15, Page 1155. 15 (2022) 1155. <https://doi.org/10.3390/EN15031155>.
- [90] 2021 International Building Code (IBC) | ICC Digital Codes, (n.d.). <https://codes.iccsafe.org/content/IBC2021P1> (accessed June 9, 2022).
- [91] B. Theis, Straw Bale Fire Safety a review of testing and experience, *Ecol. Build. Netw.* (2003). www.ecobuildnetwork.org.
- [92] A. Morrison, Fire resistance of straw bale walls outperforms conventional construction, *Strawbale*. (n.d.). <https://www.strawbale.com/fire-resistance-of-straw-bale-walls-outperforms-conventional-construction/>.
- [93] A.D. González, Energy and carbon embodied in straw and clay wall blocks produced locally in the Andean Patagonia, *Energy Build.* 70 (2014) 15–22. <https://doi.org/10.1016/j.enbuild.2013.11.003>.
- [94] B. Szasz, U. Pont, A. Mahdavi, A comparison of straw-bale and conventional brick buildings in view of energy efficiency and environmental performance, *Proceeding 2nd ICAUD Int. Conf. Archit. Urban Des.* (2014) 8. <http://dSPACE.epoka.edu.al/handle/1/950%5Cnhttp://dl.lib.mrt.ac.lk/handle/123/9222>.
- [95] L. Brojan, A. Petric, P.L. Clouston, Comparative study of brick and straw bale wall systems from environmental, economical and energy perspectives, *ARPN J. Eng. Appl. Sci.* 8 (2013) 920–926.
- [96] G. Mutani, C. Azzolino, M. Macr, S. Mancuso, Straw buildings : A good compromise between environmental sustainability and energy-economic savings, *Appl. Sci.* 10 (2020). <https://doi.org/10.3390/app10082858>.
- [97] L. Floissac, Règles professionnelles de Construction en Paille, Règles CP 2012, LeMoniteur, RFCP- Réseau Francais de la consturction en paille, 2012.
- [98] B. Belhadj, M. Bederina, Z. Makhloufi, A. Goullieux, M. Quéneudec, Study of the thermal performances of an exterior wall of barley straw sand concrete in an arid environment, *Energy Build.* 87 (2015) 166–175. <https://doi.org/10.1016/J.ENBUILD.2014.11.034>.
- [99] J. Zhang, J. Wang, S. Guo, B. Wei, X. He, J. Sun, S. Shu, Study on heat transfer characteristics of straw block wall in solar greenhouse, *Energy Build.* 139 (2017) 91–100. <https://doi.org/10.1016/J.ENBUILD.2016.12.061>.
- [100] S. Hou, F. Liu, S. Wang, H. Bian, Coupled heat and moisture transfer in hollow concrete block wall filled with compressed straw bricks, *Energy Build.* 135 (2017) 74–84. <https://doi.org/10.1016/J.ENBUILD.2016.11.026>.
- [101] K.A. Sabapathy, S. Gedupudi, On the influence of concrete-straw-plaster envelope thermal mass

- on the cooling and heating loads for different climatic zones of India, *J. Clean. Prod.* 276 (2020) 123117. <https://doi.org/10.1016/J.JCLEPRO.2020.123117>.
- [102] R. Ahmadi, B. Souri, M. Ebrahimi, Evaluation of wheat straw to insulate fired clay hollow bricks as a construction material, *J. Clean. Prod.* 254 (2020) 120043. <https://doi.org/10.1016/J.JCLEPRO.2020.120043>.
- [103] CD2E Accélérateur de l'éco-transition, *Construction en bottes de paille : Performance technique, économique et écologique*, n.d.
- [104] A travel in the straw-bale buildings in Turkey, (n.d.). <https://samanbalya.wordpress.com/building-techniques/> (accessed October 18, 2021).
- [105] A.A. Aznabaev, A.V. Ovsyannikova, A.O. Povzun, Z.A. Gaevskaya, Assessment of straw construction technologies in terms of thermal efficiency of enclosing structures, *Constr. Unique Build. Struct.* 43 (2016) 104–116. www.unistroy.spb.ru.
- [106] International Residential Code | ICC, (n.d.). <https://codes.iccsafe.org/content/IRC2018>.
- [107] La maison Feuillette | CNCP, (n.d.). <https://cncp-feuillette.fr/maison-feuillette/> (accessed September 7, 2022).
- [108] C. Searle, Straw bale building and the national building code of Canada, Canada, n.d. https://www.eng.mcmaster.ca/sites/default/files/uploads/straw_bale_building_and_the_national_building_code_of_canada.pdf.
- [109] J. Haberl, D. Claridge, C. Clup, (PDF) ASHRAE's Guideline 14-2002 for Measurement of Energy and Demand Savings: How to Determine What Was Really Saved by the Retrofit, in: *Proc. Fifth Int. Conf. Enhanc. Build. Oper.*, ResearchGate, Pittsburgh, Pennsylvania, 2005. https://www.researchgate.net/publication/26901656_ASHRAE's_Guideline_14-2002_for_Measurement_of_Energy_and_Demand_Savings_How_to_Determine_What_Was_Really_Saved_by_the_Retrofit.
- [110] A. Alcorn, M. Donn, Life cycle potential of strawbale and timber for carbon sequestration in house construction, in: *2nd Int. Conf. Sustain. Constr. Mater. Technol.*, 2010: pp. 885–895.
- [111] Thermal Mass in Buildings, (n.d.). <http://www.greenspec.co.uk/building-design/thermal-mass/>.
- [112] Instruments Regulatory Codes and standards, Regulations Regarding Latvian Construction Standard LBN 002-01 Thermotechnics of Building Envelopes, Latvia, 2002.
- [113] Physical properties of building materials or construction materials, (n.d.). <https://readcivil.com/physical-properties-of-building-materials-or-construction-materials/>.
- [114] Thermal conductivity and thermal resistance of extruded and pressed house bricks, (2002). <https://www.azom.com/article.aspx?ArticleID=1567>.
- [115] Why wood? | Wood Products, (n.d.). <https://www.woodproducts.fi/content/why-wood>.
- [116] Thermal conductivity of common materials and gases, (n.d.). https://www.engineeringtoolbox.com/thermal-conductivity-d_429.html.
- [117] Densities of solids, (n.d.). https://www.engineeringtoolbox.com/density-solids-d_1265.html.
- [118] Thermal Properties Of Building Materials | Electronics Cooling, (n.d.). <https://www.electronics-cooling.com/2008/02/thermal-properties-of-building-materials/>.
- [119] Tractor Implement Automation | Precision Ag Technology | John Deere UK & IE, (n.d.). <https://www.deere.co.uk/en/agricultural-management-solutions/guidance-automation/tractor-implement-automation/> (accessed August 22, 2022).
- [120] New Holland - Choose your brand, (n.d.). <https://www.newholland.com/Pages/index.html>

(accessed August 22, 2022).

- [121] Activ Home : Constructions Ecologiques Et Economiques - Activ Home, (n.d.). <https://www.activ-home.com/fr/>.
- [122] X. Chen, B. Zheng, H. Liu, Optical and digital microscopic imaging techniques and applications in pathology, *Anal. Cell. Pathol. (Amst)*. 34 (2011) 5. <https://doi.org/10.3233/ACP-2011-0006>.
- [123] M. Bass, C. Decusatis, J. Enoch, *Handbook of Optics: Volume I - Geometrical and Physical Optics, Polarized Light, Components and Instruments*, McGraw-Hill Education, 2010. <https://www.accessengineeringlibrary.com/content/book/9780071498890> (accessed June 16, 2022).
- [124] P. Van Soest, J.B. Roberston, *Analysis of forages and fibrous foods*, Cornell University, Ithaca, New York, 1985. <https://www.worldcat.org/title/analysis-of-forages-and-fibrous-foods/oclc/223471931> (accessed September 28, 2022).
- [125] Standard NF EN 15414-3, (n.d.). <https://www.boutique.afnor.org/en-gb/standard/nf-en-154143/solid-recovered-fuels-determination-of-moisture-content-using-the-oven-dry-/fa156279/37787> (accessed September 28, 2022).
- [126] EN 15403 - European Standards, (n.d.). <https://www.en-standard.eu/csn-en-15403-solid-recovered-fuels-determination-of-ash-content/> (accessed September 28, 2022).
- [127] K.A. Cychosz, M. Thommes, Progress in the Physisorption Characterization of Nanoporous Gas Storage Materials, *Engineering*. 4 (2018) 559–566. <https://doi.org/10.1016/J.ENG.2018.06.001>.
- [128] B. Salamon, J. Kapała, M. Gaune-Escard, Instrumentation and calibration of the Calvet calorimeter, *J. Therm. Anal. Calorim.* 2011 1082. 108 (2011) 421–424. <https://doi.org/10.1007/S10973-011-1929-3>.
- [129] ISO - ISO 24353:2008 - Hygrothermal performance of building materials and products — Determination of moisture adsorption/desorption properties in response to humidity variation, (n.d.). <https://www.iso.org/standard/42167.html> (accessed July 4, 2022).
- [130] S. Merakeb, F. Dubois, C. Petit, Modélisation des hystérésis de sorption dans les matériaux hygroscopiques, *Comptes Rendus Mécanique*. 337 (2009) 34–39. <https://doi.org/10.1016/J.CRME.2009.01.001>.
- [131] V. Cascione, D. Maskell, A. Shea, P. Walker, A review of moisture buffering capacity: From laboratory testing to full-scale measurement, *Constr. Build. Mater.* 200 (2019) 333–343. <https://doi.org/10.1016/J.CONBUILDMAT.2018.12.094>.
- [132] Hygrothermal performance of building materials and products-Determination of hygroscopic sorption properties, (2013).
- [133] Standard test methods for water vapor transmission of materials, (n.d.). https://www.researchgate.net/publication/336879226_Standard_Test_Methods_for_Water_Vapor_Transmission_of_Materials_1 (accessed July 4, 2022).
- [134] ASTM-E96/E96M, Standard test methods for water vapor transmission of materials, (n.d.).
- [135] ISO - ISO 8894-2:2007 - Refractory materials — Determination of thermal conductivity — Part 2: Hot-wire method (parallel), (n.d.). <https://www.iso.org/standard/44465.html> (accessed January 19, 2022).
- [136] Transient-Hot-Wire method method for determining thermal conductivity (THW) - tec-science, (n.d.). <https://www.tec-science.com/thermodynamics/heat/transient-hot-wire-method-method-for-determining-thermal-conductivity-thw/> (accessed September 20, 2021).
- [137] G. Tlajji, S. Ouldboukhite, F. Pennec, P. Biwole, Thermal and mechanical behavior of straw-

- based construction: A review, *Constr. Build. Mater.* 316 (2022) 125915. <https://doi.org/10.1016/j.conbuildmat.2021.125915>.
- [138] K. Kostyrko, M. Skoczylas, A. Klee, Certified reference materials for thermal analysis, *J. Therm. Anal.* 1988 331. 33 (1988) 351–357. <https://doi.org/10.1007/BF01914623>.
- [139] X. Lu, Y. Wang, L. Estel, N. Kumar, H. Grénman, S. Leveneur, Evolution of specific heat capacity with temperature for typical supports used for heterogeneous catalysts, *Process.* 2020, Vol. 8, Page 911. 8 (2020) 911. <https://doi.org/10.3390/PR8080911>.
- [140] DIN 52620 - 1991-04 - Beuth.de, (n.d.). <https://www.beuth.de/de/norm/din-52620/1672857> (accessed July 4, 2022).
- [141] Norme NF EN 1362, (n.d.). <https://m.boutique.afnor.org/fr-fr/norme/nf-en-1362/systemes-de-cartes-didentification-caracteristiques-dinterface-des-terminau/fa029801/14758> (accessed August 22, 2022).
- [142] EN 13500:2003 - Thermal insulation products for buildings - External thermal insulation composite, (n.d.). <https://standards.iteh.ai/catalog/standards/cen/6c65d7f8-9650-4618-b7c6-0f379a0b1be5/en-13500-2003> (accessed August 22, 2022).
- [143] Les référentiels ACERMI - ACERMI, (n.d.). <https://www.acermi.com/fr/documents-reference/referentiels-acermi/> (accessed August 22, 2022).
- [144] J.C. Motte, R. Escudié, N. Beaufils, J.P. Steyer, N. Bernet, J.P. Delgenès, C. Dumas, Morphological structures of wheat straw strongly impacts its anaerobic digestion, *Ind. Crops Prod.* 52 (2014) 695–701. <https://doi.org/10.1016/j.indcrop.2013.11.038>.
- [145] ISO/TS 24597:2011(fr), Analyse par microfaisceaux — Microscopie électronique à balayage — Méthodes d'évaluation de la netteté d'image, (n.d.). <https://www.iso.org/obp/ui#iso:std:iso:ts:24597:ed-1:v1:fr> (accessed January 18, 2022).
- [146] S.H. Ghaffar, M. Fan, Revealing the morphology and chemical distribution of nodes in wheat straw, *Biomass and Bioenergy.* 77 (2015) 123–134. <https://doi.org/10.1016/J.BIOMBIOE.2015.03.032>.
- [147] R. Liu, H. Yu, Y. Huang, Structure and morphology of cellulose in wheat straw, *Cellul.* 2005 121. 12 (2005) 25–34. <https://doi.org/10.1023/B:CELL.0000049346.28276.95>.
- [148] J. Straube, D. Onysko, C. Schumacher, Methodology and design of field experiments for monitoring the hygrothermal performance of wood frame enclosures, *J. Build. Phys.* 26 (2002) 123–151. <https://doi.org/10.1177/0075424202026002098>.
- [149] L. Marmoret, F. Collet, H. Beji, Moisture adsorption in glass wool products, (n.d.).
- [150] K. Harries, B. Sharma, *Nonconventional and Vernacular Construction Materials: Characterisation, properties and applications*, 2nd editio, Woodhead Publishing, 2019.
- [151] RFCP, Réseau français de la construction paille | RFCP, (n.d.). <https://www.rfcp.fr/> (accessed February 22, 2022).
- [152] M. Pfundstein, R. Gellert, M. Spitzner, A. Rudolphi, *Insulating materials: Principles, materials, applications*, Walter de Gruyter, 2012.
- [153] Y.L. He, T. Xie, Advances of thermal conductivity models of nanoscale silica aerogel insulation material, *Appl. Therm. Eng.* 81 (2015) 28–50. <https://doi.org/10.1016/J.APPLTHERMALENG.2015.02.013>.
- [154] T. Xie, Y.L. He, Z.J. Hu, Theoretical study on thermal conductivities of silica aerogel composite insulating material, *Int. J. Heat Mass Transf.* 58 (2013) 540–552. <https://doi.org/10.1016/J.IJHEATMASSTRANSFER.2012.11.016>.

- [155] M. Wang, J. He, J. Yu, N. Pan, Lattice Boltzmann modeling of the effective thermal conductivity for fibrous materials, *Int. J. Therm. Sci.* 46 (2007) 848–855. <https://doi.org/10.1016/j.ijthermalsci.2006.11.006>.
- [156] Y. Asako, H. Kamikoga, H. Nishimura, Y. Yamaguchi, Effective thermal conductivity of compressed woods, *Int. J. Heat Mass Transf.* 45 (2002) 2243–2253. [https://doi.org/10.1016/S0017-9310\(01\)00330-1](https://doi.org/10.1016/S0017-9310(01)00330-1).
- [157] A. Karamanos, A. Papadopoulos, A. Anastallos, Heat transfer phenomena in fibrous insulating materials, in: *Proc. 2004 WSEAS/IASME Int. Conf. Heat Mass*, 2014. <http://aix.meng.auth.gr> (accessed January 20, 2022).
- [158] T. Xie, Y. He, Y. Li, W. Tao, Theoretical and numerical study on thermal properties of fibrous insulation materials, in: *14th Minsk Int. Forum Heat Mass Transf.*, 2012: pp. 7–34.
- [159] A. Hoseini, C. McCague, M. Andisheh-Tadbir, M. Bahrami, Aerogel blankets: From mathematical modeling to material characterization and experimental analysis, *Int. J. Heat Mass Transf.* 93 (2016) 1124–1131. <https://doi.org/10.1016/J.IJHEATMASSTRANSFER.2015.11.030>.
- [160] D. Csanády, O. Fenyvesi, B. Nagy, Heat transfer in straw-based thermal insulating materials, *Materials (Basel)*. 14 (2021). <https://doi.org/10.3390/ma14164408>.
- [161] P. Lopez Hurtado, A. Rouilly, V. Vandenbossche, C. Raynaud, A review on the properties of cellulose fibre insulation, *Build. Environ.* 96 (2016) 170–177. <https://doi.org/10.1016/J.BUILDENV.2015.09.031>.
- [162] C.M. Popescu, Wood as bio-based building material, *Perform. Bio-Based Build. Mater.* (2017) 21–96. <https://doi.org/10.1016/B978-0-08-100982-6.00002-1>.
- [163] K. Rasmussen, Calculation methods for the physical properties of air used in the calibration of microphones, Denmark, 1997.
- [164] Kaganer, Mikhail Grigor'evich, Thermal insulation in cryogenic engineering, Israel Program for Scientific Translations, 1969.
- [165] R. Coquard, D. Baillis, V. Grigorova, F. Enguehard, D. Quenard, P. Levitz, Modelling of the conductive heat transfer through nano-structured porous silica materials, *J. Non. Cryst. Solids*. 363 (2013) 103–115. <https://doi.org/10.1016/J.JNONCRY SOL.2012.11.053>.
- [166] H. Schwab, U. Heinemann, A. Beck, H.P. Ebert, J. Fricke, Dependence of thermal conductivity on water content in vacuum insulation panels with fumed silica kernels, *J. Build. Phys.* 28 (2016) 319–326. <https://doi.org/10.1177/1097196305051792>.
- [167] Jagjiwanram, R. Singh, Effective thermal conductivity of highly porous two-phase systems, *Appl. Therm. Eng.* 24 (2004) 2727–2735. <https://doi.org/10.1016/J.APPLTHERMALENG.2004.03.010>.
- [168] S. Pradhan, V.K. Sehgal, K.K. Bandyopadhyay, P. Panigrahi, C.M. Parihar, S.L. Jat, Radiation interception, extinction coefficient and use efficiency of wheat crop at various irrigation and nitrogen levels in a semi-arid location, *Indian J. Plant Physiol.* 23 (2018) 416–425. <https://doi.org/10.1007/S40502-018-0400-X/FIGURES/8>.
- [169] R.S. Fukushima, R.D. Hatfield, Comparison of the acetyl bromide spectrophotometric method with other analytical lignin methods for determining lignin concentration in forage samples, (2004). <https://doi.org/10.1021/jf035497l>.
- [170] S.M. Grove, A model of transverse thermal conductivity in unidirectional fibre-reinforced composites, *Compos. Sci. Technol.* 38 (1990) 199–209. [https://doi.org/10.1016/0266-3538\(90\)90058-D](https://doi.org/10.1016/0266-3538(90)90058-D).

- [171] J.F. Guo, G.H. Tang, A theoretical model for gas-contributed thermal conductivity in nanoporous aerogels, *Int. J. Heat Mass Transf.* 137 (2019) 64–73. <https://doi.org/10.1016/j.ijheatmasstransfer.2019.03.106>.
- [172] P.J. Burns, C.L. Tien, Natural convection in porous media bounded by concentric spheres and horizontal cylinders, *Int. J. Heat Mass Transf.* 22 (1979) 929–939. [https://doi.org/10.1016/0017-9310\(79\)90033-4](https://doi.org/10.1016/0017-9310(79)90033-4).
- [173] S.W. Churchill, H.H.S. Chu, Correlating equations for laminar and turbulent free convection from a horizontal cylinder, *Int. J. Heat Mass Transf.* 18 (1975) 1049–1053. [https://doi.org/10.1016/0017-9310\(75\)90222-7](https://doi.org/10.1016/0017-9310(75)90222-7).
- [174] J.J. Zhao, Y.Y. Duan, X.D. Wang, B.X. Wang, Effects of solid-gas coupling and pore and particle microstructures on the effective gaseous thermal conductivity in aerogels, *J. Nanoparticle Res.* 14 (2012) 1–15. <https://doi.org/10.1007/S11051-012-1024-0/FIGURES/8>.
- [175] ISO-834, ISO - 834: Fire resistance tests-elements of building construction, 1999 (1999).
- [176] C.H. (Alex) Koh, D. Kraniotis, A review of material properties and performance of straw bale as building material, *Constr. Build. Mater.* 259 (2020) 120385. <https://doi.org/10.1016/j.conbuildmat.2020.120385>.
- [177] B. Moeller Andersen, Munch-Andersen, Houses of straw. Design and material properties; Halmhuse. Udformning og materialeegenskaber (Technical Report) | ETDEWEB, Denmark, 2004. <https://www.osti.gov/etdeweb/biblio/20502691> (accessed July 21, 2022).
- [178] V. Apte, G.J. Griffin, B.W. Paroz, A.D. Bicknell, The fire behaviour of rendered straw bales, *Fire Mater.* 32 (2008) 259–279. <https://doi.org/10.1002/FAM.963>.
- [179] RFCP, Regles Professionnelles de Construction en Paille, (2014) 163.
- [180] NF-EN-1363-1-, Essais de résistance au feu - Partie 1: exigences générales. AFNOR Normalisation., (2013).
- [181] H. Hajiloo, M.F. Green, GFRP reinforced concrete slabs in fire: Finite element modelling, *Eng. Struct.* 183 (2019) 1109–1120. <https://doi.org/10.1016/J.ENGSTRUCT.2019.01.028>.
- [182] W.Y. Gao, J.G. Dai, J.G. Teng, G.M. Chen, Finite element modeling of reinforced concrete beams exposed to fire, *Eng. Struct.* 52 (2013) 488–501. <https://doi.org/10.1016/J.ENGSTRUCT.2013.03.017>.
- [183] P. Bamonte, R. Elicetti, N. Kalaba, F. Lo Monte, N. Pinoteau, M.J. Miah, P. Pimienta, On the Structural Behavior of Reinforced Concrete Walls Exposed to Fire, *Key Eng. Mater.* 711 (2016) 580–587. <https://doi.org/10.4028/WWW.SCIENTIFIC.NET/KEM.711.580>.
- [184] J. Kang, H. Yoon, W. Kim, V. Kodur, Y. Shin, H. Kim, Effect of wall thickness on thermal behaviors of RC walls under fire conditions, *Int. J. Concr. Struct. Mater.* 10 (2016) 19–31. <https://doi.org/10.1007/S40069-016-0164-5/FIGURES/16>.
- [185] Dassault systemes, Abaqus/CAE User's Guide, Abaqus User's Guid. (2013) 1138.
- [186] Eurocode 1: Actions on structures - Part 1-2: General actions - Actions on structures exposed to fire Eurocode, 1 (2011).
- [187] N. Werther, J.W.O. Neill, P.M. Spellman, A.K. Abu, P.J. Moss, A.H. Buchanan, S. Winter, Parametric study of modelling structural timber in fire with different software packages, 7th Int. Conf. Struct. Fire. (2012).
- [188] Eurocode 5, Design of timber structures - Part 1-2: General rules - Structural fire design, 1 (2011).

- [189] J. König, L. Walleij, Timber frame assemblies exposed to standard and parametric fires Part 2: A design model for standard fire exposure, 2000. <http://www.diva-portal.org/smash/get/diva2:1079798/FULLTEXT02.pdf> (accessed September 13, 2022).
- [190] J. König, L. Walleij, One-Dimensional charring of timber exposed to standard and parametric fires in initially unprotected and postprotection situations, 1999.
- [191] Fermentation du fourrage, agir pour diminuer les risques d'incendie | Journal Paysan Breton, (n.d.). <https://www.paysan-breton.fr/2014/06/fermentation-du-fourrage-agir-pour-diminuer-les-risques-dincendie/> (accessed August 23, 2022).
- [192] H. Künzel, Simultaneous heat and moisture transport in building components one-and two-dimensional calculation using simple parameters, Fraunhofer Institute of Building Physics, 1995.
- [193] H. Künzel, A. Holm, V. Eithner, T. Schmidt, WUFI-2D: Program description, Fraunhofer-Institut for Building Physics, Holzkirchen, 2000.
- [194] T. Kalamees, J. Vinha, Hygrothermal calculations and laboratory tests on timber-framed wall structures, *Build. Environ.* 38 (2003) 689–697. [https://doi.org/10.1016/S0360-1323\(02\)00207-X](https://doi.org/10.1016/S0360-1323(02)00207-X).
- [195] J.M.P.Q. Delgado, N.M.M. Ramos, E. Barreira, V.P. De Freitas, A critical review of hygrothermal models used in porous building materials, *J. Porous Media.* 13 (2010) 221–234. <https://doi.org/10.1615/JPORMEDIA.V13.I3.30>.
- [196] F. Antretter, F. Sauer, T. Schöpfer, A. Holm, Validation of a hygrothermal whole building simulation software, in: 12th Conf. Int. Build. Perform. Simul. Assoc., Sydney, 2011. http://ibpsa.org/proceedings/BS2011/P_1554.pdf (accessed September 19, 2022).
- [197] ANSI/ASHRAE Standard 140-2007, Standard method of test for the evaluation of building energy analysis computer programs, 2008.
- [198] M. Kottek, J. Grieser, C. Beck, B. Rudolf, F. Rubel, World map of the Köppen-Geiger climate classification updated, *Meteorol. Zeitschrift.* 15 (2006) 259–263. <https://doi.org/10.1127/0941-2948/2006/0130>.
- [199] M. Ibrahim, P. Henry, E. Wurtz, P. Achard, A study on the thermal performance of exterior walls covered with a recently patented silica-aerogel-based insulating coating, *Build. Environ.* 81 (2014) 112–122. <https://doi.org/10.1016/j.buildenv.2014.06.017>.
- [200] The concrete conundrum, *Chem. World.* (2008) 62–66. www.chemistryworld.org.
- [201] I.A. De La Roche, J. O'Connor, P. Tetu, Wood products and sustainable construction, in: XII World For. Congr., Quebec city, Canada, 2003. <http://www.fao.org/3/XII/1039-A2.htm>.
- [202] M.H. Ramage, H. Burrige, M. Busse-Wicher, G. Fereday, T. Reynolds, D.U. Shah, G. Wu, L. Yu, P. Fleming, D. Densley-Tingley, J. Allwood, P. Dupree, P.F. Linden, O. Scherman, The wood from the trees: The use of timber in construction, in: *Renew. Sustain. Energy Rev.*, Elsevier Ltd, 2017: pp. 333–359. <https://doi.org/10.1016/j.rser.2016.09.107>.
- [203] I. Mundi, Cereal production (metric tons) by Country, *Index Mundi.* (2019). <https://www.indexmundi.com/facts/indicators/AG.PRD.CREL.MT>.
- [204] Athena, B. Steen, Building a home using straw bale construction, *Mother Earth News.* (1996). <https://www.motherearthnews.com/green-homes/straw-bale-construction-zmaz95djzgoe>.
- [205] S. Yevgeny, Building with bales in Belarus, *Ecol. Sustain. Dev.* (n.d.). <https://www.inforse.org/europe/iae/mae/building.html>.
- [206] K.R.G. Punhagui, É.F. Campos, J.M.B. González, V.M. John, Prospects for the use of wood in residential construction in Brazil - First results, *Key Eng. Mater.* 517 (2012) 247–260.

<https://doi.org/10.4028/www.scientific.net/KEM.517.247>.

- [207] Adventist Development and Relief Agency International, ADRA Straw bale housing becomes an eco-friendly solution for post-earthquake China, Reliefweb. (2009). <https://reliefweb.int/report/china/adra-straw-bale-housing-becomes-eco-friendly-solution-post-earthquake-china>.
- [208] Straw-bale construction gaining popularity in France, Fr. Ecotours. (n.d.). <https://www.myecostay.eu/en/blog/straw-bale-construction-gaining-popularity/>.
- [209] ASHRAE, ANSI/ASHRAE (2017) Standard 55: 2017, Thermal Environmental Conditions for Human Occupancy, 2017. www.ashrae.org.
- [210] EN 13779:2004-Ventilation for non-residential buildings-Performance requirements for ventilation and room-conditioning systems, 2004. <https://standards.iteh.ai/catalog/standards/sist/3373541e-9989-4e0b-8fe8-> (accessed January 25, 2022).
- [211] J. Straube, J. Smegal, Building America special research project: High-R walls case study analysis, 2009.
- [212] Moisture Control Guidance for Building Design, Construction and Maintenance Indoor Air Quality (IAQ), (2013). www.epa.gov/iaq/moisture (accessed August 21, 2021).
- [213] M. Ibrahim, E. Wurtz, P.H. Biwole, P. Achard, H. Sallee, Hygrothermal performance of exterior walls covered with aerogel-based insulating rendering, *Energy Build.* 84 (2014) 241–251. <https://doi.org/10.1016/j.enbuild.2014.07.039>.
- [214] K. Sedlbauer, Prediction of Mould Growth by Hygrothermal Calculation, *Therm. Environ. Build. Sci.* 24 (2002). <https://doi.org/10.1106/109719602024093>.
- [215] N.R. Bronsema, Moisture movement and mould management in straw bale walls for a Cold Climate, University of Waterloo, 2010. <http://uwspace.uwaterloo.ca/handle/10012/5536>.
- [216] MINCO | La Fenêtre HYBRIDE - Le Concept du Mieux, (n.d.). <https://www.minco.fr/> (accessed September 20, 2022).
- [217] Station météo Vantage Pro 2 Plus sans fil - 6162EU - Davis Instruments, (n.d.). <https://www.meteo-shopping.fr/Station-meteo/Station-meteo-Vantage-Pro-2-Plus-sans-fil-6162EU-Davis-Instruments> (accessed October 15, 2020).
- [218] PTS Mesures – Spécialiste en mesure physique et système d’acquisition, (n.d.). <http://www.pts-mesures.com/?dev=true> (accessed August 24, 2022).
- [219] HYT 939: Digital humidity sensor 0 - 100% RF - TO 39 at reichelt elektronik, (n.d.). <https://www.reichelt.com/fr/en/digital-humidity-sensor-0-100-rf-to-39-hyt-939-p106000.html?r=1> (accessed August 24, 2022).
- [220] EnOcean NodOn humidity and temperature sensor - Home Automation, (n.d.). <https://www.robot-advance.com/EN/art-nodon-temperature-and-humidity-sensor-2236.htm> (accessed August 24, 2022).
- [221] EnOcean motion sensor NodOn - Home Automation, (n.d.). <https://www.robot-advance.com/EN/art-enocean-motion-sensor-2242.htm> (accessed August 24, 2022).
- [222] J.E. Christensen, A Method for more specific Simulation of Operative Temperature in Thermal Analysis Programmes, (n.d.).
- [223] L. Brotas, F. Nicol, Using Passive Strategies to prevent overheating and promote resilient buildings, in: *Cities, Build. People Towar. Regen. Environ.*, 2016: pp. 135–142. https://www.researchgate.net/publication/305840500_Using_Passive_Strategies_to_prevent_ov

erheating_and_promote_resilient_buildings.

- [224] TM52: The Limits of Thermal Comfort: Avoiding Overheating in European Buildings | CIBSE, (n.d.). <https://www.cibse.org/knowledge-research/knowledge-portal/tm52-the-limits-of-thermal-comfort-avoiding-overheating-in-european-buildings> (accessed August 24, 2022).
- [225] R. Fauconnier, L'action de l'humidité de l'air sur la santé dans les bâtiments tertiaires , *Chauff. Vent. Cond.* (1992) 57–62.
- [226] EnergyPlus, (n.d.). <https://energyplus.net/documentation> (accessed September 22, 2021).
- [227] J. Yang, H. Fu, M. Qin, Evaluation of Different Thermal Models in EnergyPlus for Calculating Moisture Effects on Building Energy Consumption in Different Climate Conditions, *Procedia Eng.* 121 (2015) 1635–1641. <https://doi.org/10.1016/J.PROENG.2015.09.194>.
- [228] C. Simonson, M. Salonvaraa, OjanenTuomo, Moisture Content of Indoor Air and Structures in Buildings with Vapor-Permeable Envelopes, (n.d.).
- [229] C. Spitz, M. Woloszyn, C. Buhé, M. Labat, Simulating Combined Heat and Moisture Transfer with Energyplus: An Uncertainty Study and Comparison with Experimental Data, (n.d.).
- [230] F.A.B. Da Silva, N. Carels, M. Trindade Dos Santos, F.J. Lopes, A Tutorial on Sobol' Global Sensitivity Analysis Applied to Biological Models, (n.d.) 10. https://doi.org/10.1007/978-3-030-51862-2_6i.
- [231] A. Saltelli, P. Annoni, Sensitivity Analysis, *Int. Encycl. Stat. Sci.* (2011) 1298–1301. https://doi.org/10.1007/978-3-642-04898-2_509.
- [232] N.D. Cortiços, Improving residential building efficiency with membranes over façades: The Mediterranean context, *J. Build. Eng.* 32 (2020) 101421. <https://doi.org/10.1016/J.JOBE.2020.101421>.
- [233] A.W. Abbood, K.M. Al-Obaidi, H. Awang, A.M. Abdul Rahman, Achieving energy efficiency through industrialized building system for residential buildings in Iraq, *Int. J. Sustain. Built Environ.* 4 (2015) 78–90. <https://doi.org/10.1016/J.IJSBE.2015.02.002>.
- [234] C. Gubb, T. Blanusa, A. Griffiths, C. Pfrang, Can houseplants improve indoor air quality by removing CO₂ and increasing relative humidity?, *Air Qual. Atmos. Heal.* 2018 1110. 11 (2018) 1191–1201. <https://doi.org/10.1007/S11869-018-0618-9>.
- [235] R. Vanova, M. Vlcko, J. Stefko, Life Cycle Impact Assessment of Load-Bearing Straw Bale Residential Building, *Mater.* 2021, Vol. 14, Page 3064. 14 (2021) 3064. <https://doi.org/10.3390/MA14113064>.
- [236] X. Yin, Q. Dong, S. Zhou, J. Yu, L. Huang, C. Sun, Energy-saving potential of applying prefabricated straw bale construction (PSBC) in domestic buildings in northern China, *Sustain.* 2020, Vol. 12, Page 3464. 12 (2020) 3464. <https://doi.org/10.3390/SU12083464>.
- [237] G. Syngros, C.A. Balaras, D.G. Koubogiannis, Embodied CO₂ emissions in building construction materials of hellenic dwellings, *Procedia Environ. Sci.* 38 (2017) 500–508. <https://doi.org/10.1016/J.PROENV.2017.03.113>.
- [238] H. Li, Z. Luo, X. Xu, Y. Cang, L. Yang, Assessing the embodied carbon reduction potential of straw bale rural houses by hybrid life cycle assessment: A four-case study, *J. Clean. Prod.* 303 (2021) 127002. <https://doi.org/10.1016/J.JCLEPRO.2021.127002>.
- [239] R. Guo, Y. Zhao, Y. Shi, F. Li, J. Hu, H. Yang, Low carbon development and local sustainability from a carbon balance perspective, *Resour. Conserv. Recycl.* 122 (2017) 270–279. <https://doi.org/10.1016/J.RESCONREC.2017.02.019>.
- [240] J. Fix, S. Tynan, B. Vancouver, M. Kissinger, Carbon footprint of wood and agricultural residue

- sources of pulp 0 carbon footprint analysis for wood & agricultural residue sources of pulp, Alberta, Canada, 2011.
- [241] P. Sukontasukkul, Methodology for calculating carbon dioxide emission in the production of ready-mixed concrete, in: 1st Int. Conf. Comput. Technol. Concr. Struct., Jeju, South Korea, 2009.
https://www.researchgate.net/publication/259005796_Methodology_for_Calculating_Carbon_Dioxide_Emission_in_the_Production_of_Ready-mixed_Concrete (accessed September 8, 2022).
- [242] S. Love, Carbon footprint of New Zealand laminated veneer lumber, Rotorua, New Zealand, 2010. www.scionresearch.com (accessed September 8, 2022).
- [243] Methodology for the free allocation of emission allowances in the EU ETS post 2012 Sector report for the mineral wool industry, 2012.
- [244] Methodology for the free allocation of emission allowances in the EU ETS post 2012 Sector report for the gypsum industry, 2009.
- [245] N.G. Kulkarni, A.B. Rao, Carbon footprint of solid clay bricks fired in clamps of India, *J. Clean. Prod.* 135 (2016) 1396–1406. <https://doi.org/10.1016/J.JCLEPRO.2016.06.152>.
- [246] Choosing low-carbon windows | Features | Building, (n.d.). <https://www.building.co.uk/focus/choosing-low-carbon-windows/5060079.article> (accessed September 8, 2022).
- [247] N. Hill, E. Karagianni, L. Jones, J. Maccarthy, E. Bonifazi, S. Hinton, C. Walker, Government greenhouse gas conversion factors for company reporting: Methodology paper, London, UK, 2019. www.nationalarchives.gov.uk/doc/open-government-licence/ (accessed September 8, 2022).
- [248] S.K. Tehmina, M. Umarah, Wheat Straw: A pragmatic overview, *J. Biol. Sci.* 4 (2012) 673–675. https://www.researchgate.net/publication/320894189_Wheat_Straw_A_pragmatic_overview (accessed September 10, 2022).
- [249] S.H. Lamtom, R.A. Savidge, A reassessment of carbon content in wood: variation within and between 41 North American species, *Biomass and Bioenergy.* 25 (2003) 381–388. [https://doi.org/10.1016/S0961-9534\(03\)00033-3](https://doi.org/10.1016/S0961-9534(03)00033-3).
- [250] M. Ibrahim, P.H. Biwole, P. Achard, E. Wurtz, G. Ansart, Building envelope with a new aerogel-based insulating rendering: Experimental and numerical study, cost analysis, and thickness optimization, *Appl. Energy.* 159 (2015) 490–501. <https://doi.org/10.1016/J.APENERGY.2015.08.090>.
- [251] F. Souayfane, P.H. Biwole, F. Fardoun, P. Achard, Energy performance and economic analysis of a TIM-PCM wall under different climates, *Energy.* 169 (2019) 1274–1291. <https://doi.org/10.1016/J.ENERGY.2018.12.116>.
- [252] Natural gas prices around the world, December 2021 | GlobalPetrolPrices.com, (n.d.). https://www.globalpetrolprices.com/natural_gas_prices/ (accessed September 5, 2022).
- [253] Electricity prices around the world | GlobalPetrolPrices.com, (n.d.). https://www.globalpetrolprices.com/electricity_prices/ (accessed September 5, 2022).
- [254] Central bank rates | Worldwide Interest Rates, (n.d.). <https://www.cbrates.com/> (accessed September 6, 2022).
- [255] Hay and straw prices | AHDB, (n.d.). <https://ahdb.org.uk/dairy/hay-and-straw-prices> (accessed September 6, 2022).
- [256] Concrete prices 2022 - How much does concrete cost?, (n.d.).

- <https://www.concretenetwork.com/concrete-prices.html> (accessed September 6, 2022).
- [257] Monthly lumber price U.S. 2022, (n.d.). <https://www.statista.com/statistics/1239728/monthly-lumber-price-usa/> (accessed September 6, 2022).
- [258] The ideal wholesale glass wool price list, (n.d.). <https://www.alibaba.com/showroom/glass-wool-price-list.html> (accessed September 6, 2022).
- [259] Plastering and ceiling services | Australian Taxation Office, (n.d.). <https://www.ato.gov.au/Business/Small-business-benchmarks/In-detail/Benchmarks-A-Z/L-Q/Plastering-and-ceiling-services/?page=4> (accessed September 6, 2022).
- [260] How much does a brick wall cost to build in 2022?, (n.d.). <https://www.checkatrade.com/blog/cost-guides/cost-build-brick-wall/> (accessed September 6, 2022).
- [261] Percentage of cost breakdown between labour, materials and contractor profit in construction, (n.d.). <http://www.a4architect.com/2013/04/percentage-of-cost-breakdown-between-labour-materials-and-contractor-profit-in-construction/> (accessed September 6, 2022).
- [262] CEN/TC 169, EN 12464-1:2021 Light and lighting - Lighting of work places - Part 1: Indoor work places, (2021) 120. <https://www.en-standard.eu/bs-en-12464-1-2021-light-and-lighting-lighting-of-work-places-indoor-work-places/> (accessed September 6, 2022).
- [263] Autodesk Robot Structural Analysis Professional 2010 - Training Manual (Metric Version) - [PDF Document], (n.d.). <https://fdocuments.net/document/autodesk-robot-structural-analysis-professional-2010-training-manual-metric-version.html?page=6> (accessed August 27, 2022).
- [264] T. Cerovsek, A review and outlook for a “Building Information Model” (BIM): A multi-standpoint framework for technological development, *Adv. Eng. Informatics*. 25 (2011) 224–244. <https://doi.org/10.1016/J.AEI.2010.06.003>.
- [265] Agrafe Galva et Inox pour agrafeuse pneumatique Senco, Makita, Alsafix, (n.d.). <https://www.novi-clous.fr/81-agrafes> (accessed September 26, 2022).
- [266] EN1991-1-1 charges d’exploitation, (n.d.). <https://www.icab.fr/doc/icabforce/eurocode/en1991-1-1.htm> (accessed August 31, 2022).
- [267] Eurocode 8: Design of structures for earthquake resistance-Part 1: General rules, seismic actions and rules for buildings, (1998).
- [268] Arrêté du 22 octobre 2010 relatif à la classification et aux règles de construction parasismique applicables aux bâtiments de la classe dite «à risque normal» - Légifrance, (n.d.). <https://www.legifrance.gouv.fr/loda/id/JORFTEXT000022941755/> (accessed September 26, 2022).
- [269] Coons’ Method | Robot Structural Analysis Professional | Autodesk Knowledge Network, (n.d.). <https://knowledge.autodesk.com/support/robot-structural-analysis-professional/learn-explore/caas/CloudHelp/cloudhelp/2015/ENU/Robot/files/GUID-CC4EED46-B8FC-4509-95CB-2760B9B840D4-htm.html> (accessed August 31, 2022).
- [270] Charges de neige sur les constructions selon l’Eurocode 1-Partie 1-3 par Danielle CLAVAUD, (n.d.).
- [271] EN1991-1-4 Vent, (n.d.). <https://www.icab.eu/guide/eurocode/en1991-1-4/> (accessed August 31, 2022).

French version : Résumé détaillé

1- Introduction Générale

Le développement rapide du monde moderne nécessite une demande d'énergie sans cesse croissante, ce qui soulève de sérieuses inquiétudes quant à l'extraction et à la distribution des ressources énergétiques fossiles, avec de graves conséquences environnementales. La prise de conscience environnementale a ouvert la voie à une économie à faible émission de carbone et à un nouveau modèle de croissance verte dans tous les secteurs. Le secteur de la construction est un moteur important de la transition énergétique car il possède le plus grand potentiel inexploité d'économies d'énergie. Ce secteur est également un domaine clé dans la lutte contre le réchauffement climatique. Par exemple, en Europe, il est responsable de 40 % de la consommation totale d'énergie, de 36 % des émissions de gaz à effet de serre et de 120 millions de tonnes de CO₂ rejetés chaque année. Pour rendre ce secteur plus économe en énergie et réduire son empreinte carbone, les normes ont proposé l'utilisation de produits à faible énergie grise et biosourcés dans les bâtiments neufs. Tel est le cas en France avec la réglementation environnementale RE2020 du 1er janvier 2022 remplaçant la RT2012. Les pailles de blé, de riz, d'avoine et d'orge sont des exemples de matériaux biosourcés capables de compenser les émissions de CO₂ tout en offrant une bonne isolation thermique. La paille de céréales est produite et disponible en grandes quantités, suffisantes pour produire des bottes de paille comprimée pour le secteur du bâtiment. Le monde produit environ 2000 millions de tonnes de différents types de paille par an. Aujourd'hui, l'agriculture française produit environ 20 millions de tonnes de paille de blé, ce qui peut fournir environ 5000 bâtiments en bottes de paille.

Historiquement, les bâtiments primitifs en paille étaient construits dans les plaines africaines pendant l'ère paléolithique, il y a 3,3 millions d'années, et le renouveau de ces constructions a commencé il y a plus de 100 ans. La première construction a été localisée au Nebraska (USA) en 1886, en raison du manque de bois et d'autres matériaux de construction à cette époque. En France, ce mode de construction est apparu pour la première fois en 1920. L'intérêt pour ce type de construction a diminué à la fin du 20ème siècle en raison de l'industrialisation du bâtiment et de l'intérêt croissant pour de nouveaux matériaux. Notons que la paille, en tant que matériau structurel ou isolant, concerne la construction de bâtiments de toutes tailles : de la maison individuelle au bâtiment à plusieurs étages, du hangar industriel au bâtiment public. La paille peut être utilisée toute seule ou en la mélangeant avec d'autres matériaux conventionnels pour améliorer leurs propriétés mécaniques et thermiques. L'absence de certaines informations et explications dans la littérature a motivé le travail de cette thèse. En particulier, l'augmentation du confort hygrothermique et la diminution de la consommation d'énergie des bâtiments en paille ne sont pas suffisamment documentées scientifiquement. De même, des études expérimentales et numériques sont nécessaires pour estimer la résistance au feu et la résistance mécanique de ces structures en ajoutant de nouveaux matériaux de couverture qui pourraient améliorer les résultats. Ces questions et ces manques de données scientifiques empêchent actuellement la diffusion des bâtiments en paille. Ainsi, l'objectif de cette thèse est d'apporter des réponses scientifiques à ces questions. Le matériau composite étudié appartient aux matériaux biosourcés. Il est constitué de fibres végétales, la paille, qui agit comme isolant thermique et renfort mécanique dans un caisson de bois. La méthodologie est à la fois expérimentale et numérique à plusieurs échelles (fibre, botte, mur et bâtiment) allant de l'étude des caractéristiques thermiques et hygriques des fibres et bottes de paille à l'étude du confort de l'air intérieur et de la consommation énergétique des bâtiments en paille, en passant par les caractérisations hygrothermiques et de résistance au feu des murs.

Ce travail de thèse qui a été réalisé à l'Université Clermont Auvergne, au sein de l'Institut Pascal, dans le cadre du projet ECOMAT financé par le contrat de plan État-région 2015-2021 (CPER) est divisée en quatre parties. La première partie donne un aperçu de la littérature académique existante et de la pratique industrielle sur la construction à base de paille. Cette revue est divisée en cinq chapitres. La deuxième partie est consacrée à la caractérisation expérimentale et au développement d'un modèle analytique. Elle est divisée en deux chapitres. Le premier chapitre présente le travail expérimental effectué pour caractériser la paille à l'échelle des fibres et des bottes. Le processus de préparation du

matériau est décrit avec les méthodes expérimentales utilisées. Les résultats de la caractérisation sont présentés à la fin du chapitre. Sur la base des résultats expérimentaux, le deuxième chapitre propose un modèle analytique de la conductivité thermique dans les bottes de paille. Le modèle prend en compte la densité, la température, l'humidité et l'orientation des fibres des bottes. La troisième partie se concentre sur l'étude expérimentale et numérique des murs en paille multicouches. Un modèle WUFI est utilisé pour prédire les problèmes hygrothermiques qui peuvent survenir dans certaines conditions pour cinq murs de paille avec différentes configurations. Le nouveau mur de paille proposé par le partenaire industriel de la thèse, Activ'home, est ensuite testé pour sa résistance au feu. A l'aide du logiciel Abaqus, un modèle numérique est proposé à l'issue de l'expérimentation. La quatrième partie étudie le confort intérieur de la construction en paille. Cette partie est complétée par une étude énergétique pour prédire la consommation de telles structures en utilisant les modèles Energyplus pour différents scénarios. Une étude de sensibilité est réalisée pour déterminer les paramètres qui affectent le plus la température de l'air intérieur et l'humidité relative. En outre, la résistance mécanique est testée à l'aide du modèle d'analyse structurelle ROBOT. Enfin, une analyse économique et environnementale est réalisée pour montrer le coût des bâtiments en paille et leurs émissions nettes de carbone.

2- Objectifs et méthodologie de la thèse

Malgré de nombreuses recherches, certaines informations pour caractériser et normaliser le matériau manquent encore dans la littérature. En ce qui concerne la caractérisation thermique, davantage d'expériences concernant la variation de la conductivité thermique en fonction de la teneur en humidité pour différents types de paille sont nécessaires. De plus, les chercheurs ont mené beaucoup de travaux sur la conductivité et ses variations, tandis que la variation de la chaleur spécifique, le facteur de diffusion et le pH n'ont pas été suffisamment étudiés. Ces facteurs ont besoin d'être caractérisés en détail en fonction de la densité, l'humidité relative, l'orientation des fibres et le type de paille. A l'échelle des murs, les études sur la formation de moisissures à la surface des murs en paille font défaut. A cet égard, on ne trouve pas actuellement dans la littérature d'isoplèthes de condensation en fonction de la structure du mur pour des conditions limites hygrothermiques variables. A l'échelle du bâtiment, il existe encore très peu d'études numériques sur le comportement énergétique des bâtiments à base de paille en fonction de la structure des murs, de la localisation du bâtiment et de ses scénarios d'occupation et d'exploitation. Le rôle de la paille comme régulateur de l'humidité de l'air intérieur est également insuffisamment documenté. De telles études futures devraient prendre en compte la variabilité des résultats, due à la nature changeante des propriétés thermo-physiques de ce matériau biosourcé dans le temps. Sur la base des résultats énergétiques, la faisabilité économique de tels bâtiments devrait être étudiée de manière plus approfondie, notamment en termes de période d'amortissement et de coût du cycle de vie. Pour finir, la résistance mécanique des bâtiments en paille nécessite d'être analysée sous des charges climatiques et des accélérations sismiques. Cette thèse vise à fournir de nouvelles données scientifiques sur tous les points évoqués.

La méthodologie est à la fois expérimentale et numérique pour les aspects thermiques et mécaniques. Elle consiste en une caractérisation multi-échelle allant de l'échelle microscopique à l'échelle du bâtiment, en passant par l'échelle de la botte et du mur. Les tâches prévues sont les suivantes :

- A l'échelle de la fibre : réaliser une caractérisation expérimentale micro et macroporeuse afin de déduire la microstructure de la paille qui peut avoir un impact sur les mécanismes de transfert de chaleur et d'humidité dans la botte.
- A l'échelle de la botte : tester expérimentalement les bottes de paille pour en déduire la conductivité thermique, l'isotherme de sorption, la chaleur spécifique, le coefficient de diffusion de la résistance à la vapeur d'eau, etc. Numériquement, un modèle de transfert de chaleur doit être conçu en fonction de la microstructure du matériau et de ses caractéristiques hygrothermiques mesurées.

- A l'échelle du mur : étudier les propriétés hygrothermiques de murs en paille multicouches typiques sous différentes conditions aux limites en utilisant des modèles numériques via le logiciel WUFI. Par ailleurs, il convient de réaliser expérimentalement un test de résistance au feu d'un mur en paille recouvert de bois et de mousse minérale fourni par le partenaire industriel Activ'home. L'objectif est d'atteindre une résistance de 180 minutes.

- A l'échelle du bâtiment : étudier expérimentalement le bâtiment prototype en paille du partenaire industriel de la thèse situé à Reugny-France en analysant les variations de température et d'humidité des surfaces et de l'environnement intérieur et extérieur. Les résultats doivent permettre de valider un modèle numérique et une analyse d'incertitudes construits sur le logiciel EnergyPlus. Par la suite, le modèle EnergyPlus sera utilisé pour tester le comportement du bâtiment sous différents climats et scénarios. Pour les perspectives mécaniques, un modèle numérique devra être développé en utilisant le logiciel ROBOT. Pour les perspectives environnementales, une analyse du cycle de vie devra être réalisée pour les constructions en paille.

3- Etat de l'art

La première partie vise à résumer les connaissances actuelles sur la construction en bottes de paille. Cette partie aborde les résultats de la caractérisation thermophysique des fibres et des bottes de paille. Ensuite, elle présente le comportement hygrothermique et énergétique des murs et des bâtiments à base de paille, ainsi que leur évaluation du cycle de vie. Enfin, les principales questions de recherche ouvertes concernant les bâtiments en bottes de paille sont détaillées.

Sur l'échelle de la fibre, les chercheurs ont surtout utilisé des appareils de microscopie numérique et de microscopie électronique à balayage (MEB) pour caractériser la microstructure des entre-nœuds et des fibres. Ils ont constaté que si l'entre-nœud peut mesurer plusieurs centimètres de long, les fibres situées à l'intérieur de son enveloppe mesurent le plus souvent 2 à 7 mm de long, tandis que les pores ont une taille de 2 μm à 100 μm , selon le type de paille. Les fibres de paille sont principalement composées de cellulose (40-80 %) responsable de la propriété d'isolation thermique, de lignine (10-30 %) responsable de la stabilité mécanique, d'humidité (6-8 %) et de cendres (5-10 %).

Sur une plus grande échelle, la caractérisation concerne les bottes de paille constituées de tiges de paille empilées et compressées. La forme, la dimension et le niveau de compression de la botte dépendent de la presse utilisée. Les bottes rectangulaires utilisées dans les murs des bâtiments ont généralement une hauteur de 60 à 130 cm, une largeur de 70 à 120 cm et une longueur de 50 à 280 cm. Les chercheurs ont constaté que la densité des bottes de paille d'orge varie de 54,6 kg/m^3 à 78,3 kg/m^3 , tandis que celle des bottes de paille d'avoine et de blé, varie de 81 kg/m^3 à 106,3 kg/m^3 . De nombreuses réglementations nationales en matière de construction imposent une densité minimale de 80 kg/m^3 pour les constructions en paille. Les bottes de paille sont classées comme des matériaux hygroscopiques avec des valeurs tampon d'humidité d'environ 1,8 et une absorption capillaire d'environ 0,0155 $\text{kg}/(\text{m}^2 \cdot \text{s}^{1/2})$, en raison de leur porosité de 90 %. Plusieurs équipes ont étudié l'effet du type de paille, de l'orientation principale des fibres, de la densité de la botte, de la température moyenne et de l'humidité relative (HR), sur la conductivité thermique effective de la botte. La méthodologie était principalement expérimentale, utilisant la technique de la plaque chaude gardée ou des fluxmètres pour mesurer la conductivité thermique. Il a été constaté que cette dernière augmente avec la densité, l'humidité relative et la température, et qu'elle diminue avec une teneur plus élevée en cellulose et lorsque les fibres sont principalement orientées perpendiculairement au flux de chaleur. L'augmentation de la densité réduit la quantité d'air piégé à l'intérieur de la botte, ce qui explique l'effet négatif sur la conductivité. Une humidité relative élevée correspond à une teneur en eau plus importante dans la botte, ce qui a un effet négatif sur la conductivité en raison de la conductivité de l'eau plus élevée. Lorsque la température de la botte augmente, le nombre de molécules qui entrent en collision augmente en raison de l'énergie cinétique microscopique plus élevée, ce qui augmente la conductivité thermique. Enfin, lorsque les fibres sont perpendiculaires au flux de chaleur, il n'y a pas de chemin de conduction solide à travers la

botte alors que dans le cas parallèle, ces chemins existent à travers les fibres, qui sont moins isolantes que l'air. La conductivité thermique est comprise entre 0,033-0,19 W/m.K tandis que la densité, la température et l'humidité relative des bottes sont respectivement comprises entre 100 et 150 kg/m³, -5 et 40 °C et 5-60 %, indépendamment de l'orientation principale des fibres et du type de paille. La capacité thermique spécifique des bottes de paille varie de 1075 à 2000 J/(kg.K), la valeur mesurée augmentant avec la densité et la température des bottes. En ce qui concerne l'effusivité et la diffusivité thermiques, elles sont respectivement comprises entre 417 et 775 J/(K.m².s^{-1/2}) et entre 0,1e-06 et 3,6 e-06 m²/s, l'effusivité augmentant avec la densité des bottes et la diffusivité présentant la tendance inverse. Les propriétés hygriques des bottes sont rarement mentionnées dans la littérature. La plupart des chercheurs ont mesuré le facteur de résistance à la diffusion de la vapeur μ et ont trouvé une valeur comprise entre 1,15 et 5 qui augmente avec la densité des bottes.

A l'échelle de la paroi, les enveloppes de paille sont généralement constituées d'une couche centrale en bottes de paille sur laquelle s'ajoutent d'autres couches de finition extérieures qui peuvent comprendre du plâtre, du ciment, du bois dur, une couche d'isolation thermique supplémentaire ou encore une lame d'air non ventilé. En fonction de la structure du mur et de l'épaisseur des matériaux, les valeurs U résultantes sont généralement comprises entre 0,11 et 0,28 W/m².K, ce qui est inférieur à celles des murs de construction utilisant des matériaux conventionnels comme le béton ou les briques. Plusieurs chercheurs ont testé expérimentalement la capacité des murs de paille à réduire et à décaler dans le temps les variations de la température extérieure et de l'humidité relative. La plupart ont trouvé des déphasages et des coefficients d'amortissement d'une valeur de 6-12 heures et de 0,01-0,08 %, respectivement. En ce qui concernent les propriétés hygriques, les études s'accordent sur la très faible absorption d'humidité des murs en paille. Ceci est principalement dû à la grande résistance à la diffusion de vapeur des couches de finition et des enduits. Des tests de dégradation effectués sur un mur en paille à 28,5 % d'humidité relative n'ont montré aucun développement bactérien. Jusqu'à présent, la plupart des recherches sur la résistance au feu des murs en paille ont utilisé des méthodes expérimentales. Il a été constaté que les structures pouvaient résister à une température de feu supérieure à 1000°C sur un côté pendant deux heures, ce qui est conforme au code international de la construction. Cela est dû à la quantité limitée d'oxygène dans les bottes de densité supérieure à 80 kg/m³ et à la résistance au feu des couches de finition comme le plâtre. Enfin, en ce qui concerne les performances acoustiques, des expériences ont montré que l'indice d'affaiblissement acoustique des murs en paille varie entre 42 et 53 dB selon la disposition des murs.

À l'échelle du bâtiment, trois techniques de construction prédominantes existent pour un bâtiment en paille. Dans la méthode porteuse, les bottes de paille supportent le poids du toit. La principale limitation de cette méthode est la surface maximale des ouvertures, qui doit être inférieure à 50 % de la surface du mur. La méthode non structurelle (ou méthode de remplissage) utilise des colonnes et des poutres en bois ou en béton armé pour supporter la charge. Cette technique permet de construire des bâtiments de grande hauteur mais nécessite des opérations de construction plus complexes. Enfin, la technique du préfabriqué permet d'assembler des panneaux muraux préfabriqués sur le site de construction, réduisant ainsi la complexité et le temps de construction. L'objectif principal de l'utilisation de la paille est de réduire la consommation d'énergie et les émissions de carbone du bâtiment. Un bâtiment en paille de 300 m² de surface situé en Suisse a été évalué et a montré une consommation d'énergie finale d'environ 3800 kWh et une énergie primaire annuelle d'environ 8,9 kWh/m² de surface de plancher. Une autre étude en Italie a évalué numériquement le cycle de vie d'une maison en bois et en paille d'une superficie de 200 m². Ils ont noté une consommation d'énergie annuelle de 37,9 GJ alors qu'une maison standard avec une isolation conventionnelle en béton consomme environ 41,7 GJ par an. Par rapport à la maison standard, il a été constaté une réduction de 1 230 kg d'équivalent CO₂ par an, ce qui est presque identique à la réduction totale des émissions résultant de l'application de technologies de minimisation de l'énergie, à l'exclusion de la production d'énergie renouvelable sur place.

La littérature existante représente une étape importante vers la diffusion des bâtiments en bottes de paille. Cependant, il reste encore plusieurs lacunes dans les connaissances existantes. Les mesures des propriétés hygriques des bottes autres que le facteur de résistance à la diffusion de la vapeur sont rares. La littérature manque également de modèles détaillés du transfert de chaleur et de masse à travers les fibres de paille et les bottes, en fonction du type de paille, de la densité des bottes, de la température, de l'humidité relative et de l'orientation des fibres. De tels modèles aideraient à prévoir le comportement hygrothermique et énergétique des bâtiments en paille. De même, les trois principales méthodes de construction des bâtiments en paille n'ont pas fait l'objet d'une étude approfondie quant à leurs avantages et limites inhérents du point de vue hygrothermique et mécanique. Par exemple, on ne sait toujours pas quelle méthode offre le meilleur confort thermique, les meilleures économies d'énergie et la meilleure résistance sismique. Ces études devraient également tenir compte de l'emplacement du bâtiment et de ses scénarios d'occupation et d'exploitation. Enfin, le rôle de la paille comme régulateur de l'humidité de l'air intérieur est encore insuffisamment documenté, même si les constructeurs de bâtiments en paille annoncent parfois cette propriété. Les études futures devront prendre en compte la variabilité des résultats, due à la nature changeante des propriétés thermo-physiques de ce matériau biosourcé dans le temps. Sur la base des résultats énergétiques, la faisabilité économique des bâtiments en paille devrait être étudiée de manière plus intensive, notamment en termes de période d'amortissement et de coût du cycle de vie. Ces étapes de recherche sont cruciales pour stimuler l'intérêt privé et public pour la construction en paille.

4- Travaux réalisés à l'échelle du matériau

Cette partie montre les travaux expérimentaux réalisés sur des fibres et des bottes de paille produites dans la région auvergnate. L'étude expérimentale comprend la caractérisation de la microstructure, la composition chimique, la mesure de la valeur tampon de l'humidité, la perméabilité à la vapeur d'eau, les courbes d'adsorption/désorption, la conductivité thermique et la capacité thermique.

Un microscope digital a été utilisé pour obtenir des images microscopiques d'une section transversale d'une tige de paille au laboratoire à l'université de La Rochelle. L'image de la tige comprenant l'épiderme, le parenchyme et les faisceaux vasculaires, a montré que les fibres sont des cylindres tubulaires ayant un diamètre de 3176 μm et une épaisseur de 312 μm avec des espaces et des pores sur leur surface. L'épiderme est composé de cellules de paroi d'environ 100 μm d'épaisseur qui régulent les échanges gazeux et l'équilibre hydrique. Il protège également le système vasculaire intérieur et améliore les performances mécaniques de la fibre. Les faisceaux vasculaires s'étalent sous forme de cellules polygonales courtes et longues ayant une forme de bulle. Le diamètre des pores varie entre 5 μm et 45 μm et est distribué de façon aléatoire sur toute la section. Pour compléter la description de la morphologie de ce type de fibre, les faisceaux vasculaires ont été observés tout au long de la section longitudinale. Dans certaines parties, les faisceaux vasculaires présentent des épaississements fortement lignifiés (composés de cellulose) dans la paroi secondaire qui créent des structures en spirale pour générer des vaisseaux horizontaux. Les interconnexions et la distribution des pores sont essentielles pour déterminer le modèle de transfert de chaleur du matériau. D'une part, les interconnexions, y compris leur composition chimique, sont responsables des variations de conductivité thermique dues aux variations de masse, de température et d'humidité. La cellulose et l'hémicellulose ont de bonnes propriétés isolantes. Une augmentation de la quantité de cellulose entraîne ainsi une diminution de la conductivité thermique. D'autre part, la quantité d'air affecte significativement la conductivité thermique puisqu'elle contribue à l'isolation thermique. Ainsi, dans une fibre de blé, les trois principaux éléments responsables des variations de la conductivité thermique sont la lignine, la cellulose et l'air. Les tests chimiques sur des tiges de paille ont montré que la teneur en eau, en cellulose et en lignine sont respectivement égales à 11,5 %, 36,4 % et 7,3 %.

Les matériaux isolants sont souvent comparés par rapport à leur conductivité thermique. En raison de leur densité plus élevée, les matériaux biosourcés ont souvent une valeur légèrement supérieure à celle des isolants traditionnels comme la laine minérale et la mousse expansée (environ 0,04 W/m.K). Il est

donc important de mettre en avant les qualités hygriques des matériaux biosourcés, c'est-à-dire leur capacité à retenir ou à laisser l'humidité les traverser sous forme de vapeur ou de liquide, afin de les promouvoir. Un système isolant peut réagir de différentes manières à la vapeur d'eau. Le système peut être perspirant ou étanche à la vapeur d'eau. De même, pour le transfert d'eau liquide, un isolant peut être hydrophobe ou plus ou moins capillaire. En termes de stockage de l'humidité, les matériaux biosourcés ont, comme les autres matériaux hygroscopiques, la propriété essentielle de pouvoir échanger de l'humidité avec l'air ambiant. Une expérience a été menée sur cinq échantillons ayant les mêmes dimensions avec une surface de contact de 0,03 m² en respectant le protocole Nordtest. La phase de sorption de la paille commence à partir de 3 % d'HR avec 1 % de WC, puis augmente à 30 % d'HR avec 5 % de WC, 50 % d'HR avec 7,2 % de WC et 90 % d'HR avec environ 21 % de WC. La phase de désorption diminue de 90 % HR avec 21 % WC à 50 % HR avec 11 % WC, 30 % HR avec 8 % WC et enfin 3 % HR avec 1,8 % WC. Selon la classification IUPAC, la présence d'une telle hystérésis correspond au motif II H3 décrivant un échantillon macroporeux constitué de pores de différentes tailles. La valeur tampon d'humidité moyenne (MBV) de la paille est d'environ 3,07 g/(m².%RH). Les fibres de paille sont considérées comme excellentes pour réguler l'humidité relative intérieure puisque leur capacité tampon est supérieure à 2 g/(m².%RH). Quant à la perméabilité à la vapeur d'eau de la paille, elle se situe entre 0,00036 g/m.h.Pa et 0,00057 g/m.h.Pa, ce qui signifie que ce matériau est hautement hygroscopique.

La caractérisation thermique du matériau paille est importante puisqu'elle détermine la performance énergétique de l'ensemble du bâtiment. Tout d'abord, la conductivité thermique est analysée en fonction de plusieurs paramètres : la température, l'humidité relative, la densité et l'orientation des fibres. Ensuite, la chaleur spécifique est mesurée en fonction de la température de l'échantillon. Ces deux paramètres permettent d'utiliser des modèles de simulation de bâtiments entiers avec une plus grande précision. La conductivité thermique de trois bottes de paille ayant une densité de 80 kg/m³, 100 kg/m³ et 120 kg/m³ est mesurée par la méthode du fil chaud transitoire sous différentes températures (15 °C – 55 °C) et HR (15 % - 95 %). La gamme de températures et d'humidités relatives des matériaux contrôlés à l'aide d'une enceinte climatique reflète les conditions d'utilisation des matériaux d'isolation des bâtiments dans leur environnement réel. La conductivité thermique d'une botte ayant une orientation de fibres perpendiculaire au flux thermique augmente de 0,048 W/mK mesurée à 15 °C, 15 % d'HR et pour une densité de 80 kg/m³, à 0,09 W/mK obtenue à 55 °C, 95 % d'HR et 120 kg/m³. En ce qui concerne les autres paramètres étudiés, la variation de la conductivité thermique suit la même évolution, pour des orientations perpendiculaire et parallèle des fibres. La température, l'humidité et la densité contribuent toutes à une augmentation de la conductivité thermique, ce qui entraîne une dégradation des caractéristiques d'isolation. Ces facteurs sont tous liés à la quantité d'air dans le matériau. Tout d'abord, l'augmentation de la densité réduit la porosité, ce qui réduit la fraction d'air et les propriétés isolantes, entraînant une augmentation de la conductivité thermique. L'augmentation de la densité de 40 kg/m³ par la compression des bottes se traduit par une augmentation de 9 % de la conductivité thermique à une température et une humidité relative spécifiques. Deuxièmement, lorsque la température augmente, l'énergie cinétique des molécules de gaz augmente en conséquence, et le nombre de molécules qui entrent en collision augmente, ce qui accroît la conductivité thermique. Au cours de l'expérience, on a remarqué qu'une élévation de température de 10°C entraîne une élévation moyenne de la conductivité thermique de 6 %. Troisièmement, une humidité relative élevée reflète une augmentation de la quantité de vapeur d'eau dans les interstices des bottes et de la teneur en eau du matériau, ce qui réduit les propriétés isolantes du matériau. Dans chaque mesure, une augmentation de 10 % de l'humidité relative entraîne une augmentation de la conductivité thermique de 7 % en moyenne.

Pour étudier la chaleur spécifique de la paille, la technique de calorimétrie différentielle à balayage DSC est utilisée pour tester des fibres de paille sur une plage de températures allant de -10 °C à 40 °C qui correspond à la température de fonctionnement de la plupart des bâtiments dans les climats tempérés. Ce test est fait au laboratoire à l'université de La Rochelle. La chaleur spécifique des fibres de paille augmente presque linéairement avec la température, de 1000 J/kg.K à 1600 J/kg.K dans cette plage de

température. À mesure que la substance se réchauffe, l'énergie cinétique moyenne des molécules augmente. Les collisions transmettent suffisamment d'énergie pour permettre une rotation. La rotation des molécules contribue alors à l'énergie interne et augmente la chaleur spécifique.

Ces essais expérimentaux ont été suivis par une étude numérique concernant la conductivité thermique des bottes de paille. Vu que la conductivité thermique d'une botte de paille est variable, un modèle mathématique est proposé pour prédire la conductivité thermique effective des bottes de paille en fonction de sa densité, de l'orientation des fibres, de sa composition chimique, de la température et de l'humidité relative. Les résultats numériques ont été comparés avec les résultats expérimentaux pour valider le modèle. Les fibres contenant 38 % de cellulose ont une conductivité thermique effective en moyenne 25 % supérieure à celle des fibres qui contiennent 48 % de cellulose. La différence de 10 % dans la teneur en cellulose n'affecte que la composante solide, tandis que la conductivité gazeuse et la composante radiative restent les mêmes dans les deux cas. La conductivité effective de la botte de paille augmente de 9 % avec la température en raison de l'augmentation de la conductivité du gaz et du rayonnement. La conductivité effective de la botte de paille augmente avec l'humidité relative en raison de l'augmentation de la conductivité solide de 17 %, de la conductivité gazeuse de 4 % et d'une diminution de la conductivité radiative à travers l'air de 3 %. La conductivité thermique des bottes de paille de blé est également fortement affectée par l'orientation des fibres. La conductivité thermique des bottes ayant des fibres perpendiculaires est environ 16 % inférieure à celle des bottes ayant des fibres parallèles. Le modèle proposé permet ainsi d'évaluer la conductivité thermique optimale en fonction des principaux facteurs d'influence. Une telle étude permet de trouver un compromis entre la composition chimique des fibres, leur densité, leur HR et leur orientation. Les résultats obtenus dans cette partie seront utilisés dans les parties suivantes pour étudier leur effet sur le comportement des murs et des bâtiments.

5- Travaux réalisés à l'échelle de la paroi

Cette partie examine, en premier lieu, la résistance au feu d'un nouveau type de mur fait de bottes de paille et recouvert de bois et de mousse minérale en utilisant un four dédié. À l'intérieur du four la température suit la courbe ISO-834. Les observations visuelles d'indices d'inflammation tels que la combustion, la fumée et des fissures sur les surfaces extérieures, ainsi que les valeurs de température à différents endroits du mur, sont utilisées pour étudier et analyser la performance de l'échantillon contre le feu. L'échantillon est classé EI 180, ce qui signifie que le mur exposé d'un côté empêche le feu de progresser vers l'autre côté. Cette classification s'explique par l'étanchéité à la flamme en direction de la surface non exposée et l'absence de fissures avec une augmentation limitée de la température sur cette surface non exposée. Malgré ce résultat performant, le mur a passé plusieurs tests qui ont nui à sa stabilité mécanique et sa résistance. Les premières traces de fumée ont été observées pendant l'expérience à la minute 77 entre la mousse minérale et le panneau fermacell en raison d'un défaut dans la pâte d'étanchéité au feu qui les lie. La pâte utilisée étant de type EI 180, la seule explication raisonnable est qu'elle n'a pas été appliquée correctement ou en quantité suffisante. La détérioration de la pâte d'étanchéité au feu à certains endroits a permis au feu d'atteindre le panneau fermacell puis la surface de la paille au bout de 165 minutes, lorsque la fumée a été observée. La capacité thermique de la mousse minérale, de la plaque fermacell et de la paille a permis d'éviter la combustion totale du mur. Par conséquent, l'ajout de mousse minérale du côté intérieur du mur est validé par cette expérience puisqu'au bout de 180 minutes la surface non exposée de l'échantillon a enregistré une augmentation de température de seulement 60 °C. Concernant la variation de la température, les premières observations ont montré une augmentation progressive de 22°C à 50°C, entre 40 mm et 75 mm du feu, au bout de 10 minutes. Cette température a atteint un maximum de 750 °C à la fin de l'expérience (au bout de 180 minutes). Un comportement similaire a été obtenu au milieu de la botte de paille après 40 minutes et a conduit à une température stable de 100 °C entre les minutes 60 et 130 expliquée par un changement de phase dans le matériau. Par la suite, la température a augmenté jusqu'à atteindre un maximum de 390°C. Toujours à l'intérieur de la botte, à 32 cm de l'extérieur, la température est restée à 28 °C pendant 100

minutes, puis elle a augmenté jusqu'à 100 °C après 180 minutes. Le faible transfert de chaleur vers la surface non exposée s'explique par la forte épaisseur, la résistance thermique élevée et la faible diffusivité thermique de la paroi. De plus, il est important de mentionner que la présence initiale de 15 % d'humidité dans la paille a empêché l'augmentation de la température pendant un temps significatif. La température du four a suivi la norme ISO-834 pendant 140 minutes en atteignant un maximum de 1088 °C, puis elle a commencé à diminuer sachant que la puissance des brûleurs reste la même pendant le test. Cette baisse de température a été expliquée par la pénétration du feu qui a provoqué le contact direct de l'intérieur du four et du fermacell ayant une température plus basse (500 °C). Au bout de 180 min, les brûleurs se sont éteints et l'expérience s'est arrêtée. La paroi a été démontée pour inspecter le côté exposé. L'hypothèse précédente a été confirmée puisqu'un trou s'est formé dans la plaque fermacell qui a provoqué la combustion de la botte de paille. En conséquence, environ 36 % de la paille a été endommagée puisque l'épaisseur de paille gale à 45 cm en début d'expérience mesurait 29 cm à la fin. La mousse minérale qui était en contact direct avec la flamme a été endommagée à environ 50 %. Lors des essais, il a été constaté que la présence de cette mousse retardait la propagation de la chaleur à la paille. Ainsi, le mur a réussi à résister au feu pendant plus de 180 min. Le problème principal a été la mauvaise application de la pâte coupe-feu qui a accéléré le processus. Cet essai a été reproduit numériquement sur Abaqus, ce qui a permis d'obtenir des nouvelles caractéristiques pour la paille à haute température. Le modèle a été utilisé pour tester le même mur en éliminant la colle entre les plaques de mousse minérale. Dans le cas précédent, la température maximale à la jonction des plaques était de 650 °C et le maximum à l'intérieur de la botte était de 500 °C. Dans la nouvelle simulation, ces valeurs diminuent pour atteindre une valeur de 500 °C et un maximum de 300 °C aux mêmes endroits, respectivement. De plus, le feu ne s'est pas propagé dans le mur et il n'y a pas eu de trou dans le panneau fermacell. Le modèle numérique sous Abaqus confirme ainsi la résistance au feu du mur testé pendant plus de 180 minutes.

En deuxième lieu, le comportement hygrothermique de cinq murs multicouches à base de paille a été évalué numériquement en utilisant WUFI-2D dans quatre conditions météorologiques différentes. Dans le premier cas (cas 1), une couche de ciment de 20 mm d'épaisseur recouvre la paille des deux côtés et donne une épaisseur totale au mur d'environ 400 mm. Le ciment est utilisé comme finition de surface pour protéger la paille contre le feu et les moisissures, même si ce matériau augmente l'empreinte carbone du mur. Dans le second cas (cas 2), des panneaux de bois dur de 30 mm d'épaisseur recouvrent la couche de paille des deux côtés, ce qui donne une épaisseur d'assemblage du mur de 420 mm. Les planches de bois dur sont utilisées pour protéger la couche de paille, pour augmenter la performance thermique et pour réduire l'impact environnemental du mur à condition que la source de bois soit exploitée de manière durable. Dans les cas 3 et 4, une lame d'air non ventilée est ajoutée à différents endroits pour augmenter la propriété d'isolation du mur, réduire le transfert de masse et fournir de l'espace pour les câbles électriques et les canalisations. L'épaisseur de la paille est différente dans ces deux cas, et donc l'épaisseur totale du mur, qui est de 520 mm et 470 mm dans le cas 3 et le cas 4, respectivement. Dans le dernier cas (cas 5), une couche de laine de bois a été ajoutée pour augmenter la résistance thermique du mur. L'épaisseur totale de la structure est de 533 mm. Ce dernier assemblage a été récemment proposé par des entrepreneurs français (Activ'home) pour augmenter le confort thermique des bâtiments en paille. Les quatre climats ont été choisis en fonction de leurs profils de température et d'humidité extrêmement différents, selon la classification de Köppen-Geiger, et en fonction de la disponibilité des céréales. Par conséquent, les villes choisies dans cette étude sont Nice-France, Xinjiang-Chine, Arkhangelsk-Russie et Brasilia-Brésil.

L'évaluation hydrique s'est basée sur les critères de teneur en eau totale (TWC), de taux de séchage (DR), de risque de condensation (CR), de développement de moisissures (MG) et de la recommandation

ASHRAE (ASH). TWC montre la capacité du mur à sécher sur une durée de quatre ans en comparant la teneur en eau initiale et finale. Le mur passe ce critère si la valeur finale est inférieure à la valeur initiale. DR calcule la différence entre la teneur en humidité finale et initiale. Un taux de séchage plus élevé signifie une plus grande capacité de séchage. CR est le pourcentage de temps pendant lequel la température de surface tombe en dessous du point de rosée. La condensation apparaît sur la surface intérieure si la température du matériau est inférieure à la température du point de rosée de l'air intérieur. MG consiste à tracer l'HR d'un matériau en fonction de la température à un instant donné. Les moisissures peuvent se développer lorsque les conditions de HR et T d'un mur atteignent ou dépassent la limite des isoplèthes (LIM). ASH prévient les problèmes de moisissure en limitant la quantité d'humidité dans tous les matériaux et les surfaces à l'exception des couches externes. La norme exige sur une période de 30 jours une HR de surface moyenne inférieure à 80 % dans des enveloppes ayant une température de surface moyenne comprise entre 5 °C et 41 °C. En plus, les coefficients d'amortissement et le déphasage de chaque mur ont été calculés et comparés.

D'après les résultats obtenus, certains problèmes sont détectés pour toutes les configurations de murs dans le climat continental subarctique d'Arkhangelsk, en Russie. Un tel climat froid et humide avec un niveau élevé d'humidité relative de l'air est susceptible de causer de sérieux problèmes de condensation dans la paroi. Le temps froid génère des températures de surface basses qui sont proches de la température du point de rosée, ce qui augmente le risque de condensation même pour des niveaux d'HR intérieurs modérés. La différence entre la pression de saturation et la pression de la vapeur d'eau est également réduite, ce qui entraîne des risques de condensation à l'intérieur du mur. Cela peut expliquer le risque élevé de condensation des quatre premiers cas, qui peut atteindre 80 % du temps simulé, en particulier pour le climat subarctique continental russe et le climat froid désertique chinois. Ce problème peut être évité en renforçant l'isolation extérieure. Les conditions climatiques d'Arkhangelsk-Russie expliquent également le taux de séchage plus faible par rapport aux autres climats simulés. Les premier et quatrième cas présentent des risques de développement de moisissures et de décomposition uniquement pour le climat continental subarctique. Les problèmes de taux de séchage et de développement de moisissure peuvent être évités en ajoutant un panneau pare-vapeur ou en augmentant l'épaisseur de la paille. Le risque de décomposition peut être évité en ajoutant un pare-pluie ventilé à l'extérieur et une couche de chaux des deux côtés du mur de paille. Dans le troisième cas, sous tous les climats sauf celui d'Arkhangelsk-Russie, la teneur totale en eau est stable et l'humidité relative est inférieure à 80 % sur quatre ans, grâce à la couche d'air du côté intérieur et à la forte épaisseur de la paille. Ces résultats sont différents pour le cas 3 en Russie. L'isolation intérieure est responsable en effet d'une faible température de surface intérieure. Les couches intérieures dans les cas 4-Russie, 4-Chine, 3-Chine, and 5-Russie ont entraîné une baisse de la température de la surface intérieure, réduisant ainsi la capacité de séchage de l'enveloppe du bâtiment. L'inertie thermique a été évaluée en comparant le déphasage et le coefficient d'amortissement, associés à la capacité de stockage de la chaleur de chaque mur. Le déphasage des cas 1 et 2 était de 6 heures et 30 minutes, tandis que pour les cas 3 et 4, il était de 7 heures. Le cas 5 ayant dans sa structure plusieurs couches de bois, une couche de laine de bois et une couche de paille, a enregistré le déphasage le plus élevé d'environ 8 heures et 30 minutes. Tous les cas montrent un faible coefficient d'amortissement variant entre 0,05 et 0,07. Ces résultats montrent que les murs ayant la plus grande épaisseur et la plus faible diffusivité thermique présentent des déphasages plus élevés et des coefficients d'amortissement plus faibles. Cette étude visait à associer à chaque climat la composition optimale des murs d'un point de vue hygrique et thermique. Il a été remarqué que les

problèmes hygrothermiques se produisaient principalement dans les climats froids ou/et humides. Les première, deuxième et quatrième configuration de murs ont un comportement similaire et peuvent être utilisées dans des climats tempérés-méditerranéens (Csa) et de savane (Aw) tels que Nice et Brazilia. Le troisième cas présente de bonnes propriétés thermiques et peut être utilisé dans des climats désertiques froids (BWk) tels que le Xinjiang. Le dernier cas ne présente pas de problème hygrothermique ni de développement de moisissures sous tous les climats avec des conditions intérieures normales et peut donc être utilisé sous tous les climats, y compris les climats continentaux subarctiques (Dfc) comme Arkhangelsk. La présence de la laine de bois comme isolant extérieur et de la lame d'air intérieure dans le cas cinq a permis d'éviter les problèmes d'humidité dans la paroi. Pour cette raison, il a de meilleures performances pour toutes les conditions.

6- Travaux réalisés à l'échelle du bâtiment

Dans cette partie, les bâtiments en paille sont testés expérimentalement et numériquement pour étudier leurs performances hygrothermiques, énergétiques, environnementales et économiques. Tout d'abord, la campagne expérimentale a utilisé un bâtiment ayant une surface totale de 120 m² situé à Reugny (03190), en France. La valeur U des murs préfabriqués composant le bâtiment est d'environ 0,137 W/m².K. L'évaluation comprend la performance hygrothermique des enveloppes et le confort hygrothermique intérieur en se basant sur des normes telle que la norme ASHRAE.

Les résultats ont montré que la température intérieure moyenne quotidienne au deuxième étage se situait tout au long de l'année entre 5 °C et 30 °C, tandis que les variations saisonnières de la température extérieure moyenne quotidienne se situaient entre -3 °C et 28 °C. La propriété d'isolation de la paille est alors prouvée par la différence de température de l'air intérieur et extérieur pendant l'hiver puisque les murs ont la capacité d'augmenter les températures extérieures minimales de 25 % et jusqu'à 15 °C. En ce qui concerne les valeurs d'humidité relative, malgré les valeurs importantes de l'humidité relative extérieure, l'humidité relative intérieure est relativement stable. La moyenne quotidienne de l'HR intérieure au deuxième étage a varié tout au long de l'année entre 36 % et 56 %, alors que les variations saisonnières moyenne quotidienne de l'HR extérieure étaient comprises entre 44 % et 90 %. Le mur a la capacité de réguler l'HR intérieure aux alentours de 50 % HR. Ce comportement est dû aux propriétés combinées de tampon d'humidité des couches de paille et de bois. En outre, il a été constaté que le mur bois-paille contrôle les pics externes d'humidité relative et de température pour offrir un meilleur confort intérieur. L'humidité relative externe de la face nord a augmenté de 58 % le 1er août pour atteindre une valeur maximale de 70 % le 1er février. Sur la face interne, elle a commencé à 46 % d'HR et l'HR maximale atteinte était de 55 % à la fin du mois de février. La même tendance est obtenue pour la face sud mais avec une HR externe maximale d'environ 60-65 % pendant la saison hivernale. La différence de 5 % entre le nord et le sud s'explique par la pluie qui provoque l'absorption d'humidité avec un ensoleillement plus faible et augmente ainsi l'HR selon la courbe isotherme de sorption de la paille et des matériaux de couverture. Une diminution d'environ 10 % s'est produite le jour 90. Elle peut s'expliquer par la ventilation naturelle du bâtiment causée par l'entrée des travailleurs dans le bâtiment. Cette période de ventilation a conduit à un air ambiant plus sec. Pour les courbes de température des surface interne et externe, ils ont suivi la courbe de température intérieure. La température externe a diminué de 30 °C à 0 °C tandis que la température interne a diminué de 30 °C à 5 °C. Les valeurs de température de surface interne et externe des murs sud et nord étaient proches, avec une différence de 3 °C et 7 °C, respectivement, en raison d'un rayonnement solaire plus important au sud. En février et mars, la température de surface externe a atteint un minimum quotidien moyen de -3 °C qui était à peine perceptible sur le côté interne du mur, avec un écart de 8 °C malgré l'absence de système de chauffage. De même, lorsque la température de surface externe a atteint 30 °C en août, la température de surface interne était de 25 °C sans aucune ventilation ni refroidissement. Le déphasage du mur testé s'avère être de 9 heures avec un coefficient d'amortissement de 0,16. Ces valeurs indiquent un stockage de la chaleur

dans l'enveloppe pendant la journée. Cela permet de réduire le temps nécessaire au refroidissement pendant la période chaude et au chauffage pendant la période froide. Le mur libère la chaleur stockée 9 heures après avoir atteint la température maximale, ce qui augmente la température intérieure de 16 %. Les deux paramètres montrent une configuration bénéfique pour le confort intérieur avec un temps de chauffage minimal pendant l'hiver. Pour la période estivale, une surchauffe peut se produire certains jours, car l'écart entre les températures de surfaces et la température intérieure n'était pas important. Ces deux points sont étudiés en détail dans les sections suivantes.

Concernant le confort thermique, l'indice de confort (TCI) moyen au premier étage a été mesuré à 1,5 °C en été et 4 °C en hiver alors qu'au deuxième étage a été mesuré 2 °C en été et 6 °C en hiver. Cette différence entre le premier et le deuxième étage est causée par le tirage thermique du bâtiment qui affecte la température intérieure et l'humidité relative. La température opérationnelle intérieure diminue lorsque la température extérieure diminue. Notons que pendant l'hiver, la température extérieure moyenne mensuelle atteint 3,2 °C et en été elle atteint 20 °C. Par rapport aux limites de la CIBSE, le mur de paille testé n'assure pas le confort thermique intérieur de novembre à mars, et un système de chauffage est nécessaire pour diminuer l'indice TCI. La situation est bien meilleure en été (entre juillet et septembre) où une légère surchauffe peut se produire. L'application des limites de l'ASHRAE présente la même situation en été où il n'y a pas besoin d'un système de refroidissement alors qu'en hiver on obtient des résultats différents. La température opérationnelle intérieure dépasse les limites 31 % du temps. Par conséquent, on peut conclure que la température opérationnelle intérieure est acceptable sur la base de la température moyenne mensuelle extérieure.

Concernant le confort hygrique, les limites d'humidité relative de l'ASHRAE sont respectées tout le temps, sauf pendant quelques jours en août, février et mars. L'impact de la sorption des murs sur l'humidité relative de l'air intérieur a été démontré expérimentalement. En hiver, les valeurs d'humidité relative de l'air intérieur sont plus élevées qu'en été en raison de la faible température intérieure et de l'humidité relative extérieure élevée, ce qui peut causer des problèmes hygrothermiques dans le mur. Ces résultats ne sont pas suffisants et ne permettent pas de décider si le confort intérieur est atteint ou non. Concernant le confort hygrothermique, il a été constaté que la température opérative et l'HR intérieures sont en dehors de la zone de confort 62 % du temps pendant un an. L'inconfort hygrothermique est causé par les valeurs élevées de température (25 °C - 30 °C) pendant l'été et les basses températures (10 °C - 15 °C) pendant l'hiver à des niveaux d'HR entre 30 % et 60 %.

Ensuite, un modèle numérique Energyplus (EP) est validé en utilisant les résultats expérimentaux. En outre, une étude de sensibilité est réalisée en calculant les indices de Sobol pour déterminer les paramètres les plus influents, notamment la conductivité thermique, les isothermes de sorption, la teneur en humidité initiale et la densité. Les indices ont montré que les variations de la conductivité thermique ont un effet plus important sur la température de l'air intérieur et que les variations des isothermes ont un effet plus important sur l'humidité relative de l'air intérieur. Le deuxième paramètre le plus influent est l'isotherme de sorption. Ces deux entrées sont importantes dans un modèle HAMT et doivent être choisies avec soin pour obtenir des résultats exacts. Pour une meilleure analyse, la combinaison des entrées doit être étudiée car, par exemple, la densité affecte les valeurs de conductivité thermique. Par la suite les mêmes cas proposés dans la troisième partie ont été testés numériquement à l'aide du modèle EP sous les mêmes climats. En ce qui concerne le confort intérieur, sous le climat brésilien, les cas 1, 2 et 5, respectent les limites ASHRAE pendant 60 %, 64 % et 61 % du temps, respectivement. Le cas 3 présente une température opérationnelle intérieure qui ne respecte les limites que pendant 20 % du temps. Ce cas suggère des problèmes de surchauffe pendant la saison chaude, en particulier de janvier à mars. Le cas 4 présente la meilleure température opérationnelle intérieure, qui reste dans les limites pendant 96 % du temps. Les cas 1, 2 et 5, dans le climat chinois, respectent les limites ASHRAE pendant 49 %, 42 % et 52 % du temps, respectivement. Le cas 4 a la température opérationnelle intérieure la plus basse, qui respecte les limites pendant 37 % du temps. Le cas 3 présente la meilleure température opérationnelle intérieure, qui reste dans les limites pendant 64 % du temps. Pendant la saison chaude,

tous les cas sont exempts de risque de surchauffe. Le principal problème survient pendant la saison froide (de novembre à juin), lorsque la température de fonctionnement intérieure est basse. Les cas 1, 2, 4 et 5 du climat français respectent les limites ASHRAE pendant 76 %, 65 %, 51 % et 71 % du temps, respectivement. Le problème est découvert entre décembre et mars. Le cas 3 présente la meilleure température opérationnelle intérieure, qui reste dans les limites pendant 88 % du temps tout au long de l'année, sauf en novembre et décembre. Les cas 1, 2, 3, 4 et 5, dans un climat russe, respectent les limites de l'ASHRAE pendant 28 %, 23 %, 39 %, 18 % et 23 % du temps, respectivement. La température opérationnelle intérieure n'est respectée que pendant la période chaude entre avril et septembre. Pendant le reste de l'année, la température reste basse en raison de la basse température extérieure.

En l'absence d'un système de CVC, il est nécessaire d'assurer le confort intérieur des occupants en été et en hiver. Les murs en paille testés et le mur conventionnel ont des résistances thermiques différentes qui sont de 6,41 m².K/W pour le premier cas, 6,15 m².K/W pour le deuxième, 7,87 m².K/W pour le troisième, 6,71 m².K/W pour le quatrième, 7,46 m².K/W pour le cinquième et 2,5 m².K/W pour un mur conventionnel qui a été rajouté aux cinq cas pour comparer la paille aux matériaux standards. De plus, les enveloppes ont des propriétés hygriques différentes qui affectent le confort intérieur.

Le mur conventionnel a assuré le confort hygrothermique 80 % du temps à Brazilia, 5 % à Xinjiang, 45 % à Nice et 11 % à Arkhangelsk. Pour tous les cas de murs en paille, le confort intérieur n'a pas été assuré sous le climat chinois en raison de l'humidité relative extérieure élevée de 85 % en hiver avec une température moyenne de -10 °C et de l'humidité relative faible de 40 % en été avec une température moyenne de 25 °C. La faible température en hiver entraîne une faible température de l'air intérieur, ce qui montre l'inefficacité de la résistance thermique des murs, tandis que la faible HR en été entraîne une faible HR de l'air intérieur. Pour le climat russe, le confort hygrothermique intérieur est assuré 18 % du temps dans le cas 1, 22 % dans le cas 2, 4 % dans le cas 3, 20 % dans le cas 4, et 7 % dans le cas 5. Le problème est lié aux faibles valeurs de température intérieure et d'humidité relative au cours de l'année. Il faut noter que presque tous les cas dépassent les limites ASH qui indiquent une HR élevée dans les murs. Cela peut s'expliquer par les couches intérieures qui empêchent la diffusion de l'humidité vers l'intérieur. Pour le climat brésilien, le confort hygrothermique intérieur est assuré 26 % du temps dans le cas 1, 28 % dans le cas 2, 1 % dans le cas 3, 44 % dans le cas 4 et 6 % dans le cas 5. Ce type d'enveloppe, sous des températures extérieures élevées, provoque des surchauffes comme on le constate dans les cas 3 et 5. De plus, l'humidité relative intérieure est faible en raison des couches intérieures. Pour le climat français, le confort hygrothermique intérieur est assuré 48 % du temps dans le cas 1, 59 % dans le cas 2, 25 % dans le cas 3, 55 % dans le cas 4, et 40 % dans le cas 5. Le temps de confort le plus faible du cas 3 est dû à la faible HR intérieure entre février et août. La comparaison entre les bâtiments en paille et les bâtiments conventionnels montre que les constructions en paille ne sont pas adaptées à un climat chaud comme celui de Brasilia. En outre, les bâtiments en paille améliorent en moyenne de 10 % le confort hygrothermique intérieur par temps froid comme celui d'Arkhangelsk, en Russie.

Concernant le besoin net en énergie, deux cas peuvent être distingués en fonction du climat simulé. Pour un climat tropical (Aw), la part de la demande de refroidissement est prédominante entre septembre et février. Pendant les autres mois, le confort intérieur est assuré sans système CVC. Pour les climats subarctique (Dfc), méditerranéen (Csa) et aride (BWk), la part de la demande de chauffage est prédominante pendant la période hivernale de chaque pays. Tous les cas de murs en paille ont une faible demande de chauffage de 1,5 à 3,5 kWh/m² et une forte demande de refroidissement de 65 à 92 kWh/m² par temps brésilien. Le cas 3 présente la demande de chauffage la plus faible, soit 85 % de moins que le cas conventionnel. Le cas 4 a la demande de refroidissement la plus faible, qui est de 58 % supérieure à celle du cas conventionnel. En Chine, tous les cas de paille ont une faible demande de refroidissement de 4,1 à 4,9 kWh/m² et une forte demande de chauffage de 84 à 94 kWh/m². Le cas 3 présente la demande de chauffage et de refroidissement la plus faible, soit 42 % et 48 % de moins que le cas conventionnel. En raison de sa faible résistance thermique, le cas 1 a une demande de chauffage la plus élevée des

configurations de paroi paille. Dans le climat français, tous les cas ont une faible demande de refroidissement de 1 à 2 kWh/m² et une faible demande de chauffage de 16 à 29 kWh/m². Le cas 3 a une demande de chauffage et de refroidissement la plus faible, soit 75 % et 70 % de moins que le cas conventionnel. Toutes les configurations de paroi paille ont une faible demande de refroidissement de 8 à 9,6 kWh/m² et une forte demande de chauffage de 129 à 142 kWh/m² en climat russe. Comme pour les conditions météorologiques précédentes, le cas 3 a une demande de chauffage et de refroidissement la plus faible, soit 39 % et 46 % de moins que le cas conventionnel. La comparaison entre les bâtiments en paille et les bâtiments en brique montre une amélioration dans tous les cas, sauf au Brésil où la charge de refroidissement augmente de 30 % pour les bâtiments en paille. Cela peut s'expliquer par la résistance thermique élevée des murs en paille qui convient au temps froid et la résistance thermique plus faible du mur en brique isolé qui convient au temps chaud.

L'étude des performances thermiques et énergétiques du bâtiment test a été complétée par une évaluation environnementale et économique. Les analyses économiques basées sur les coûts de la construction sur son cycle de vie et les périodes d'amortissement pour les bâtiments en paille sont peu documentées dans la littérature. Par conséquent, cette étude effectue de telles analyses sur les cas proposés, afin de comparer leur impact environnemental et leur coût économique. Chaque enveloppe est censée être incorporée dans un bâtiment similaire au bâtiment test. L'évaluation environnementale est faite en calculant les émissions carbone dû à la production des matériaux de construction et à la consommation énergétique et le coefficient de neutralité carbone. Les résultats montrent que le cas conventionnel (bâtiment en briques standard) présente la plus forte émission de carbone liée à la production des matériaux avec 253,51 kg de CO₂/m². L'utilisation de la brique dans le cas conventionnel est à l'origine de 35 % des émissions totales. La deuxième émission de carbone la plus élevée due à la production de matériaux est obtenue dans le cas 4 avec 209,26 kg de CO₂/m². Ce cas est fortement affecté par les émissions du plâtre extérieur qui représentent 75 % des émissions totales. Le cas 2 présente la valeur la plus faible avec 111,85 kg de CO₂/m² en raison des faibles émissions du bois et de la paille. Les émissions totales du cas 5 sont similaires à celles du cas 4 en raison de l'utilisation de plâtre extérieur et intérieur et de la quantité de bois employé. La laine de bois a un impact très faible de 1 % sur les émissions totales dans les cas 5 et 6. On remarque que la couche de ciment est la principale cause de l'augmentation de l'émission totale des bâtiments en paille. En outre, la comparaison entre le cas 2 et le cas conventionnel montre que les bâtiments en paille peuvent réduire les émissions de carbone de 44 % par rapport aux bâtiments en briques standard. Les matériaux issus de la biomasse, tels que les bottes de paille, la laine de bois et le bois d'œuvre, ont un effet de séquestration du carbone. Le puits de carbone permet de réduire les émissions totales de carbone du bâtiment. La paille de blé et le bois contiennent respectivement 40 % et 50 % de carbone. La quantité de CO₂ stockée dans le matériau est utilisée pour calculer les émissions nettes de carbone en la soustrayant des émissions liées à la production des matériaux. Le stockage de carbone des bottes de paille uniquement se situe entre 45,8 kg de CO₂/m² dans le cas 3 et 36,7 kg de CO₂/m² dans les autres cas. Le stockage de carbone du bois atteint 38,4 kg de CO₂/m² dans le cas 1 et 243 kg de CO₂/m² dans le cas 2. Ces valeurs incluent la quantité de bois utilisée pour la structure de l'ensemble du bâtiment. Ainsi, l'émission nette de carbone calculée à partir des émissions totales et du carbone stocké des matériaux de la biomasse diminue de 20 % dans le cas 1, de 205 % dans le cas 2, de 61 % dans le cas 3, de 83 % dans le cas 4 et dans le cas 5 et de 2 % dans le cas conventionnel. La valeur nette des émissions de carbone la plus élevée est ainsi obtenue dans le cas 1 qui comprend la plus grande quantité de ciment. Le stockage du carbone a un effet direct sur la réduction des émissions de carbone. En classant les différents cas étudiés en fonction des émissions nettes de carbone causées par les matériaux employés, on remarque que le cas 2 est la meilleure configuration tandis que les cas 4 et 5 viennent en deuxième position. Le coefficient de neutralité carbone (CNC) du cas conventionnel n'est que de 0,005 avec seulement de la laine de bois comme matériau biologique. Le CNC le plus élevé est celui du cas 2 avec 0,59 car il est fortement basé sur les bottes de paille et le bois. Pour les cas 3, 4 et 5, le CNC est d'environ 0,25 tandis que pour le cas 1, il est de 0,12. Les valeurs CNC des bâtiments en paille indiquent que le bâtiment a un effet de neutralité carbone en fonction des

matériaux de couverture et que la paille réduit les émissions de carbone par unité de surface du bâtiment. Ces résultats changent lorsque les émissions de carbone causées par le chauffage et la climatisation du bâtiment chaque année sont considérés. Cette partie dépend de la région climatique qui fixe la demande de chauffage et de climatisation du bâtiment déterminée dans la section précédente. Les deux premiers cas ont des émissions annuelles similaires d'environ 16 kg de CO₂/ m², 26 kg de CO₂/ m², 8 kg de CO₂/ m² et 40 kg de CO₂/ m², respectivement sous les climats brésilien, chinois, français et russe. Pour le climat tropical (Aw), le cas conventionnel a les émissions de carbone les plus faibles en raison de sa demande de refroidissement plus faible chaque année. Pour les climats désertiques froids (BWk), le climat méditerranéen (Csa) et le climat continental subarctique (Dfc), les bâtiments en paille ont des émissions inférieures à celles des bâtiments en briques de 36 % en moyenne. Les bâtiments en paille ne sont pas efficaces sur le plan environnemental en climat tropical. En outre, les cas 5 et 3 peuvent être associés à un climat subarctique et méditerranéen, respectivement. Les cas 1, 2 et 4 devraient être utilisés dans un climat désertique froid.

L'évaluation économique est faite en calculant le coût du cycle de vie (LCC), le coût initial des matériaux (IC), le coût énergétique annuel et la période de d'amortissement. Le prix total des matériaux des bâtiments en paille est inférieur d'environ 45 % à celui des bâtiments standards. Les cas 1 et 5 présentent respectivement les prix des matériaux les plus bas et les plus élevés, car dans le premier cas, les murs sont composés de paille et de ciment avec une structure en bois, tandis que dans le cinquième cas, des panneaux de bois dur sont ajoutés, ce qui augmente la quantité de bois. Le remplacement du plâtre de ciment par des panneaux de bois dans le cas 2 augmente le prix total des matériaux de 34,6 %, tandis que dans le cas 3, le remplacement du plâtre de ciment par des planches de bois sur un côté n'augmente le prix total que de 30 %. L'ajout de panneaux de bois dur dans le cas 4 augmente le prix total de 31,6 %. Le coût énergétique annuel dépend fortement des prix de l'électricité et du gaz naturel du pays considéré. La Russie a les prix de l'énergie les plus bas, ce qui conduit au coût énergétique le plus faible malgré la demande élevée de chauffage et de climatisation calculée précédemment. La faible demande de chauffage et de refroidissement à Nice donne un faible coût énergétique qui est néanmoins supérieur à celui de la Russie de 51 % à 59 %, selon le cas. Au Xinjiang, le coût est plus élevé que dans les cas français et russe pour deux raisons, la demande annuelle de chauffage et le prix du kWh. La demande de refroidissement au Brésil augmente le coût annuel de refroidissement de plus de 70 % pour les bâtiments en paille. Enfin, le bâtiment en briques a un coût énergétique annuel supérieur à celui de la paille dans tous les cas, à l'exception du cas brésilien, en raison de la demande de refroidissement. Le coût initial de tous les types de murs varie à peine selon les pays, puisqu'il est affecté par le prix total des matériaux à hauteur de 75 %, qui est le même dans tous les pays. Le coût énergétique affecte le coût du cycle de vie de 9 %, 38 %, 45 % et 26 %, respectivement en Russie, en Chine, en France et au Brésil. Les matériaux de couverture utilisés ne contribuent pas à supprimer la demande de chauffage des bâtiments et augmentent le prix total des matériaux. Le cas 1 a le plus faible LCC de 518,5 \$/m², 687,2 \$/ m², 632 \$/ m², et 396,4 \$/ m², respectivement, au Brésil, en France, en Chine et en Russie. Le cas 5 présente le LCC du bâtiment en paille le plus élevé, mais il reste inférieur à celui du bâtiment conventionnel de 30 % en moyenne. On peut conclure que les bâtiments en paille permettent d'économiser sur le coût initial dans tous les pays et sur les coûts énergétiques, sauf dans les climats chauds et tropicaux (Aw). Les bâtiments en paille ont besoin de beaucoup d'années pour rembourser leur coût initial. Le délai moyen est de 47 ans, 32 ans et 187 ans, respectivement dans les régions désertiques froides, méditerranéennes et subarctiques. Sous un climat tropical, l'utilisation de la paille n'est pas rentable car le délai d'amortissement est négatif, ce qui signifie que dans les cinq cas, la consommation d'énergie des bâtiments en briques est inférieure à celle des bâtiments en paille.

Enfin, la dernière section porte sur le comportement mécanique du bâtiment expérimental en appliquant des charges de vent, de neige permanentes et des charges sismique en se basant sur l'Eurocode. Le bâtiment est alors supposé situé dans une zone montagneuse française (Isola). Les résultats ont montré que les cadres de contreventement de la fondation sont fortement affectés par les forces horizontales telles que le vent. Ces cadres qui relient les pieux en diagonale travaillent en tension afin d'empêcher les

pieux de s'effondrer. La contrainte maximale observée sur un cas de charge de vent est seulement de 10 MPa. Cette valeur est très faible comparée à la limite d'élasticité de l'acier S235 (235 MPa), ce qui indique une bonne résistance aux forces latérales. Pour les pieux, la contrainte maximale calculée est de 146 MPa, ce qui peut également être supporté par les profils en acier S235. Pour le caisson en bois, la contrainte maximale appliquée est de 2,75 MPa. Cette valeur est vérifiée pour un élément en bois lamellé-collé GL24h qui peut supporter une contrainte allant jusqu'à 19,2 MPa. Les hypothèses faites pour les cadres de contreventement et les pieux sont donc acceptables pour le dimensionnement du bâtiment. Elles montrent la stabilité de la structure face aux sollicitations permanentes et climatiques. Pour évaluer la résistance des panneaux, le critère de Von Mises est utilisé car il tient compte des composantes de la force de traction, de compression et de cisaillement, afin de fournir un niveau isotrope de force de cisaillement constant dans toutes les directions. Pour rester dans le domaine élastique du matériau, la contrainte équivalente doit être inférieure à la contrainte plastique. Les valeurs maximales des contraintes restent assez faibles par rapport à la résistance des matériaux utilisés pour la construction. Les poutres en I qui sont des éléments des panneaux en bois lamellé-collé GL24h ont une résistance à la compression et à la flexion de 24 MPa. L'essai montre que la contrainte maximale appliquée est d'environ 5 MPa, ce qui est inférieur à la contrainte admissible. En plus, le bâtiment est étudié sous une charge sismique avec une accélération horizontale de $1,6 \text{ m/s}^2$. La connaissance de la période de la structure est nécessaire pour déterminer le spectre de réponse élastique défini comme la réponse maximale (déplacement, vitesse ou accélération) d'une série d'oscillateurs qui sont mis en mouvement par la même vibration de base. La période naturelle calculée du bâtiment bois-paille modélisé est de 0,16 seconde. Cette période se situe entre la limite inférieure (0,15 s) et la limite supérieure (0,4 s) de la période du domaine à accélération spectrale constante. Ainsi, la structure est considérée comme rigide et capable de résister à un séisme ayant une accélération horizontale de $1,6 \text{ m/s}^2$.

7- Conclusion générale

Les objectifs de cette thèse étaient d'apporter des réponses scientifiques aux questions qui empêchent encore la diffusion des bâtiments en bottes de paille. Ces questions sont liées au confort hygrothermique intérieur, à la consommation énergétique, au bénéfice environnemental, à la rentabilité et à la résistance mécanique et au feu des bâtiments en paille. La première partie contient une revue de la littérature multi-échelle (fibre de paille - bottes - bâtiments) menée pour définir les lacunes dans les connaissances existantes. La paille est un coproduit agricole formé après la récolte des grains de diverses variétés de pailles : blé, orge, avoine et autres. Dans de nombreuses applications, les fibres organiques naturelles deviennent des alternatives viables aux fibres synthétiques. Comme le montre la revue, peu d'études ont été réalisées sur la caractérisation de ces matériaux.

Les travaux expérimentaux décrites dans la deuxième partie répondent à ce manque. L'étude expérimentale comprend la caractérisation de la microstructure, la mesure de la valeur tampon de l'humidité, la perméabilité à la vapeur d'eau, les courbes d'adsorption/désorption, la conductivité thermique et la capacité thermique spécifique. Ensuite, le transfert de chaleur a été traité dans les bottes de paille. La littérature comprend un nombre limité de modèles car une seule étude a été trouvée pour les bottes de paille. Les fibres naturelles ont de bonnes propriétés thermiques car elles contiennent de la cellulose et ont un faible impact environnemental en raison de leur énergie grise et de leurs émissions de gaz à effet de serre limitées. Dans l'application de construction de bâtiments, les composites naturels peuvent être utilisés pour leurs caractéristiques d'isolation thermique, qui dépendent de plusieurs facteurs tels que T et RH. Pour cette raison, cette partie fournit un modèle mathématique qui prédit la conductivité thermique effective des bottes de paille en fonction de la température, de l'humidité relative, de la teneur en cellulose et en lignine, de l'orientation des fibres et de la densité. Le modèle est construit à partir de la caractérisation de la microstructure et validé par les mesures expérimentales de la conductivité thermique. L'étude de caractérisation des matériaux s'est limitée à des échantillons de petites dimensions en fonction des exigences des tests. Les résultats auraient pu varier légèrement si une botte entière avait été testée. En outre, le modèle mathématique de la conductivité thermique s'est limité

à la lignine, à la cellulose et à l'humidité. D'autres composants chimiques pouvant affecter la conductivité thermique n'ont pas été pris en compte. Pour compléter l'étude, les travaux futurs pourraient inclure une comparaison de différents types de pailles comme le riz, l'avoine et l'orge. Cette comparaison permettrait de normaliser les propriétés de chaque type. Le modèle numérique proposé permet d'évaluer la conductivité thermique optimale en fonction des principaux facteurs d'influence. Une telle étude permet de trouver un compromis entre la composition chimique des fibres, leur densité, leur RH et leur orientation. Les futurs modèles numériques pourraient inclure l'effet de la longueur des fibres et des fissures qui peuvent se produire dans le composant solide. Le même travail pourrait être répété pour obtenir un modèle de la chaleur spécifique effective et de la formulation de l'hystérésis de sorption pour les matériaux de paille, basé sur leur microstructure et en fonction de leur densité, température, humidité, orientation des fibres, etc. Ces modèles sont importants pour estimer les caractéristiques thermiques et hygriques d'un type spécifique de botte de paille dans des conditions spécifiques, sans avoir à effectuer des tâches expérimentales longues et fastidieuses. Au final, de tels modèles augmenteront la précision des modèles de simulation thermique et énergétique des constructions incluant ce type de matériaux dans leur enveloppe.

La partie suivante a traité de la résistance au feu d'un nouveau type de mur en paille proposé par Activ'home, le partenaire industriel de cette thèse. Une couche de mousse minérale est ajoutée sur la face intérieure de manière à protéger la structure paille-bois qui est déjà recouverte de plaques fermacell sur les deux faces. L'expérience est réalisée à l'aide d'un four de 1 m³ équipé de thermomètres et reproduisant la courbe de feu ISO-834. L'objectif de l'étude est de tester une résistance au feu de 180 minutes. Ensuite, un modèle numérique est conçu à l'aide du logiciel ABAQUS. Le modèle est validé à l'aide de données expérimentales. Malgré les caractéristiques prometteuses du matériau paille, il peut comporter des risques d'humidité et de condensation entraînant des problèmes de santé, de stabilité et de durabilité. La température et l'humidité intérieures et extérieures, les pluies battantes, l'humidité du sol et les fuites peuvent toutes générer de l'humidité dans les murs en paille. Pour cette raison, cette partie étudie numériquement le comportement hygrothermique de diverses compositions de murs en paille multicouches en utilisant le logiciel WUFI. La validation du modèle se fait par la comparaison des données aux résultats trouvés dans la littérature. Cette étude associe à chaque climat la composition de mur optimale d'un point de vue hygrique et thermique. Cette partie a présenté quelques limitations. Notamment, la colle utilisée lors de l'essai de résistance au feu était classée EI 180, ce qui signifie une durée de résistance au feu supérieure à 180 minutes. Cependant, les expériences ont montré une destruction de la colle. Par conséquent, de nouvelles expériences devraient être menées sur la paroi déjà testée en assurant une application correcte de la colle. Le modèle numérique Abaqus a considéré un coefficient de convection externe constant comme recommandé par l'Eurocode 8. Des modèles plus précis peuvent considérer des coefficients variables basés sur la différence de température entre la surface externe et l'air environnant. Des tests supplémentaires de résistance au feu sont nécessaires et devraient tenir compte du type de paille, de sa composition chimique, de la densité des bottes de paille, de la composition et de la conception des différents parois constituées de bottes de paille. De même des tests approfondis qui ne sont pas seulement effectués sur des éléments de construction individuels mais aussi sur des structures entières permettraient d'évaluer les effets des autres éléments de construction sur le feu. Une étude complète devrait être réalisée pour examiner l'effet de la pluie battante sur les propriétés hygrothermiques des cinq murs de paille choisis. Il serait intéressant de faire varier l'épaisseur des bottes de paille dans le mur afin de choisir l'épaisseur optimale en fonction de ses propriétés hygrothermiques. La paille devrait également être étudiée comme matériau d'isolation extérieure pour les murs standards sous différents climats afin de montrer l'effet de la paille sur la température et l'humidité relative du mur. Sur le plan mécanique, les murs en paille devraient être testés pour mesurer leurs capacités de traction et de cisaillement.

La dernière partie concerne l'étude à l'échelle du bâtiment. Des bottes de paille sont utilisées pour construire un bâtiment expérimental selon la méthode du préfabriqué. Le bâtiment prototype est élaboré par le partenaire industriel. L'objectif est d'évaluer le confort intérieur dans le bâtiment en paille en été

et en hiver. En outre, ce chapitre permet de valider les caractéristiques déjà obtenues pour les murs en paille. En plus, la consommation thermique et énergétique des bâtiments en paille a été examinée sous différentes conditions climatiques et pour différentes compositions de murs. À cette fin, un modèle EnergyPlus est construit et validé en utilisant les données expérimentales du chapitre précédent. Le modèle est ensuite utilisé pour associer chaque climat à la composition de paroi appropriée du point de vue du confort hygrothermique et de la consommation d'énergie. En outre, le chapitre étudie la sensibilité de la température et de l'humidité relative de l'air intérieur aux variations de la densité, de la conductivité thermique, de la teneur en humidité initiale et des isothermes de sorption du matériau paille. De même, les différents bâtiments en paille ont été évalués d'un point de vue économique et environnemental en fonction des conditions météorologiques. L'évaluation environnementale est basée sur le calcul des émissions de carbone de chaque paroi. Le calcul comprend les émissions nettes de carbone des matériaux et les émissions générées par les charges de chauffage et de refroidissement de chaque cas. Sur le plan économique, le coût du cycle de vie et le délai de recouvrement sont calculés en fonction des prix des matériaux, du chauffage et de la climatisation dans chaque pays. À la fin, la résistance mécanique des bâtiments en paille a été étudiée. L'objectif ici est d'étudier le comportement mécanique du bâtiment expérimental face aux aléas sismiques et climatiques. Le travail est réalisé numériquement en utilisant un modèle de calcul de structure avec le logiciel Robot. Cette étape est indispensable avant toute construction afin d'assurer la sécurité des futurs occupants et la pérennité de la maison face à des conditions extrêmes. Cette partie a présenté quelques limitations. L'analyse de sensibilité actuelle considère l'effet de chaque paramètre, pris séparément, sur la température et l'HR. Les études futures devraient prendre en compte l'influence croisée des paramètres car, par exemple, la densité des bottes affecte leur conductivité thermique. L'étude numérique s'est concentrée sur l'effet du climat extérieur sur le confort intérieur dans un bâtiment résidentiel. Cependant, il serait intéressant d'étudier les mêmes cas dans différents scénarios intérieurs et pour différents types de bâtiments. Le confort intérieur des bâtiments standards pourrait être étudié en ajoutant de la paille comme isolation extérieure ou en variant l'épaisseur de la paille comme solution dans certains climats comme le climat tropical. En outre, l'impact thermique des bâtiments en paille doit être examiné sur le microclimat en mettant en œuvre une étude de voisinage. De tels cas devraient être complétés par le calcul des économies d'énergie réalisées après l'isolation du bâtiment et la détermination de la période d'amortissement. De même, les trois principales méthodes de construction des bâtiments en paille n'ont pas fait l'objet d'une étude approfondie quant à leurs avantages et limites inhérents du point de vue hygrothermique et mécanique. Par exemple, on ne sait toujours pas quelle méthode offre le meilleur confort thermique, les meilleures économies d'énergie et la meilleure résistance sismique. Ces études devraient également tenir compte de l'emplacement du bâtiment et de ses scénarios d'occupation et d'exploitation. En ce qui concerne l'évaluation environnementale, en cas de large diffusion de la construction en bottes de paille, des travaux supplémentaires devront être consacrés à l'impact des camions lourds transportant les pailles à proximité des sites de construction. À cet égard, l'utilisation du transport par train ou par bateau pourrait être une alternative respectueuse de l'environnement. D'un point de vue mécanique, le bâtiment doit être testé à différents endroits qui peuvent inclure des charges supplémentaires telles que l'accélération sismique verticale

Appendices

Appendix A1: Isolation method

At first, to determine the weight of ash (wash), a sample was ignited in a muffle furnace at 525 °C and burnt for 3 hours (TAPPI T211 om-12). For ash calculation, a separate sample was analyzed for the percentage of moisture by the Sartorius moisture analyzer. Ash content was calculated as follows:

$$W_{\text{ash}} = \left(\frac{m_1 - m_2}{m_u} \right) \cdot 100 \quad (\text{A13.1})$$

Where W_{ash} is the content of the ash, m_1 is the weight of the moisture-free sample before ignition, m_2 is the weight of the sample after ignition, and m_u is the oven-dry weight of the sample. Then for the determination of solvent extractives, a weight chopped sample was extracted with a mixture of benzene–ethanol ($\text{C}_6\text{H}_6 - \text{C}_2\text{H}_5\text{OH}$) solvent in a ratio of 1:1 for 8 hours in the Soxhlet apparatus. The material, extracted in a round bottom flask, was dried in an oven at the temperature of 80°C to constant weight (TAPPI T204 cm-07). The extracted content was calculated as follows:

$$W_{\text{SE}} = \left(\frac{m_2 - m_1}{m_u} \right) \cdot 100 \quad (\text{A1.2})$$

Where W_{SE} is the weight of the solvent extractives, m_1 is the oven-dry weight of the flask, m_2 is the oven-dry weight of extract in the flask and m_u is the oven-dry weight of the sample. In addition, for the determination of klasons lignin, the extracted sample, before being cooked in distilled water for 4 hours, had been pre-treated by 72 % sulphuric acid (H_2SO_4) for 2.5 hours. The solid residue lignin was obtained by filtration and drying in an oven at the temperature of 105 °C to constant weight (TAPPI T222 om-11). The Klason lignin content was calculated as follows:

$$W_{\text{lignin}} = \left(\frac{m_2 - m_1}{m_u} \right) \cdot 100 \quad (\text{A1.3})$$

Where W_{Lignin} is the content of the klasons lignin, m_1 is the oven-dry weight of filter paper, m_2 is the oven-dry weight of filtrated lignin plus the weight of filter paper, and m_u is the oven-dry weight of the sample. By using Küschner–Hoffer method for the determination of cellulose. The extracted sample was cooked in a mixture of nitric acid–ethanol ($\text{HNO}_3 - \text{C}_2\text{H}_5\text{OH}$ with a ratio of 1:4) in a hot water bath at the temperature of 100°C. The solid/liquid ratio was 1:25. Cooking was done through four extraction cycles until the sludge became completely bleached. Its filtration and drying in an oven at the temperature of 105°C to constant weight provided Küschner–Hoffer cellulose, which was calculated as follows:

$$W_{\text{cellulose}} = \left(\frac{m_1 - m_2}{m_u} \right) \cdot 100 \quad (\text{A1.4})$$

Where $W_{\text{cellulose}}$ is the content of the cellulose, m_1 is the oven-dry weight of filter paper funnel, m_2 is the oven-dry weight of funnel + extracted cellulose, and m_u is the oven-dry weight of the sample. Cellulose extracted from a sample had been obtained through several consecutive extractions with 17.5 % sodium hydroxide (NaOH) solution at 25 °C and then neutralized with 10 % acetic acid solution (CH_3COOH) (TAPPI T203 cm-09). The α -cellulose, as an insoluble fraction, was isolated by filtration and drying in an oven at the temperature of 105 °C to constant weight. The α -cellulose content was calculated as follows:

$$S = 100 - W_{\text{moisture}} \quad (\text{A1.5})$$

$$W_{\alpha\text{-cellulose}} = \frac{m_{\alpha\text{-cellulose}} \cdot 10^4}{S \cdot m_{\text{cellulose}}} \quad (\text{A1.6})$$

Where S is the weight of moisture-free cellulose sample, $W_{\alpha\text{-cellulose}}$ is the content of α -cellulose, W_{moisture} is the content of moisture, $m_{\text{cellulose}}$ is the weight of cellulose and $m_{\alpha\text{-cellulose}}$ is the weight of α -cellulose.

Appendix A2: Mechanical properties of Glued Laminated Timber GL24h and Steel S 235

Table A2. 1: Mechanical properties of GL24h and S235

Mechanical characteristics	GL24h (EN1194)	S 235 (EN10025)
Tension strength (N/mm ²)	16.5	360
Shear strength (N/mm ²)	2.7	83.1
Compression strength (N/mm ²)	24	--
Yield strength (kN/mm ²)	--	235
Young's modulus (kN/mm ²)	11.6	210
Density (kg/m ³)	440	7850

Appendix A3: Staple dimensioning based on Eurocode 5

Table A3. 1: Dimensions of the two staples used in the assembling step

Dimensions (mm)	Staple 1	Staple 2	comments
b	10.8	10.8	> 6.d (based on EC5)
l	1.4	1.4	
L	1.6	1.6	
d	1.5	1.5	
Length	40	64	

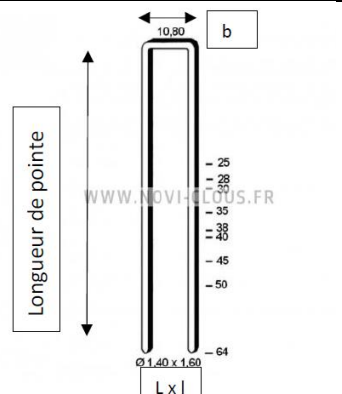


Table A3. 2: Dimensions of the two staples used in the assembling step

	Staple 1	Staple 2	comments
Timber thickness t (mm)	10	40	
Timber Density ρ (kg/m ³)	500	500	
Characteristic embedment strength $f_{h,1,k}$ (MPa)	105.82	243,12	$30 \cdot d^{-0.3} \cdot t^{0.6}$
Characteristic embedment strength $f_{h,2,k}$ (MPa)	36.33	36.33	
characteristic yield moment M_y (N.mm)	688.75	688.75	$240 \cdot d^{2.6}$
characteristic load-carrying capacity $F_{v,rk_{min}}$ (N)	382.9	413.94	EC5 8.6
characteristic load-carrying capacity $F_{v,rk}$ (N)	766	828	$2 \cdot (F_{v,rk_{min}})$

The bracing resistance is calculated then by:

$$F = \frac{\sum F_{v,rk} \cdot L_{wall}}{d} = \frac{(766+828) \cdot 6.5}{0.25} = 41 \text{ kN} \quad (\text{A3.1})$$

where L_{wall} is the maximum length of the wall and d is the spacing between staples.

Appendix A4: French regions location category

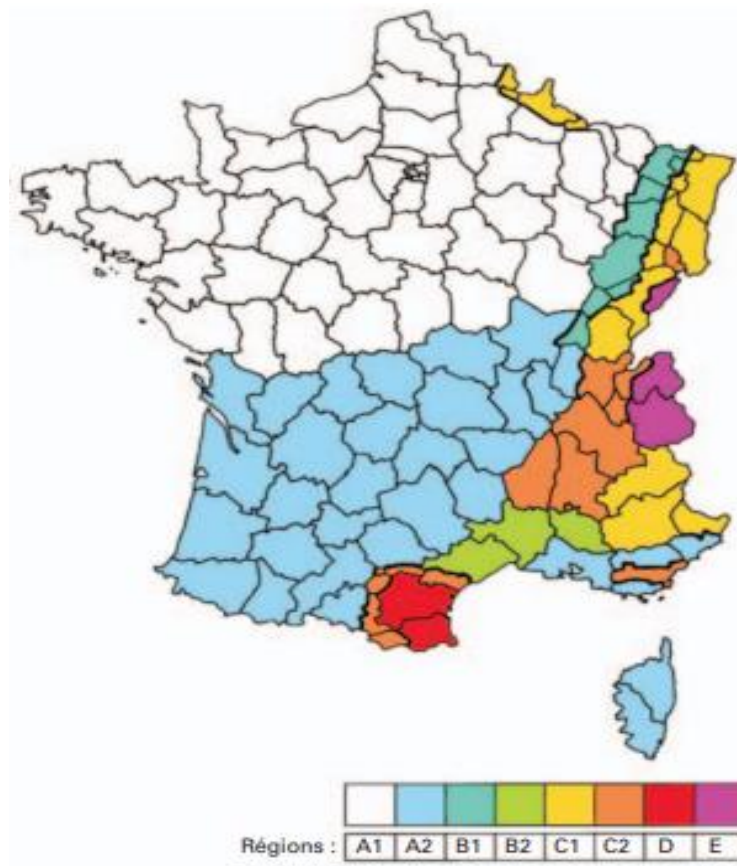


Figure A4. 2: France map showing the location categories based on the snow charge [270]

Table A4. 1: Snow charge in the different location categories [270]

Region		A1	A2	B1	B2	C1	C2	D	E
Snow charge S (kN/m ²) at an altitude of 200 m		0.45	0.45	0.55	0.55	0.65	0.65	0.9	1.4
ΔS based on the site altitude above sea level A	200 m – 500 m	$\frac{A}{1000} - 0.2$							$(1.5 \cdot \frac{A}{1000}) - 0.3$
	500 m – 1000 m	$(1.5 \cdot \frac{A}{1000}) - 0.45$							$(3.5 \cdot \frac{A}{1000}) - 1.3$
	1000 m – 2000 m	$(3.5 \cdot \frac{A}{1000}) - 2.45$							$(7 \cdot \frac{A}{1000}) - 4.8$

The snow load is calculated by:

$$F = \mu \cdot C_e \cdot C_t \cdot S + \Delta S = 0.65 + 2.8 = 3.45 \text{ kN} \quad (\text{A4.1})$$

Where C_e is the exposure coefficient, C_t is the thermal coefficient, μ is the snow load shape coefficient. All coefficients are equal to 1.

Appendix A5: Wind load calculation in France

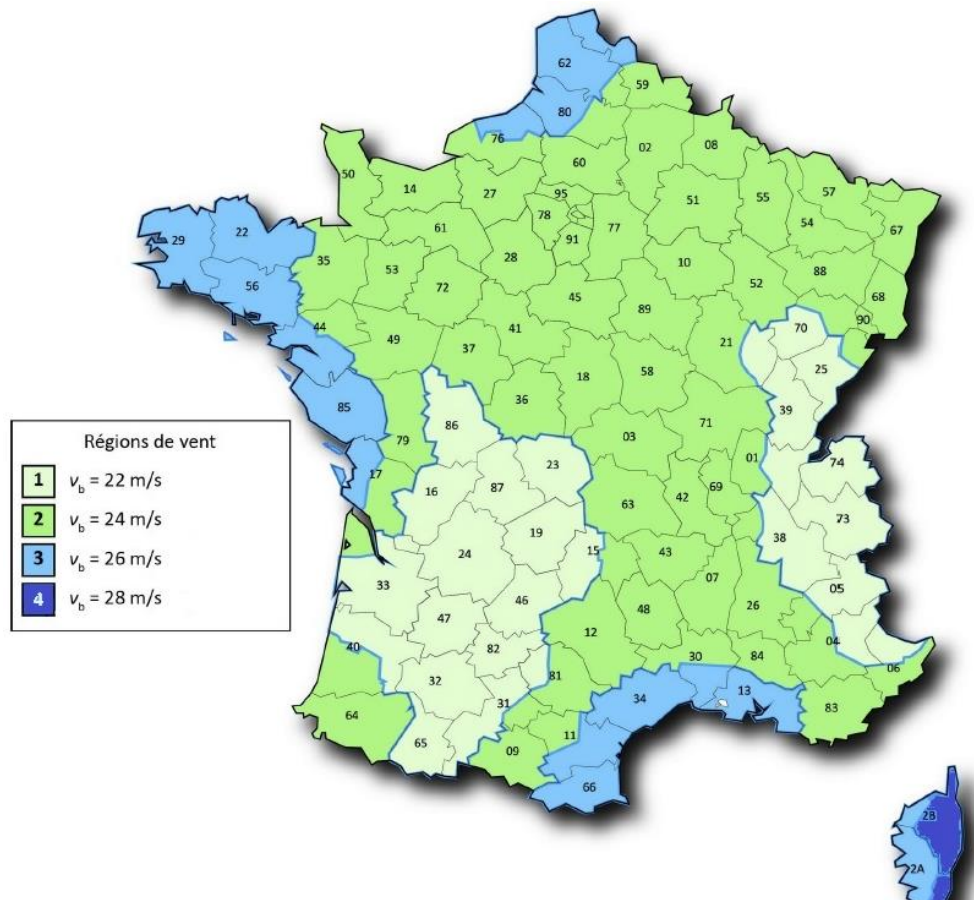


Figure A5. 3: France map showing the location categories based on the wind speed [271]

Table A5. 1: Roughness length and minimum height of a building based on its land category [271]

Land Category	Roughness length (m)	Minimum height (m)
0: sea wind	0.005	1
II: open countryside	0.05	2
IIIa: countryside with hedges	0.2	5
IIIb: urbanized area	0.5	9
IV: urbanized area covered by buildings (minimum 15 % of the surface)	1	15

Eurocode gives us the formulas allowing us to calculate the intensity of the wind, the average speed, and the peak dynamic pressure which ultimately corresponds to the pressure exerted on the south facade of our building.

Table A5. 2: Calculation of the wind intensity [271]

Parameters		Value
Orography factor	$C_0(z)$	1
Reference height	$Z_{0,II} = 0,05 \text{ m} ; Z_0 = 0,20\text{m} ; Z_{min} = 5,00\text{m}$	
Land Factor	$k_r = 0.19 \cdot \left(\frac{Z_0}{Z_{0,II}}\right)^{0.07}$	0.209
Roughness Factor	$C_r(z) = k_r \cdot \ln\left(\frac{z}{Z_0}\right)$	0.808
Wind turbulence factor	$K_t = C_0(z) \cdot [1 - 2 \cdot 10^{-4} \cdot (\log_{10}(z_0) + 3)^6]$	0.974
Turbulence intensity (EC1-4 - Exp. 4.7)	$I_v(z) = \frac{K_t}{C_0(z) \cdot \ln\left(\frac{z}{Z_0}\right)}$	0.251
Wind reference speed	$v_{b,0}$ (zone 1)	22 m.s ⁻¹
Orientation coefficient	Cdir	1
Season coefficient	Cseason	1
Basic Wind Velocity	$v_b = C_{dir} \cdot C_{season} \cdot v_{b,0}$	22 m.s ⁻¹
Wind velocity at height	$v_m(z) = C_r(z) \cdot C_0(z) \cdot v_b$	17,85 m.s ⁻¹
Peak velocity pressure at a height (ρ is the air pressure)	$(z) = [1 + 7 \cdot I_v(z)] \cdot 0.5 \cdot \rho \cdot v_b^2$	53,9 DaN/m ²

For the roofs, the Eurocode recommends a pressure coefficients (Cpe) calculation based on area type:

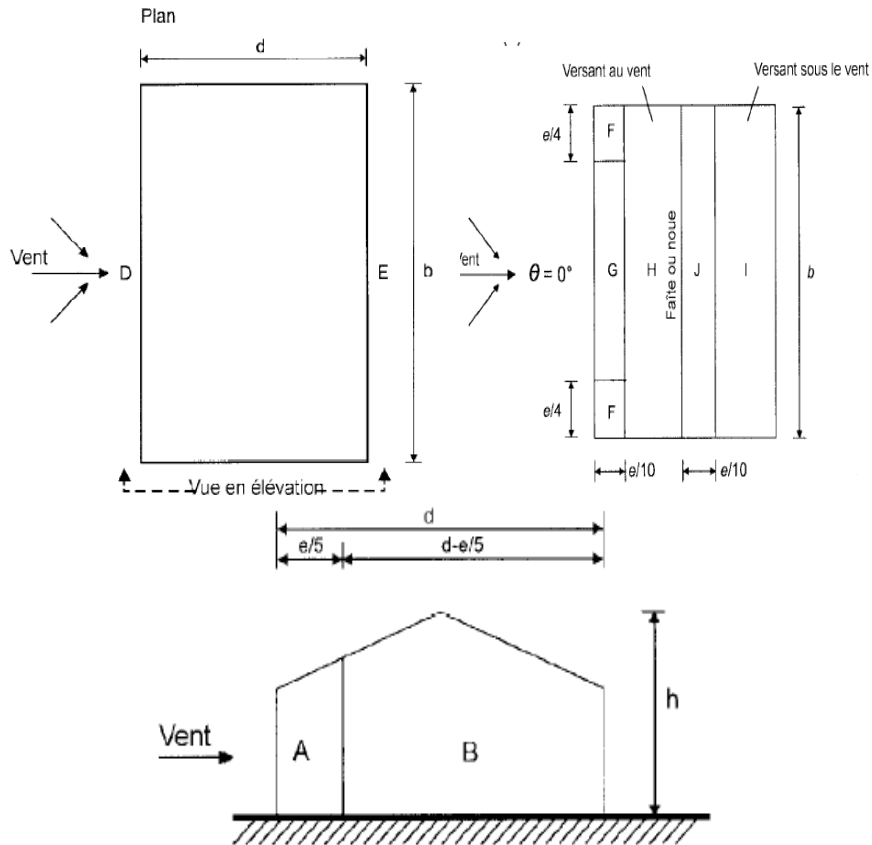


Figure A5. 4: Pressure coefficient based on the zone of the building [271]

Table A5. 3: Calculation of the pressure coefficient [271]

Zone	$C_{pe,10}$	Aerodynamic pressure applied over the surfaces $We = q_p \cdot C_{pe}$ (DaN/m ²)
A	-1,2	-64,68
B	-0,8	-43,12
D	0,8	43,12
E	-0,5	-26,95
F	0,7	37,73
G	0,7	37,73
H	0,4	21,56
I and J	0	0

Appendix A6: List of publications

At the time of the submission of this manuscript, two journal papers are published, and two are submitted.

Journal papers:

- Tlaji G., Biwole P., Oulboukhite S., Pennec F., (2022) “**A mini review of straw bale construction**” – *Energies 15 (21)*
- Tlaji G., Pennec F., Oulboukhite S., Ibrahim M., Biwole P., (2022) “**Hygrothermal performance of multilayer straw walls in different climates**” – *Construction and Building Materials, Volume 326, pp. 126873*
- Tlaji G., Oulboukhite S., Pennec F., Biwole P., (2022) “**Thermal and mechanical behavior of straw-based construction: A review**” – *Construction and Building Materials, Volume 316, pp. 125915*
- Tlaji G., Biwole P., Oulboukhite S., Pennec F., “**Effective thermal conductivity model of straw bales based on microstructure and hygrothermal characterization**” – Submitted to *Construction and Building Materials*

Conference papers:

- Tlaji G., Pennec F., Oulboukhite S., Ibrahim M., Biwole P., “**Performance hygrothermique des enveloppes multicouches utilisant le matériau paille**”- *Conférence IBPSA France – Châlons en Champagne – 19-20 May 2022 – PowerPoint presentation*
- Tlaji G., Biwole P., Pennec F., Oulboukhite S., “**Analyse bibliographique du comportement thermique et mécanique de la construction en paille**”- *Congres National de la Recherche des IUT (CNRIUT) – Lyon – 3-4 June 2021 – Poster and online participation*